

Dissertation
submitted to the
Combined Faculty of Natural Sciences and Mathematics
of the Ruperto Carola University Heidelberg, Germany
for the degree of
Doctor of Natural Sciences

Presented by
Renè Sahm, M. Sc.
born in Offenbach am Main, Germany
Oral examination: 02.06.2020

In Vitro Analysis of HIV-1 Proteolytic Maturation Kinetics

Referees: Prof. Dr. Hans-Georg Kräusslich
Prof. Dr. Stephan Urban

Eidesstattliche Erklärung

Hiermit erkläre ich, Renè Sahm, Wingertstr. 40, 69207 Sandhausen, geboren am 22.11.1989 in Offenbach am Main, dass ich die vorliegende Dissertation am Lehrstuhl für Virologie an der Ruprecht-Karls-Universität Heidelberg unter Anleitung von Prof. Dr. Barbara Müller selbständig verfasst habe und nur mit den angegebenen Hilfsmitteln angefertigt habe und das alle Stellen, die dem Wortlaut oder dem Sinne nach anderen Werken entnommen sind, durch Angabe der Quellen als Entlehnung kenntlich gemacht worden sind. Ich habe an keiner anderen Stelle ein Prüfungsverfahren beantragt bzw. die Dissertation in dieser oder anderer Form bereits anderweitig als Prüfungsarbeit verwendet oder einer anderen Fakultät als Dissertation vorgelegt. Ich erkläre hiermit, dass die Dissertation unter Verwendung elektronischer Datenverarbeitungsprogramme auf die Einhaltung allgemein geltender wissenschaftlicher Standards überprüft werden darf.

Sandhausen, den 05.03.2020

1 Summary

Human Immunodeficiency Virus-1 (HIV-1) assembles and buds as non-infectious particles at the plasma membrane of host cells. During assembly, it forms an irregular hexameric ordered lattice consisting of the structural polyproteins Gag and GagProPol. To facilitate infectivity, the intrinsic protease (PR) of HIV-1 drives the maturation by processing these polyproteins at 5 and 9 cleavage sites (CS), respectively, after self-cleavage. This proteolytic part is tightly regulated temporally and sequentially, to ensure a correct morphological rearrangement by a specific release of subdomains inside the viral particle. Gag comprises the matrix (MA), capsid (CA), and nucleocapsid protein (NC) as well as two spacer peptides (SP1 and SP2) and the C-terminal p6-domain. After maturation, CA encapsulates a condensed complex of NC and the RNA genome copies as the conical core. Already subtle dynamical or structural changes can prevent a successful maturation and therefore impair viral infectivity. The concomitant start of maturation and assembly/budding processes so far prevented a precise time-course analysis of maturation in connection with structural and cofactor interactions, and the determination of pH during maturation.

Previous proteolytic cleavage studies with *in vitro* translated Gag and viral particles already led to the categorization of the CSs regarding their processing rates: rapid (SP1-NC), intermediate (MA-CA, SP2-p6), and slow (CA-SP1, NC-SP2). However, these dynamics differ from the processing of synthetic CS peptides. That is why this work aimed to analyze the impact of Gag assembly, which is usually induced by the binding of nucleic acid, and other factors as specific mutations upon the dynamics of maturation. In previous studies, only the final products of maturation were analyzed in viral particles regarding morphology and processing results. Other time-course analyses excluded the verification of the Gag multimerization or the influence of nucleic acid as present in virus-producing cells. Thus, I wanted to compare the processing of Gag in an assembled structure or non-assembled state and additionally introduced specific cleavage site mutants and maturation altering compounds into my system. In order to tackle these open questions for Gag processing dynamics, an *in vitro* based processing approach for the analyses of proteolytic maturation was chosen, including non-assembled Gag and *in vitro* assembled Δ MACANCSP2, a truncated Gag variant.

Therefore, I produced recombinant Gag with a C-terminal His-tag (Gag-His) in *E. coli* and optimized the protocol to yield high purity and no nucleic acid contamination, to avoid preliminary assembly. A given protocol to assemble Δ MACANCSP2 was optimized, which increased assembly efficiency and stability to endure the inconvenient conditions of the following processing experiment. Additionally, this newly created protocol could achieve assembly of Δ MACANCSP2 in the absence of any nucleic acid into curved filaments instead of spherical particles. As these filamentous structures are a novelty, further structural analysis of them could give more insight into the assembling properties of Gag in the future.

Gag-His featured, independent of its intrinsic homodimerization, an altered order of processing in contrast to the assembled Δ MACANCSP2. The initial cleavage occurred at MA-CA and CA-SP1, followed by SP1-NC and SP2-p6, and at last, NC-SP2. In comparison, the processing of assembled Δ MACANCSP2 reproduced the same processing order shown in the literature, which was only marginally affected by the application of longer NA than 68 nt. The processing of assembled protein was finished up to six times faster than for the non-assembled, while the absence of or very short (5 nucleotides) NA during the processing of assembled Δ MACANCSP2 caused a mixture of both results. While MA-CA and CA-SP1 are processed like

assembled Δ MACANCSP2 with nucleic acid, SP1-NC and NC-SP2 are processed significantly slower than in the case of non-assembled Gag-His. These results suggest that the cleavage events of non-assembled Gag is dependent on the amino acid sequence of the CSs, and assembly causes for MA-CA and CA-SP1 a maturation restriction.

Changing the pH of the processing procedure had a severe impact on the processing of CA-SP1 and NC-SP2 in an assembled or non-assembled protein. While the processing was fastest at pH 6.0, the optimum for PR activity, the processing was strongly reduced at pH 6.5 and even more at pH 7.0. The remaining three CSs were only marginally affected. Consequently, CA-SP1 and NC-SP2 might comprise pH-dependent structural domains or interactions, and a theoretical pH shift during maturation of viral particles could enable fast processing.

The introduction of mutations known to inhibit proteolytic cleavage or a maturation inhibitor showed that the processing of each site, but CA-SP1, is independent of the cleavage of the other CSs. By inhibiting the processing at SP1-NC, the cleavage of CA-SP1 got delayed, which was observed in the presence and absence of nucleic acids. Interestingly, the inhibition of MA-CA cleavage led to the processing of a new cryptic CS, which was determined to be at the N-terminal region of CA.

In summary of this work, assembly of Gag in the presence of nucleic acid accelerates maturation notably, whereas the single cleavage events are independent of each other and only temporally ordered. While assembly delays the processing at MA-CA and CA-SP1, the presence of nucleic acid is the actual key player to shorten the maturation, but it is not essential for Gag assembly.

2 Zusammenfassung

Das Humane Immundefizienz-Virus-1 (HIV-1) assembliert und knospt als nicht infektiöse Partikel an der Plasmamembran infizierter Zellen. Dort formt es ein unregelmäßig hexamer-geordnetes Gitter aus den Strukturproteinen Gag und GagProPol. Für die Infektiösität der Partikel treibt die Protease (PR) des HIV-1 die Maturation an, indem die Struktureproteine jeweils an fünf bzw. neun Schnittstellen (CS) prozessiert werden. Dieser proteolytische Schritt ist sowohl zeitlich wie auch sequenziell strikt reguliert, um für die nötige Verfügbarkeiten der Untereinheiten für eine morphologische Neuordnung innerhalb der viralen Partikel zu sorgen. Gag enthält neben dem Matrix- (MA), Capsid- (CA) und Nucleocapsidprotein (NC) zwei Spacerpeptide (SP1 und SP2) sowie eine C-terminaler p6-Domäne. Nach der Maturation schließt CA als konischer Kern einen verdichteten Komplex aus NC und den Kopien des RNA-Genoms ein. Bereits leichte dynamische oder strukturelle Abweichung können eine erfolgreiche Maturation und eine Neuinfektion an Wirtszellen verhindern. Die Überschneidung der Maturation und der Assemblierung/Knospfung verhinderte bisher jedoch eine präzise zeitlich aufgelöste Analyse der Maturation mit dem Augenmerk auf strukturelle und Cofaktor-Interaktionen sowie des vorliegenden pH-Wertes.

Basierend auf vorausgegangen Studien mit *in vitro* translatiertem Gag und viralen Partikeln konnte die sequenzielle Prozessierung genauer untersucht und die einzelnen CSs gemäß ihrer Prozessierungsraten kategorisiert werden: rapide (SP1-NC), intermediär (MA-CA, SP2-p6) und langsam (CA-SP1, NC-SP2). Dies variiert jedoch gegenüber der Prozessierung synthetischer Peptide aus den CSs. Daher befasst sich diese Arbeit mit dem Einfluss der Gagassemblierung, welche künstlich durch Bindung mit Nukleinsäuren (NA) induziert wird, und der Präsenz der NA selbst auf die Dynamiken der Maturation. Bisher konnten die meisten anderen Forschungen nur die finalen Ergebnisse der Maturation in viralen Partikeln auf ihre Morphologie und Prozessierungsprodukte untersuchen. Andere zeitaufgelöste Analysen bezogen nicht die Multimerisierung von Gag oder Präsenz möglicher NA mit ein. Darauf aufbauend wollte ich die Prozessierung des Gag-Proteins in assemblierter oder nicht-assemblierter Form vergleichen, wobei zusätzlich spezifische CS-Mutanten und maturationsverändernde Substanzen getestet werden sollten. Um die offenen Fragen der Maturation anzugehen, wurde ein *in vitro* basierter Prozessierungsansatz gewählt unter Einbezug der nicht assemblierten Gag und dem *in vitro* assemblierten Δ MACANCSP2, eine verkürzte Gag-Variante.

Zu Beginn wurde dazu rekombinantes Gag mit C-terminalen His-tag (Gag-His) in *E. coli* produziert, welches im Anschluss mit Hilfe eines optimierten Protokolls separiert wurde. Ein bereits etabliertes Protokoll wurde für die Assemblierung des Δ MACANCSP2 optimiert, so dass eine höhere Ausbeute und Stabilität der Partikel erreicht wurde, wodurch diese sogar unter den widrigen Bedingungen der folgenden Prozessierungsexperimente stabil blieben. Mittels des neuen Protokolls konnte Δ MACANCSP2 sogar ohne anwesende NA assembliert werden, wenn es auch in diesem Fall nicht sphärische Partikeln sondern kurvige Filamente bildete. Da diese Filamentstrukturen eine Neuheit sind, könnte in Zukunft die strukturelle Analyse mehr Details über die Assemblierungseigenschaften des Gag-Proteins preis geben.

Die Prozessierung des gereinigten Gag-Proteins zeigte unabhängig der intrinsischen Fähigkeit zur Homodimerisierung eine Veränderung in der Prozessierungsreihenfolge im Vergleich zu assemblierten Δ MACANCSP2. Der initiale Schnitt war an MA-CA und CA-SP1 gefolgt von SP1-NC und SP2-p6. Die

Prozessierung des assemblierten Δ MACANCSP2 reproduzierte dieselbe Reihenfolge, wie sie in der Literatur beschrieben wird, was nur geringfügig durch die Verwendungen länger NA als 68 Nukleotide beeinflusst wurde. Die gesamte Prozessierung assemblierten Proteins geschah sechsmal schneller im Vergleich zum nicht assemblierten, während die Abwesenheit von oder nur sehr kurze (5 Nukleotide) NA während der Prozessierung des assemblierten Δ MACANCSP2 eine Mischung aus den beiden zuvor beobachteten Ergebnissen erzeugte. Während MA-CA und CA-SP1 wie im assemblierten Zustand verdaut wurden, vollzog sich dies bei SP1-NC und NC-SP2 deutlich langsamer wie im Falle des nicht assemblierten Gag-His. Diese Ergebnisse sprechen dafür, dass die Kinetiken des CSs-Verdaus des nicht assemblierten Gag-His durch die Aminosäuresequenz der CSs bestimmt sind und dass das Assembly für MA-CA und CA-SP1 eine Maturationrestriktion verursacht.

Die Veränderung des pH-Wertes zeigte großen Einfluss auf die Prozessierung von CA-SP1 und NC-SP2 im assemblierten und nicht-assemblierten Zustand. Während die Prozessierung bei pH 6.0 am schnellsten war, wurde sie bei pH 6.5 und noch deutlicher bei pH 7.0 reduziert. Folglich weisen CA-SP1 und NC-SP2 wohlmöglich pH abhängige strukturellen Domänen oder Interaktionen auf und eine theoretische Veränderung des pH könnte eine schnelle Prozessierung während der Maturation viraler Partikel ermöglichen.

Durch Inhibierung einzelner CSs durch Mutation oder die Zugabe eines Maturationsinhibitors konnte nachgewiesen werden, dass alle CSs, abgesehen von CA-SP1, unabhängig voneinander prozessiert werden. Die Inhibierung von SP1-NC verzögerte die Prozessierung an CA-SP1, was unabhängig von der Anwesenheit an Nukleinsäuren war. Überraschenderweise förderte die Inhibierung von MA-CA die Prozessierung einer bisher unbekanntem aberranten CS im N-terminalen Bereich von CA.

Zusammenfassend kann festgehalten werden, dass die Maturation sichtlich durch die Assemblierung von Gag in Gegenwart von Nukleinsäuren beschleunigt wird, wobei die einzelnen CSs unabhängig voneinander und nur zeitlich geordnet prozessiert werden. Während die Assemblierung die Prozessierung von MA-CA und CA-SP1 verzögert, ist die Verfügbarkeit von Nukleinsäuren der ausschlaggebende Punkt für die Verkürzung der Maturation, auch wenn sie nicht essenziell für Gag-Assembly ist.

3 Table of content

1	Summary	i
2	Zusammenfassung	iii
3	Table of content	v
4	Introduction	1
4.1	Retroviruses and HIV-1.....	1
4.1.1	HIV-1 genome and proteome.....	2
4.2	HIV-1 replication cycle.....	3
4.3	HIV-1 particle maturation.....	5
4.3.1	Architecture of Gag and immature viral particles.....	5
4.3.2	Proteolysis and structural rearrangement during maturation.....	7
4.3.2.1	HIV-1 protease and protease inhibitors	10
4.3.3	<i>In vitro</i> systems for HIV-1 assembly and proteolytic maturation.....	11
4.4	Maturation altering conditions	13
4.4.1	pH dependency of proteolytic activity	14
4.4.2	Regulation of maturation by nucleic acid.....	14
4.4.3	Dynamical impact of cleavage site mutations.....	15
4.4.4	Maturation inhibitors	16
4.5	Aim of this work	17
5	Materials and methods	18
5.1	Materials.....	18
5.1.1	Laboratory equipment.....	18
5.1.2	Kits	20
5.1.3	Chemicals and consumables.....	20
5.1.4	Antibodies and dyes	23
5.1.5	Enzymes.....	23
5.1.6	Buffers recipes.....	24
5.1.7	Primer and plasmids.....	26
5.1.8	Bacterial and eukaryotic strains	28
5.2	Methods	28
5.2.1	Molecular biological methods.....	28
5.2.1.1	Isolation of plasmids.....	28

5.2.1.2	Transformation	29
5.2.1.3	Gene amplification by polymerase chain reaction (PCR)	29
5.2.1.4	Restriction digest.....	30
5.2.1.5	Ligation	30
5.2.1.6	Agarose Gel Electrophoresis.....	30
5.2.1.7	Cloning procedure and used plasmids	31
5.2.2	Biochemical methods	34
5.2.2.1	Protein production	34
5.2.2.2	Protein purification and preparation	34
5.2.2.3	Antiserum purification.....	36
5.2.2.4	<i>In vitro</i> assembly.....	37
5.2.2.5	Protein processing.....	39
5.2.2.6	Protein analysis.....	40
6	Results.....	46
6.1	Establishment of a purification method for recombinant Gag and its characterization	46
6.2	Efficient assembly of stable virus-like particles.....	51
6.3	Quantitative workflow for the analysis of Gag processing	59
6.3.1	Establishment of conditions for proteolytic processing.....	59
6.3.2	Identification of processing products.....	62
6.3.3	Protein stability under processing conditions.....	67
6.3.4	Quantitative analysis and plotting.....	68
6.4	Processing of Gag	70
6.4.1	Gag in mono- and dimeric states	70
6.4.2	Impact upon cleavage events by the structural arrangement of Gag.....	72
6.4.3	Maturation altering conditions	76
6.4.3.1	Impact of physiological vs. active protease pH	77
6.4.3.2	The effect of nucleic acid on Gag processing	80
6.4.3.3	Inhibition of single cleavage events by point mutations.....	83
6.4.3.4	Analysis of protease inhibitor resistance conveying and cleavage rate altering mutations of Gag	90
6.4.3.5	Influence of the maturation inhibitor bevirimat on Gag processing.....	93
7	Discussion.....	95
7.1	Non-assembled Gag reveals an altered sequential processing independent of the oligomerization state.....	95

7.2	IP6 and pH: Assembly stabilizer and maturation accelerator	97
7.3	Assembly and nucleic acid: Structural agents and proteolytic maturation modulators?	99
7.4	Synchronized but independent cleavage events.....	101
7.5	Aberrant cleavage of MA-CA: Biological compensation or possible target in HIV-1 replication?	102
7.6	Gag mutations for PI resistance without accelerating effect on processing	103
7.7	Kinetic modeling of maturation	103
8	Abbreviations	105
9	Appendix	109
10	Index	125
11	Acknowledgments.....	127
12	Plasmid maps.....	128
13	References	129

4 Introduction

In 1981, the immune disease acquired immune deficiency syndrome (AIDS) was observed clinically for the first time (CDC, 1981). In 1983, two groups reported isolation of the principal causative agent, the retrovirus human immunodeficiency virus (HIV) (Gallo, et al., 1983; Barré-Sinoussi, et al., 1983). While the oldest known case of an HIV infection is derived from 1959 (Zhu, et al., 1998), statistical approaches predict the first infection in the middle of the 1900s (Faria, et al., 2014). Since then, the disease evolved into a global pandemic influencing human society and medical research.

In 2018, about 37.9 million people were living with an HIV infection, while 770000 people died due to AIDS-related illnesses (reviewed in GLOBAL HIV STATISTICS , 2019). In spite of intense research on HIV for more than three decades, there is still no vaccination available. In 1987, the reverse transcriptase (RT) inhibitor azidothymidine (AZT) became available for the treatment of HIV infected patients (Nakashima, et al., 1986). However, HIV rapidly developed resistance against monotherapy, demanding a more complex therapy scheme. The development of drugs targeting the viral protease (PR) allowed for a combination therapy. Today, compounds targeting the steps of viral entry, reverse transcription, genome integration and proteolytic maturation are available for combination antiretroviral therapy (cART) (reviewed in Deutsche AIDS-Gesellschaft, 2019). Together with public health initiatives, the combination antiretroviral therapy cART resulted in a dramatic decrease in AIDS-related deaths. Thus, the number of newly infected people and AIDS-related deaths per year is globally decreasing steadily since 1997 (UNAIDS Press release, 2016), whereas the fraction of antiretroviral therapy accessing people has increased to 24.5 million (reviewed in GLOBAL HIV STATISTICS , 2019). However, currently available drugs can only control the viral load and prevent progression of the disease, but do not cure the infection. Besides the research for cures against HIV, the remaining challenges are to reduce the burden of infected people being on medication of antiretroviral drugs for their lifetime, and to treat resistant strains derived from the high mutation rate.

4.1 Retroviruses and HIV-1

Viruses of the *Retroviridae* family are membrane enveloped viruses containing two copies of a single-stranded (ss) (+) strand-RNA genome. After cell entry, the genome is reverse transcribed into double-stranded (ds) DNA by the virus-encoded RT, and the newly synthesized DNA is integrated into the host genome by the viral integrase (IN) resulting in permanent infection of the cell. These two enzymes are the hallmark of retroviruses.

Retroviruses are part of the group VI viruses (Baltimore, 1971) and are divided taxonomically into its subfamilies *Alpharetroviruses*, *Betaretroviruses*, *Gammaretroviruses*, *Deltaretroviruses*, *Epsilonretroviruses*, and *Lentiviruses*. Human pathogenic retroviruses are the human T-cell leukemia viruses (HTLV) type I and II from the subfamily *Deltaretroviruses* and HIV type I and type II of the family *Lentiviruses* (Stoye, et al., 2011). While HIV-1 and HIV-2 are morphologically similar and are part of the same genus, HIV-2 is phylogenetically more related to Simian immunodeficiency virus (SIV) than to HIV-1

(Keele, et al., 2006). Without treatment, HIV-2 can also cause AIDS, even though it has a reduced infection rate and pathogenicity (reviewed in Reeves and Doms, 2002; reviewed in Campbell-Yesufu, et al., 2011). Due to the significantly higher medical relevance of HIV-1, this study is only focusing on HIV-1.

4.1.1 HIV-1 genome and proteome

After reverse-transcription of the 9.7 kb long HIV-1 genome (vRNA) (Wain-Hobson, et al., 1985; Ratner, et al., 1985), the resulting ds DNA is integrated into the human genome, which is described as the provirus. The highly conserved genomic organization comprises nine open reading frames (ORFs) (Figure 1) encoding for proteins that can be divided into (i) structural polyproteins Gag (group-specific antigen), Pol (polymerase) and Env (envelope), which are common among retroviruses, (ii) regulatory proteins Tat (transactivator of transcription) and Rev (regulator of virion), and (iii) accessory proteins Vif (virion infectivity factor), Vpr (viral protein R), Vpu (viral protein U) and Nef (negative factor). During viral replication, transcriptional regulation and multiple site splicing are required for the expression of viral proteins in chronological order.

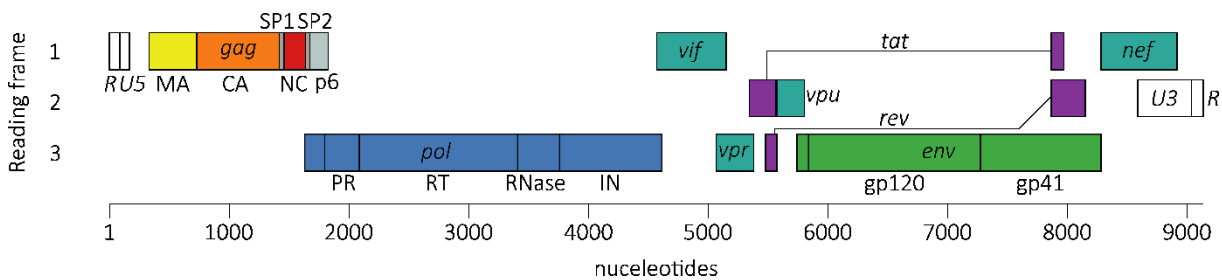


Figure 1: Organization of the HIV-1 genome. The coding regions for viral proteins are indicated in black-framed boxes. Junction sites in polyproteins are depicted as solid vertical lines. X-axis describes the position of encoded regions in the whole HIV-1 genome RNA string. The major genes are gag (group-specific antigen), pol (polymerase), and env (envelope). Gag is coding for MA (matrix, yellow), CA (capsid, orange), SP1 (spacer peptide 1, grey), NC (nucleocapsid, red), SP2 (spacer peptide 2, grey) and p6 (light gray), pol (blue) for PR (protease), RT (reverse transcriptase), RNase H and IN (integrase), and env (green) for subunits gp120 and gp41. Other regions provide genes for regulatory proteins (purple) Tat (transactivator of transcription) and Rev (regulator of virion), and accessory proteins (turquoise) Vif (virion infectivity factor), Vpr (viral protein R), Vpu (viral protein U) and Nef (negative factor). Adapted from Watts, et al., 2009.

The main structural polyprotein Gag (Figure 2) comprises matrix (MA), capsid (CA), and nucleocapsid (NC) domains (Wills, et al., 1991; Mervis, et al., 1988; Henderson, et al., 1990). In addition to these domains, which are conserved among all retroviruses, HIV-1 Gag contains two spacer peptides, SP1 and SP2, separating CA from NC and NC from a C-terminal phosphoprotein (p6), respectively. The globular shaped MA consists of 5 α -helices and is guiding Gag to the plasma membrane (PM) of host cells via an N-terminal myristoyl group (Tang, et al., 2004; Veronese, et al., 1988). MA has a surface exposed highly basic region (HBR), essential for regulated membrane association (Murray, et al., 2005), and a long C-terminal helix linking to CA. CA displays two independently folded regions - an N-terminal domain (CA-NTD) and a C-terminal domain (CA-CTD). The C-terminal domain contains two critical parts for HIV-1 assembly and

replication: the dimerization interface (Gamble, et al., 1997) and the major homology region (MHR), which is highly conserved among retroviruses (Patarca, et al., 1985; Wills, et al., 1991). The key player for the incorporation of two copies of vRNA in viral particles is the flexible protein NC. A globular domain of NC yields two zinc finger motifs (CCHC) displaying a hydrophobic pocket to bind to unpaired nucleotides. Basic residues of NC stabilize those interactions electrostatically with the charged nucleic acid (NA) backbone (De Guzman, et al., 1998; reviewed in Muriaux, et al., 2010). Additionally, NC also exhibits the function of a NA chaperone (reviewed in Levin, et al., 2005; reviewed in Rein, 2010).

A translational frameshift, occurring with a probability of ~5 %, at a so-called slippery site in the p6 sequence causes the expression of an extended version of Gag, namely GagProPol (Jacks, et al., 1988), carrying the essential viral enzymes PR, RT, and IN. A homodimer of the PR domain promotes the cleavage of Gag and GagProPol into their functional subdomains to initiate HIV-1 maturation (reviewed in Sundquist and Kräusslich, 2012). RT consists of two subunits, p51 and p66, which exhibit the reverse transcription of vRNA into the ds proviral DNA, and an RNase H activity cleaving RNA in RNA/DNA hybrids (Arnold, et al., 2008). The IN then inserts the double-stranded proviral DNA into the host cell genome (Li, et al., 2006; reviewed in Engelman, 2010).

Env consists of two glycoproteins of 120 kDa (gp120) and 41 kDa (gp41). While gp41 is incorporated into the plasma membrane, gp120 is presented on the membrane surface showing variable loops and extensive glycosylation to evade immune response (Mascola and Montefiori, 2003; Chen, et al., 2009). Both proteins form trimeric heterodimers (7 - 14 trimers per viral particle), which interact with cellular receptors for infection of new target cells (Chertova, et al., 2002; Zhu, et al., 2003; Center, et al., 2002).

The two regulatory proteins, Tat and Rev, play essential roles for transcription and transport of viral RNA during HIV-1 replication. Four accessory proteins, Vif, Vpr, Vpu, and Nef, counteract antiviral activity and bind to several host cell factors during infection and viral production ensuring viral pathogenesis (reviewed in Anderson and Hope, 2004; reviewed in Abraham, et al., 2012; reviewed in Sauter, et al., 2016; reviewed in Fabryova, et al., 2019).

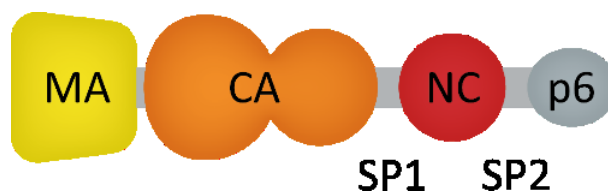


Figure 2: Schematic monomeric structures of Gag. Gag consists of six subunits, beginning with N-terminal MA (yellow), CA (orange), SP1 (grey), NC (red), SP2 (grey), and C-terminal p6 (dark grey).

4.2 HIV-1 replication cycle

The starting point of HIV-1 infection is the attachment of viral particles to the cell surface, which can occur via non-specific binding of various factors (reviewed in Wilen, et al., 2012). The essential part for infection is the binding of the gp120 subdomain of Env to CD4 on the cell surface of T cells or macrophages, enabling

interaction of Env with a cellular co-receptor molecule (β -chemokine receptor CCR5 or α -chemokine receptor CXCR4 (reviewed in Berger, 1997; McDougal, et al., 1986; Kwong, et al., 1998; reviewed in Capon, et al., 1991; Wu, et al., 1996). These binding events of Env lead to a dramatic structural shift within gp41, which inserts a hydrophobic fusion protein into the host cell plasma membrane, and a subsequent formation of a six-helix bundle at the terminal regions of gp41 (Lu, et al., 1997; Swanstrom, et al., 2012; reviewed in Sattentau, et al., 1988) causes a close proximity of viral and cellular membranes (Liu, et al., 2008), followed by membrane fusion (Chan, et al., 1997). The conical capsid core, which is composed of \sim 1100 - 1300 molecules of CA (Li, et al., 2000; Briggs, et al., 2003; reviewed in Mattei, et al., 2016) and encapsulates a complex of NC and vRNA (reviewed in Sundquist and Kräusslich, 2012), is then transferred through a fusion pore into the cytoplasm.

Although it is known that the viral capsid is crucial for the early phase of infection and that its disassembly is required for productive infection, the fate of the capsid and the dynamics of this so-called “uncoating” process in the early post-entry phase are highly discussed (Ambrose, et al., 2014; reviewed in Campbell and Hope, 2015; reviewed in Yamashita and Engelmann, 2017). In the cytoplasm, the reverse transcription of vRNA by the RT initiates within a poorly-defined subviral complex, termed reverse transcription complex/ pre-integration complex (RTC/PIC). While RTC defines the viral complex after fusion and initiation of reverse transcription, the PIC is formed upon the completion of the vDNA synthesis, which precedes the integration into the host genome (reviewed Campbell and Hope, 2015). Even though it remains elusive, when and where the reverse transcription is finished and PIC is generated, there is some indirect evidence showing that reverse transcription can still be partially proceeded in the host cell nucleus (Bejarano, et al., 2019). Although the exact composition of the RTC/PIC is not known, several viral proteins such as NC, RT, and IN, have been found in association with these subviral complexes. (Fassati, et al., 2001). The association of CA has been observed in multiple cell types, but the extension of this association is controversial. The RTC/PIC is actively transported along the microtubular network of the host cell to the nuclear pore complex (reviewed in Gaudin, et al., 2013; McDonald, et al., 2002), where several interactions with a multitude of nucleoporins takes place, enabling the active translocation of RTC/ PIC into the nucleus (reviewed in Di Nunzio, 2013; reviewed in Yamashita and Hope, 2017). The precise mechanism of nuclear entry is not fully clarified. Once inside the nucleus, the vDNA is integrated into the host genome in a process catalyzed by the IN.

The linear vDNA is integrated into host cell DNA preferably into active genes (Schröder, et al., 2002) by IN, which binds as a dimer at each of the two vDNA flanking repetitive sequences, called long terminal repeats (LTR), and forms the intasome (Krishnan, et al., 2010). Where vDNA gets integrated is mainly defined by the interaction of the PIC with host cellular proteins. It is hypothesized that CPSF6 targets the integration to specific genes and LEDGF to the position inside those genes (Sowd, et al., 2016). While the 5' LTR functions as a eukaryotic promoter, the 3' LTR terminates transcription via a polyadenylation site (Bushman, et al., 1990). The integrated vDNA (provirus) can stay latent for several years until transcription is activated (reviewed in Van Lint, et al., 2013; reviewed in Lusic and Siliciano, 2017). Early gene expression is initiated by the recruitment of transcription factors and results in a multi-spliced viral transcript enabling the production of the early proteins, Tat and Rev. Tat recruits cellular factors like the cyclin T1-CDK9 complex for hyperphosphorylation of the RNA polymerase II (Kao, et al., 1987; Feinberg, et al., 1991) and binds to the transactivating responsive sequence (TAR) (Feng, et al., 1988), which, in turn, facilitates the

transcription of full-length RNA constructs starting at the LTR promoter. Rev induces the transition from the early to late phase of gene expression during HIV-1 infection and binds to the Rev Response Element (RRE) (Malim, et al., 1989), enabling the transport of spliced and unspliced RNA from the nucleus into the cytoplasm, which encodes for structural and accessory proteins among others (reviewed in Hope, 1999).

In the late phase of the replication cycle, the structural proteins need to be synthesized and assembled at the plasma membrane for the formation of viral particles. Therefore, Env is initially derived as gp160 from a single-spliced RNA transcript and glycosylated in the Golgi apparatus (reviewed in Checkley, et al., 2011), where it is subsequently cleaved by cellular furin protease into gp120 and gp41 (Hallenberger, et al., 1992). Gag and GagProPol are translated on free ribosomes from unspliced RNA in the cytoplasm, and an N-terminal myristoyl group is covalently attached. This group is proposed to be packaged in the globular domain of MA, as Gag remains in the cytoplasm (Spearman, et al., 1997; Tang, et al., 2004). It is thought that upon binding of phosphatidylinositol 4,5-bisphosphate (PIP2), attached to the plasma membrane, to HBR exposes the myristoyl group for membrane targeting of Gag (Saad, et al., 2006), as it was proven that HBR interacts *in vitro* with PIP2 (Chukkapalli, et al., 2008; Dick, et al., 2012; Mercredi, et al., 2016).

Gag exists mono- or oligomeric in the cytoplasm (Kutluay and Bieniasz, 2010), where it binds via MA to cellular tRNA, as a mechanism to suppress the promiscuous binding of Gag to the PM (Alfadhli, et al., 2011; Kutluay, et al., 2014). The multimerization of Gag starts the assembly reaction in microdomains at the PM, recruiting numerous Gag molecules to form the budding site. At these assembly sites, MA, attached to the cell membrane, facilitates the incorporation of Env trimers into the PM at the assembly site (Dorfman, et al., 1994). ~ 2500 Gag molecules, together with ~ 125 GagProPol molecules, form a semispherical lattice necessary for viral budding, whose interactions in combination with the single-stranded vRNA enable membrane curvature (reviewed in Sundquist and Kräusslich, 2012; Briggs, et al., 2003). A ~ 200 bases long packaging signal sequence near to the 5' end abbreviated as “Ψ”, drives the specific incorporation of two copies of vRNA (Lever, et al., 1989) into newly forming particles by binding to NC in combination with the kissing loop hairpins (Skripkin, et al., 1994; Laughrea and Jetté, 1994).

Following assembly, the p6 domain of Gag promotes the recruitment of components of the cellular endosomal complex required for transport (ESCRT) machinery by two distinct so-called late-domain motifs within p6, facilitating the membrane scission and release of non-infectious, immature particles (reviewed in Meng, et al., 2013; Göttlinger, et al., 1991). Those viral particles undergo a process called maturation to transform into infectious and mature particles (Figure 3 C). Briefly, structural proteins Gag and GagProPol are cleaved by the viral PR, and structural rearrangement takes place. As this process is the main focus of this work, it is explained in detail in the following chapter 4.3.

4.3 HIV-1 particle maturation

4.3.1 Architecture of Gag and immature viral particles

As mostly researched by cryo-electron tomography (cryo-ET), retroviruses form enveloped particles, including a lipid bilayer membrane (reviewed in Coffin, 1992). Viral particles of HIV-1 have a spherical form

of 120 – 150 nm diameter, which is determined by the interaction of Gag subunits in hexamers lining on the inside of the viral membrane (Briggs, et al., 2003; Briggs, et al., 2006; Briggs, et al., 2009). While the peripheral parts of Gag are excluded from the organization of the highly ordered hexameric structure, CA forms cup-shaped hexamers as the central part of the lattice (Briggs, et al., 2009; Wright, et al., 2007). Around 70 % of the inner membrane is covered by this lattice (Carlson, et al., 2008), which is studded by irregular structures and small gaps that are caused by the impossibility to ensure a closed curved form built by Gag hexamers (Briggs, et al., 2009). Additionally, it is proposed that the Gag lattice shows a large gap (Figure 3 A), where membrane scission occurred during the budding step (Carlson, et al., 2010), which is, consequently, missing upon *in vitro* assembly (compare Figure 3 A and B). The interactions of the Gag molecules predefine the formation and the shape of spherical particles. Consequently, the expression of only Gag in cell culture leads to the formation of virus-like particles (VLPs) of the same immature morphology and diameter compared to HIV-1 particles (Gheysen, et al., 1989; Jacobs, et al., 1989; Karacostas, et al., 1989).

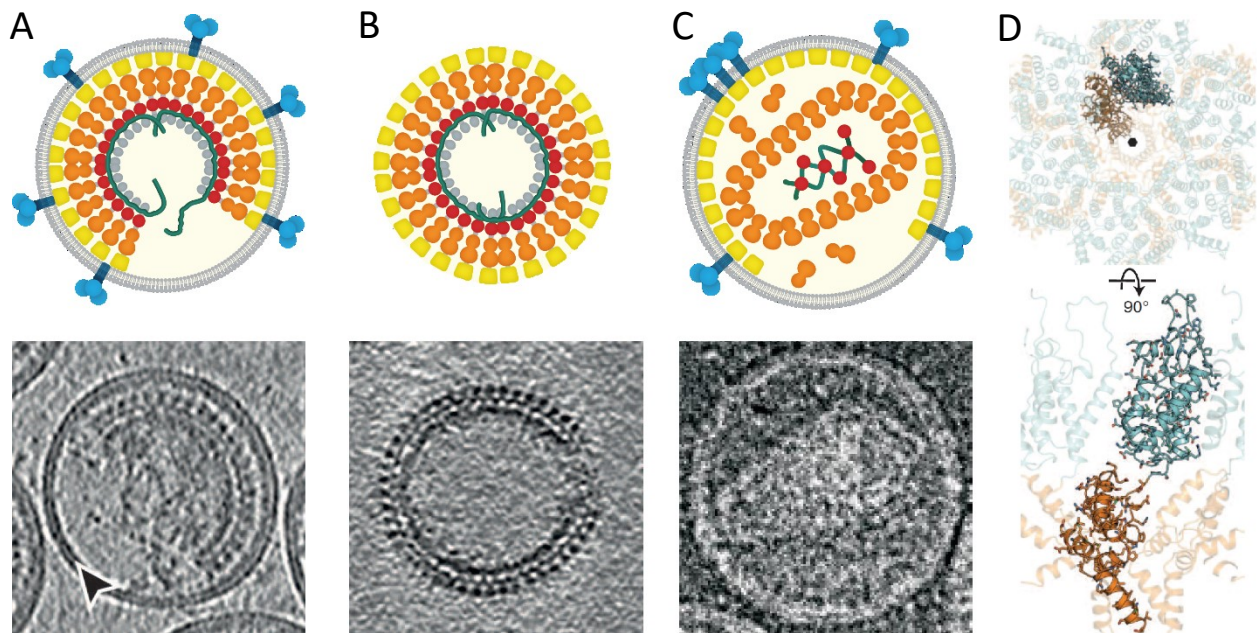


Figure 3: Schematic assembled Gag structures of immature and mature HIV-1 in comparison to tomograms made by cryo-EM. (A) In immature viral particles, the myristoylated N-terminus of MA is attached at the inner face of the membrane, where viral particles leave major gaps in their spherical lattice. (B) *In vitro* assembled particles build a fully closed spherical arrangement without membrane. (C) In the mature particle, MA is still attached to the membrane, while CA forms a conical core encapsidating a complex of NC and the HIV-1 RNA genome. Cryo-electron tomograms from (A, B) Schur, et al. (2016) and (C) Briggs, et al. (2004). (D) Refined atomic model of CA in an immature lattice from top view (top) and side view (bottom) based on cryo-electron tomograms with CA-NTD (turquoise) and CA-CTD (orange) including the C-terminal junction helix to SP1, which is part of the hexameric substructure in immature lattice (Schur, et al., 2016).

Gag proteins, as explained in chapter 4.2, are attached via MA to the plasma membrane and oriented with the following subunits to the particle center (Figure 3 A). While the NC-p6 subdomain was not yet seen to arrange in a specific order, MA can arrange as a hexamer of trimers *in vitro* (Alfadhli, et al., 2009). In

contrast, the leading key players for the immature structure of the Gag lattice are CA and SP1. CA is divided into its N-terminal domain (CA-NTD) and C-terminal domain (CA-CTD), which both contribute with a variety of interactions to the hexameric organization. While CA-NTD mold with a ring-like structure into the upper part of the cup-shaped hexamer, CA tapers towards the end of CA-CTD to fill the center of the hexamers with a dense rod-shaped structure in SP1 (Briggs, et al., 2009; Wright, et al., 2007).

On the one hand, CA-CTD organizes at the C-terminus as an α -helical structure (junction helix; Figure 3 D), which ranges to the first half of the downstream SP1 confirmed by X-ray crystallography (Wagner, et al., 2016), solid-state NMR (Bayro, et al., 2016), and with high resolution by cryo-electron tomography (Schur, et al., 2016). Cell culture and *in vitro* based results confirmed that this region is essential to form the α -helical structure of SP1 (Kräusslich, et al., 1995; Gross, et al., 2000; Accola, et al., 1998). In solution, SP1 is flexibly unstructured in an extended conformation and is structured during assembly by anisotropic attractions of other helical regions of the CA-SP1 junction (Accola, et al., 1998; Datta, et al., 2011). These helices build the core of the hexameric bundle (Schur, et al., 2015; Bharat, et al., 2014).

On the other hand, CA-NTD bridges the hexameric units along with two- and threefold symmetry axes with an 8 nm inter-hexamer spacing (de Marco, et al., 2010), even though observations conclude that CA-NTD is dispensable for the assembly of an immature lattice (Wang, et al., 1993).

In comparison to the assembled protein, Gag stays in solution in an equilibrium of mono- and homodimers, based on *in vitro* experiments of purified Gag. Consequently, a tendency to the formation of dimers is occurring in case Gag is present at higher concentrations. The leading causative site for this is a dimerization site inside CA-CTD consisting of a tryptophan residue and a methionine residue at position 184 and 185 in CA (Gamble, et al., 1997). The determined dissociation constant (K_d) for homodimers of Gag is 5.5 μ M (Datta, et al., 2007b), which covers the critical threshold of the cytoplasmic Gag concentration at the low μ M range for the Gag-membrane association (Fogarty, et al., 2014). After assembly, the concentration of Gag in the immature virion is at a millimolar concentration (reviewed in Briggs and Kräusslich, 2011). In contrast, upon introducing the WM mutation (W184A M185A), the dimerization site is disrupted, causing an increased K_d of 0.53 mM (Datta, et al., 2007b), with the result that Gag stays mainly in a monomeric mode even at higher concentrations.

4.3.2 Proteolysis and structural rearrangement during maturation

HIV-1 particles are released after assembly as immature particles by budding at the plasma membrane. Remaining in this state, the particles are not infectious until the maturation takes place (Figure 4). The starting point of maturation is a proteolytic process driven by the HIV-1 protease, where structural proteins Gag and GagProPol are cleaved into their subunits in a highly controlled sequential pattern (Erickson-Viitanen, et al., 1989; Pettit, et al., 1994; Pettit, et al., 2003). Processing is proposed to start concomitantly with virus particle formation or shortly after the virion release (Kräusslich, et al., 1991; reviewed in Sundquist and Kräusslich, 2012). The liberation of Gag subunits, in turn, initiates the morphological maturation leading to infectious particles (Figure 3 C; reviewed Ganser-Pornillos, et al., 2008; Pettit, et al., 1994; reviewed in Swanstrom and Wills, 1997; reviewed in Vogt, 1997). Both parts of

maturation are not happening separately but overlapping, and the proteolysis sets maturation in a temporal order to enable the correct sequence of the rearrangement of the final products. Even slight changes in proteolysis can lead to morphologically aberrant particles and a decrease in viral infectivity (Müller, et al., 2009; Wagner, et al., 2016; de Marco, et al., 2012; Pettit, et al., 1994; Datta, et al., 2011; Lee, et al., 2009) (Müller, et al., 2009; de Marco, et al., 2012; Pettit, et al., 1994; Datta, et al., 2011).

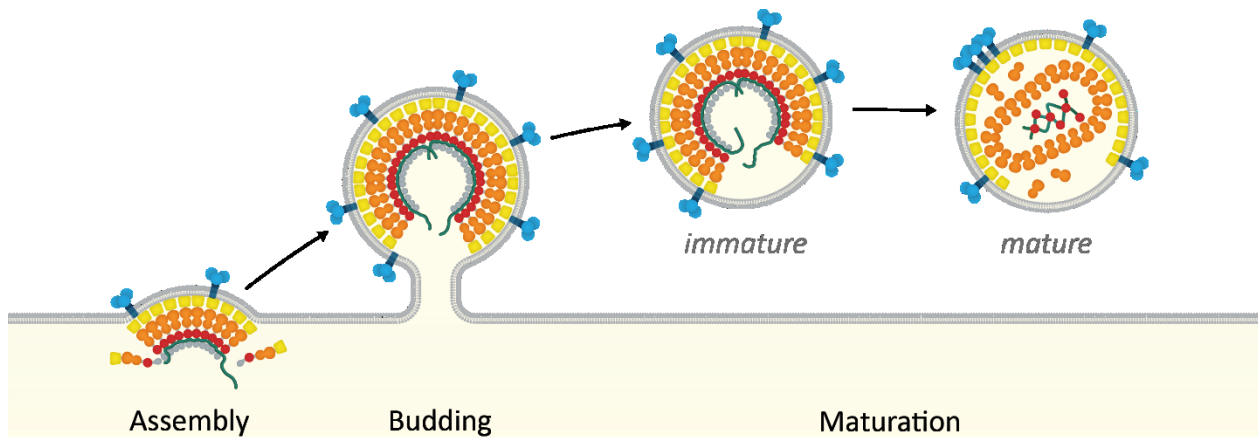


Figure 4: Schematic illustration of assembly, budding, and maturation of HIV-1 particles. Gag protein assembles at the plasma membrane, binding the genomic RNA to form a budding site. After release, the virion undergoes maturation to become infectious. After proteolysis, CA (orange) forms the conical core containing the complex of genomic RNA (green line) and NC (red). MA (yellow) remains at the plasma membrane, while envelope glycoproteins (Env, blue) form clusters on the surface of the particle.

During maturation, the structural proteins Gag (Figure 5 B) and GagProPol are proteolytic cleaved by PR at five and nine different cleavage sites (CS), respectively, which led to their classification into the processing rates: rapid (SP1-NC), intermediate (MA-CA; SP2-p6), and slow (CA-SP1; NC-SP2). In principle, the primary sequence at the CS (Figure 5 A) affects the catalytic efficiency of PR. Mutational analysis revealed that several amino acids up- and downstream of the scissile bond in the CSs are of importance (Figure 5), determine the binding, and cleavage properties of PR (Partin, et al., 1990; Partin, et al., 1991). While variable residues at the position 3 up- and downstream of the scissile bond are tolerated (Tözsér, et al., 1991; Pettit, et al., 1991), position 2 reveals majorly hydrophobic as well as small and position 1 large hydrophobic amino acids (Pettit, et al., 2002). Contrarily, several structural interactions and limitations prevent rapid processing at specific sites. As described in chapter 4.3.1, the helical structure at the CA-SP1 junction prevents direct access of PR to the amino acid chain, while the helix bundle is conserving the structure (Schur, et al., 2015; Mattei, et al., 2018). Additionally, Gag is tightly packed in an immature lattice, which should impair spatial access for PR, but which may facilitate fast processing due to proximity of one CS to another in the same layer (Mirambeau, et al., 2007).

After proteolytic cleavage, MA remains attached to the membrane, but displays an increased exchange of position in the membrane sheet, facilitating the clustering of Env trimers on the particle surface (Chojnacki, et al., 2017). Liberated NC stays with the RNA genome building a complex, dense structure (ribonucleoprotein particle = RNP), whereas the spacer peptides (SP1 and SP2) regulate proteolytic maturation and structural rearrangement (reviewed in Sundquist and Kräusslich, 2012). While it is

proposed that the C-terminal destabilization at the helix-bundle is the mainspring for structural maturation, cleavage at both ends of CA is crucial for the formation of the conical capsid core (Mattei, et al., 2018). After cleavage, free CA forms a conical core encapsulating the RNP. It is still unclear by which mechanism CA is transformed from its immature form to its mature, although high-resolution structures of both are known (Briggs, et al., 2009; reviewed in Mattei, et al., 2016; Mattei, et al., 2018).

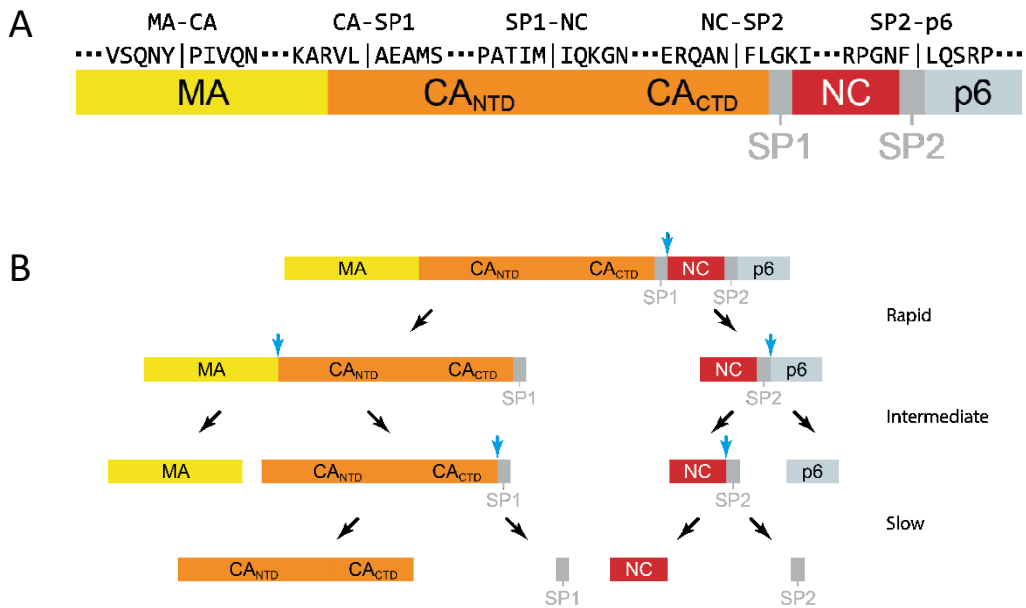


Figure 5: Gag sequences at protease cleavage sites and schematic depiction of sequential proteolysis of Gag during maturation. (A) The sequences of all cleavage sites are shown with their prequel and sequel amino acids. (B) The HIV-1 protease processes Gag at five distinct cleavage sites. The reactions are occurring with rapid speed at SP1-NC, intermediate at MA-CA and SP2-p6, and slow at CA-SP1 and NC-SP2 in viral particles. Blue arrows indicate the order of the cleavages, and black arrows show the resulting products of certain cleavage events.

Existing literature suggests a total disassembly-reassembly of CA or only a partial disassembly conserving a small sheet from the original lattice as a nucleation source for mature assembly (Keller, et al., 2013; Bharat, et al., 2012; Woodward, et al., 2015; Ning, et al., 2016). If *in vitro* assembled particles build mature or immature particles was shown to be only dependent on how the nucleation for assembly started (Wagner, et al., 2016). Other results indicated that CA-SP1 needs to disassemble before it can be processed, which is essential for the formation of mature cores (de Marco, et al., 2010).

Furthermore, based on a correlation between capsid length and membrane diameter and the observed appearance of multiple capsids in mature VLPs (Briggs, et al., 2003), models were predicted for conical capsid assembly starting from the narrow or broad end of the capsid. Upon almost full inhibition of processing at CA-SP1, the CA shell remains immature but less complete than immature Gag, suggesting for a disassembly mechanism of CA (Keller, et al., 2011).

Moreover, literature also refers to a fully displacive mechanism (Frank, et al., 2015; Meng, et al., 2012). *In vitro* CA-SP1-NC assembles into tubes, and upon processing by PR, the lattice is transformed into mature tubes of CA without disassembly (Meng, et al., 2012). Additionally, the inhibition of CA-SP1 can lead to spherical shells, which arrange displacive as mature-like lattices (Keller, et al., 2013), whereas large membrane-enclosed structures, derived by the supernatant of HIV-1 infected cells, contain multiple normal-sized capsid cores arguing for a rolling sheet mechanism for the transition into mature cores (Frank, et al., 2015).

However, both cleavage events at the terminal sites of CA were shown to be necessary to form proper mature cones. Due to cleavage by PR, the N-terminal end of CA is forming a β -hairpin structure, and the C-terminal helices are unfolded (Mattei, et al., 2018). It is proposed that cleavage at CA-SP1 represents the main switch between forming mature or immature assemblies (Datta, et al., 2011) and for morphological maturation of the immature lattice (Mattei, et al., 2018). Overall, CA is changing its orientation at both ends inside the hexameric layer forming new interactions with surrounding CA (Briggs, et al., 2009; Schur, et al., 2015). With the help of seven pentameric structures of CA at the broad end and five at the narrow end, the curvature of the conical capsid core is enabled (Ganser, et al., 1999).

Nevertheless, the critical step of maturation is tightly regulated, and yet poorly understood in terms of initiation, kinetics, and duration. Because particle formation and maturation occur asynchronously, elucidation of the pathway of structural changes in every detail is prevented. Thus, the impact of structural interactions in the immature lattice on the proteolytic maturation and the dependencies of the single cleavage events among themselves remain elusive.

4.3.2.1 HIV-1 protease and protease inhibitors

Homodimerization of PR in its precursor GagProPol leads to autoproteolysis in a specific order, resulting in a fully active enzyme (Pettit, et al., 1991; Pettit, et al., 1994; Pettit, et al., 2005; Tessmer, et al., 1998). The proteolytic part of maturation is only driven by the catalytic activity of the aspartyl-protease of HIV-1, where the active catalytic triad is made of three amino acid residues (Asp25-Thr26-Gly27; reviewed in Blundell, et al., 1998). While the dimerization is preferentially built *in vitro* in a high ionic environment (>1 M NaCl) by non-covalent interactions, lower salt concentrations shift the equilibrium partially towards the monomeric structure (Todd, et al., 1998). The activation of PR is thought to take place during the budding of particles, as premature activation of PR inhibits particle production (Kräusslich, et al., 1991). Since assembly is occurring asynchronously between different particles and cells, investigation of this process with biochemical approaches is limited. Until today it remains uncertain how and when the formation of the PR homodimer is induced.

In combination with other antiretroviral compounds, AIDS-related deaths could be decreased over the years. Meanwhile, the drugs used in antiretroviral therapy (ART) were optimized, one of whom is the protease inhibitor (PI). HIV-1 infected people depend on medical treatment for their lifetime. That is why PR inhibitors were not only designed for optimal biological availability but also to reduce the number of side effects as well as the actual necessary dose during treatment. The first clinically approved protease

inhibitors (PI) were saquinavir (SQV; reviewed in James, 1995) and indinavir (IDV; reviewed in Lacy, et al., 1996). Today, there are seven more compounds approved for ART: ritonavir (RTV), nelfinavir (NFV), amprenavir (APV), lopinavir (LPV), atazanavir (ATV), tipranavir (TPV), and darunavir (DRV).

PIs were mainly structurally designed to bind to the active site of PR, mimicking potential substrates. Based on this, most PIs were synthesized to have a peptide-like structure and a low biodegradability in the host. They bind competitively to the PR and thereby prevent the cleavage of Gag in total. Thus, HIV-1 releases immature particles, which are unable to undergo maturation and infect new cells (Patick and Potts, 1998). Due to the estimated error rate of RT about 3×10^{-5} per base during the replication of the HIV-1 genome, a fast adaptation to critical and suboptimal environments for viral replication is ensured (reviewed in Rambaut, et al., 2004). Consequently, HIV-1 compensates the PI treatment with mutations, to rescue viral replication and infectivity. Primary mutations of PR decrease the binding capability of PIs by a structural adaptation of the active site (Gulnik, et al., 1995; reviewed in Wensing, et al., 2010). Secondary and tertiary mutations, which can occur over time, enhance the effect of primary mutation or instead enhance the catalytic activity (Nijhuis, et al., 1999; Callebaut, et al., 2011; van Maarseveen, et al., 2007). As a result, a smaller amount of PR not bound to PIs compensate for the lost activity of PR bound to PI and, because PIs have structural similarities, mutations of PR may also affect resistance to other PIs. Given this fact, it is a compelling necessity to develop new drugs addressing as well as other mechanisms of PR inhibition.

4.3.3 *In vitro* systems for HIV-1 assembly and proteolytic maturation

The knowledge up to now about the assembly and maturation of retroviruses has been mainly obtained by *in vitro* experiments with Gag derivatives. Using *in vitro* applications to examine the assembly and structure of HIV-1 has certain advantages to the analysis of intact viruses and should be applied to scientific research as long as they can mimic naïve systems accurately. Firstly, viral particles and their compartments yield full functionality only for a restricted time after budding and are easily damaged during purification. *In vitro* experiments utilizing artificial particles or other proteins are additionally uncoupled from viral processes and other viral proteins. By that, specific parts of the viral life cycle can be analyzed in a distinct pattern giving a more detailed insight, which may also be a disadvantage as the coupled dependency of individual processes is lost. However, the main benefits of these experiments are easy scalability, reproducibility, and low amount of impurities or other confounding factors.

It was previously shown that Gag and a truncated version, missing the globular domain of MA from residue 16 – 99 and the C-terminal p6 domain, called Δ MACANCSP2 (Figure 6), are capable of assembling *in vitro* in the presence of NA into spherical particles (Gross, et al., 2000). These particles can be easily detected negatively stained as characteristic electron-dense ring structures in transmission electron microscopy (TEM). In contrast to the larger particles released from Gag expressing cells (100 – 150 nm), full-length Gag only forms small particles (10 – 30 nm) *in vitro* (Campbell, et al., 2001; Datta, et al., 2007a; McKinstry, et al., 2014). Unfortunately, there is yet no efficient protocol for the *in vitro* assembly of recombinant full-length Gag into correctly sized particles.

In most publications, NA is implemented in the *in vitro* generation of VLPs. As presented before in chapter 4.1.1, NC binds preferentially to Ψ sequences in vRNA, to incorporate it into viral particles, whereas NC was revealed to bind to any single-stranded NA (Campbell, et al., 2001; Campbell and Rein, 1999), supporting assembly by binding on average five bases of the NA strand (Fisher, et al., 1998; Stephen, et al., 2007). Even though the binding of NC is independent of the NA sequence and length, it only leads to proper assembly with a minimum length of 12 - 30 bases (Chen, et al., 2017; Campbell and Rein, 1999; reviewed in Rein, et al., 2011). If this is the only source of nucleation is questionable since it is possible to assemble Gag Δ MACASP1NC *in vitro* based on protein-protein interaction induced by tartrate instead of NA (Wagner, et al., 2016). Consequently, this argues for a sole dependency on protein-protein interaction of the nucleation for *in vitro* assembled Gag. It is congenial proposed that the molecular switch of CA-SP1 structured into the hexameric lattice is the central constituent driving assembly (Datta, et al., 2011; Pak, et al., 2017), while binding of MA to membrane and NC to RNA acts as critical scaffolding parameters (Pak, et al., 2017; Yang, et al., 2018).

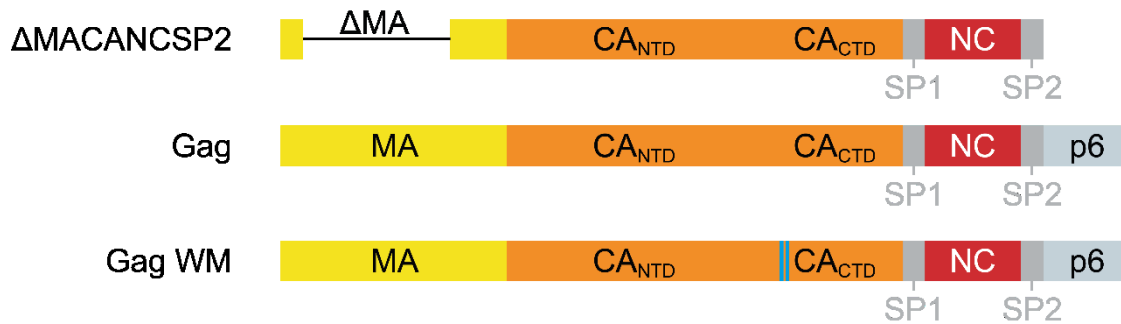


Figure 6: HIV-1 Gag derivatives and *in vitro* assembly systems. Predominantly used Gag derivatives for *in vitro* assembly and biochemical analyses comprise full-length Gag with and without WM mutation to disrupt the dimerization site. To enable a highly reproducible assembly, Δ MACANCS P2 is commonly applied, which is missing the p6 domain and a major part of MA.

Closely above the hexameric helix bundle formed by CA-CTD and SP1, two positively charged rings, each composed of six lysines, are complexing the highly negatively charged cellular substance inositol hexakisphosphate (IP6; Dick, et al., 2018). Upon the addition of IP6, the efficiency and stability of Gag assembly *in vitro* are severely enhanced (Dick, et al., 2018). IP6 is abundant in mammalian cells ranging in the concentration of 10 – 40 μ M (Letcher, et al., 2008) and by this enabling an easy access of assembly sites to bind IP6. Potently, it is facilitating the formation and stability of the CA-SP1 junction helix in the immature lattice (Dick, et al., 2018). Due to the proteolytic maturation, IP6 bound near to this area is released and bound again by CA in the mature form, this time in a hexa-arginine ring at the N-terminal region near the newly formed β -hairpin (Dick, et al., 2018).

In the solution of Gag present in a mono-/dimeric equilibrium, IP6 is bound by Gag and causes a mono- and trimeric equilibrium, which is speculated to mimic a precursor for Gag assembly (Datta, et al., 2007b). Depending on the ionic strength in solution different ratios of Gag: IP6 may arise, but the K_d of a single bound molecule to Gag is 18 μ M (Datta, et al., 2007b).

Even though the *in vitro* assembly of Δ MACANCSP2 is well established, the standard classification of CSs into its processing speeds is derived from experiments on *in vitro* translated Gag protein mixed with recombinant PR (Erickson-Viitanen, et al., 1989; Pettit, et al., 1994). According to the results, the eventual cleavage at CA-SP1 and NC-SP2 are 400- and 350-fold slower, respectively, compared to the initial cleavage at SP1-NC (Pettit, et al., 1994). The processing at these sites is dependent on a couple of factors, and, while this processing is similar to processing results of actual viral particles, the processing of synthetic CS peptides shows different processing dynamics (Tözsér, et al., 1991; Darke, et al., 1988; Mascher, et al., 1996). There, mainly CA-SP1 is processed more rapidly, which indicates a high impact of secondary, tertiary, and quaternary structure upon the maturation. While CA-SP1 shows a presumably hindering structure for processing in an immature form, other observations showed that the connection of the solely N-terminal part of Gag from SP1-p6 is arranging a quinary interaction additionally and by that inducing the processing of CSs implemented (Lyonnais, et al., 2019).

Nevertheless, the processing based on *in vitro* translated Gag excludes a variety of factors, which are essential to reconstruct the proteolytic maturation in viral particles. Thus, there was no clear evidence for the oligomerization state of Gag nor the presence and quality of assembled particles. Since RNA is applied for the translation, it seems likely that at minimum, some preliminary assembly structures are built, which could lead to a heterogenic mixture of non-assembled and assembled Gag. The direct impact of the type and length of NA on the proteolytic maturation is yet only marginally examined, and, until now, there was no quantitative research been done to elucidate the kinetic impact of structural arrangement and substructures of immature Gag upon proteolytic maturation of all CSs under defined parameters.

4.4 Maturation altering conditions

Because the sequential processing during maturation is tightly controlled, even small interferences, e. g. blocking particular CSs cause a dramatic loss of infectivity and lead to morphologic dysfunctional particles. Hindering or altering the processing of Gag can be targeted at different levels in HIV-1. The crucial part for maturation is the activity of the PR, which needs to be activated at the right time during or after assembly and acts, as mentioned before in chapter 4.3.2.1, catalytically for the maturation. In order to prevent viral particles from maturation, there are several protease inhibitors (PIs), which are capable of binding to the PR and prevent any catalytical activity. Additionally, a mutation in the catalytic center of the PR completely also eliminates activity. In comparison, other mutations in Gag can inhibit the cleavage at specific sites by the PR, while others have an in- or decreasing effect on the processing rates. Another group of compounds, called maturation inhibitors, bind to some areas of Gag, reducing the spatial access for the PR or inducing high stability of immature structures. Virus intrinsic factors also influence the processing speed by providing spatial proximity or quickening cofactors to the HIV-1 PR.

4.4.1 pH dependency of proteolytic activity

The effect of pH upon the dynamics of the proteolytic maturation can be divided into two branches. First, the HIV-1 PR, as mentioned before in chapter 4.3.2.1, is highly sensitive to the pH regarding its activity and self-cleavage. A plethora of analyses revealed a high catalytic activity of PR in a pH range of 5 – 6, although a notable activity can be measured between 4.0 and 7.5 (Tamburini, et al., 1990; Kräusslich, et al., 1989; Szeltner, et al., 1996; Cheng, et al., 1990; Ido, et al., 1991). On the contrary, the pH of the human cytoplasm is around 7.0 – 7.2, and blood plasma is highly regulated around 7.32 – 7.42 (reviewed in Diem, et al., 1970). If HIV-1 yields a mechanism for the lowering of pH and if the pH plays a crucial role in the initiation and duration of maturation is not yet understood.

In order to measure the pH optimum for PR activity, most studies used synthetic peptides comprising a CS of Gag or GagProPol, excluding the impact of structural parts of Gag on the pH-dependent maturation. Δ MACANCSP2, the most commonly used protein for *in vitro* assembly, and CA-SP1-NC assemble at higher pH from 7.0 to 8.0 into thick-walled immature particles, which complies with the cytoplasmic pH. At a lower pH of 6.0, they arrange as mature-like tubes, cones, and spheres (Gross, et al., 2000; Briggs, et al., 2009; Dick, et al., 2018). Interestingly, the pH for *in vitro* assembly of mature CA and high activity of PR coincide (pH ~6.0), and digestion by the recombinant protease of *in vitro* translated Gag (Pettit, et al., 1994), *in vitro* assembled particles, and VLPs (Ning, et al., 2016) showed that in particular the CA-SP1 CS is effected most by a pH change. Lowering the pH from 7.0 to 5.0 increased the processing rate 20-fold (Pettit, et al., 1994), while most CA-SP1 remained unprocessed at a pH of 7.5 (Ning, et al., 2016). However, it was proposed that the processing acceleration at CA-SP1 is caused at lower pH by a sequence-based mechanism instead of a conformational or spatial effect (Pettit, et al., 1994). In contrast, MA-CA and SP1-NC are not majorly affected by lower pH, and SP2-p6 is processed around threefold faster at pH of 5.0 instead of 7.0 (Pettit, et al., 1994). Even though the altering effect of pH on maturation is shown, it remains unknown, at which pH proteolytic maturation in viral particles takes place and what exactly is changed for sequential release of individual Gag subunits.

4.4.2 Regulation of maturation by nucleic acid

NC contains two zinc finger motifs and is binding during assembly to the HIV-1 RNA genome copies. Upon the first cleavage at SP1-NC, released NC-SP2-p6 starts forming intermediate complex structures with the RNA (Lyonnais, et al., 2019). This complex detaches from the outer ring of MA-CA-SP1, and the second cleavage occurs at SP2-p6. It has been shown that the presence of single-stranded NA enhances the processing of NC intermediates *in vitro* (Mirambeau, et al., 2007; Sheng, et al., 1997; Deshmukh, et al., 2015; Potempa, et al., 2015). One reason for this is that PR can bind productively to RNA and, by this enhances its activity independently of the RNA sequence or substrate. Another reason is that NC-SP2-p6, NC-SP2, and NC are providing different binding capacities for RNA and spacial proximities of several CSs (Lyonnais, et al., 2019; reviewed in Mirambeau, et al., 2010). In viral particles, PR gets sequestered during maturation in the ribonucleoprotein complex precursors. There, spatially concentrated CSs and the presence of RNA lead to an intricate partnership, which drives PR to complete maturation and the final

NC/RNA condensation within minutes (Lyonnais, et al., 2019). *In vitro* assembly of SP1-NC-SP2-p6 revealed a quinary network of RNA and NC (Lyonnais, et al., 2019). While there are no clear preferences shown, if the processing enhancement is stronger for DNA or RNA, a clear relationship between the length of NA and the maturation speed had been determined. Starting at length of 10 – 20 nucleotides, processing of all implemented CSs in *in vitro* assembled SP1-NC-SP2-p6 had been boosted the longer the NA string was (Lyonnais, et al., 2019). If the processing of assembled Gag reveals the same correlation of NA length and processing acceleration remains unclear. Additionally, the complete interplay of present NA and processing dynamics is not fully understood. As described before (4.3.3), Δ MACASP1NC is capable of assembling *in vitro* in the absence of NA, which could easily give insight about relevant changes in the proteolytic maturation upon binding to NA.

4.4.3 Dynamical impact of cleavage site mutations

Blocking of protease cleavage sites affects functional mechanisms in viral maturation, sequential processing, and impairs the infectivity of the viral particles. For all five CSs in Gag, mutations are described, which inhibit the processing at the corresponding site in the case of viral particles or synthetic peptides. In general, these are point mutations exclusively at the last amino acid of the upstream sequence.

MA-CA is inhibited by the mutation Y132I (Wyma, et al., 2004) and is most sensitive to incomplete processing in terms of viral infectivity than any other CS (Lee, et al., 2012). Already 4 % of this mutation in Gag molecules leads to a 50 % loss of infectivity (Lee, et al., 2009). While subsequent CSs are processed, MA-CA stays at the plasma membrane preventing Env clustering and the formation of the conical core (Mattei, et al., 2018), even though the cleavage of MA-CA per se is not prerequisite for cleavage at CA-SP1 (Müller, et al., 2009). Almost 75 % of the viral particles carrying this mutation are still forming a condensed ribonucleoprotein complex (Mattei, et al., 2018).

In contrast to the other CSs, CA-SP1 needs theoretically two mutations to prevent processing by HIV-1 PR. The CS is carrying a second aberrant CS four amino acids downstream (Wieggers, et al., 1998). Consequently, L363I inhibits cleavage at the actual CS and M367I at the aberrant. CA-SP1 is part of the discussion in many publications in the last years. As it is shown to be one of the switches for morphological maturation of the immature lattice (Mattei, et al., 2018), mutations at this site lead to vanished infectivity, too (Müller, et al., 2009). Here again, the blocking of this CS does not prevent the formation of the ribonucleoprotein complex, and the majority of viral particles were shown to have similar morphologies like mature particles but no correct capsid core (Mattei, et al., 2018; Wieggers, et al., 1998). Unlike MA-CA, the inhibition of CA-SP1 does not conserve the immature structure at the plasma membrane. However, even the marginal presence of uncleaved CA-SP1 inflicts a high reduction upon viral infectivity (Checkley, et al., 2010). With the mutation M377V, SP1-NC is protected from being cleaved from the PR and viral particles form irregular ribonucleoprotein complexes (Wieggers, et al., 1998). In parallel, the processing rate at CA-SP1 is increased 20-fold upon SP1-NC blocking or complete SP1 deletion in the case of *in vitro* translated Gag (Pettit, et al., 1994). In viral particles, especially the intermediate of maturation, CA-SP1-NC, is accumulating (Wieggers, et al., 1998). The two C-terminal cleavage sites, NC-SP2 and SP2-p6, are inhibited with the mutations N432I and M448I, respectively (Wyma, et al., 2004). Using N432I in viral

particles solely had only a minor effect on infectivity and formation of mature particles equivalent to the deletion of the entire SP2 region in Gag. Blocking SP2-p6 has a reducing effect on infectivity and the amount of correctly formed viral cores. Combining both mutations is severely enforcing the effects of M448I (Müller, et al., 2009; de Marco, et al., 2012; Coren, et al., 2007). Even though there are numerous observations for the impact of CS inhibitions regarding the viral morphology and infectivity, it is still elusive, how single cleavage events are dependent on each other.

Besides the known mutants for inhibition of CSs in Gag, other Gag mutations have an effect on the processing speed of Gag at individual sites. Based on *in vitro* translated Gag cleavage, between 12 and 17 mutations in all 5 CSs were analyzed for their effect on the cleavage at the relevant site. While for MA-CA, CA-SP1, and NC-SP2, at least one or more mutations could enhance the processing rate up to 60 fold, no mutation is known to maximize the processing rate at SP1-NC and SP2-p6 (Pettit, et al., 2002). If the accelerating effect is of kinetic nature or just a destabilizing factor like most mutations in CA-SP1 for immature Gag (Wagner, et al., 2016), is not investigated yet. N432L at NC-SP2 and F448M at SP2-p6 are known for boosting and reducing the cleavage rate at the specific site, respectively (Pettit, et al., 2002). Because the quantitative kinetic effect of CS inhibitions is unclear, the question also arises, which effect acceleration of processing at a particular CS and, beyond this, what the directed altered sequential processing bears.

As mentioned before (0), HIV-1 comprises a high mutation rate during the replication due to a lack of a proofreading capability of the RT. Consequently, mutations provide a fast adaptation to critical and suboptimal environments for viral replication (reviewed in Rambaut, et al., 2004), and HIV-1 compensates the PI treatment of infected patients, to rescue viral replication and infectivity. Resulting mutations are mainly found in PR (4.3.2.1) frequently combined with mutations in Gag (reviewed in Shafer, et al., 2008). For this, the C-terminal region of Gag is mostly carrying the adaptation, mainly showing the mutations A431V or I437V in NC-SP2. MA, CA, and SP1 do not seem to contribute a lot in mutational changes (Dam, et al., 2009; Malet, et al., 2007). These two mutations are often found in correlation with mutations in PR like L76V (Lambert-Niclot, et al., 2008), enabling an increased Gag processing in the presence of PIs (Nijhuis, et al., 2007) and correcting a loss of replicative capacity due to PI treatment (Dam, et al., 2009). Summarizing, substitutions in NC-SP2 or SP2-p6 can contribute to the adaption of HIV-1 to become PI resistant, showing an alternative way besides solely PR mutations. However, it is not yet clarified if these mutations enable a better binding affinity of the CS to PR in the presence of PI or if they compensate by increased processing rates the lost PR activity due to primary mutations.

4.4.4 Maturation inhibitors

As described before (4.3.2), CA is an essential key player for the HIV-1 life cycle. The main structural component for immature assembly undergoes a structural rearrangement after release from the lattice by PR and forms the capsid core. Recently, a particular class of compounds, the maturation inhibitor (MI), for the potential implementation into the cART was developed. Unlike PI or assembly inhibitors, MIs do not bind to the HIV-1 PR or prevent Gag assembly. MIs interact with Gag in the immature state and thereby prevent maturation from proceeding. The first MI, bevirimat (BVM), is binding to the CA-SP1 region of

immature assembled Gag. In the last years, cryo-ET based analysis of BVM bound to Gag showed that it stabilizes the hexameric region of CA-SP1, preventing unfolding and the following proteolysis (reviewed in Pornillos, et al., 2019; Schur, et al., 2016; Purdy, et al., 2018). This stabilization is even conserved after NC and MA are cleaved off, leading to an accumulation of sole CA-SP1 protein during the processing of in *in vitro* assembled Δ MACANCSP2 or VLPs by PR (Li, et al., 2003; Zhou, et al., 2004). Even though BVM shows high inhibition potential in *in vitro* based experiments, it failed to impair the viral load in a patient group of a phase II clinical trial as a polymorphism in the SP1 sequence enables a fast resistance to BVM (Adamson, et al., 2010).

The binding of BVM and the consequent protection of CA-SP1 seem to be pH-dependent since the effect is stronger at a higher pH of 7.4 than at a lower pH of 6.0, where it had only a slight effect (Ning, et al., 2016). Up to this point, there is still no quantitative analysis of the maturation in the presence of BVM regarding a high time-resolution to interpret the data on a kinetic level.

4.5 Aim of this work

This project focuses on the elucidation of sequential processing of Gag and its underlying conditions derived from inter- and intramolecular interactions. Therefore, the impact of pH and subdomains binding to secondary compounds on the processing of mono-/dimeric or assembled Gag was examined. Additionally, the effect on all cleavage sites caused by specific mutations, inhibiting, or altering cleavage at certain sites, are analyzed.

2014, the first protocols for purification of full-length Gag were published. As the processing analysis of Gag had been done so far with truncated versions or purified VLPs, this work aims to establish a reproducible protocol for purification of full-length Gag. Furthermore, the purification is developed to deliver complete NA-free protein samples to prevent preliminary aggregation or assembly. With this achievement, Gag and truncated versions are used for the generation of a highly efficient assembly providing high stability of *in vitro* assembled Gag for further experiments. The processing of both, non-assembled and assembled Gag, is then dynamically analyzed in a time-resolution.

The length of NA used for assembly has an influence on the assembly of Gag at certain levels. Therefore, the processing of non-assembled and assembled protein is performed with different NA types and lengths. So far, the dependency of the cleavage at specific sites on other cleavage sites is not yet completely revealed. Because of this, we used inhibiting mutations in certain cleavage sites to address this question. Additionally, mutations with an altering effect on the processing and mutations derived from protease inhibitor-resistant strains of HIV-1 were tested. Furthermore, the exact pH during and at the initiation of maturation is not clear yet. For a better understanding, Gag in a non-assembled and assembled state is processed and analyzed at different pH-values. Finally, the effect of the maturation inhibitor bevirimat, which binds and stabilizes the hexa-helix bundle of assembled Gag at CA-SP1, is also targeted. With this, we provide insight into a variety of open questions regarding the conditions, dynamics, and duration of maturation.

5 Materials and methods

5.1 Materials

5.1.1 Laboratory equipment

Table 1: Laboratory equipment used for experiments or preparation and the respective manufacturer.

Name	Company
Agarose gel electrophoresis system	Bio-Rad, Hercules, CA, USA
Air-Cooled Vertical Electrophoresis Systems SE 400 Series Sturdier	Hoefer, Inc., Holliston, USA
Bacterial Shaker Multitron Pro	Infors HT, Bottmingen, Switzerland
Capto Core 700, 1 mL	General Electric, Boston, USA
Centrifuge 5417C	Eppendorf AG, Hamburg, Germany
Centrifuge Avanti J-26 XP with JA-10 rotor	Beckman Coulter, Brea, USA
Electrophoresis power supply EPS 601	Amersham Biosciences, Little Chalfont, UK
Fine scale Entris	Sartorius, Göttingen, Germany
FPLC	Äkta Purifier, GE Healthcare, Uppsala, Sweden
Gel iX Imager (Agarose gel UV-imager)	INTAS Science Imaging, Göttingen , Germany
Gel filtration column Superdex 200 16/60 PG	General Electric, Boston, USA
Gel filtration column Superdex 75 30/100 GL	General Electric, Boston, USA
Glow discharger ACE I	GaLa Instrumente GmbH, Bad Schwalbach, Germany
Gyratory shaker Duomax 1030	Heidolph Instruments, Schwabach, Germany
Heraeus Megafuge 40R Centrifuge	Thermo Scientific, Waltham, USA
High Vacuum Sputter Coater EM ACE600	Leica Camera, Wetzlar, Germany
HiTrap FF,1 ml and 5 ml	General Electric, Boston, USA
HiTrap Heparin HP affinity columns 5 mL	General Electric, Boston, USA
HiTrap NHS activated HP 1 mL	General Electric, Boston, USA
HiTrap Q FF 5 mL	General Electric, Boston, USA
HiTrap Q FF 5 mL	General Electric, Boston, USA
Ice Maker AF 103	Scotsman, Sprockhövel
Incubator B12	Heraeus, Hanau, Germany
Incubator C200	Labotect Labor-Technik-Göttingen, Rosdorf

JEM1400	JEOL Ltd., Akishima, Japan
L8-70M Ultracentrifuge with SW28, SW32 and SW60 TI rotor	Beckman Coulter, Brea, USA
LiCor Odyssey Imager CLx	LiCor Bioscience, Lincoln, USA
Magnetic stirrer MR 3001	Heidolph Instruments, Schwabach, Germany
MBP Trap HP 5 mL	General Electric, Boston, USA
Micro fluidizer LM10	Microfluidics Corporation, Newton, USA
Microbiological Cabinet	Envair, Emmendingen
Microscope DM IL LED	Leica Camera, Wetzlar, Germany
Microwave for Agarose gels	Sharp, Cologne
NanoPhotometer	Implen, Munich
NanoSight NS300	Malvern Panalytical, Kassel, Germany
PCR FlexCycler2	Analytik Jena, Jena
pH Meter Benchtop FiveEasy	Mettler Toledo, Gießen, Germany
PipetBoy	INTEGRA Biosciences AG, Zizers, Switzerland
Plate Reader Infinite M200 Pro	Tecan, Männedorf, Switzerland
Refractometer	Schmidt + Haensch GmbH & Co., Berlin, Germany
SDS-PAGE electrophoresis chamber Mighty small	Hoefer, Inc., Holliston, USA
Semi-Dry Blotter Fastblot B32	Whatman Biometra, Göttingen
Sonifier	Branson Ultrashall, Dietzenbach, Germany
Spectrofluorometer FP-8500	Jasco, Pfungstadt
Thermomixer, Eppendorf, Thermomixer® comfort	Eppendorf, Hamburg
TLC syringe 702, 25 µL, 22s	Hamilton Company, Reno, Nevada
Transmission electron microscope EM10	Zeiss, Oberkochen, Germany
Vacuum pump 2522Z-02	Welch, Mt. Prospect, USA
Vortex Genie 2	Scientific Industries, Bohemia, USA
Warming Cabinet	Memmert, Schwabach
Water Filtering System	Stakpure, Niederahr
Waterbath MP	Julabo, Seelbach
XS40025 Deltarange Weight Scale	Mettler Toledo, Gießen, Germany

5.1.2 Kits

Table 2: Commercial kits used for DNA purification, including their origin.

NucleoBond MaxiPrep Kit	Macherey-Nagel, Düren, Germany
NucleoSpin Gel and PCR Clean-up	Macherey-Nagel, Düren, Germany

5.1.3 Chemicals and consumables

Table 3: List of chemicals used in experiments for this work, including their origin.

Chemical	Company
(NH ₄) ₂ SO ₄	VWR, Radnor, USA
2-(N-morpholino)ethanesulfonic acid (MES)	Carl Roth, Karlsruhe, Germany
4-(2-hydroxyethyl)-1-piperazineethanesulfonic acid (HEPES)	Carl Roth, Karlsruhe, Germany
96 Well Plates	Greiner Bio-One GmbH, Frickenhausen, Germany
Acrylamide (AA) 30 %	AppliChem, GmbH, Darmstadt, Germany
Acrylamide 4K - solution (30 %) - Mix 29 : 1	AppliChem, GmbH, Darmstadt, Germany
Acrylamide 4K 30% 29:1	AppliChem GmbH, Darmstadt, Germany
Acrylamide 4K Ultrapure	AppliChem GmbH, Darmstadt, Germany
Agarose NEE0	Carl Roth, Karlsruhe, Germany
Amicon Ultra-15 10k MWCO centrifugal filters	Merck, Darmstadt, Germany
Ammonium persulfate (APS)	Sigma Aldrich, St. Louis, USA
Ampicillin	Carl Roth, Karlsruhe, Germany
Bisacrylamid (BAA) 4K Ultrapure	AppliChem GmbH, Darmstadt, Germany
Blotting paper	3 MM Chr, Whatman, Dassel, Germany
Bromophenol blue	Chroma, Fürstfeldbruck, Germany
BSA 100x	NEB, Ipswich, USA
CaCl ₂	Sigma-Aldrich, St. Louis, USA
Cellulose phosphate	Polyscience, Warrington, USA
cOmplete, EDTA-free Protease Inhibitor Cocktail	Hoffmann-La Roche, Basel, Switzerland
Coomassie brilliant blue G-250	Biomol Feinchemikalien, Hamburg, Germany
Dialysis tubing Spectrapor 4	Carl Roth, Karlsruhe, Germany

Dithiothreitol (DTT)	Carl Roth, Karlsruhe, Germany
DMSO	Merck, Darmstadt, Germany
DNA ladder 1 kb Plus	Thermo Scientific, Waltham, USA
dNTP Set	Thermo Scientific, Waltham, USA
Dulbecco's Modified Eagle Medium (DMEM)	Invitrogen, Karlsruhe, Germany
Ethanol (99 %) (EtOH), denatured	Zentralbereich INF, Heidelberg, Germany
Ethylenediaminetetraacetic acid (EDTA)	Carl Roth, Karlsruhe, Germany
Fetal Calf Serum (FCS)	Biochrom, Berlin, Germany
Gel Filtration Cal Kit Low Molecular Weight	General Electric, Boston, USA
Gel Loading Dye, Purple (6x) for DNA	New England Biolabs, Ipswich, USA
Glycerol	Honeywell, Bucharest, Romania
Glycine	Labochem international, Heidelberg, Germany
HIV Protease Substrate 1	Sigma-Aldrich, Steinheim, Germany
Imidazole	Sigma-Aldrich, Steinheim, Germany
Isopropanol	Zentralbereich INF, Heidelberg, Germany
K ₂ HPO ₄	Grüssing, Filsum, Germany
Kanamycin	Carl Roth, Karlsruhe, Germany
KCl	Thermo Fisher Scientific, Hampton, USA
KH ₂ PO ₄	Grüssing, Filsum, Germany
LI-COR Blocking Buffer (TBS)	LI-COR Bioscience, Lincoln, USA
Methanol (MeOH)	Sigma-Aldrich, St. Louis, USA
MgCl ₂	Grüssing, Filsum, Germany
NativePAGE cathode buffer	AppliChem, GmbH, Darmstadt, Germany
NativePAGE Novex Bis-Tris gels	Invitrogen, Carlsbad, CA, USA
Nitrocellulose membrane	Protran, Schleicher & Schull/Whatman, Dassel, Germany
OptiPrep	Abbott Diagnostics Technologies AS, Oslo, Norway
PageRuler prestained	Thermo Scientific, Waltham, USA
Penicillin Streptomycin (PenStrep)	Thermo Scientific, Waltham, USA
Phytic acid sodium salt hydrate (IP6)	Sigma-Aldrich, St. Louis, USA
Pierce 660nm Protein Assay Reagent	Thermo Fisher Scientific, Hampton, USA

Polyethylenimine (PEI)	Sigma-Aldrich, St. Louis, USA
Reaction tubes (0.5-2ml)	Sarstedt, Nümbrecht, Germany
Serological pipettes	Sarstedt, Nümbrecht, Germany
Single Channel Pipettes, PIPETMAN classic™ (0.1-1000 µl)	Gilson, Middleton, USA
Sodium Acetate	Sigma-Aldrich, St. Louis, USA
Sodium azide	Merck, Darmstadt, Germany
Sodium Chloride	Sigma-Aldrich, St. Louis, USA
Sodium dodecyl sulfate (SDS)	Applichem, Karlsruhe, Germany
Stericup filter units 0.2 and 0.45 µM	Merck, Darmstadt, Germany
Sucrose	AppliChem GmbH, Darmstadt, Germany
Tetramethylethylenediamine (TEMED)	Sigma Aldrich, St. Louis, USA
Tricine	Carl Roth, Karlsruhe, Germany
Tris(2-carboxyethyl)phosphine (TCEP)	Carl Roth, Karlsruhe, Germany
Tris(hydroxymethyl)-aminomethane (TRIS)	Carl Roth, Karlsruhe, Germany
TritonX-100	Merck, Darmstadt, Germany
Tryptone	BD GmbH, Heidelberg, Germany
Tween-20	Carl Roth, Karlsruhe, Germany
Vivaspin 500 Centrifugal Concentrators 5k PES	Sartorius, Göttingen, Germany
Whatman Puradisc 30 syringe filters 0.2 and 0.45 µM	General Electric, Boston, USA
Yeast extract	Carl Roth, Karlsruhe, Germany
Yeast tRNA	Thermo Fisher Scientific, Waltham, USA
Zinc acetate	Fisher Scientific, Hampton, USA
β-Mercaptoethanol	Sigma-Aldrich, St. Louis, USA

5.1.4 Antibodies and dyes

Table 4: List of antibodies or dyes used in this work and the respective source.

Antibody and dyes	Source or company
Coomassie brilliant blue G-250	Biomol Feinchemikalien, Hamburg, Germany
Midori Green	Nippon Genetics Europe GmbH, Dueren, Germany
Monoclonal mouse antibody against (His) ₆	General Electric, Boston, USA
Polyclonal antibody goat serum against NC	Own lab
Polyclonal antibody rabbit serum against MA	Own lab
Polyclonal antibody rabbit serum against p6	Own lab
Polyclonal antibody rabbit serum against SP1	This work
Polyclonal antibody rabbit serum against SP2	This work
Polyclonal antibody sheep serum against CA	Own lab

5.1.5 Enzymes

Table 5: List of enzymes applied in experiments and their respective origins.

Enzyme	Company
Benzonase	Merck-Millipore, Billerica, MA, USA
DNase A	NEB, Ipswich, US
HIV-1 Protease	AG Jan Konvalinka, Prague, Czech Republic
Lysozyme	Merck-Millipore, Billerica, MA, USA
Phusion High Fidelity-DNA-Polymerase	NEB, Ipswich, US
Restriction enzymes	NEB, Ipswich, US
T4 DNA Ligase	NEB, Ipswich, US
Trypsin	BioChrom AG, Berlin, Germany

5.1.6 Buffers recipes

Table 6: List of relevant and self-prepared buffers, including the recipe.

Buffer	Recipe
20 x NativePAGE running buffer	1 M BisTris, 1 M tricine, pH 6.8
2xYT medium	1 % peptone, 1 % yeast extract, 171 mM NaCl
3 x sample buffer – SDS-PAGE	125 mM TRIS, pH 6.8, 2 % SDS, 10 % (w/v) glycerol, 0.02 % bromophenol blue
3 x TricinePAGE casting buffer	3 M TRIS, pH 8.45, 0.3 % SDS
3 x TricinePAGE glycerol solution	40 % (w/v) glycerol
4 x NativePAGE sample buffer	200 mM BisTris, 24 M HCl, 200 mM NaCl, 40 % glycerol, 0.004 % Ponceau S, pH 7.2
4 x separation gel buffer – SDS-PAGE	1.5 M TRIS, pH 8.8, 0.4 % SDS
4 x stacking gel buffer – SDS-PAGE	0.5 M TRIS, pH 6.8, 0.4 % SDS
Acrylamide stock solution	30 % Acrylamide, 0.15 % bisacrylamide
Antibody purification elution buffer	100 mM glycine, pH 2.5 – 3
Assembly buffer	50 mM HEPES, pH 8.0, 200 mM NaCl, 1 mM EDTA, 1 mM TCEP, 20 % methanol, 0 – 120 μ M IP6
Calcium transfection buffer	250 mM CaCl ₂
Colloidal coomassie	0.12 % Coomassie brilliant blue G-250, 10 % (NH ₄) ₂ SO ₄ , 10 % (ortho-) phosphoric acid, 20 % ethanol
Fixation solution	40 % (v/v) MeOH, 10 % (v/v) acetic acid
Gag assembly buffer	50 mM HEPES, pH 8.0, 200 mM NaCl, 1 mM EDTA, 1 mM TCEP, 20 % methanol
Gag processing buffer	100 mM MES, pH 6.0, 150 mM NaCl, 1 mM DTT, 0.02 % (v/v) TX-100
Gag storage buffer	50 mM TRIS, pH 8.0, 1 M NaCl, 5 mM DTT
Gag-His elution buffer	50 mM TRIS-HCl pH 8.0, 1 M NaCl, 250 mM imidazole, 5 mM MgCl ₂ , 10 mM imidazole, 1 % (v/v) Tween-20, 10 % (v/v) glycerol, 5 mM DTT
Gag-His PEI solution	10 % PEI
Gag-His resuspension buffer	50 mM TRIS-HCl pH 8.0, 1 M NaCl, 10 mM imidazole, 5 mM MgCl ₂ , 10 mM imidazole, 1 % (v/v) Tween-20, 10 % (v/v) glycerol, 5 mM DTT

Gag-His washing buffer	50 mM TRIS-HCl pH 8.0, 1 M NaCl, 25 mM imidazole, 5 mM MgCl ₂ , 10 mM imidazole, 1 % (v/v) Tween-20, 10 % (v/v) glycerol, 5 mM DTT
Gag-TEV-His cleavage buffer	50 mM Tris, pH 8.0, 500 mM NaCl, 0.5 mM EDTA, 1 mM DRR
LB medium	1 % peptone, 0.5 % yeast extract, 171 mM NaCl
NHS coupling buffer	0.2 M NaHCO ₃ , pH 8.3, 0.5 M NaCl
PBS	137 mM NaCl, 2.7 mM KCl, 10 mM Na ₂ HPO ₄ , 1.8 mM KH ₂ PO ₄
PEI transfection reagent	1 mg/mL PEI
SDS-PAGE running buffer	25 mM TRIS, 200 mM glycine, 0.1 % SDS
TAE buffer	40 mM TRIS, pH 8.3, 20 mM NaAc, 2 mM EDTA
TB	0.017 M KH ₂ PO ₄ , 0.072 M K ₂ HPO ₄ , 0.04 % (v/v) glycerol, 2.4 % yeast extract, 2 % peptone
TBST	10 mM TRIS, pH 7.5, 150 mM NaCl, 0.1% (v/v) Tween 20
TricinePAGE AB-3 solution	48 % acrylamide, 1.5 % bisacrylamide
TricinePAGE AB-6 solution	49.5 % acrylamide, 3 % bisacrylamide
TricinePAGE anode buffer	0.2 M TRIS, pH 8.9
TricinePAGE cathode buffer	0.1 M TRIS, pH 8.25, 0.1 M Tricine, 0.1 % SDS
WB blocking buffer	50 % (v/v) LI-COR buffer in PBS
WB transfer buffer I	0.3 M TRIS, 20 % (v/v) methanol
WB transfer buffer II	0.025 M TRIS, 20 % (v/v) methanol
ΔMACANCSP2 binding buffer	50 mM Pi, 500 mM NaCl, pH 7.5, 1 mM DTT
ΔMACANCSP2 elution buffer	50 mM Pi, 500 mM NaCl, pH 7.5, 1 mM DTT, 50 mM imidazole
ΔMACANCSP2 lysis buffer	50 mM TRIS, 1M NaCl, 10% w/v glycerol, 1 mM EDTA, 2 mM DTT, pH 8.3
ΔMACANCSP2 storage buffer	50 mM HEPES, 500 mM NaCl, 5% glycerol, 1 mM TCEP, 10 μM ZnCl ₂

5.1.7 Primer and plasmids

Table 7: List of used plasmids with a short description of containing constructs and sources.

Name	Description	Source
Gag-His A431V	Gag with CS mutation A431V fused C-terminally to internal (His) ₆ -tag of pET28	This work
Gag-His CA-SP1	Gag with CS mutations L363I M367I fused C-terminally to internal (His) ₆ -tag of pET28	This work
Gag-His F448M	Gag with CS mutation F448M fused C-terminally to internal (His) ₆ -tag of pET28	This work
Gag-His I437V	Gag with CS mutation I437V fused C-terminally to internal (His) ₆ -tag of pET28	This work
Gag-His MA-CA	Gag with CS mutation Y122I fused C-terminally to internal (His) ₆ -tag of pET28	This work
Gag-His MUT	Synthetic construct of Gag MUT fused C-terminally to internal (His) ₆ -tag of pET28, containing inhibiting mutation of MA-CA, CA-SP1, NC-SP2, SP2-p6, and the WM mutation	This work
Gag-His N432L	Gag with CS mutation N432L fused C-terminally to internal (His) ₆ -tag of pET28	This work
Gag-His N432L F448M	Gag with CS mutations N432L and F448M fused C-terminally to internal (His) ₆ -tag of pET28	This work
Gag-His NC-SP2	Gag with CS mutation N432I fused C-terminally to internal (His) ₆ -tag of pET28	This work
Gag-His SP1-NC	Gag with CS mutation M377V fused C-terminally to internal (His) ₆ -tag of pET28	This work
Gag-His SP2-p6	Gag with CS mutation F448I fused C-terminally to internal (His) ₆ -tag of pET28	This work
Gag-His WT	Synthetic construct of Gag WT fused C-terminally to internal (His) ₆ -tag of pET28	This work
Gag-TEV-His	Gag WT fused C-terminally to internal (His) ₆ -tag of pET28 with a separating TEV cleavage site	This work
GagΔp6	Gag without p6 in pET28	This work
GagΔp6-His	Gag without p6 fused C-terminally to internal (His) ₆ -tag of pET28	This work

pCHIV PR D25N	pcDNA3.1 derived, non-infectious HIV-1 proviral construct, lacking LTRs and parts of Nef; D25N active site mutation in PR	(Hanne, et al., 2016)
Δ MACANCSP2	Gag without amino acids 16 – 99 of MA and p6 in pET11c	Own laboratory
Δ MACANCSP2 MA-CA	Gag MA-CA without amino acids 16 – 99 of MA and p6 in pET28	This work
Δ MACANCSP2 CA-SP1	Gag A-SP1 without amino acids 16 – 99 of MA and p6 in pET28	This work
Δ MACANCSP2 SP1-NC	Gag SP1-NC without amino acids 16 – 99 of MA and p6 in pET28	This work
Δ MACANCSP2 NC-SP2	Gag NC-SP2 without amino acids 16 – 99 of MA and p6 in pET28	This work

Table 8: List of oligonucleotides used for cloning procedures, including sequence, relevant restrictions sites, and orientation.

Primer	Sequence	Relevant restriction site	Direction
GagCOPR28Nc olfw	atatccATGGGCGCACGTGCAAG	NcoI	forward
GagCOPR28Xh olrv	tataCTCGAGTTGAGAAGAAGGGTCAG	XhoI	reverse
GagtodMA16_99 fw	tataCCATGGGCGCACGTGCAAGTGTATTGTCGGGAGG CGAATTGGATAAGGCACTGGATAAGATTGAAGAGG	NcoI	forward
Gc dp6	atatCTCGAGtcaAAGAAAATTACCGGGCCGGCC	XhoI	reverse
GHc dp6	atatCTCGAGAAGAAAATTACCGGGCCGGCC	XhoI	reverse
GHcA431Vmut fw	GTACAGAGCGTCAAGTGAATTTCTTAGGC	-	forward
GHcA431Vmut rv	GCCTAAGAAATTCACCTTGACGCTCTGTAC	-	reverse
GHcF448Mmut fw	CCCGTAATATGCTTCAATCTCG	-	forward
GHcF448Mmut rv	CGAGATTGAAGCATATTACCGGG	-	reverse
GHcI437Vmutfw	CTTAGGCAAGGTGTGGCCGAGTCAC	-	forward

GHcl437Vmutr v	GTGACTCGGCCACACCTTGCCTAAG	-	reverse
GHcMfeSP1NC mutrv	atatCCACAATTGAAACATTTAACCGTCTTACGTTGGTTA CGGAAATTCCCTTTCTGAATCACAATCG	MfeI	reverse
GHcN432Lmut fw	GCGTCAAGCGCTGTTCTTAGGC	-	forward
GHcN432Lmut rv	GCCTAAGAACAGCGCTTGACGC	-	reverse
G-TEV-Hc rv	atatCTCGAGAGACTGGAAGTACAGGTTTTCTTGAGAAG AAGGG	XhoI	reverse
I437VMfeI	CGGTTAAATGTTTCAATTGTGG	MfeI	forward
WMcaAA fw	GGTAAAAAATGCGGCGACAGAAACC	-	forward
WMcaAA rv	GGTTTCTGTCCCGCATTTTTTACC	-	reverse

5.1.8 Bacterial and eukaryotic strains

Table 9: List of *E. coli* strains for cloning and expression.

Strain	Genotype	Reference
<i>E. coli</i> BL21 (DE3)	F ⁻ <i>ompT gal dcm lon hsdS_B(r_B⁻m_B⁻)</i> λ(DE3 [<i>lacI lacUV5-T7p07 ind1 sam7 nin5</i>]) [<i>malB</i> ⁺] _{K-12} (λ ^S)	(Studier, et al., 1986)
<i>E. coli</i> DH5α	F ⁻ <i>endA1 glnV44 thi-1 recA1 relA1</i> <i>gyrA96 deoR nupG purB20</i> φ80d <i>lacZ</i> ΔM15 Δ(<i>lacZYA-argF</i>)U169, <i>hsdR17(r_K⁻m_K⁺)</i> , λ ⁻	(Grant, et al., 1990)
<i>E. coli</i> STBL2	F ⁻ <i>endA1 glnV44 thi-1 recA1 gyrA96</i> <i>relA1</i> Δ(<i>lac-proAB</i>) <i>mcrA</i> Δ(<i>mcrBC- hsdRMS-mrr</i>) λ ⁻	(Trinh, et al., 1994)

5.2 Methods

5.2.1 Molecular biological methods

5.2.1.1 Isolation of plasmids

According to Table 12, 400 mL LB-medium with antibiotics were inoculated by a single colony and incubated for 16 h at 37 °C and 150 rpm. For the plasmid isolation, the whole culture was used according to the manufacturer's guide (Macherey-Nagel, Düren, Germany). Isolated DNA was reconstituted in 300 μL of nuclease free water (high copy vectors) or 150 μL (low copy vectors). Isolation of retroviral constructs

was performed with *E. coli* STBL2, and other constructs were isolated from *E. coli* DH5 α or TOP10. If necessary, newly synthesized plasmids with the pET28 vector were sequenced by Eurofins Scientific (Luxembourg, Luxembourg) with T7 or specific primers of Table 8.

5.2.1.2 Transformation

For 10 min, 50 μ L of chemically competent bacteria were thawed on ice and mixed cautiously by pipetting with 2 μ L (10 – 150 ng) of the chosen plasmid, 5 μ L site-directed mutagenesis PCR product or 2 μ L ligation reaction sample. After 10 min incubation at 4 $^{\circ}$ C, cells were heat-shocked for 45 s at 37 $^{\circ}$ C or 42 $^{\circ}$ C. Afterward, the cells were cooled again for 2 min on ice before adding 400 μ L of LB-medium and incubating for 45 min at 37 $^{\circ}$ C. Cell pellet of the transformation was resuspended in 50 μ L of LB medium after centrifugation (Ligation transformation or PCR transformation) or 50 μ L of the transformation without centrifugation (retransformation) were plated on selective agar and incubated for 16 h at 37 $^{\circ}$ C.

5.2.1.3 Gene amplification by polymerase chain reaction (PCR)

The polymerase chain reaction (PCR) was performed with specifically designed primers (Table 8) to synthesize new DNA fragments with flanking restriction sites (standard) or site-directed mutagenesis (sdm). The following protocol (Table 10 and Table 11) was oriented towards the manufacturer's guide of the used Phusion High Fidelity-DNA-Polymerase (NEB, Ipswich, US). Before further use, resulting PCR samples were processed by 1 μ L DpnI/50 μ L for 1 h (standard PCR) or 4 h (sdm-PCR) to remove parental DNA. If necessary, PCR products were purified according to the manufacturer's guide of NucleoSpin Gel and PCR Clean-up (Macherey-Nagel, Düren, Germany).

Table 10: Pipetting scheme for a PCR for DNA amplification.

Compounds	Volume [μ L]	Final concentration
Nuclease-free water	to 50 μ L	
5X Phusion HF	10	1x
10 mM dNTPs	2.5	500 μ M
10 μ M Forward Primer	2.5	0.5 μ M
10 μ M Reverse Primer	2.5	0.5 μ M
Template DNA	1	10 – 50 ng
DMSO (sdm-PCR)	1 - 3	
Phusion DNA Polymerase	0.5	1.0 units/50 μ l PCR

Table 11: PCR cyclor program for generation of chosen DNA fragments by PCR.

Step	T [°C]	Time
Initial Denaturation	98	30
35 cycles (standard)	98	5 – 10 s
26 cycles (sdm)	45 – 72	10 – 30 s
	72	15 – 30 s/kb
Final Extension	72	5 – 10 min
Hold	4 - 10	-

5.2.1.4 Restriction digest

For cloning by ligation, plasmids or PCR products of desired DNA were digested with restrictions enzymes from New England Biolabs (Ipswich, USA) as recommended by the manufacturer. DNA was incubated with the appropriate enzyme for 2 h at 37 °C. Resulting fragments were separated by agarose gel electrophoresis and purified with NucleoSpin Gel and PCR Clean-up (Macherey-Nagel, Düren, Germany).

An analytical standard restriction digest was prepared in 20 µL, including 1 µL of each restriction enzyme, 2 µL 10 x reaction buffer and 0.5 – 2 µg of DNA. Plasmids, inserts, and PCR products were digested with the flanking enzymes for cloning. For reaction volumes of 50 µL, the whole PCR product or 5 µg of plasmids, 1 µL of each restriction enzyme, and 5 µL 10 x reaction buffer were mixed.

5.2.1.5 Ligation

Cloning of constructs was mainly done by ligation with T4 DNA Ligase (NEB, Ipswich, US) as recommended by the manufacturer. In 20 µL ligation mix, 1 µL ligase, 2 µL 10 x reaction buffer, 100 ng vector and insert with threefold molar excess to vector were added. The reaction was performed either at room temperature for 1 h or at 4 °C over night. Afterward, the ligase was denatured by incubation at 65 °C for 10 min.

5.2.1.6 Agarose Gel Electrophoresis

For separation of DNA fragments according to size, agarose gel electrophoresis was applied in 1% (w/v) gels. For DNA staining Midori Green dye was added to the agarose solution (1:10000) prior to pouring the gel. Samples were mixed with 6 x loading dye before loading. DNA ladder 1 kb Plus was used as a size

standard and gels were run at 90V (unlimited amperage) for 45min for a 10cm gel in a 1 x TAE buffer. The final documentation was performed by the Gel iX Imager (INTAS Science Imaging, Göttingen, Germany).

5.2.1.7 Cloning procedure and used plasmids

For production in *E. coli*, the pET28 vector encoding the gene of choice was used or pET11c encoding Δ MACANCSP2. The pET28-vector with an inserted Gag gene at NcoI and XhoI sites (fused C-terminal His-tag to Gag) was a kind gift of the Johnson Mak group (McKinstry, et al., 2014). To optimize the production of the Gag in *E. coli* (5.2.2.1.2), two codon optimized synthetic constructs were used as blunt end constructs in this thesis. One was the wild type (Gag WT) and the other was containing mutations for inhibition of MA-CA, CA-SP1, NC-SP2, SP2-p6 cleavage as well as the WM mutation (Gag MUT). Besides the codon optimization, single unique restriction sites for Gag and pET28 were inserted into the Gag coding sequence in order to enable a simple exchange of subparts between the two constructs (Figure 7). Therefore the sites AgeI (blue), SbfI (green), SrfI (yellow), MfeI (red), and FseI (purple) were used. Restriction sites of NcoI and XhoI were added at the C- and N-terminal end, respectively, using PCR. The sequences of both are listed below:

Gag WT

```
catATGGGGCGCACGTGCAAGTGTATTGTCGGGAGGGCGAATTGGATAAGTGGGAGAAAATTCGCTTACGCCCTGGAGGGAAAAAGCAGTATAAAATTAAGCATAT
CGTGTGGGCCTCACGGAATTGGAACGCTTTGCTGTTAACCCGGGATTATTAGAACTTCGGAAGTTGTCGCCAAATCTGGGACAACTTCAGCCGTCGTTGCA
GACCGGTAGTGAAGAATTGCGCAGCTTATACAACACCATCGCTGTCTTTATTGCGTACACCAACGTATTGACGTCAAGGACACGAAAGAGGCACTGGATAAGA
TTGAAGAGGAAACAAAATAATCGAAAAAAAAGCACAACAAGCTGCTGCCGACACGGGCAACAATTCTCAAGTTTCACAAAATTACCCGATTGTGCAAAACCTG
CAGGGCCAAATGGTTCATCAAGCAATTTGCGCCGTCAGTTGAACGCTGGGTAAGTTCGTTGAGGAAAAGCGTTCTCACTGAAGTATTCCCATGTTCTCA
GCTTTGTCGAAGGGGCAACCCACAAAGATTTAAATACCATGCTGAACACGGTTGGCGGTACCAGGCTGCAATGCAAATGCTGAAGGAAACGATTAACGAAGA
GGCTGCAGAATGGGACCGCTTCATCCAGTCCACGCGGGCCGATTGCTCCTGGACAATGCGTGAGCCTCGTGGGTCTGACATCGCAGGTACCACTAGTACCT
TACAGGAGCAAATGGGTGGATGACCCATAATCCACCGATCCCCGTGGGGGAGATCTACAAGCGCTGGATTATCTTAGGTCTGAATAAGATTGTCCGCATGTATT
CCCCGACGTCGATCTTAGATATCCGCCAAGGCCAAAAGAGCCTTTTCGTGATTATGTTGATCGCTTCTATAAGACTCTGCGTGCAGAGCAAGCTTCGCAAGAAG
TAAAAAAGTGGATGACGGAGACTCTGTTAGTCCAGAACGCCAACCTGACTGTAAGACAATCTTGAAAGCCCTTGGTCCAGGGGCCACACTTGAAGAAATGATG
ACAGCATGTACGGGGTGGGGGCCCGGGCCATAAGGCCCGCTCTTAGCCGAGGCGATGTCGCAGGTAACCAATCCCGCAACGATTATGATTAGAAAGGGA
ATTTCCGTAACCAACGTAAGACGGTTAAATGTTTCAATTGTGGAAAAGAGGGACACATTGCGAAGAATTGTAGGGCCCCACGCAAGAAAGGGTGTGAAATG
CGGGAAGGAGGGGCATCAAATGAAGGACTGTACAGAGCGTCAAGCGAATTTCTTAGGCAAGATCTGGCCGAGTACAAAGGCCGGCCCGGTAATTTCTTCAA
TCTCGTCCAGCCAAACAGCCCCCGAAGAGACTTCCGTTTCGGTGAGGAGACACTACGCCAGTCAGGTCAGGAACCTATCGACAAGGAACCTTATCCC
CTCGGAGCCTTCGCTCACTGTTTGGGTCTGACCCTTCTCAAGAAAACCTGTACTTCCAGTCTAAAATCGAAGAAAGGCAAACCTGTTATCTGGATCAACGGCG
ATAAAGGCTATAATGGCCTGGCGGAAGTGGGCAAAAATTCGAA
```

Gag MUT

```
catATGGGGCGCACGTGCAAGTGTATTGTCGGGAGGGCGAATTGGATAAGTGGGAGAAAATTCGCTTACGCCCTGGAGGGAAAAAGCAGTATAAAATTAAGCATAT
CGTGTGGGCCTCACGGAATTGGAACGCTTTGCTGTTAACCCGGGATTATTAGAACTTCGGAAGTTGTCGCCAAATCTGGGACAACTTCAGCCGTCGTTGCA
GACCGGTAGTGAAGAATTGCGCAGCTTATACAACACCATCGCTGTCTTTATTGCGTACACCAACGTATTGACGTCAAGGACACGAAAGAGGCACTGGATAAGA
TTGAAGAGGAAACAAAATAATCGAAAAAAAAGCACAACAAGCTGCTGCCGACACGGGCAACAATTCTCAAGTTTCACAAAATATCCCGATTGTGCAAAACCTG
CAGGGCCAAATGGTTCATCAAGCAATTTGCGCCGTCAGTTGAACGCTGGGTAAGTTCGTTGAGGAAAAGCGTTCTCACTGAAGTATTCCCATGTTCTCA
GCTTTGTCGAAGGGGCAACCCACAAAGATTTAAATACCATGCTGAACACGGTTGGCGGTACCAGGCTGCAATGCAAATGCTGAAGGAAACGATTAACGAAGA
GGCTGCAGAATGGGACCGCTTCATCCAGTCCACGCGGGCCGATTGCTCCTGGACAATGCGTGAGCCTCGTGGGTCTGACATCGCAGGTACCACTAGTACCT
TACAGGAGCAAATGGGTGGATGACCCATAATCCACCGATCCCCGTGGGGGAGATCTACAAGCGCTGGATTATCTTAGGTCTGAATAAGATTGTCCGCATGTATT
CCCCGACGTCGATCTTAGATATCCGCCAAGGCCAAAAGAGCCTTTTCGTGATTATGTTGATCGCTTCTATAAGACTCTGCGTGCAGAGCAAGCTTCGCAAGAAG
TAAAAAAGCGGCGACGGAGACTCTGTTAGTCCAGAACGCCAACCTGACTGTAAGACAATCTTGAAAGCCCTTGGTCCAGGGGCCACACTTGAAGAAATGATG
ACAGCATGTACGGGGTGGGGGCCCGGGCCATAAGGCCCGCTCATCGCGAGGCGATTTGCGAGGTAACCAATCCCGCAACGATTATGATTAGAAAGGGA
ATTTCCGTAACCAACGTAAGACGGTTAAATGTTTCAATTGTGGAAAAGAGGGACACATTGCGAAGAATTGTAGGGCCCCACGCAAGAAAGGGTGTGAAATG
CGGGAAGGAGGGGCATCAAATGAAGGACTGTACAGAGCGTCAAGCGAATTTCTTAGGCAAGATCTGGCCGAGTACAAAGGCCGGCCCGGTAATATCTTCAA
```

TCTCGTCCAGAGCCAACAGCCCCCGAAGAGAGCTTCGGTTTCGGTGAGGAGACGACTACGCCAGTCAGCGTCAGGAACCTATCGACAAGGAACTTTATCCC
 CTCGCGAGCCTTCGCTCACTGTTTGGGTCTGACCCTTCTCAAGAAAACCTGTACTTCCAGTCTAAAATCGAAGAAGGCAAACCTGGTTATCTGGATCAACGGCG
 ATAAAGGCTATAATGGCCTGGCGGAAGTGGGCAAAAAATTCGAA

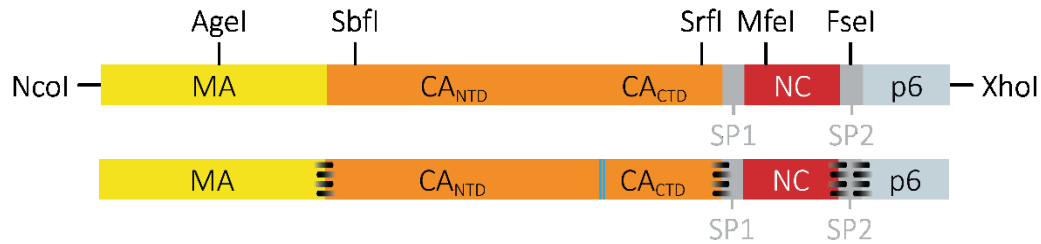


Figure 7: Cloning scheme of ordered synthetic DNA constructs of Gag. Two synthetic DNA constructs for Gag were ordered, one as WT (upper) and the other one (lower) carrying the WM (blue) and point mutations for inhibiting CSs at MA-CA, CA-SP1, NC-SP2 and SP2-p6 (black stitches). Both were codon-optimized for expression in *E. coli* BL21 (DE3) and contained Gag in full length (MA, CA_{NTD}, CA_{CTD}, SP1, NC, SP2, and p6). Additionally, they are flanked by the restriction sites of NcoI (N-terminus) and XhoI (C-terminus) for cloning with pET-vectors. Other unique restriction sites for changing parts between the constructs are indicated above.

Table 12: List of cloning procedures with numeration, original vector, added insert, plasmid name, used restriction enzymes, and antibiotic resistance encoded by the vector.

Plasmid number	Vector	Insert	Plasmid name
1353	1356	Mutagenesis PCR (whole plasmid)	pET28 Gag-His N432L
1354	1356	Mutagenesis PCR (whole plasmid)	pET28 Gag-His F448M
1355	1356 x NcoI XhoI	PCR x NcoI XhoI	pET28 ΔMACANCSP2 MA-CA
1356	pET28 x NcoI XhoI	PCR Gag WT x NcoI XhoI	pET28 Gag-His WT
1357	pET28 x NcoI XhoI	PCR Gag MUT x NcoI XhoI	pET28 Gag-His MUT
1358	1356 x NcoI XhoI	PCR x NcoI XhoI	pET28 ΔMACANCSP2 CA-SP1
1360	1356 x NcoI XhoI	1357 x NcoI XhoI	pET28 Gag-His WM
1412	1357 x SrfI XhoI	1356 x SrfI XhoI	pET28 Gag-His WM MA-CA CA-SP1
1413	1412 x SbfI XhoI	1356 x SbfI XhoI	pET28 Gag-His WM MA-CA

1414	1356 x NcoI SbfI	1357 x NcoI SbfI	pET28 Gag-His WM CA-SP1 NC-SP2 SP2-p6
1415	1356 x MfeI XhoI	1357 x MfeI XhoI	pET28 Gag-His NC-SP2 SP2-p6
1416	1356 x FseI XhoI	1415 x FseI XhoI	pET28 Gag-His NC-SP2
1417	1356 x NcoI SbfI	1357 x NcoI SbfI	pET28 Gag-His MA-CA
1417	1356 x NcoI SbfI	1357 x NcoI SbfI	pET28 Gag-His MA-CA
1418	1415 x FseI XhoI	1356 x FseI XhoI	pET28 Gag-His SP2-p6
1428	1356	PCR mutagenesis (whole plasmid)	pET28 Gag-His A431V
1429	1360 x SbfI MfeI	PCR 1417 x SbfI MfeI	pET28 Gag-His SP1-NC
1430	1415 x SbfI MfeI	1414 x SbfI MfeI	pET28 Gag-His WM CA-SP1
1431	1430 x XhoI SrfI	1418 x XhoI SrfI	pET28 Gag-His CA-SP1
1432	1418 x XhoI SrfI	1430 x XhoI SrfI	pET28 Gag-His CA-SP1 SP2-p6
1433	1356 x NcoI XhoI	PCR 1356 x NcoI XhoI	pET28 Gag-TEV-His
1434	1356 x NcoI XhoI	PCR 1356 x NcoI XhoI	pET28 Gagdp6-His
1435	1356 x NcoI XhoI	PCR 1356 x NcoI XhoI	pET28 Gagdp6
1436	1354 x NcoI MfeI	1353 x NcoI MfeI	pET28 Gag-His N432L F448M
1437	1354 x MfeI XhoI	Synthetic constrict x MfeI XhoI	pET28 Gag-His I437V
1518	1356 x NcoI XhoI	PCR x NcoI XhoI	pET28 ΔMACANCSP2 NC-SP2
1519	1518 x SbfI FseI	PCR x SbfI FseI	pET28 ΔMACANCSP2 SP1-NC

5.2.2 Biochemical methods

5.2.2.1 Protein production

5.2.2.1.1 Glycerol stocks

For permanent storage of transformed *E. coli* strains, single colonies of a chosen plasmid were inoculated in 50 mL LB medium with the respective antibiotic. The culture was incubated at 37 °C and 150 rpm and centrifuged afterward at 4 °C at 10000 RCF for 20 min after reaching a high optical density on the next day. The pellet was resuspended in 1 mL of 50 % (v/v) glycerol in LB medium, flash-frozen in liquid nitrogen and stored at -80 °C.

5.2.2.1.2 Expression

A day before protein production, a small part of a glycerol stock or a single colony, containing the plasmid with the coding sequence for the chosen proteins, was inoculated in 200 mL LB medium with added respective antibiotic as a pre-culture and incubated over night at 37 °C and 150 rpm. The grown pre-culture was added to 4 L LB-medium for the production culture. After the addition, the culture should feature an OD₆₀₀ of ~ 0.1. This suspension was grown at 37 °C and 150 rpm until OD₆₀₀ of 0.6 was reached after which 1mM IPTG was added to induce expression. After 3 – 5 h of expression, the cells were harvested by centrifugation at 10000 RCF at 4 °C for 30 min and pooled in 50 mL tube. Subsequently, the cells were flash-frozen in liquid nitrogen before storing at -80 °C until further use.

During expression, a sample of the preculture, the culture before, and each full h after induction was taken for analysis by SDS-PAGE and WB (5.2.2.6.2). Therefore, a volume of 400 µL divided by OD₆₀₀ at a given timepoint was centrifuged at 14000 RCF for 5 min. The resulting pellet was resuspended in 60 µL SDS-PAGE sample buffer and incubated at 95 °C in a heating block for 10 min. For analysis by SDS-PAGE or WB 5 – 10 µL were applied.

5.2.2.2 Protein purification and preparation

At the beginning of the protein purification, the frozen, harvested cell pellet was thawed on ice and resuspended by stirring in 10 mL of the respective lysis or resuspension buffer per g of pellet until no more cell aggregates were detectable by eye. If not differently noted, samples, yielding cells or protein, were kept on ice or at 4 °C during the purification. For cell lysis, 1 mg/mL lysozyme was added and the cells were incubated for 30 min while stirring. In the case of the purification of His-tagged proteins, 50 µL benzonase (25 U/µL) and 1 mL DNaseI (2 U/µL) were added per 100 mL. The lysis was performed subsequently by two runs of a cell fluidizer at 15000 psi.

Gag versions with C-terminal His-tag

To remove all remaining NA in the sample after cell lysis, these were precipitated at a concentration of 0.14 % PEI while stirring for 10 min at RT. Cell debris and precipitated NA were removed by centrifugation at 15000 RCF for 30 min. While stirring, Gag protein in the remaining supernatant was precipitated at 45 % of $(\text{NH}_4)_2\text{SO}_4$ saturation (25 % in case of Gag-His WM) for 1 h at 4 °C and afterward pelleted by centrifugation at 15000 RCF for 30 min at 4 °C. Precipitated Gag protein was solubilized again in resuspension buffer of the same volume as before the precipitation and centrifuged as before to remove non-solubilized protein. The protein-containing supernatant was applied to a HisTrap FF 5 ml column loaded with Ni^{2+} and equilibrated with resuspension buffer. The flow-through was fractionated in 15 mL steps. Subsequently, the column was washed with 8 column volumes with washing buffer. Protein was eluted by a linear gradient to 100 % of elution buffer over 20 min with a flow-rate of 2 mL/min. The elution was recorded in real-time with the absorption at 280 nm. Fractions, yielding protein according to the absorption, were pooled with fractions of the same concentration and dialyzed against dialysis tubes (MWCO 8 – 10 kDa) against storage buffer ON at 4 °C. On the following day, the protein solutions were aliquoted and flash-frozen in liquid nitrogen for storage at -80 °C.

In the case of Gag-TEV-His, the resulting samples after purification by HisTrap were dialyzed instead against 50 mM Tris/HCl, pH 8.0, 0.5 mM EDTA, 500 mM NaCl, and 1 mM DTT at 4 °C ON. Afterward, the sample was centrifuged at 14000 RCF and TEV protease was added in a molar ratio to Gag-TEV-His of 1:50, continuing the dialysis. On the next day, the sample was again applied to a 5 mL HisTrap column. The protocol of washing and elution was the same as previously using the HisTrap column. Solely His-tag was binding to the column and the remaining part of Gag (Gag-TEV) was in the flow-through, which was dialyzed one more time ON against the Gag-His storage buffer at 4 °C. Final samples were flash-frozen in liquid nitrogen and stored at -80 °C.

Resuspension buffer: 50 mM TRIS-HCl pH 8.0, 1 M NaCl, 10 mM imidazole, 5 mM MgCl_2 , 10 mM imidazole, 1 % (v/v) Tween-20, 10 % (v/v) glycerol, 5 mM DTT

Washing buffer: 50 mM TRIS-HCl pH 8.0, 1 M NaCl, 25 mM imidazole, 5 mM MgCl_2 , 10 mM imidazole, 1 % (v/v) Tween-20, 10 % (v/v) glycerol, 5 mM DTT

Elution buffer: 50 mM TRIS-HCl pH 8.0, 1 M NaCl, 250 mM imidazole, 5 mM MgCl_2 , 10 mM imidazole, 1 % (v/v) Tween-20, 10 % (v/v) glycerol, 5 mM DTT

Storage buffer: 50 mM TRIS, pH 8.0, 1 M NaCl, 5 mM DTT

Δ MACANCSP2

Δ MACANCSP2 was purified according to an internal protocol based on previously published ones (Gross, et al., 2000; Voráčková, et al., 2011). The pellet of the protein production was resuspended in 10 mL lysis buffer and lysed according to the protocol mentioned before. Afterward, the content of NA was removed by precipitation at 0.2 % PEI, while stirring for 10 min at RT. With centrifugation at 15000 RCF for 25 min, the cell debris and NA precipitate were removed. The remaining supernatant was precipitated by

(NH₄)₂SO₄ at 25 % saturation, while stirring at 4 °C for 1 h, and pelleted at 15000 RCF for 25 min. The protein pellet was solubilized in binding buffer of equal volume to buffer used for the initial resuspension. Insoluble protein was removed by centrifugation at 14000 RCF for 25 min at 4 °C. The resulting supernatant was filtered through a syringe filter with a cellulose acetate membrane of 0.45 µm pore size and was applied to a HisTrap FF 5 mL column. The flow-through was fractionated in 15 mL steps and the column was washed with 40 mL binding buffer. Elution was performed as an immediate step gradient from 0 – 100 % of the elution buffer. Total eluted protein was rebuffed by dialysis with dialysis tubes (MWCO 8 – 10 kDa) against storage buffer ON at 4 °C. Final protein solutions were pooled, aliquoted and flash-frozen in liquid nitrogen before storing at -80 °C.

Lysis buffer: 50 mM TRIS, 1M NaCl, 10% w/v glycerol, 1 mM EDTA, 2 mM DTT, pH 8.3

Binding buffer: 50 mM Pi, 500 mM NaCl, pH 7.5, 1 mM DTT

Elution buffer: 50 mM Pi, 500 mM NaCl, pH 7.5, 1 mM DTT, 50 mM imidazole

Storage buffer: 50 mM HEPES, 500 mM NaCl, 5% glycerol, 1 mM TCEP, 10 µM ZnCl₂

10 µL of all samples before elution of the His-Trap were mixed with 110 µL SDS-PAGE sample buffer and incubated at 95 °C in a heating block for 10 min. After elution, 5 µL of all samples for analysis with SDS-PAGE were mixed with 115 µL of sample buffer instead.

If protein samples yielded too low concentration for following assembly or processing experiments, these samples were concentrated in a centrifugal filter with 2 mL capacity and membrane of regenerated cellulose with MWCO of 500 Da for sample volumes less than 2 mL and in the case of samples larger than 2 mL a centrifugal filter with 15 mL capacity and MWCO of 15 kDa was used, according to the manufacturer's guide. Samples of purified Gag proteins were applied to Superdex 70 30/100 columns equilibrated in respective storage buffer to control for purity and structural integrity, which was recognizable by a homogenous peak exhibiting no other peaks or shoulders.

5.2.2.3 Antiserum purification

For this work, polyclonal sera of antibodies against MA (rabbit), CA (sheep), NC (goat), and p6 (rabbit) and a monoclonal serum against the C-terminal His-tag (mouse) were used for immunoblotting. The antibodies against SP1 and SP2, however, needed to be purified from blood sera before they could be applied for immunoblotting. In both cases, the full-length peptides recognized by the antibodies were synthesized by PSL Peptide Specialty Laboratories GmbH (Heidelberg, Germany) and each was bound according to the manufacturer's guide to HiTrap NHS-activated HP 1mL columns. For SP1 3 mg and SP2 5 mg were attached with an efficiency of ~ 70% to the column resin. The activation of the column was also performed according to the manufacturer's guide.

Before use, the columns were equilibrated in phosphate-buffered saline (PBS) and the respective antibody-containing blood sera were diluted 2:1 with PBS. In total, 20 mL blood serum of SP1 and 17.5 mL of SP2 were applied to the columns and washed by 15 column volumes of PBS, respectively. The antibodies were eluted in an immediate step gradient from 0 – 100 % with 0.1 M glycine, pH 2.5 in 100 μ L fractions, and immediately diluted with 500 μ L of 100 mM Tris/HCl, pH 7.5 to neutralize the acidic conditions. The pooled samples of the antibodies were dialyzed against PBS + 0.02 % sodium azide at 4 °C ON in dialysis tubes of MWCO 8 – 10 kDa. The final concentration measurement was done by spectrophotometer and plate reader (Pierce protein assay).

5.2.2.4 *In vitro* assembly

The assembly of Δ MACANCSP2 was performed adapted to a formerly published protocol (Gross, et al., 2000). A maximum yield from *in vitro* assembly was achieved by dialysis of the protein (30 – 100 μ M) against assembly buffer (50 mM HEPES, pH 8.0, 200 mM NaCl, 1 mM EDTA, 1 mM TCEP, 20 % methanol, 0 – 120 μ M IP6) in the presence of 4 % (m/m) DNA or RNA (NA:protein) in a dialysis tube of 0.5 – 1 kDa MWCO for oligonucleotides consisting of 5 nucleotides or 6 – 8 kDa MWCO for oligonucleotides consisting of 25 nucleotides and more. Additionally, IP6 was added to the assembly buffer at experimentally based concentrations as described in the results part. After 16 h of dialysis at 4 °C with gentle stirring, particles were either applied directly to analysis and experiments or harvested at 10000 RCF for 5 min. Pellet particles were then resuspended in fresh assembly or processing buffer.

After dialysis or other treatments, samples of assembled protein were centrifuged at 10000 g for 10 min, to determine the amounts of soluble and assembled protein. Therefore, the pelleted particles were resuspended with an appropriate buffer in the same volume as the supernatant. Protein concentrations in the supernatant and resuspended particles were measured with the Pierce Protein Assay or Coomassie-stained SDS-PAGEs with rectangular signal quantification of Image Studio Lite. From this data, efficiency of assembly and the stability of particles under certain conditions were determined.

5.2.2.4.1 Negative staining and electron microscopy

Four hundred hexagonal mesh copper grids coated with 1.2 % pioloform and 2 nm carbon layer were used for TEM analysis of assembled Gag. Minimum 30 min before use grids were glow discharged for 30 s. One grid was applied for 5 min on top of a drop of 5 μ L sample, which was to be analyzed. Grids were washed two times afterward with water drops, shortly pretreated with a 3 % uranyl-acetate drop and stained on a second uranyl-acetate drop for 30 s. After each step, the remaining liquid on the grid was removed by blotting with filter paper. The grids were air-dried for a minimum of 2 min before storage or analysis at the electron microscope operated at 80 kV.

5.2.2.4.2 Gradient centrifugation

To separate non-assembled protein contaminations from the Δ MACANCSP2, which was assembled without IP6, 200 μ L sample was loaded on a sucrose step gradient. 0.9 mL of 70, 50, 30, and 10 % sucrose in assembly buffer, including 20 % methanol and 0.3 μ M IP6, was layered in a centrifugal tube before the application of the sample, starting with the highest concentration on the bottom. The centrifugation was performed in an SW60 rotor for 16 h at 60000 rpm. 21 fractions of 200 μ L were analyzed by EM with negative-staining for particle presence, by SDS-PAGE and immunoblot for protein content, and by a refractometer for sucrose concentration or density.

5.2.2.4.3 Gel filtration of assembled Δ MACANCSP2

For the purification of Δ MACANCSP2, which was assembled without IP6, 400 μ L sample was applied to a Superose 6 column equilibrated in processing buffer without IP6, which was also the elution buffer for the purification. During the purification, the absorption at 280 nm was chosen as an indicator of protein elution. After the initial slope of the first peak, samples were taken in 500 μ L aliquots until the absorption reached the baseline again. For SDS-PAGE analysis, 5 μ L of the unpurified sample was mixed with 115 μ L of 3 x sample buffer (SB) while 80 μ L from each fraction was mixed with 40 μ L 3x SB. Samples were incubated for 10 min at 95 $^{\circ}$ C. 5 μ L from all relevant samples were analyzed by EM, according to the protocol mentioned above.

5.2.2.4.4 Capto Core purification

After assembly and dialysis of Δ MACANCSP2 in processing buffer, including 60 μ M IP6, 100 μ L sample was applied via a 100 μ L sample loop to a 1 mL Capto Core 700 column pre-equilibrated in processing buffer including IP6. During the purification, the absorption at 280 nm was chosen as an indicator of protein elution. The resin was washed with 7 mL processing buffer, including IP6. The fraction sizes were according to the volume of the respective elution peak. 5 μ L of the resulting peak fractions were taken for EM analysis and 10 μ L were mixed with 10 μ L of 3x sample buffer, before incubation at 95 $^{\circ}$ C in a heating block for 10 min for SDS-PAGE. In order to strip the column from bound protein contaminations, it was cleaned with a solution of 1 M NaOH and 20 % isopropanol. Bound proteins were also analyzed the same way by SDS-PAGE and immunoblot.

5.2.2.5 Protein processing

Protein samples of 27 μM for *in vitro* processing in an unassembled state were thawed on ice. Buffers were replaced with processing buffer (100 mM MES, pH 6.0, 150 mM NaCl, 1 mM DTT, 0.02 % (v/v) TX-100) by dialysis in dialysis tubes (14 kDa MWCO) at 4 °C ON. The samples were centrifuged at 14800 rcf for 10 min to remove precipitates. The supernatant was afterward transferred in a fresh reaction tube.

For processing of *in vitro* assembled particles, protein samples of 60 μM were thawed on ice and subsequently centrifuged at 14800 g for 10 min to remove precipitated protein. The concentration of the supernatant was measured by Pierce 660 nm Protein Assay. Before dialysis in assembly buffer (50 mM HEPES, pH 8.0, 200 mM NaCl, 1 mM EDTA, 1 mM TCEP, 20 % methanol) using a dialysis tube (14 kDa MWCO) at 4 °C ON, the protein samples were mixed with 4 % (m/m) of DNA-oligonucleotides or RNA (NA:protein) and incubated on ice for ~ 5 min. On the following day, the sample was dialyzed against processing buffer containing 60 μM IP6 at 4 °C ON.

For the processing of VLPs, 3×10^7 HEK 293T cells were seeded prior to transfection in a T175 flask, containing 25 mL DMEM including 10 % fetal calf serum (FCS), 10 mM HEPES, penicillin, and streptomycin. After 24 h incubation at 37 °C, 5 % CO₂, and 90 % relative humidity, cells were transfected by the addition of a mixture of 70 μg of pCHIV (D25N; Table 7) and 210 μg PEI in 7 mL DMEM without supplements. Supernatant was harvested after 40 – 48 h by centrifugation at 1500 rpm and 4 °C for 5 min and passed through a 0.45 μm filter. Approx. 32 mL of supernatant per T175 flask were layered carefully on 6 mL sucrose cushion (20 % sucrose (w/v) in PBS) and pelleted in an SW32 rotor for 2 h at 28000 rpm at 4 °C. Resulting pellets were resuspended in 20 μL ice-cold processing buffer w/o TX-100 by incubation and slight shaking for 1 h on ice. Subsequently, TX-100 was added to a concentration of 0.1 % and the particles were incubated for 30 min at room temperature to remove particle membranes before processing.

To measure the concentration of the samples, unassembled and *in vitro* assembled Gag were analyzed by Pierce 660 nm Protein Assay. Because of co-purification of other proteins, samples of protease deficient particles, were instead dot blotted with 100 μL samples on nitrocellulose membrane with 0.4 μm pore size with a primary antiserum against CA (sheep) together with a serial dilution of a Gag standard as a calibration. For the blot, samples were serially diluted (1:30 – 1:840) in 3 x sample buffer in the case of VLPs and from 40 μM to 10 nM in the case of Gag-His, before incubation at 95 °C in a heating block for 10 min. The membrane was dried before the application of antibodies.

Highly concentrated samples were diluted by fresh processing buffer to the desired concentration before processing was started. For the analysis of standard processing, the concentration of Gag was 27 μM (or 11 μM in the case of protease deficient particles). The protein solutions were prewarmed for 5 to 10 min at 37 °C at 1000 rpm in a shaking heat block before the addition of recombinant PR in a molar ratio of 40:1 (Gag:PR dimer) and further incubation. At specific time points (0, 0.5, 1, 2, 4, 8, 15, 30, 60, 120, 240, 480 and 1440 min), 8 μL samples were taken while shaking and immediately mixed 2:1 with 3 x sample buffer for SDS-PAGEs before boiling for 10 min at 95 °C in a heating block to stop the reaction. 10 μL of the taken samples were analyzed later by SDS-PAGE or Tricine-PAGE and respective WB. The used recombinant

protease of 16 μM concentration was a kind gift from Jiri Schimer and Jan Konvalinka (IOCB Prague). All processing experiments were performed as triplicates.

As the PR activity drops over time, PR was incubated at a concentration of 1 μM in PB at 37 °C and 1000 rpm as in the standard processing experiment but without Gag or any other protein. At certain time points (0, 1, 2, 4, 8, 24 h), 4 μL of the sample were added to 150 μL of 2 μM HIV-1 PR substrate I in PB pre-warmed to 37 °C. The reaction was performed in a 10 x 2 mm quartz cuvette and measured by a fluorescence spectroscope with 0.5 s between every measurement. The reaction mix was excited at 340 nm, and the emission was measured at 490 nm, while an increase in emission would indicate the cleavage of the substrate. Consequently, the slope of the increasing emission is equal to the remaining relative activity of the PR. The ratio of the activity at a particular time point and the initial activity of PR describes the percental activity remaining at the specific time point.

5.2.2.6 Protein analysis

5.2.2.6.1 Concentration measurement

In order to define the concentration of protein samples, different methods were used. For samples with major impurities, concentration was determined by Coomassie-stained SDS-PAGEs or WB with the help of a protein standard quantifying the staining or signal of the protein of interest with Image Studio Lite. Pure protein samples were analyzed by Pierce 660 nm Protein Assay using a serial dilution of BSA between 0 and 2 mg/mL as a standard for calibration. 2.5 – 10 μL of protein samples were mixed with 150 μL of Pierce 660 nm Protein Assay sample and incubated for 5 min at RT. With a plate reader, the samples were shaken for 1 min at room temperature in 96-well flat-bottom plates before absorbance measurement at 660 nm. Additionally, pure protein samples were measured at a spectrophotometer. After using the protein-free buffer solution as blank, the concentration was calculated with the detected absorbance at 280 nm of 1 μL sample and the extinction coefficient of the specific protein (Table 13).

Table 13: Extinction coefficient of proteins for concentration determination. The values represent the extinction at 280 nm in the case that all cysteine residues are reduced and are determined by the standard calculation software (Gasteiger, et al., 2003).

Protein	Extinction coefficient [$\text{M}^{-1} \text{cm}^{-1}$]
Gag-His	1.105
$\Delta\text{MACANCSP2}$	1.140

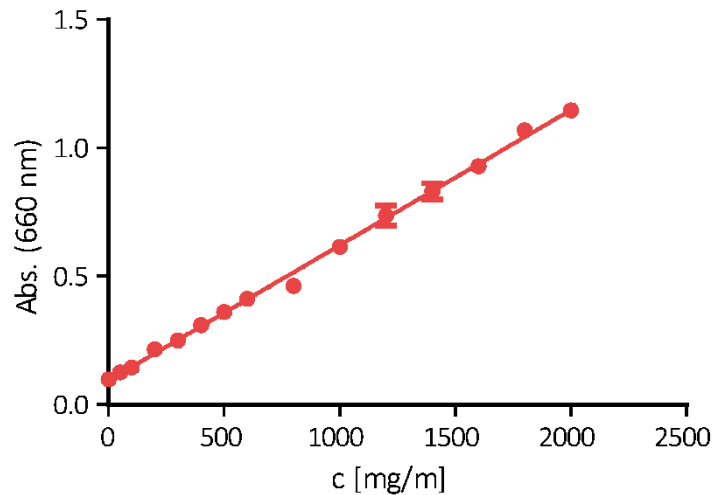


Figure 8: Pierce 660 nm protein assay calibration. For determination of protein concentration, a calibration of the Pierce 660 nm protein assay was done with BSA in storage buffer for Gag-His, varying the concentration between and 2000 $\mu\text{g}/\text{mL}$. Measurements were performed as triplicates in a plate reader. Red dots indicate the median of the measurements for one concentrations and red bars represent the standard deviation.

5.2.2.6.2 SDS-Polyacrylamide gel electrophoresis (SDS-PAGE) and immunoblotting

Samples for SDS-PAGE analysis were boiled at 95 °C in a heating block for 10 minutes and centrifuged down subsequently before analysis. All samples not related to processing analysis were applied to standard SDS-PAGE (12.5 – 17.5 % separating gel; Table 14).

Table 14: Ingredients of standard SDS-PAGE separation gel

Chemicals	12.5 %	15 %	17.5 %
AA/BAA (30:0.8)	2.5 ml	3 ml	3.5 ml
4 x separating gel buffer	1.5 ml	1.5 ml	1.5
H ₂ O	1 ml	1 ml	1 ml

The separation gel for standard SDS-PAGE was polymerized with the addition of 50 μL 10 % APS and 10 μL TEMED and overlaid with 1 mL isopropanol. After the polymerization was finished, the remaining isopropanol was removed by decantation and blotting with cellulose filter paper. 1.5 mL stacking gel was mixed with 1.5 parts of acrylamide stock, 2.5 parts of separating gel buffer, and six parts of water. After the polymerization was started with the addition of 37.5 μL TEMED and 10 % APS, respectively, the solution was layered on the separating gel and a 15-well comb was put on top. After finished polymerization, the

gel was installed in the according holder and the comb was removed. 2 – 10 μL of the sample was loaded on the gels. Electrophoresis was run at 25 mA per 72 cm^2 for 60 min.

For analysis of processing experiments, Tricine PAGEs based on Schägger (2006) were used:

Table 15: Ingredients of Tricine-PAGE.

Chemicals	Separating gel	Spacer gel	Stacking gel
AA/BAA (48:1.5)	6	1.5	-
3 x casting buffer	6	2.5	2.5
3 x glycerol solution	6	-	-
AA/BAA (29:1)	-	-	1.5
H ₂ O	-	3.5	8
10 % APS	150	60	25
TEMED	12.5	5	25

17 mL of polymerizing separating gel was overlaid with 5 mL polymerizing spacer gel and 5 mL H₂O. After the end of the reaction, water was removed by decantation and blotting with cellulose filter paper. The stacking gel was applied on top of the spacer gel with a 14-well comb on top. 1 – 50 μL samples were loaded depending on the protein concentration on the gel before electrophoresis was performed at 25 mA per 285 cm^2 for 16 h.

If needed, the proteins were plotted afterward onto nitrocellulose membrane with 0.4 μm pore size by a semidry blotting method with 50 mA per 72 cm^2 (standard SDS-PAGE) or 1 mA per 1 cm^2 (Tricine-PAGE) for 60 min. In the case of immunoblots for the detection of p6 protein, the membrane had a 0.2 μm pore size and was dry-baked for 30 min at 80 °C. Subsequently, the membrane was incubated ON at 4 °C with 33 % LI-COR buffer/PBS including primary antiserum (Table 4). On the next day, the membrane was washed three times for 10 min with TBS-T and incubated for 1 h at room temperature with secondary antibodies conjugated to infrared dye 700/800 (Table 4) in 33 % LI-COR buffer/PBS. After three final washing steps for 10 min in TBS-T, the membrane was imaged with a digital infrared scanner (LiCor Odyssey Imager CLx).

For in-gel staining, the gels were fixated and washed by smooth shaking in fixation solution (40 % (v/v) MeOH, 10 % (v/v) acetic acid) for at least 1 h, following the end of the gel electrophoresis. Gels were washed shortly twice with desalted water to remove remaining SDS and covered with colloidal Coomassie solution for staining ON. On the next day, the Coomassie solution was decanted and gels washed at least three times in desalted water for 10 min or longer until the unspecific staining was majorly removed. Measurement was performed with a digital infrared scanner (LiCor Odyssey Imager CLx) at 700 nm. For quantitative analysis of stained standard SDS-PAGEs, the Odyssey Image Studio software was used.

5.2.2.6.3 Calculation of Gag dimerization

To calculate the dissociation constant (K_d) for purified Gag-His, samples of different concentrations (50, 5.5, 4, 2, and 0.5 μM) higher and lower than the published K_d of 5.5 μM (Datta, et al., 2007b) were prepared in storage buffer (50 mM TRIS, pH 8.0, 1 M NaCl, 5 mM DTT) and applied as 500 μL samples to Superdex 75 30/100 equilibrated in storage buffer. The maximum value of the absorption at 214 nm represented the elution volume of a specific concentration. The turning point of a sigmoidal regression line in a plot of logarithmic protein concentration and elution volume represents the K_d (shown in the results section). To set this in correlation with the molecular mass, the used Superdex 75 30/100 was calibrated with a standard calibration kit for low molecular weight according to the manufacturer's guide. The elution volume of the resulting peaks (Figure 9 A) was plotted versus the common logarithm of the respective molecular mass of the calibration implemented proteins (Figure 9 B and Table 16)

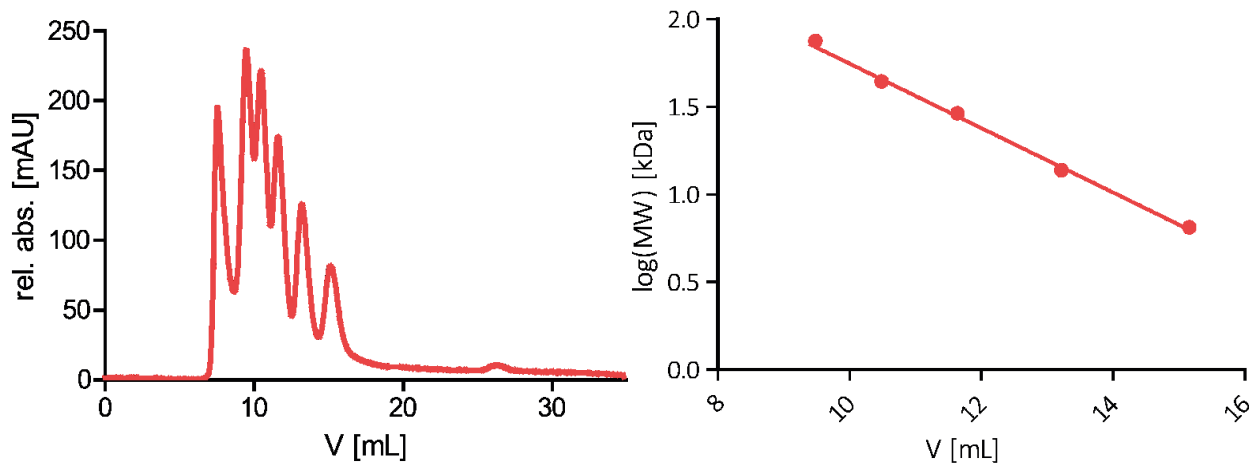


Figure 9: Gel filtration calibration. Gel filtration column Superdex 75 10/300 was calibrated with 500 μL of a low molecular weight calibration kit. (A) The absorption was measured at 280 nm. Peaks are representative for Blue dextran 2000 (2 MDa, Peak 1), Conalbumin (75 kDa, Peak 2), Ovalbumin (43 kDa, Peak 3), Carbonic anhydrase (29 kDa, Peak 4), Ribonuclease A (13.7 kDa Peak 5), and Aprotinin (6.5 kDa, Peak 6). (B) Logarithm of molecular mass was plotted against the elution volume of the peaks enabling a linear regression with R^2 of 0.997.

Table 16: Protein molecular weight of the standard calibration kit for low molecular weight applied to the Superdex 75 30/100 column.

Protein	Molecular weight [kDa]
Blue Dextran	= Running front
Coalbumin	75
Ovalbumin	44
Carbonic Anhydrase	29
Ribonuclease A	13.7
Aprotinin	6.5

5.2.2.6.4 Mass spectrometry

In order to determine the exact molecular weight of the primary intermediates of Gag processing, 750 μ L sample of the POI 32 μ M was processed according to the protocol (5.2.2.5) and applied afterward as 500 μ L to a Superdex 75 300/10 column equilibrated in processing buffer without TX-100. All distinguishable peaks were taken as fractions and analyzed by intact protein mass spectrometry performed by the Core Facility for Mass Spectrometry and Proteomics (CFMP) at the Ruprecht Karl University of Heidelberg.

For measurement, the sample was applied to a POROS 10R1 column equilibrated in 0.3 % formic acid (= mass spec buffer A). With isocratic gradient to 50 % of mass spec buffer B (80 % isopropanol, 10 % acetonitrile, and 0.3 % formic acid). Eluted fractions were immediately measured in a maXis mass spectrometer. The analysis was performed in Data Analysis 4.2 (Bruker) and ESI Compass 1.3 Maximum Entropy Deconvolution Option. Masses of dominant present proteins or peptides were compared to possible partial peptide sequences of the full-length protein with the help of the Protein Calculator (<http://protcalc.sourceforge.net/>).

5.2.2.6.5 Quantitative analysis of Coomassie-stained Tricine-PAGE

For the quantitative analysis of stained Tricine-PAGEs, the image file was first cut into shape and background was subtracted with IMAGE J (Figure 10 upper lane). A signal mask was then generated by pixel classification with ilastik and used for signal analysis with IMAGE J (Figure 10 right lane). Each signal was multiplied with the ratio of the sum of measured signals at the initial time point without processing and the sum signals of the signal's time point. With this, the sum of signals at each time point was set to the same value. Afterward, all protein signals were divided by the number of containing amino acids responsible for the Coomassie staining plus one for the N-terminal amino group. Residues of tyrosine, histidine, lysine, and arginine bind Coomassie (de Moreno, et al., 1986). The resulting values were subsequently divided by the signal of the original uncleaved protein at the time point = 0. Finally, these

results indicated the changes in concentration of uncleaved protein, intermediates, and products over time (Figure 10 Protein concentrations). In order to calculate the amount of a specific unprocessed cleavage site, the signals of proteins containing the uncleaved site at each time point were summarized (Figure 10 bottom lane).

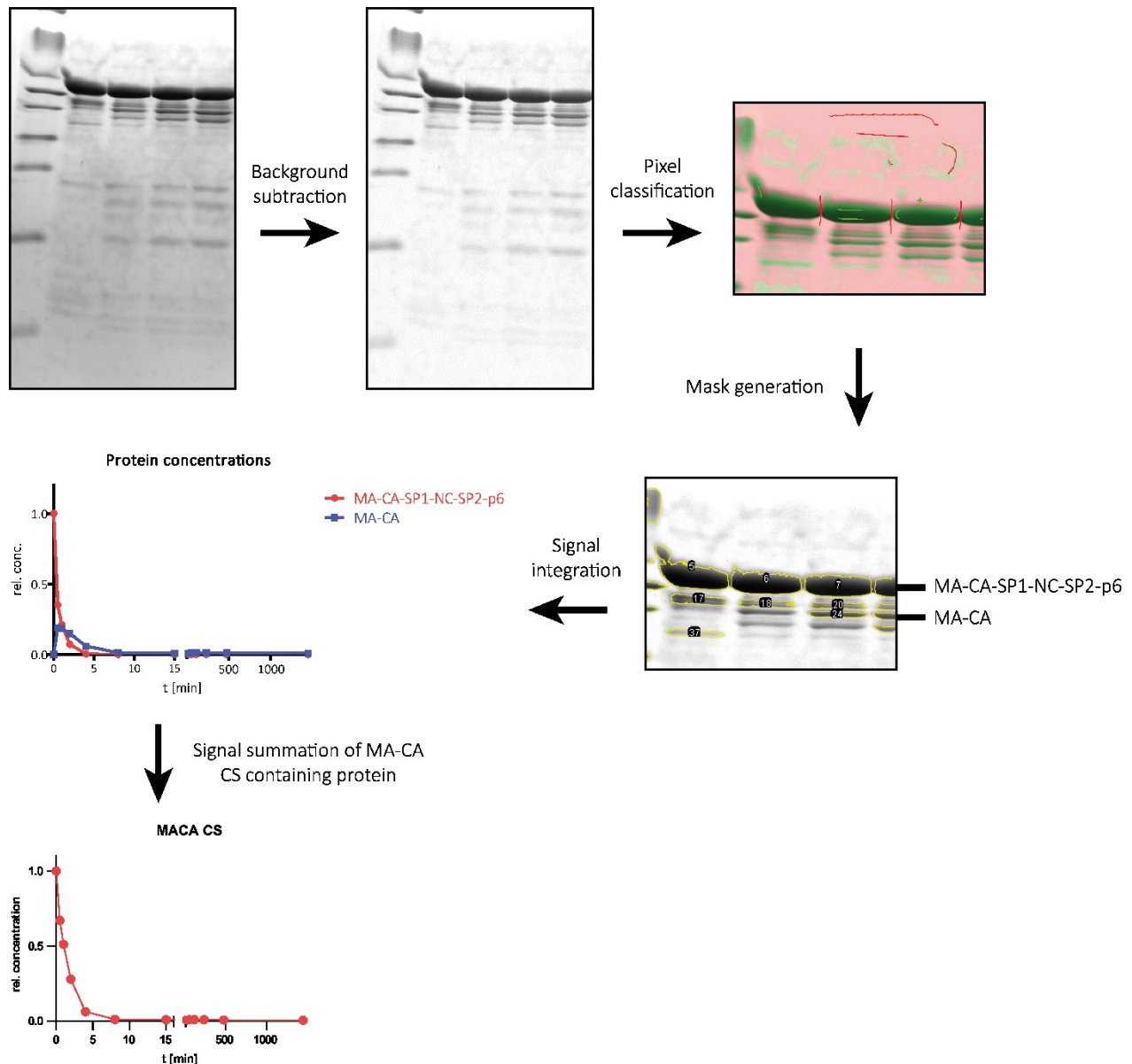


Figure 10: Simplified schedule of the quantitative analysis of processing samples with Coomassie-stained Tricine-PAGEs. Processing samples taken in experiments as described in 5.2.2.5 were applied to Tricine-PAGEs (16 % PAA, crosslinking ratio 1:32 BAA/AA and 9.6 % PAA, 1:32 BAA/AA). The resulting gels were stained by Coomassie G-250 and recorded by an infrared scanner (LiCor Odyssey Imager CLx) at 700 nm excitation (upper-left). With the help of IMAGE J, the background of the image was subtracted (upper-mid), and the signal mask was generated with ilastik by pixel classification (right lane). Based on this, the temporal changes in concentrations of uncleaved protein, intermediates or products (middle-left) and the concentration of uncleaved CS were calculated (bottom lane). As an example, only partial gels, as well as the analysis for the proteins MA-CA-SP1-NC-SP2-p6 and MA-CA and the uncleaved cleavage site MA-CA, are shown.

6 Results

6.1 Establishment of a purification method for recombinant Gag and its characterization

The proteolytic maturation of Gag was targeted in a plethora of previous research studies. Since the viral particles are asynchronously produced, the tracking of maturation has not been achieved yet. The introduction of PR deactivating mutation or protease inhibitors (PI) enabled at least partially an induction of maturation by artificial addition of recombinant PR (Müller, et al., 2009) or elution of the PIs from viral particles (Mattei, et al., 2014), respectively. However, these techniques still cannot analyze the processing in full detail, due to intrinsic interference factors and reduced precision of the analysis tools, immunoblots. To this day, *in vitro* translated Gag processed by recombinant PR (Erickson-Viitanen, et al., 1989; Pettit, et al., 1994) is the basis for our knowledge about the proteolytic maturation. However, these experiments were not performed under clearly defined conditions as the NA content and without correlation to the oligomeric state of Gag. The studies did not cover in high detail the processing in a quantitative manner, regarding the comprehensive detection of potential intermediates and the time-schedule (Pettit, et al., 1994; Ning, et al., 2016). Furthermore, no research has yet analyzed processing in full detail regarding the analysis of intermediates, products, assembly state, and other factors on a quantitative level.

This thesis aimed to characterize the processing of Gag as close as possible to its natural state in viral particles and track the concentration of unprocessed cleavage sites as well as processing intermediates and products over time. Therefore, the first prerequisite was to purify Gag in high yields and purity. There are two Gag derivatives that were used in former publications for the biochemical analysis of Gag and *in vitro* assembly, the Δ MACANCSP2 and Gag carrying a C-terminal His-Tag (Gag-His).

Due to its efficient assembly, the truncated version of Gag, Δ MACANCSP2 (Gross, et al., 2000), is most commonly used in literature, and our lab already established a high yield purity protocol. In 2014, McKinstry developed the first high-efficiency protocol for the purification of full-length Gag-His (McKinstry, et al., 2014). Unspecific binding of two zinc-finger motifs in NC to any NA results in aggregation and oligomerization of Gag. Because this would reduce purification yields and interfere with our subsequent processing analysis, any NA needed to be strictly avoided. The cited publication targeted this issue by adding benzonase during the purification but did not include clear evidence for the removal of NA below the detection limit in addressed Gag samples. Thus, the given protocol for purification needed to be further optimized.

For optimal expression and production in bacteria, the full-length Gag coding sequence with a C-terminal His-tag was cloned codon-optimized for production in *E. coli* into the bacterial expression vector with a C-terminal His-tag (= Gag-His; 5.1.7). The production was performed in transformed *E. coli* BL21 by induction with IPTG (5.2.2.1 and Figure 11 B + C). The production of Gag-His was not fully suppressed without IPTG, because of the already present translated Gag-His in small amounts of the starting culture (Figure 11 B + C SC) and at point of induction (Figure 11 B + C lane 0 h), which was ~ 10 – 15 % compared to the later yield of Gag-his after induction. However, the mass expression was achieved after IPTG addition in the

following hours (Figure 11 B + C lanes 1, 2, and 3 h). Because the signal for Gag-His on the immunoblot at 1, 2, and 3 h was almost of the same intensity, the maximum concentration of Gag-His per cell was achieved already within 1 h, post induction, the total yield of cells in culture, measured by OD_{600} , was steadily increasing up to 3 – 4 hours (Figure 11 A). In order to reduce the amount of Gag-His degraded by bacterial proteases, the expressing culture was grown to a maximum of 1.9 – 2.1 g/L. Besides Gag, a variety of degradation products at lower concentrations was present in the bacterial cells, as shown by immunoblots (Figure 11 C). These, however, were present in sufficiently low amounts < 5 %, according to the signal intensity calculated by Image Studio Lite.

The cell lysis was achieved with high efficiency by a cell microfluidizer. According to the analysis of the purification by SDS-PAGE (Figure 11 D) and immunoblot (Figure 11 E), the solubilized fraction after cell lysis (Figure 11 D + E lane S1) contained the same pattern and intensity of proteins compared to the cell pellet before lysis (Figure 11 D + E lane PC). The cell debris and insoluble proteins (Figure 11 D + E lane P1), however, contained only minor concentrations of Gag-His. Gag-His was precipitated in final concentration of 45 % ammonium sulfate and centrifuged, which gave the best separation between Gag-His and major contaminations of bacterial proteins. The remaining supernatant solution (Figure 11 D + E lane S2) contained only other proteins, but not Gag-His. The pellets after centrifugation were quite unstable and needed to be handled carefully to prevent any loss during decantation. The protein was brought back into solution (Figure 11 D + E lane S3) by repeated shaking in an appropriate buffer for the following purification step. The last centrifugation step removed precipitated remaining protein (Figure 11 D + E lane P3). The analysis of the insoluble pellets showed a similar composition compared to the supernatant, but the loss of Gag due to decreased solubility was less than 1 %, according to signal quantitation.

The supernatant was then applied to a HisTrap column where Gag is bound specifically to the resin, and major contaminations by other proteins as well as truncated versions of Gag were eluted in the flow-through (Figure 11 D + E lane FT; Figure 11 F blue and red line). Subsequent to a washing step, Gag was eluted by a linear gradient of imidazole (Figure 11 F green line). After several runs, the purification conditions, mentioned in chapter 5.2.2.2, achieved the best results regarding the concentration and purity of the eluted protein (Figure 11 D + E lanes F1 – F4). Since protein concentrations of above 5 mg/mL led to irreversible precipitation of Gag, the elution step was designed to result in protein samples of lower concentration but more than 1.8 mg/mL, which was necessary for the following experiments. As quantified by signal intensity, Coomassie-stained SDS-PAGE and immunoblots displayed a purity of > 95 % for purified Gag-His WT after final dialysis in storage buffer (Figure 11 D + E lanes I, II, and III). The remaining contaminations were composed of mainly truncated Gag, as indicated by protein bands of lower mass than Gag-His, which were detected by Coomassie-stain and CA specific antiserum. The total yield of Gag-His ranged in different purifications around 12 – 16 mg/L of bacterial culture, while the purified Gag yield in comparison to the yield after production in *E. coli* was ~ 80 % (Table 17).

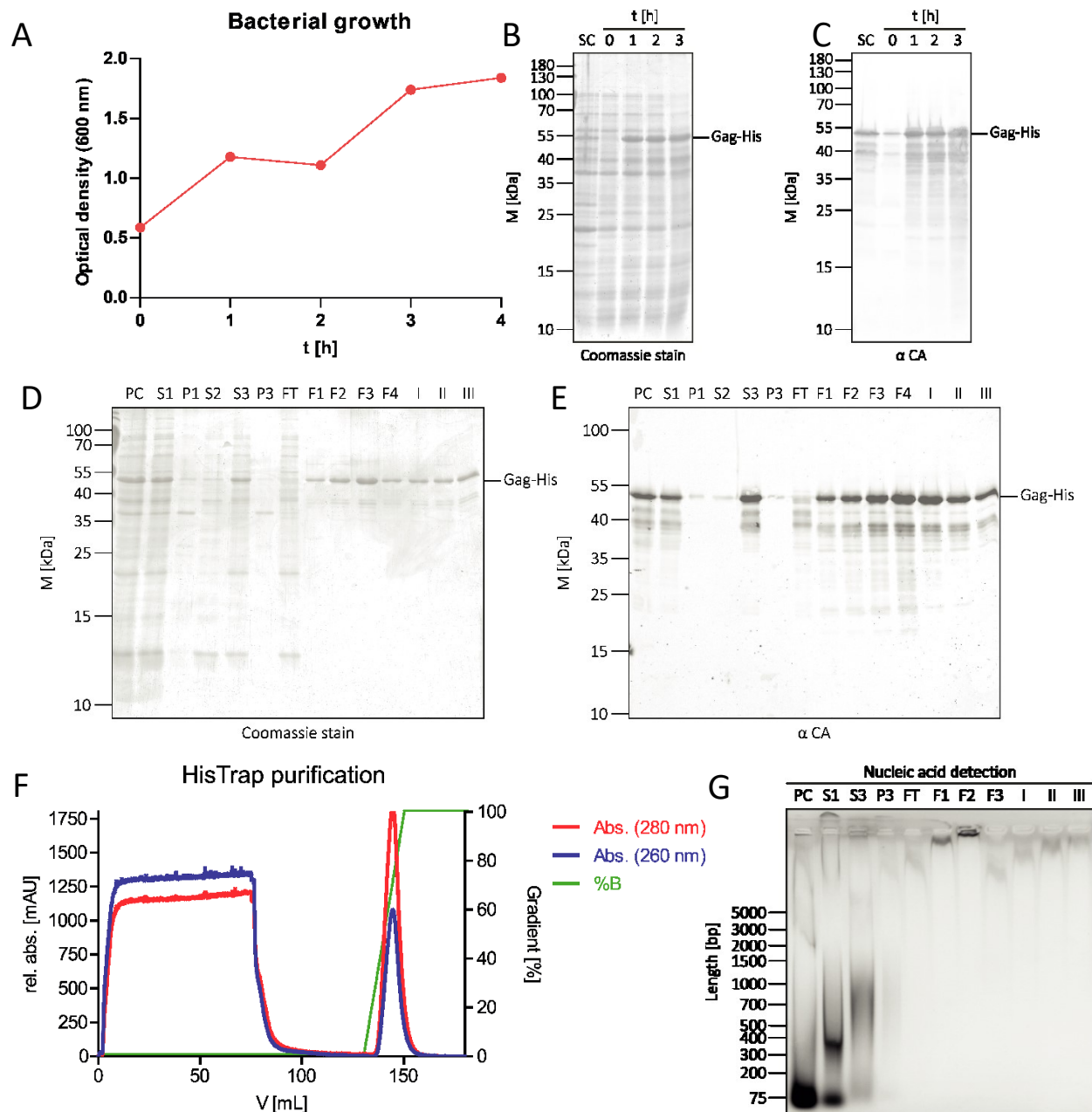


Figure 11: Production and IMAC-purification of Gag-His. A starter culture (SC) of *E. coli* BL21 (DE3) transformed with plasmid pET28a(+) was diluted in 4 L LB-medium to OD₆₀₀ 0.1 and induced at an OD₆₀₀ of 0.6 using 1 mM IPTG. The culture was incubated at 37 °C and 150 rpm. Samples were taken at the indicated times post induction and analyzed for their optical density at 600 nm. Cell pellets (0 – 3 h) were lysed in SDS sample buffer (A, B). Lysate (PC) from *E. coli* BL21 (DE3) cells expressing Gag-His protein was prepared and subjected to precipitations with 0.14 % PEI as described in materials and methods. The resulting pellet (P1) was removed, and the supernatant (S1) was precipitated with 45 % (NH₄)₂SO₄. After centrifugation, the new supernatant was removed (S2), and the pellet (P2) resolved. The remaining precipitate (P3) was removed by centrifugation. The remaining supernatant (S3) was further purified over a 5 mL HisTrap FF column. Flow-through (FT) did not contain the major yield of Gag-His. Elution was performed with an imidazole step gradient. Fractions (F1 – F4) of the elution were pooled and dialyzed overnight at 4 °C in storage buffer (I – III). Samples from the purification were analyzed for nucleic content by agarose gel electrophoresis (G; 1 % agarose) or by SDS-PAGE (17.5 % PAA, 1:200 AA/BAA) followed by Coomassie G-250 staining (B, D) or immunoblot using polyclonal antiserum raised against CA (C, E). Positions of molecular mass standards marker are shown left, and the position of the Gag-His variants is indicated at the right. (F) Absorption of the eluate from the HisTrap column was measured at 280 (red line) and 260 nm (blue line). The relative concentration of the imidazole is depicted as % buffer B (green line).

Table 17: Efficiency of single Gag purification steps. The purification of Gag contained several steps. In this table, the total protein concentration was measured by a colorimetric protein quantitation assay, Gag concentration, the sample volume, total Gag amount and the remaining yield of Gag normalized to the initial are listed as percentage values according to signal analysis of immunoblots signals by Image Studio Lite. After the production of Gag-His WT in *E. coli* BL21 cells (Cell pellet), the lysis was performed and centrifuged. The supernatant yielding Gag (Cell lysis) was treated with $(\text{NH}_4)_2\text{SO}_4$ for precipitation of Gag-His. After centrifugation, the new supernatant was removed, and the pellet resolved. The remaining precipitate was removed by centrifugation. The remaining supernatant (Precipitation) was further purified over a HisTrap column. Subsequent to the elution, the Gag containing fractions (HisTrap) were dialyzed in storage buffer (Dialysis) as the final purification step.

Purification step	Total protein [mg]	Gag concentration [mg/L]	Volume [mL]	Total Gag amount [mg]	Remaining Gag yield [%]
Cell pellet	x	0.668	80	53.4	100
Cell lysis	212.3	0.679	73.2	49.7	93
Precipitation	192.7	0.568	80	45.4	85
HisTrap	43.68	1.56	28	43.8	82
Dialysis	42.36	1.19	35.6	42.2	79

The main challenge during the establishment of the purification protocol was to ensure the complete removal of NAs in the product, to prevent any preliminary aggregation or assembly. In order to tackle this problem, methods from different publications (McKinstry, et al., 2014; Tanwar, et al., 2017; Bewley, et al., 2017) were applied in combination to the lysed solution after production and yielded a NA-free Gag protein after purification (Figure 11 G). DNase I and benzonase were added for the degradation of NA (Figure 11 G lane NA) strands after cell lysis. Remaining non-degraded NA was precipitated with PEI, which reduced the NA amount (Figure 11 G lane S1) compared to the initial NA yield of the cell pellet (Figure 11 G lane PC). During further purification steps (Figure 11 G lanes S3, F1, F2, and F3), the NA concentration is continuously decreased, until the degree was further reduced below the detection limit of agarose gels and absorption at 260 nm (Figure 11 G lanes I, II, and III). The ratio of absorption at 260 nm and 280 nm was lower than 0.6 for final protein samples, which implies no detectable traces of NA after the purification.

As described in 4.3.1, a truncated Gag version ($\Delta\text{MACANCSP2}$) features in solution a mono-/dimeric equilibrium of a high dissociation constant of 5.5 μM proven by light scattering (Datta, et al., 2007b). This thesis aimed to analyze the processing of Gag in an assembled pattern as well as monomeric state. To determine if the purified Gag-His WT protein displays a dimerization state in solution at concentrations of 1.8 mg/mL (= $\sim 30 \mu\text{M}$) and higher, the dissociation constant needed to be evaluated; thus, an size exclusion based assay was established for Gag-His to prove that the dissociation constant of the purified Gag-His had similar value with the truncated Gag version (5.5 μM). Therefore, Gag-His WT was applied as 500 μL samples of different concentrations (50, 5.5, 4, 2, and 0.5 μM) to a gel filtration column Superdex 200 16/60 PG with a 500 μL sample loop. The running agent was the Gag-His storage buffer. The peak maximum at 214 nm absorption of Gag-His fraction shifted with higher concentrations to a lower elution volume (Figure 12 A). One peak, which represented the mono-/dimeric equilibrium, was detected instead of one peak for the monomer and one for the dimer, indicating that the dissociation and dimerization reaction of Gag-His was occurring quite fast. Thus, a low elution volume is implicating a higher yield of Gag-His dimers compared to lower concentrations.

In order to check for the reversibility of the dimerization reaction, the eluted sample of 5.5 μM was applied to gel filtration, where it was diluted due to the process. This diluted sample was concentrated by a centrifugal filter (MWCO: 30 kDa) and reapplied to the column at 4 μM . The elution volume of the re-concentrated sample was similar as for the initial sample, while the diluted sample (0.5 μM) revealed a higher elution volume (Figure 12 A; blue, green, and purple line).

With the results of different concentrations of Gag applied to gel filtration, a sigmoidal fitting was performed on the elution volume of Gag at different concentrations (Figure 12 B), as explained in chapter 5.2.2.6.3. From this fit, the calculated dissociation constant (K_d) was derived to be $\sim 8.3 \mu\text{M}$ (Figure 12 B green triangle). As high concentrations ($> 20 \mu\text{M}$) are needed for the following experiments (assembly and processing) with Gag-His, the protein is consequently mainly present as a homodimer. Because this project targets the processing analysis of Gag in different multimerization states including fully monomeric Gag, a mutant for Gag-His carrying a double mutation at the dimerization site of CA (W184A M185A) was introduced (= Gag-His WM) and also purified according to the before-mentioned protocol. The K_d of this mutant was shown to be 100-fold higher at 0.53 mM (Datta, et al., 2007b). With the purification of Gag-His WT and Gag-His WM in high yield and purity, a comparison of processing monomeric and dimeric Gag could be performed. The results of these experiments and the assembled protein are described in chapters 6.4.2 and 6.4.2, respectively.

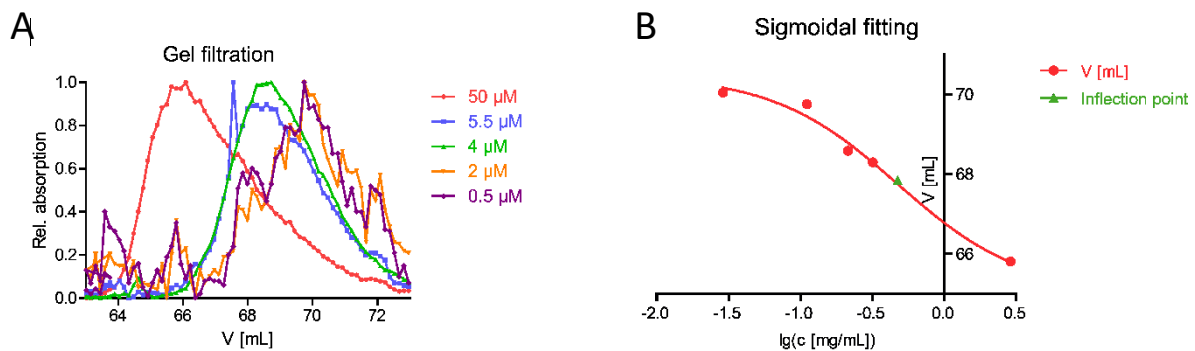


Figure 12: Analysis of Gag dimerization by gel filtration. Purified Gag-His WT was applied in 500 μL storage buffer to a Superdex 200 16/60 PG gel filtration column at different concentrations. For control, absorption was measured at 280 nm (aromatic residues) and 214 nm (peptide bond). (A) The absorption at 214 nm of Gag-His WT solutions of 50 μM (red), 5.5 μM (blue), 4 μM (green), 2 μM (orange), and 0.5 μM (purple) is plotted against the volume. The peak maximum (= elution volume) is shifted to a higher volume with a lower concentration. (B) The maxima of running peaks (red) were plotted against the log of their concentrations. The inflection point of the sigmoidal fit (green) indicates the K_d of Gag-His.

6.2 Efficient assembly of stable virus-like particles

In order to compare the processing of Gag-His as mono- or dimer with assembled Gag, two different approaches are possible. The first approach is to purify immature virus-like particles (VLP) from eukaryotic cells expressing HIV-1 particles carrying a deficient protease (PR), which are later treated with purified active PR (Konvalinka, et al., 1995). However, contaminations, the confounding factors such as the viral envelope, other viral proteins, and a mixture of different NAs can substantially influence the processing. Furthermore, the purification of viral particles usually results in lower concentrations of Gag than needed for later experiments ($> 20 \mu\text{M}$). The second option is to assemble recombinant Gag *in vitro* (Gross, et al., 2000) by the addition of NA in specific buffers. Consequently, the processing can be accomplished with the highly pure protein under defined parameters such as the type and amount of applied NA. Due to the ability to avoid confounding factors, the latter method was chosen to be used for the processing analysis of assembled Gag.

Previously, a protocol for the assembly of $\Delta\text{MACANCSP2}$ was established, enabling a highly reproducible system for morphological analyses by TEM (Schur, et al., 2016; Gross, et al., 2000). The assembly was performed by dialysis of purified protein against 50 mM HEPES, pH 8.0, 100 mM NaCl, 1 mM EDTA and 1 mM TCEP after addition of 4 % deoxyoligonucleotide of minimum 20 nucleotides length. In this work, first assembly reactions were performed with an oligonucleotide of 25 adenosines, according to a former publication (Munro, et al., 2014).

The described buffer conditions were used as a starting point for *in vitro* assembly experiments with purified Gag-His WT protein. However, this was not sufficient to trigger an assembly reaction for the full-length Gag at a concentration of 1.8 mg/mL. Due to the transition of solubilized protein into particles in suspension, the assembly of $\Delta\text{MACANCSP2}$ caused slight turbidity detectable by eye, which is a common indicator for assembly. Gag-His, on the other hand, stayed in solution, as there was no pelletable fraction, and no turbidity appeared. With TEM, spherical particles could be detected for $\Delta\text{MACANCSP2}$ (Figure 13 D). In the case of Gag-His, the analysis did not reveal any detectable structures.

In order to achieve the assembly of Gag-His, certain parameters had to be optimized: Gag concentration, NA length, NaCl concentration etc.. While a low concentration of $\Delta\text{MACANCSP2}$ of 2 μM (Munro, et al., 2014) can achieve an assembly, most commonly recommended and used are higher concentrations than the dissociation constant for Gag dimerization (Datta, et al., 2007; Datta, et al., 2017; Gross, et al., 2000; Schur, et al., 2016). Hence, the concentration used before ($\sim 30 \mu\text{M}$) would be high enough, thus no lower concentration was tested. A high pH (8.0) favors the immature form of CA and lower pH (6.0) the mature (Gross, et al., 2000). Because of this, no other pH was applied to the assembly experiments of this work, even though there is a protocol for immature assembly of $\Delta\text{MACANCSP2}$ at pH 6.0 (Ning, et al., 2016).

As mentioned in 4.3.1, it was recently shown that inositol hexakisphosphate (IP6) is an essential cofactor for HIV-1 Gag assembly efficiency and particle stability (Dick, et al., 2012). To improve the assembly rate, IP6 was added to the following assembly experiments, where it was applied in a range between 0.1 to 10 μM based on the literature (Munro, et al., 2014; Tanwar, et al., 2017; Dick, et al., 2018). The concentration range of 0.1 – 3 μM IP6 in the reaction yielded $\Delta\text{MACANCSP2}$ to assemble with uniform

shape and size shown by negative-stained TEM images (Figure 13 C). Gag-His WT, however, was still not assembled according to TEM, and no turbidity was detected. The presence of IP6 of more than 3 μ M during assembly resulted in Gag-His WT precipitation, which could not be resuspended. The insolubility indicated that the precipitate was not consisting of assembled particles but rather of damaged or denatured protein. Based on these results, 0.3 μ M IP6 was used to the following experiments for assembly, to prevent irreversible precipitation of Gag-His.

Commonly, purified Gag proteins are stored at concentrations of 500 – 1000 mM NaCl (Datta, et al., 2017; McKinstry, et al., 2014; Schur, et al., 2016), which prevents protein-protein interactions (Dumetz, et al., 2007), to prevent the induction of an preliminary assembly reaction. According to different publications, assembly of Δ MACANCSP2 is initiated by the change of buffer conditions to low NaCl concentrations (< 300 mM) and the addition of NA. Oligonucleotides used for assembly consisted of RNA, as yeast tRNA (reviewed in Datta, et al., 2017), or single-stranded DNA with 25 nt (Munro, et al., 2014), 73 nt (Schur, et al., 2016), or 92 nt (Gross, et al., 2000). As described in 4.3.3, NC of Gag is, in principle, capable of binding any NA, for which reason I also tested an oligonucleotide of 68 nucleotides (referred to as “standard oligonucleotide for assembly”). This oligonucleotide included all four types of bases and was chosen based on results in the former work of our laboratory that a length of \sim 70 nucleotides works optimally for assembly. The concentrations of NaCl reported to be used in the assembly of Δ MACANCSP2 varied between \sim 50 mM (Ning, et al., 2016) and 100 mM (Gross, et al., 2000; Schur, et al., 2016; Wagner, et al., 2016).

For the purpose of assembling Gag-His WT with the standard oligonucleotide for assembly, NaCl concentrations of 0, 50, 100, 150, 200, 250, or 300 mM were tested. However, Gag-His WT was assembled only in \sim 20 % of the cases at 200 mM NaCl, which yielded particles on the negative-stained TEM images (Figure 13 A + B). Preparations displayed two different populations regarding the particle size. More than 60 % of the particles had a diameter of 90 – 110 nm ($n = 14$), while the remaining particles were of \sim 60 nm ($n = 12$). This assembly, however, was not reproducible, preventing further analyses.

In contrast to the full-length Gag, Δ MACANCSP2 assembled reproducibly and formed uniform particles in the presence and absence of IP6 (Figure 13 C). The diameter of the particles ranged from \sim 80 nm up to 130 nm with a mean of 98 ± 14 nm (Figure 13 D), and they were mainly dispersed or sticking as small aggregates together (Figure 13 E, F, G, and H). Centrifuging those particles revealed that the percental yield of protein bound in particles after assembly was \sim 20 %, according to the determination of protein content with a colorimetric protein quantitation assay. Based on the results of former work on the assembly of Δ MACANCSP2 in this laboratory, it is known that 20 % of methanol induces the assembly reaction to higher efficacy. Introducing 20 % methanol to the assembly buffers, increased the assembly yield substantially to > 90 % of proteins bound in particles (Table 18), as determined by the protein content of the centrifugable fraction. However, experimental setups with Gag-His, including different concentrations of methanol (10, 20, 30, 40, and 50 %), did not achieve an assembly. With increasing methanol concentration, the amount of precipitated protein, as observed in the presence of high IP6 concentrations, was increasing, and the precipitate was not solubilizable.

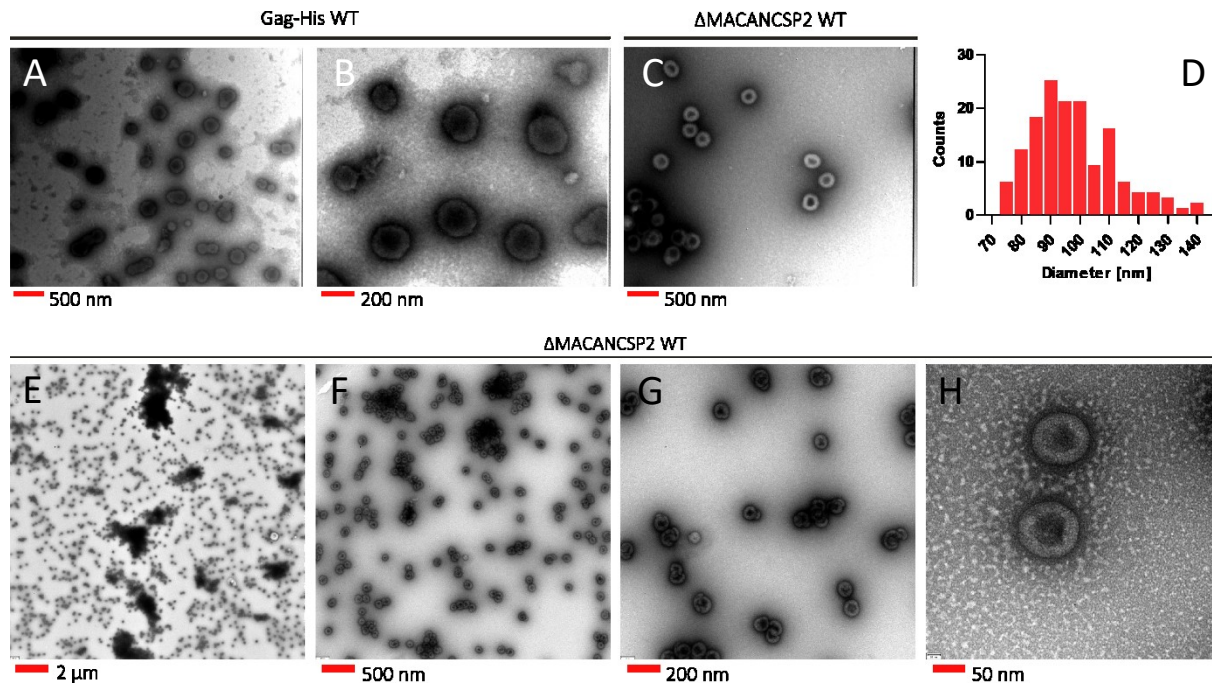


Figure 13: Visualization of *in vitro* assembled Gag-His WT and Δ MACANCSP2 WT by TEM. Samples of recombinant purified Gag-His WT (A, B) and Δ MACANCSP2 WT (C, E, F, G, H) were assembled *in vitro* by dialysis in assembly buffer (50 mM HEPES, pH 8.0, 200 mM NaCl, 1 mM EDTA, 1 mM TCEP, 20 % methanol) in presence of 0.3 μ M (A, B, C) or 60 μ M (E, F, G, H) IP6, 4 % standard oligonucleotide for assembly (5.1.7) at 4 °C. The resulting particles were analyzed by TEM with negative staining of 3 % uranyl acetate. Different magnifications show the spatial and size distribution of the particles of the assembled protein. The scale bars (red) depict indicated sizes (500, 200, 100, 80, and 20 nm). (D) Analyzed particles of three experiments with assembled Δ MACANCSP2 WT are plotted according to their diameter in a histogram. The protein assembled reproducibly in comparable size distributions among the different experiments and showed a mean size of 90 – 100 nm ($n = 148$).

Several different conditions were tested to assemble the self-purified Gag-His protein, however, without achieving efficient and reproducible assembly. Therefore, I decided to perform further assembly experiments only with Δ MACANCSP2. Additionally, as Δ MACANCSP2 is capable of assembling in a high percentage, all following experiments for processing of *in vitro* assembled protein were performed with Δ MACANCSP2.

After reaching a high yield assembly of Δ MACANCSP2, the particles needed to be transferred into the buffer optimized for processing experiments (5.2.2.5; processing buffer = 100 mM MES, pH 6.0, 150 mM NaCl, 0.02 % TX-100, 1 mM DTT). The buffer conditions are based on the fact that HIV-1 PR was shown to be most active *in vitro* at pH 5.0 – 6.0 and inactive at pH 8.0, which was determined with processing of synthetic peptides representing Gag CS (Tamburini, et al., 1990; Cheng, et al., 1990; Ido, et al., 1991). For rebuffing, the particles would be dialyzed or purified by suitable gel filtration related systems. To roughly analyze the stability of assembled Δ MACANCSP2, particles were spun down after assembly and resuspended in indicated buffers (Table 18). Subsequently, the amount of solubilized protein and protein bound in particles was determined by separation of both fractions by centrifugation.

Table 18: Solubilizing effect of different buffer conditions on assembled Δ MACANCSP2 WT. Recombinant purified Δ MACANCSP2 WT was assembled in the presence of 4 % standard oligonucleotide for assembly with or without 0.3 μ M IP6. Resulting samples of assembled protein were centrifuged. Pelleted particles were resuspended in different compositions of assembly or processing buffer (AB and PB, respectively) and were centrifuged again to separate the fractions of solubilized protein and protein bound in particles of the resuspended sample. Their concentrations were determined by a colorimetric protein quantitation assay (5.2.2.6.1). The percental values represent the amount of protein solubilized after resuspension or of protein, which remained in the pelletable fraction. (AB: 50 mM HEPES, pH 8.0, 200 mM NaCl, 1 mM EDTA, 1 mM TCEP, 20 % methanol, 0 – 120 μ M IP6; PB: 100 mM MES, pH 6.0, 150 mM NaCl, 1 mM DTT, 0.02 % (v/v) TX-100)

Buffer	Solubilized [%]	Pelleted [%]
Assembly buffer	4	96
Assembly buffer + TX-100	15	85
Processing buffer pH 6.0	80	20
Processing buffer – TX-100	69	31
Processing buffer pH 8.0	39	61
Processing buffer pH 6.0 + 0.3 μ M IP6	82	18

As \sim 80 % of Δ MACANCSP2 particles were dissolved during resuspension in PB, different conditions were tested to determine the leading critical cause of disassembly in the PB. The rebuffing in AB caused only minimal solubilization (4 %). Additionally, the presence of 0.02 % of TX-100 in AB (Table 18) only reduced the percentage of assembled protein from 96 % to 85 %. In contrast, PB without TX-100 reduced disassembling properties of PB only slightly. While the addition of 0.3 μ M IP6 (Table 18) had no detectable effect on the stability of assembled Δ MACANCSP2 in PB, the pH shift from 8.0 to 6.0 was shown to be the leading cause of disassembly (Table 18). Resuspending assembled Δ MACANCSP2 in PB at pH 8.0 tripled the percentage of protein bound in particles to \sim 60 % compared to PB at pH 6.0 with 20 % assembled protein.

Although particles showed to be more stable in PB with a pH of 8.0, this high pH is not suitable for processing experiments, because PR activity is extremely low above pH 7.5. Recent research by Dick *et al.* (2018) using CA and CANC revealed that high concentrations of IP6 of 10 μ M or more boosted assembly efficiency for immature particles. Therefore, higher IP6 concentrations were tested in order to compensate for low particle stability at a pH of 6.0. The absence as well different concentration of IP6 ranging between the minimum concentration 0.3 μ M used previously (Munro, et al., 2014) and the maximum concentration of 60 μ M which is approximately the concentration found in natural T-helper cells (Bunce, et al., 1993) were applied in the PB buffer.

Without IP6, the amount of resolubilized protein after resuspension was similar to before at \sim 80 % (Table 19). In the presence of 0.3 and 3 μ M, this yield was reduced to \sim 60 – 70 %. Only with 60 μ M IP6, which equates to the Gag-IP6 ratio of 1:1, the percentage of Δ MACANCSP2 bound in particles stayed at \sim 80 % after resuspension. This yield was not further increased with higher concentrations of IP6 but was instead leading to fewer morphologically correct particles or a higher yield of actual precipitates. Based on this

result, following assembly and processing experiments using *in vitro* assembled Δ MACANCSP2 or purified VLPs contained 60 μ M IP6 in all used buffers.

Table 19: Fraction of assembled Gag dependent on higher IP6 concentration. Recombinant purified Δ MACANCSP2 WT was assembled in the presence of 4 % standard oligonucleotide for assembly with 0 – 60 μ M IP6. Subsequently, the samples were centrifuged, and the pelleted particles were resuspended in processing buffer (5.2.2.5). By another centrifugation step, the fraction of solubilized protein and particles still in suspension were separated and their concentrations were determined by a colorimetric protein quantitation assay (5.2.2.6.1). The percental values represent the amount of protein solubilized after resuspension or of protein, which remained in the pelletable fraction. (PB: 100 mM MES, pH 6.0, 150 mM NaCl, 1 mM DTT, 0.02 % (v/v) TX-100)

IP6 [μ M]	Molar ratio (Gag: IP6)	Solubilized [%]	Pelleted [%]
0	1:0	81	19
0.3	190:1	69	31
3	19:1	64	36
60	1:1	20	80

In order to remove disassembled Δ MACANCSP2 derived by rebuffering in PB, including 60 μ M IP6, a purification by Capto Core 700 was tested. This column is based on core beads, which work with the same principle as beads in gel filtration but are furthermore functionalized. These beads have a molecular weight cut off of 700 kDa. The inside of the particles is multimodally functionalized. The beads contain hydrophobic and positively charged ligands and bind proteins in a variety of conditions. By using these columns, soluble proteins could be removed from the sample. After equilibration of the column in PB + 60 μ M IP6, 200 μ L of assembled Δ MACANCSP2 were applied to the column. The major amount of protein was present in the flow-through of the column (Figure 14 A). During the cleaning of the column, a small fraction of Δ MACANCSP2 was eluted, too. According to the Coomassie-stained SDS-PAGE (Figure 14 B) and the immunoblot with CA antibodies (Figure 14 C), the sample of peak 1 (Figure 14 A; P1) contained Δ MACANCSP2 with the same purity as the non-purified assembled sample (Figure 14 B+ C; 0). The protein bound to the column contained small traces of Δ MACANCSP2 (Figure 14 A; P2). Even though the resulting sample of P1 showed correctly shaped particles in TEM analysis, only 66 % of Δ MACANCSP2 was bound in pelletable material, which was determined by centrifugation and measuring of the protein content in the supernatant as well as in the pellet. With the application of dialysis for rebuffering in PB with 60 μ M IP6 instead of Capto Core, the proportion of protein bound in pelletable material was, however, higher. According to the measurement of protein content with a colorimetric protein quantitation assay after centrifugation, more than 80 % of Δ MACANCSP2 was still assembled, which is \sim 14 % more compared to the usage of Capto Core. Confirmed by Coomassie-stained SDS-PAGE, the assembled fraction contained full-length Δ MACANCSP2 in high purity (Figure 16 C). Since the dialysis achieved better results, it was applied in future experiments for the rebuffering of assembled Δ MACANCSP2 in PB. The optimization of assembly and particle stability in combination with the established system to transfer particles from assembly conditions to the processing buffer were consequently suitable to prepare particles for the

following experiments, which focus on the comparison in processing between non-assembled and assembled protein.

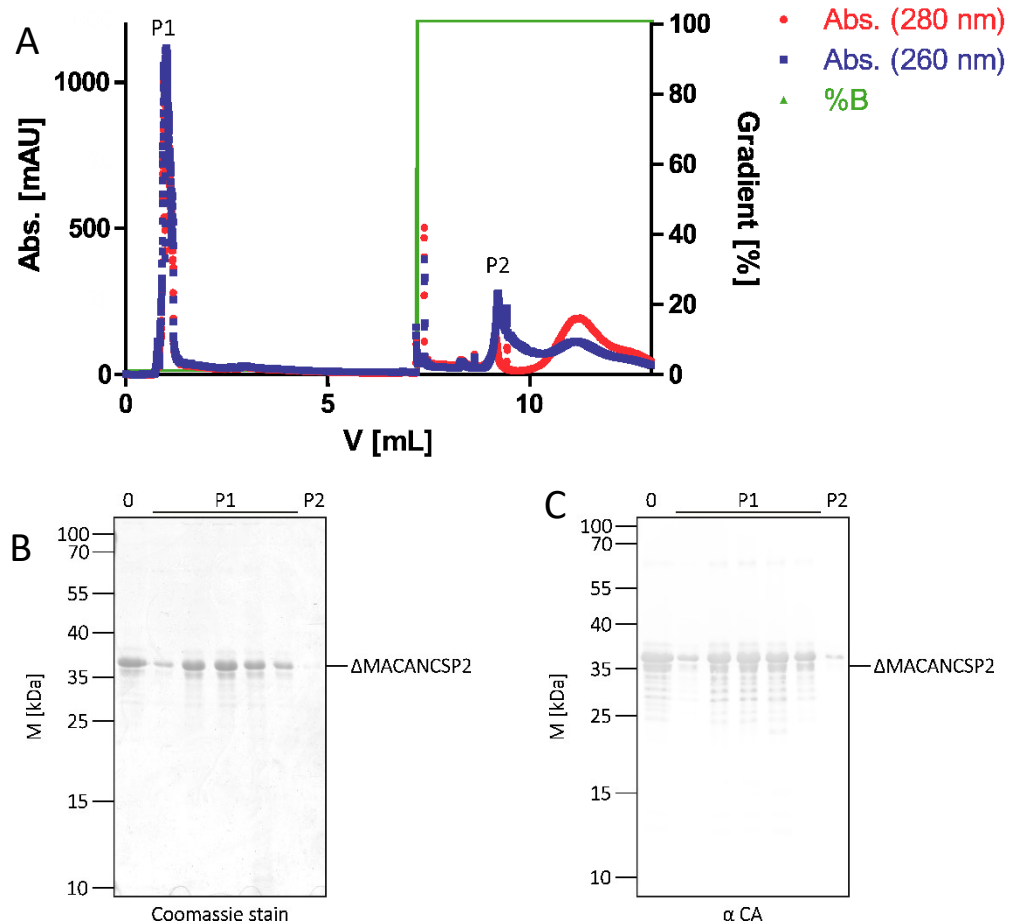


Figure 14: Capto Core purification of *in vitro* assembled Δ MACANCSP2. Recombinant purified Δ MACANCSP2 was *in vitro* assembled according to the protocol (5.2.2.4) with the standard oligonucleotide for assembly. (A) The resulting sample was loaded on a Capto Core 700 column. The elution of protein-containing samples was measured by absorption at 280 nm (red) and 260 nm (blue). After application of the sample, the column was washed. Bound material was removed by 100 % of buffer B (green), which contained 20 % isopropanol and 1 M NaOH. (B) Samples from peak 1 (P1) and peak 2 (P2) were analyzed by SDS-PAGE (17.5 % PAA, 1:200 AA/BAA) followed by Coomassie G-250 staining (left) or immunoblot using polyclonal antiserum raised against CA (right). The positions of molecular mass standards marker are shown left, and the position of the Gag-His variants is indicated at the right.

Assembly of Gag is known to be driven by protein-protein interactions as well as the binding of the NC domain to NA (Liu, et al., 2017). To date, the only way to assemble a truncated Gag version (Δ MACASP1NC) without NA is in the presence of tartrate at a high concentration of 375 mM (Wagner, et al., 2016; Kucharska, et al., 2019). For this work, it was of interest to analyze the impact NA has on the processing of assembled Δ MACANCSP2. Therefore, the protein was dialyzed overnight for assembly under the optimized conditions of the AB with methanol but in the absence of any NA. The applied concentration of

Δ MACANCSP2 was 70 μ M. The resulting sample showed the same turbidity as the assembly with NA as observed by the eye. The yield of assembled protein was > 90 %. After transfer to PB with 60 μ M IP6 stable particles were still at > 80 % present comparable to assembled Δ MACANCSP2 with NA. The particles seemed to be spherical and mainly sticking together (Figure 15 A). However, analysis at higher resolution scanning transmission electron microscopy (STEM) tomography of these aggregates was able to show that they were not built by spherical particles but elongated structures formed as filaments of a curved morphology (Figure 15 B). Only some separated and closed structures were observed of the same size and shape of correctly assembled Δ MACANCSP2.

According to an *in silico* prediction based on cleavage rates of synthetic peptides, the morphological part of maturation is induced after 30 min (Könnnyű, et al., 2013), while in the experiments for processing of *in vitro* translated Gag under different conditions, not all CS were fully processed after 6 h by HIV-1 PR (Pettit, et al., 1994). Consequently, the particles of Δ MACANCSP2 for processing experiments needed to be stable for a minimum of 24h; thus, no preliminary decay of the particles could result in artifacts. In order to analyze the stability under processing conditions, assembled particles with and without NA were incubated for several days in PB at 37 °C and 1000 rpm. In the case of assembled Δ MACANCSP2 with NA, particles were stable for more than five days (Figure 15 D; + NA). Particles were still of roughly 90 – 100 nm in diameter and spherical. The yield of protein in the non-solubilized fraction was > 65 %, which was the same for the assembly without NA. The initially observed structures after assembly rearranged for the most part after incubation at 37 °C (Figure 16 E). However, some correctly shaped rings of spherical particles had also been detected. Nevertheless, the particle aggregation after assembly which was made by curved filament-like structures were mostly transformed into elongated filament-like structures, which often were attached with at least one of their terminal regions to the remaining curved aggregated structures (Figure 16 A). With the help of high-resolution STEM and TEM, a twisted structure of these filaments could be visualized (Figure 15 A right + Figure 16 A). However, the structural arrangement of Δ MACANCSP2 in these twisted filaments is not known yet, and detailed structural analysis by cryo-EM is planned. Analyzed from the given data by STEM, the filaments were $\sim 22.6 \pm 1.2$ nm wide and 16.0 ± 1.2 nm high in the section. A half rotation of the filament occurred after 99.9 ± 9.9 nm (Figure 16 B). Even though Δ MACANCSP2 assembled without NA into macromolecular structures, these particles were also implemented in the following processing experiments, as the lack of NA had an impact on the morphology of assemblies.

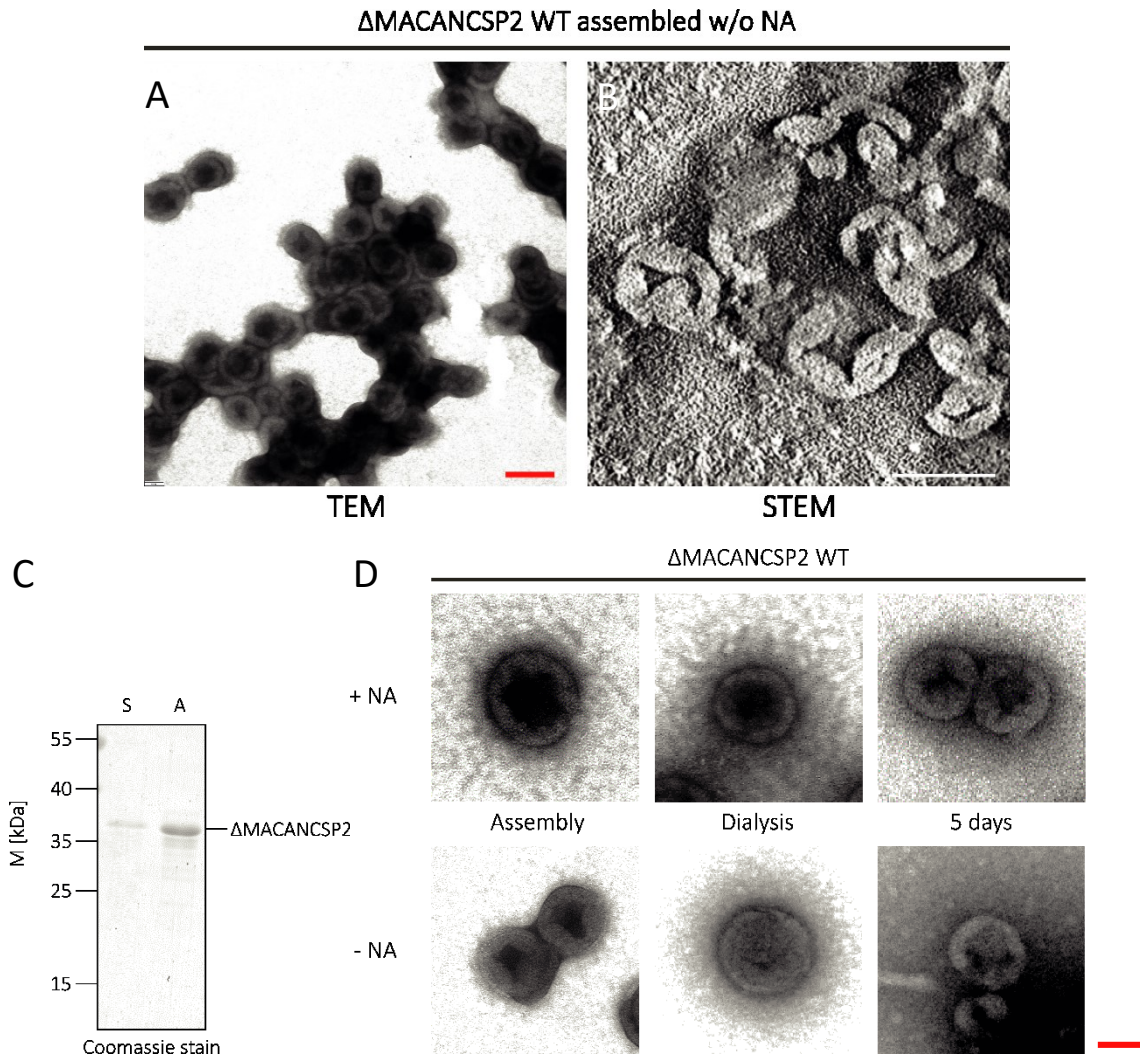


Figure 15: Long-term stability of assembled particles and aberrant assembly induced in the absence of nucleic acid. Recombinant purified Δ MACANCSP2 WT was dialyzed against assembly buffer (5.2.2.4) in the tubing of 8 – 9 MWCO at 4 °C overnight. After assembly without NA, the particles or protein aggregations stuck together, as shown by TEM (A) and STEM (B). (C) The resulting assembled sample was centrifuged. Supernatant and pellet were analyzed by SDS-PAGE (17.5 % PAA, 1:200 AA/BAA) followed by Coomassie G-250. The positions of the molecular mass standard are shown left, and the position of the Gag-His variants is indicated at the right. (D) To show the stability of assembled Δ MACANCSP2 WT samples were additionally analyzed by negative stained TEM with 3 % uranyl acetate. One sample of Δ MACANCSP2 WT was assembled with present standard oligonucleotide for assembly (5.1.7) and another without (Assembly). Subsequently, the particle suspension was dialyzed against processing buffer (Dialysis; 5.2.2.5) and incubated for five days at 37 °C and 1000 rpm in a heated agitator (5 days).

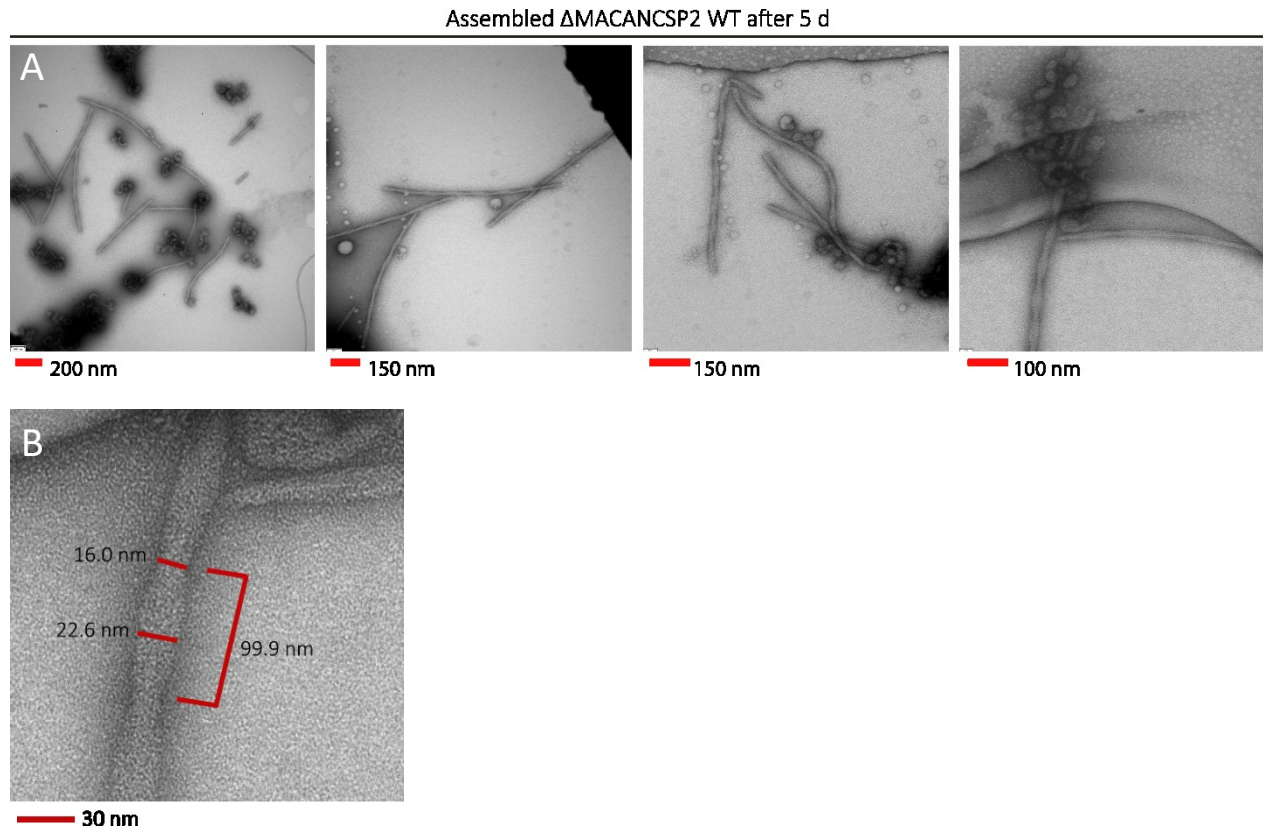


Figure 16: Morphological analysis of elongated filament-like assemble of Δ MACANCSP2. Recombinant purified Δ MACANCSP2 WT was dialyzed against assembly buffer (5.2.2.4) in the tubing of 8 – 9 MWCO at 4 °C overnight in the absence of NA. Afterward the sample was incubated for five days at 37 °C at 1000 rpm in a heated agitator and analyzed by negative stained TEM with 3 % uranyl acetate. (E) After five days, the samples showed an aberrant morphological rearrangement as twisted filaments, which were analyzed further in TEM with different magnification. (F) On average, the elongated filaments display a repetitive rotation with an interval of 99.9 nm, a width of 22.6 nm and a height of 16.0 (n = 10 filaments).

6.3 Quantitative workflow for the analysis of Gag processing

6.3.1 Establishment of conditions for proteolytic processing

With the establishment of the purification system for highly pure Gag-His and an efficient protocol for stable assembly of Δ MACANCSP2, the next step was to set up an experimental procedure for Gag processing and its analysis. Buffers and conditions for the experiment were based on a previously described protocol for *in vitro* processing of immature virions (Mattei, et al., 2014). As mentioned in chapter 5.2.2.5, PB was prepared at pH 6.0, containing 100 mM MES, 150 mM NaCl, 0.02 % (v/v) TX-100, 1 mM DTT. The processing was performed at 37 °C and shaking in a heated agitator for 1.5 mL reaction tubes, to prevent any sedimentation. The first experiment was performed with Gag-His WT at a concentration of 27 μ M. At this concentration, Gag should be present at \sim 70 % as dimers. To start the processing recombinant dimeric PR was added 1:40 molar ratio to Gag, mimicking the natural ratio between Gag and PR (as a dimer) in actual viral particles (Carlson, et al., 2008).

In the initial experiments, samples were taken after several hours for analysis by SDS-PAGE, which was only capable of visualizing a few bands mainly of protein mass higher than MA (~ 14 kDa) with Coomassie staining. Even though this method could not visualize all primary intermediates or products (data not shown), it did show that, under the chosen parameters, the processing did take place in ~ 8 – 24 h. Consequently, the maximum time frame for analysis was set to 24 h.

For the quantification of processing products and intermediates, I adapted a Tricine-PAGE based approach. Ideally, the method should allow quantification of all possible processing intermediates and products covering a range from ~ 1 - 2 kDa (SP1 and SP2) to 57 kDa (full-length Gag-His). Therefore, the Tricine-PAGE, according to Schägger (2006), was tested in order to capture small proteins and peptides and resolve proteins in the desired range. Samples for the time course analysis were taken at 0, 0.5, 1, 2, 4, 8, 15, 30, 60, 120, 240, 480, and 1440 (= 24 h) min. For the staining of the finished gel, colloidal Coomassie was chosen, which accomplishes a 5 – 50 x higher sensitivity and less background compared standard Coomassie staining (Dyballa, et al., 2009). Silver staining achieves a similar sensitivity, but it yields a significantly smaller linear dynamic range for protein quantification (Grove, et al., 2009; Butt, et al., 2013) and is more sensitive to contamination of used preparation solutions.

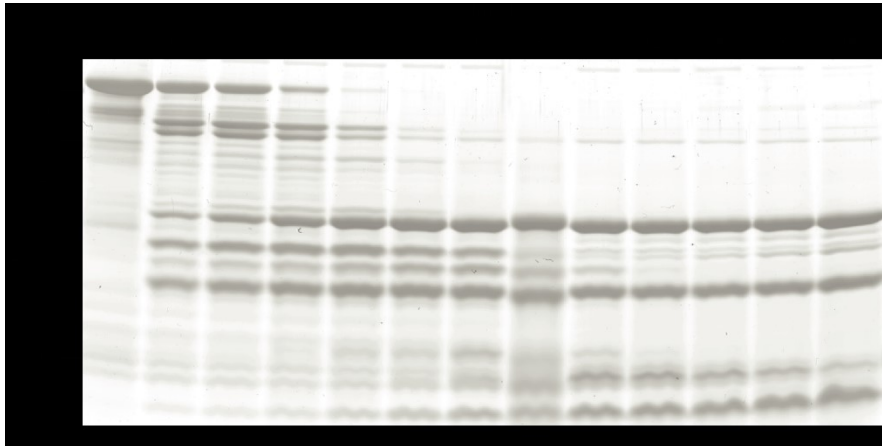


Figure 17: Time course of Gag-His WT processing analyzed by Tricine-PAGE. Recombinant purified Gag-His WT was dialyzed against processing buffer and processed *in vitro* by the addition of recombinant purified HIV-1 PR over 24 h (= 1440 min) at 37 °C and 450 rpm. After successive increasing time steps (0, 0.5, 1, 2, 4, 8, 15, 30, 60, 120, 240, 480 and 1440 min) samples were taken for analysis by Coomassie G-250 stained Tricine-PAGEs (16 % PAA, crosslinking ratio 1:32 BAA/AA and 9.6 % PAA, 1:32 BAA/AA). Positions of molecular mass standards marker are shown at the left, and the position of bands indicating processing products are shown at the right.

The processing of Gag-His was performed, as described, and the samples were applied to a Tricine-PAGE. In Figure 17, the resulting gel with Coomassie stain shows a diversity of protein bands, with electrophoretic mobilities corresponding to ~ 8 kDa to ~ 57 kDa. The bands were all nicely separated and not overlapping. In total, several prominent bands of different proteins were detected. While the initial unprocessed full-length Gag-His vanishes within 4 min, several intermediates appear in parallel at a size between 25 and

45 kDa. As these are also processed over time, other intermediates are present, finally leading to the end products. Additionally, two end products are already detected after 0.5 min at ~ 24 and 13 kDa.

Nevertheless, only based on the stained gel, the assignment of the bands with their respective protein is not possible. In theory, there are 21 possible configurations of uncleaved Gag-His, intermediates, and processing products (Table 20). As some of the bands may be assigned according to their masses, most of the theoretical proteins reveal masses closely to other variants, and because proteins display electrophoretic mobilities differing from their masses, other methods for clear identification needed to be applied.

Table 20: Theoretical intermediates and products of Gag-His WT processing. During the processing of Gag-His WT by the HIV-1 PR, a variety of intermediates and final products can appear theoretically composed of different combinations of Gag subunits as matrix protein (MA), capsid protein (CA), nucleocapsid protein (NC), the p6-domain with the C-terminal His-tag, and the two spacer peptides, SP1 and SP2. For all theoretical products, the molecular mass without the initial methionine of the start codon and antisera, which would recognize a contained subunit, are listed.

Potential processing products	Molecular mass [Da]
MA-CA-SP1-NC-SP2-p6-His	56780.52
MA-CA-SP1-NC-SP2	49898.07
MA-CA-SP1-NC	48074.95
CA-SP1-NC-SP2-p6-His	42086.95
MA-CA-SP1	41741.61
MA-CA	40295.95
CA-SP1-NC-SP2	35204.52
CA-SP1-NC	33381.40
CA-SP1	27048.05
CA	25602.39
SP1-NC-SP2-p6-His	16502.59
NC-SP2-p6-His	15056.92
MA	14711.58
SP1-NC-SP2	9620.15
SP2-p6-His	8723.58
NC-SP2	8287.64
SP1-NC	7797.02
p6-His	6900.46
NC	6351.35
SP2	1841.14
SP1	1463.68

6.3.2 Identification of processing products

As the identity of the individual bands of Gag-His processing by its subunits was unknown, the immunoblot was chosen for analysis. For all subunits, primary antisera raised against purified recombinant proteins or synthetic peptides (SP1, SP2) had been prepared in the lab. While most of these antisera had been validated by immunoblot, sera against SP1 and SP2 showed weak reactivity and specificity in early experiments. Thus, these sera were subjected to affinity chromatography. For this purpose, synthetic peptides of SP1 and SP2 were bound to NHS-activated columns (HiTrap NHS activated HP 1 mL, 5.2.2.3) according to the manufacturer. The surfaces in these columns display an N-hydroxysuccinimide group esterified with a good leaving group. This active reagent binds preferably to primary amino groups of peptides and proteins.

After the rabbit sera containing antibodies against SP1 or SP2 were diluted in PBS, they were applied to the respective column (Figure 18) and purified according to a standard protocol given by the manufacturer of the column (5.1.1). After binding to the column, the columns were washed with PBS and bound protein antibodies eluted by acidic glycine buffer (pH 3.0), which prevents the interactions of bound antibody and column-bound peptides (Gendusa, et al., 2014). In subsequent immunoblot experiments, the optimal dilution as a primary antibody was determined to be 1:1000 for SP1 antiserum and 1:2000 in the case of SP2 antiserum.

Table 21: Antibody samples used for subunit identification during Gag-His processing. For the assignment of the bands in the gel of Gag-His processing (Figure 17), the contained subunits needed to be identified. Therefore, polyclonal antisera from different sources against MA, CA, SP1, NC, SP2, and p6 and a monoclonal antibody against the C-terminal His-tag were used in immunoblots at the indicated dilutions.

Antiserum	Source	Applied dilution
Polyclonal serum against MA	Rabbit	1:3000
Polyclonal serum against CA	Sheep	1:5000
Polyclonal serum against SP1	Rabbit	1:1000
Polyclonal serum against NC	Goat	1:3000
Polyclonal serum against SP2	Rabbit	1:2000
Polyclonal serum against p6	Rabbit	1:1000
Monoclonal antibody against His-tag	Mouse	1:1000

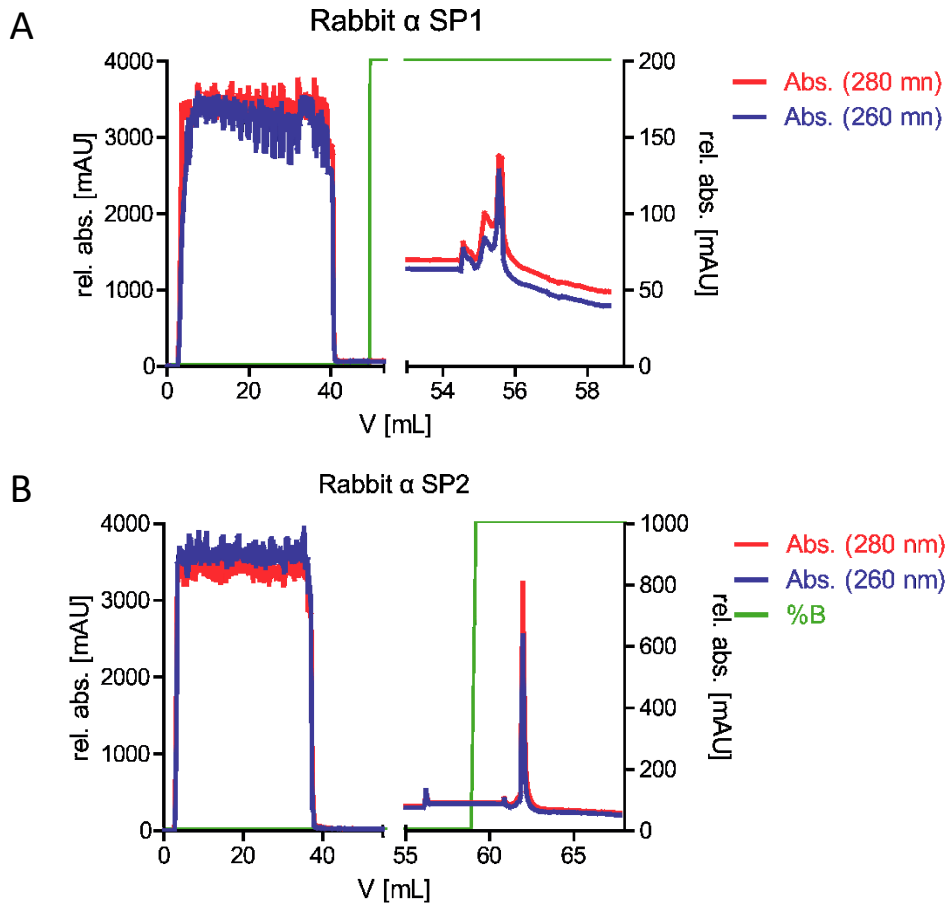
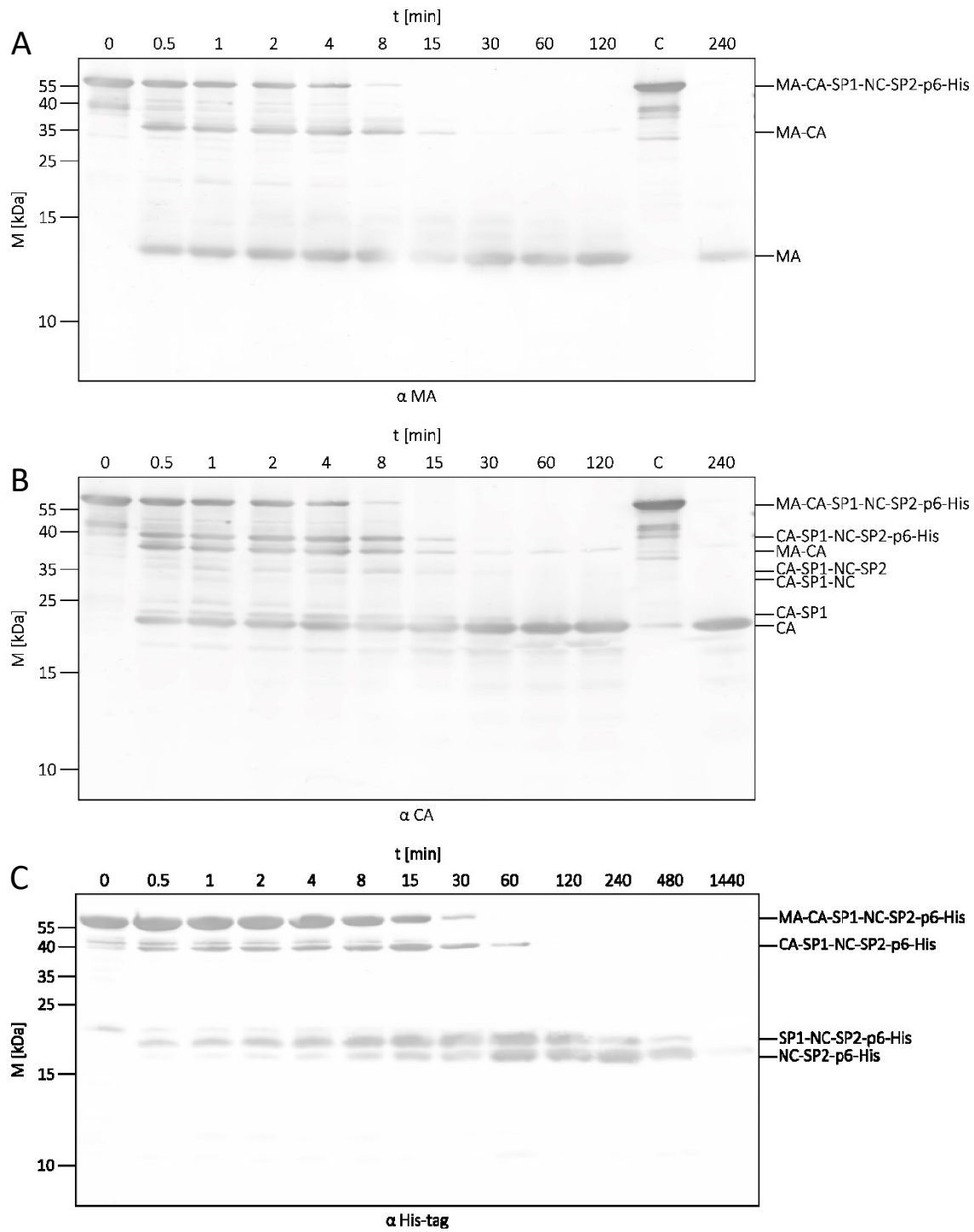


Figure 18: Affinity chromatography of polyclonal antibodies against SP1 and SP2. Rabbit serum containing polyclonal antibodies against SP1 (A) or SP2 (B) were applied to HiTrap NHS-activated HP columns carrying the respective synthetic peptide of SP1 or SP2. The bound antibodies were eluted in one step. Absorption at 280 nm (red) and 260 nm (blue) was measured to detect the protein elution.

In order to identify the subunits during Gag-His processing, samples were again separated with Tricine-PAGE and afterward transferred to nitrocellulose immunoblot membranes (5.2.2.6.2). The different listed antisera (Table 21) were applied for the determination of the contained subunits at each band. If two bands were in close proximity on the gel, but only one was recognized by a certain antiserum, a second antiserum was added, which recognized both bands. The resulting blots (Figure 19) show that the initial uncleaved sample was recognized by the antisera for MA and His-tag (Figure 19 A t=0, Figure 19 C t=0), indicating that the protein contained as expected all six subunits. According to the Coomassie-stained gel (Figure 17), the next proteins after the addition of PR were missing MA or SP1-NC-SP2-p6-His at the termini of the protein (Figure 19 A + B t=0.5), i.e., the bands represented CA-SP1-NC-SP2-p6-His and MA-CA. MA-CA was processed to the final products MA and CA, detectable at their expected sizes of around 15 and 25 kDa, respectively (Figure 19 A + B t=1440). The other two bands in the range of 25 – 35 kDa represented contained both a CA subunits (Figure 19 B t=1), while only the upper one displayed an SP2 domain (Figure 19 E t=12). Consequently, they indicated further processing of CA-SP1-NC-SP2-p6-His to CA-SP1-NC-SP2 and CA-SP1-NC, but each only in low amounts (Figure 17 t=1). Instead, there is a high



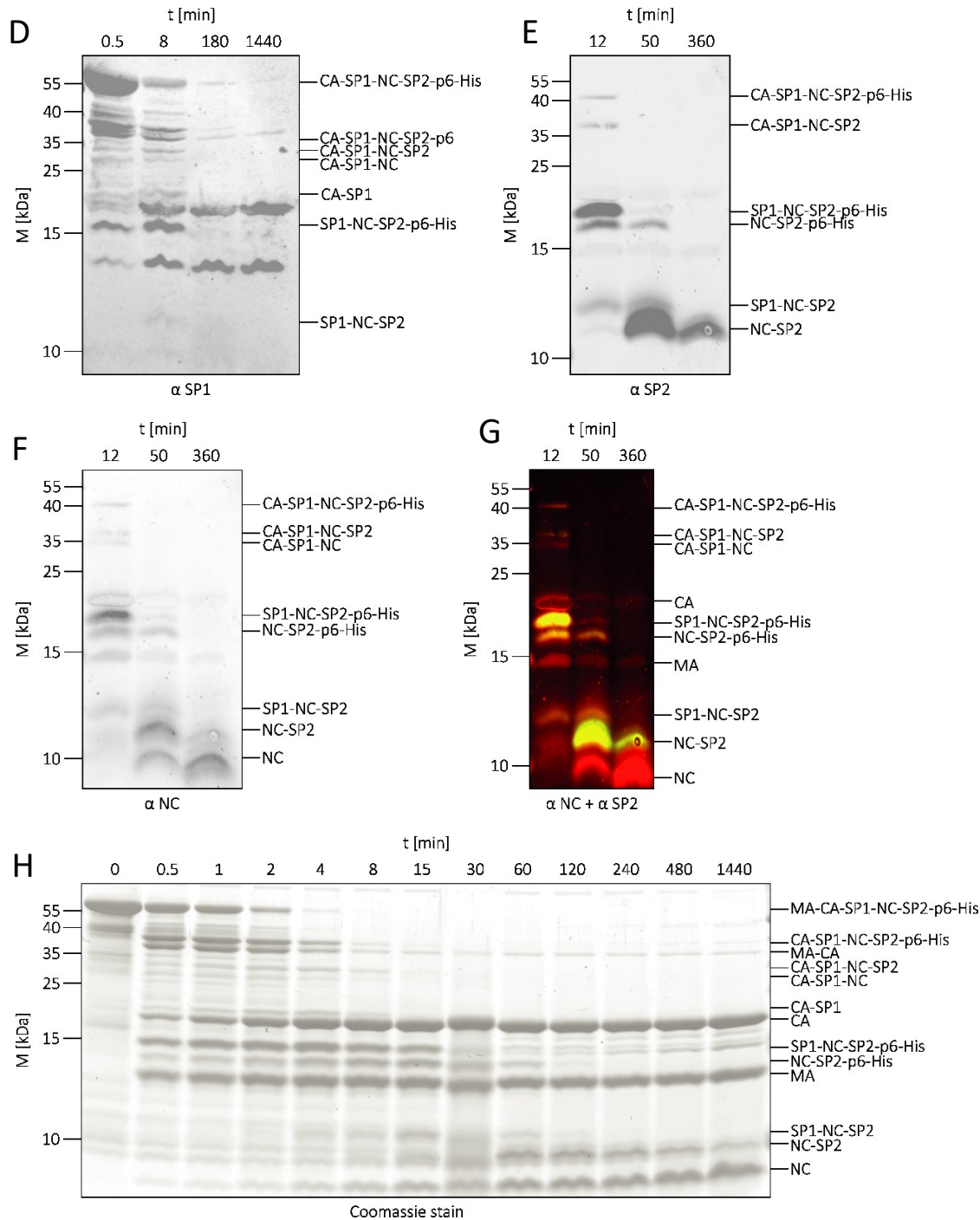


Figure 19: Intermediate and product identification of Gag-His WT processing analyzed by immunoblotting. 27 μ M recombinant purified Gag-His WT was dialyzed against processing buffer and processed in a reaction tube *in vitro* by the addition of dimeric recombinant purified HIV-1 PR in a ratio of 1:40 for 24 h (= 1440 min) at 37 °C, while the sample was permanently shaken in a thermal agitator at 450 rpm. Samples were taken at the indicated time points (0 – 1440 min) as well as one sample without PR treatment after 8 h (C) and analyzed Tricine-PAGEs (16 % PAA, crosslinking ratio 1:32 BAA/AA and 9.6 % PAA, 1:32 BAA/AA) and immunoblot using polyclonal antisera raised against MA (A), CA (B), SP1 (D), NC (F, G) or SP2 (E, G) or a monoclonal antibody against His-tag (C). In the dual-color image, red color symbolizes the presence of NC and green the presence of SP2 in bands. For both domains present in one band, the bands are colored yellow (G). Tricine-PAGE and colloidal Coomassie staining of processing products as shown in Figure 17. Processing products identified by immunoblot are indicated to the left (H). Positions of molecular mass standards marker are shown at the left, and the position of Gag-His and processing products are indicated at the right.

concentration of two proteins between 0.5 and 30 min roughly higher than 15 kDa, which were not detected from CA antiserum but from the antisera for SP1 or NC and His-tag (Figure 19 D t=0.5; Figure 19 F t=12; Figure 19 C t=30). They were consequently composed of SP1-NC-SP2-p6-His and NC-SP2-p6-His, respectively. Final processing steps at these proteins lead to three bands below MA (Figure 17 t=15), of which the upper one contained SP1-NC-SP2 (Figure 19 D t=8 + E t=12), the middle one NC-SP2 (Figure 19 E + F t=50), and the lowest was only NC (Figure 19 F t=360). However, this analysis showed that there was no staining for SP1, SP2, or p6-His as a singular protein in the gel by Coomassie, even though p6-His was minimally visible on immunoblots (Figure 19 C t=60). In summary, 13 prominent bands of proteins during the processing of Gag-His could be assigned precisely, and quantitation of these bands for processing analysis could be designed now.

Other detectable bands as those between MA and CA (Figure 17) could not be assigned with the help of the used antisera and were consequently derived from contaminations by truncated Gag-His with aberrant termini or copurified proteins of *E. coli*. Therefore, they were not included in further analysis. Additionally, these results for band assignments were easily adaptable to the processing analysis of Δ MACANCSP2. The main differences here were the missing p6 domain and the His-tag, why there was especially no SP1-NC-SP2-p6 and NC-SP2-p6 present during processing, and due to the missing part of MA, the respective band was running slightly lower than NC (Figure 45 in chapter 9).

Even though the processing products were assigned to their subunits with the help of immunoblots, evidence was needed that Gag-His was processed at the correct sites by HIV-1 PR. In order to verify this, the masses of the products after processing were analyzed by intact protein mass spectrometry (5.2.2.6.4). If the masses of primary detected proteins fit with the expected theoretical masses, Gag-His is processed at the expected sites. The advantage of this method compared to peptide mass fingerprint is that not only cleavage at the CS can be proven, but it also reveals if residues of amino acids are oxidized or deleted as in the case of deamination, as well as if there is aberrant cleavage present.

As the amount of proteins measurable in one sample is limited, the sample after processing had to be separated first. 500 μ L sample of 22 μ M Gag-His WT was digested according to the before conditions described above for 40 h to ensure full processing. Afterward, the sample was applied to a Superdex 75 10/300 column (Figure 20 A). One fraction for peak 1 (Figure 20 P1) and peak 2 (Figure 20 P2) and a sample of peak 3 (Figure 20 P3) were examined by a Tricine-PAGE and Coomassie staining (Figure 20 B). As a control, the samples were analyzed prior to separation by gel filtration (Figure 20 B; C0) as well as the precipitate after processing (Figure 20 B; P). P1 and P2 contained a notable amount of CA and MA, while P3 showed prominent bands for MA and NC. Furthermore, in P1 and P2, a small amount of protein at the size of full-length Gag-His was present, indicating unprocessed protein. According to the mass spectrometry of these samples, prominent masses were 6350.6, 6900.3, 14711.0, and 25601.7 Da (Figure 41), corresponding to the calculated molecular masses of NC (= 6351,4 Da), p6-His (= 6900.5 Da), MA, lacking the N-terminal methionine (=14711.6 Da), and CA (=25602.4 Da). Both spacer peptides were, however, not detectable. According to the measured masses, all subunits were cleaved at their termini correctly by the HIV-1 PR under the given conditions.

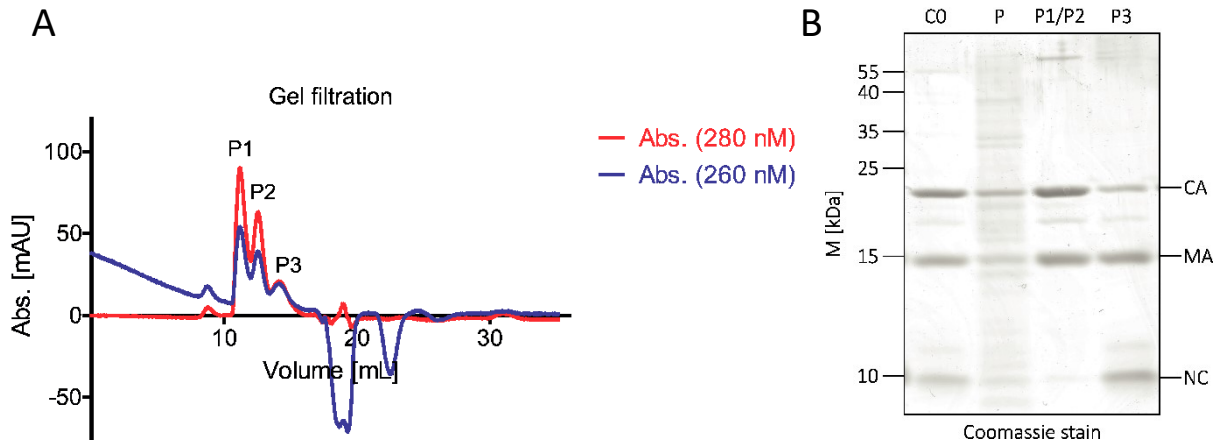


Figure 20: Gel filtration analysis of non-assembled Gag-His WT processing products. 22 μ M recombinant Gag-His WT was processed according to material and methods with 0.5 μ M recombinant protease in 1 mL for 40 h. (A) The resulting sample was loaded on a Superdex 75 10/300, and absorption was measured at 280 nm (red) and 260 nm (blue). (B) Fractions taken from the size exclusion column (1 = P1 and P2, 2 = P3) and a non-purified control sample (CO) were analyzed by Tricine-PAGE stained by Coomassie G-250 staining. Positions of molecular mass standards marker are shown left, and the position of the Gag-His and processing products are indicated at the right. Fractions 4 and 8 were used for later intact mass spectrometry.

6.3.3 Protein stability under processing conditions

For the quantitative analysis and its interpretation, the reliability of the experimental setup, regarding the stability and activity of Gag-His and PR, in the timeframe of 24 h needed to be validated. Therefore, 27 μ M Gag-His WT was incubated in processing buffer at 37 °C for several days without the addition of PR. After each day, samples were taken for the analysis by SDS-PAGE with Coomassie staining (Figure 21 A). The analyzed samples were applied onto the gel at high quantity (4 μ g) for sensitive detection of bands corresponding to proteins with lower masses and concentrations. Over four days of incubation, the band intensity of Gag-His remained unchanged, and products of lower molecular mass were not detected, indicating that Gag-His is not autoproteolyzing or precipitating under the processing conditions. Consequently, all cleavage events occurring during the processing experiments should be attributed to the activity of HIV-1 PR.

In order to track the loss of activity of the recombinant protease during processing experiments, HIV protease substrate I was introduced, which is a synthetic peptide comprising an artificial cleavage site sequence for HIV-1 PR. Additionally, this peptide carries two covalently modified amino acids, one connected to the fluorophore EDANS (5-((2-aminoethyl)amino)naphthalene-1-sulfonic acid) and another to the respective acceptor chromophore DABCYL (4-(4-dimethylaminophenylazo)benzoic acid). When the modified amino acids are flanking the introduced cleavage site region in the uncleaved substrate, the spatial proximity of both modifications causes quenching of EDANS at 490 nm. Upon cleavage emission at 490 nm can be detected (Matayoshi, et al., 1990; Gaber, et al., 2013). The processing of this compound was performed at three different pH values pH 6.0, 6.5, and 7.0. The pH higher than 6.0 was also tested for the processing, which is described in chapter 6.4.3.1.

Recombinant PR was diluted 1:25 with PB to ~ 650 nM as used for the processing experiments and incubated at 37 °C while shaking in a thermal agitator at 1000 rpm. After several time intervals (0, 1, 2, 4, 8, and 24 h), 4 μ L of PR were taken and added to prewarmed 150 μ L PB at 37 °C containing HIV protease substrate I at 2 μ M concentration. The linear slope of the emission at 490 nm was taken as the value relative enzyme activity. Normalizing for the activity value of the initial PR without incubation, the proportion of remaining PR activity was determined. The resulting fit of a one-phase decay for the mean values of triplicates including the standard deviation shows that the activity vanished within 24 h (Figure 21 B). The respective half-lives were 286 min at pH 6.0 (Figure 21 B red line), 78 min at pH 6.5 (Figure 21 B blue line), and 55 min (Figure 21 B green line), indicating that the PR activity was reduced considerably within the time frame used for processing experiments. Thus, for analysis and discussion of the processing experiments, this result needed to be taken into account. The processing during the later stages of the experimental setup would be therefore influenced by the reduced activity and could not be compared to processing events of the early phase one-on-one.

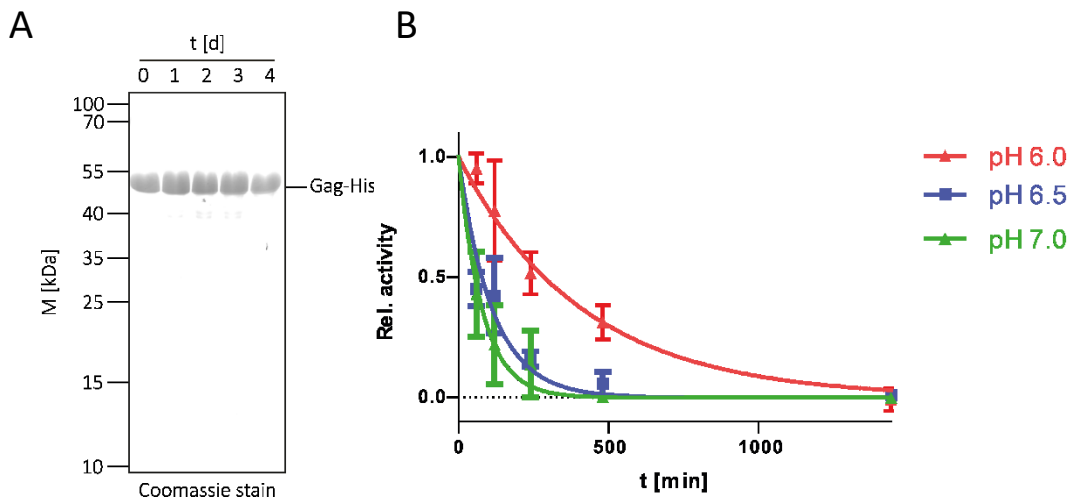


Figure 21: Gag-His and PR stability under processing conditions. (A) Gag-His WT was incubated for four days in processing buffer at 37 °C. After each day, a sample was taken for analysis by SDS-PAGE (17.5 % PAA, 1:200 AA/BAA) followed and Coomassie G-250 staining. Positions of molecular mass standards marker are shown left, and the position of the Gag-His variants is indicated at the right. (B) Recombinant HIV-1 PR was incubated in processing buffer for 0, 1, 2, 4, 8, and 24 h at 37 °C as done in the standard processing experiment as triplicates but without Gag at pH 6.0 (red), 6.5 (blue) and 7.0 (green). At the mentioned time points, the activity was measured by the processing of HIV-1 PR substrate I by the PR. All calculated activities were set relative to the activity of the initial measurement at $t = 0$. Error bars indicate the standard deviation of the measured data points. A one-phase decay fit was set with $y(t=0) = 1$. While the goodness of fit (R^2) is 0.98, the half-life is 316 min, with a decay rate of 0.22 ± 0.036 %.

6.3.4 Quantitative analysis and plotting

After proving for protein stability and intermediate identity of Gag processing, an approach for the qualitative analysis of the Coomassie-stained Tricine-PAGE was developed. Therefore, the gel was imaged by an infrared scanner (LiCor Odyssey Imager CLx) since Coomassie can emit at 700 nm (Butt, et al., 2013). In order to quantify the amount of proteins per band, the background was subtracted from the raw data

image, to reduce the impact of heterogenic staining. The signals of the bands were integrated (5.2.2.6.5), and the sum of signals per time point normalized. Proteins are stained by Coomassie primarily at N-terminal amino groups and residues of arginine, lysine, serine, and histidine (de Moreno, et al., 1986), therefore the ratio of signal intensity and the quantity of stainable residues are representative for the protein concentration of an individual band. Finally, the data were normalized with the concentration of the initially uncleaved Gag-His. Because the starting concentration is set consequently to the relative value of 1, this last step simplified the comparison of different processing experiments if not the same concentration of Gag had been used.

Moreover, different ways to present the data of the processing experiments are shown in Figure 22, including explanations, which method I applied in this work primarily. The quantitative characterization of the processing and comparison of different experiments will be described in the following chapter 6.4.

The first way to plot the quantified processing included all detectable intermediates and products (Figure 22 A). However, since the interpretation and description of twelve different proteins during the analysis are challenging to be done without bioinformatical modeling, other ways to present the quantitative analysis were also performed. A second option was to track the concentration of Gag subunits included in all signals at a given time point (Figure 22 B). The concentrations of SP1, SP2, and p6 were decreasing over time until they had almost or entirely vanished after 24 h because they were not detected by the Coomassie staining of Tricine-PAGEs. The relative concentration of MA, CA, and NC remained constant for over ~ 1 h, while towards the 24 h endpoint, the concentration is going slowly higher than 1 to a maximum of ~ 1.2 in the case of CA (Figure 22 B orange line). These relative concentrations of > 1 were mainly derived by the signal loss of SP1, SP2, and p6 over time, which is to be taken into account for the interpretation of the results during the later phase (8 – 24 h).

Since this thesis aimed at the elucidation of cleavage events under certain conditions on an *in vitro* based level, further analysis was focused almost exclusively on individual cleavage events. Therefore, the concentration of the respective intact CSs at a given time point were summed up (Figure 22 C). The resulting plot illustrates the processing of intact CSs over time. Thus, this type of analysis had been used in most cases to compare the results of the following experiments for Gag processing. Especially the rapidly processed CSs reveal a roughly single exponential decay typically for enzyme-catalyzed reactions. Albeit, the condition and complexity of the overall reaction did not justify the application of a single exponential fit, this was used to approximate changes to the processing under different conditions.

Based on the calculation used for Figure 22 C, the release of the subunits in Gag after cleavage at all terminal cleavage sites could be plotted (Figure 22 D). This visualizes the temporal sequential release of subunits, which could be applied for dynamical predictions and interpretations on how followingly to proteolytic maturation, the morphological rearrangement could be structured.

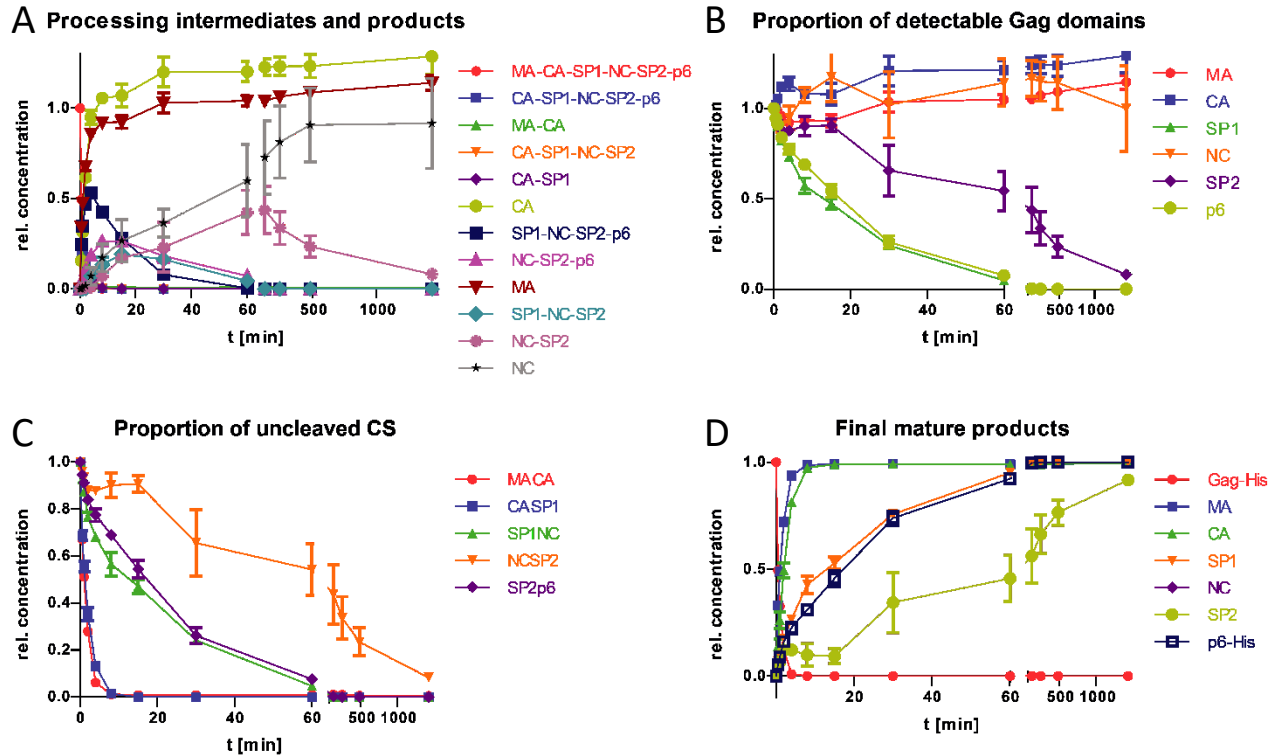


Figure 22: Different representations of the quantitative analysis for Gag-His processing. 27 μM recombinant purified Gag-His WT was dialyzed against processing buffer and processed in a reaction tube *in vitro* by the addition of dimeric recombinant purified HIV-1 PR in a ratio of 1:40 for 24 h (= 1440 min) at 37 °C, while the sample was permanently shaken in a thermal agitator at 450 rpm. Samples were taken at the indicated time points (0 – 1440 min) and analyzed with Coomassie-stained Tricine-PAGEs (16 % PAA, crosslinking ratio 1:32 BAA/AA and 9.6 % PAA, 1:32 BAA/AA), as described before (5.2.2.6.5). The concentrations shown are normalized to the initial concentration of Gag-His ($t=0$). (A) The concentration of the uncleaved Gag-His, intermediates, and products detectable with the Coomassie stain are plotted for the respective time points. Signals were detected for MA-CA-SP1-NC-SP2-p6 (red), CA-SP1-NC-SP2-p6 (blue), MA-CA (green), CA-SP1-NC-SP2 (orange), CA-SP1 (purple), CA (yellow), SP1-NC-SP2-p6 (dark blue), NC-SP2 (bright purple), MA (dark red), SP1-NC-SP2 (turquoise), NC-SP2 (rose), and NC (gray). (B) For quality control, the concentrations of the Gag subunits MA (red), CA (blue), SP1 (green), NC (orange), SP2 (purple), and p6 (yellow) among all signals at one time point are summed up. (C) To track the processing of cleavage sites, all signals for proteins containing the respective unprocessed cleavage sites of MA-CA (red), CA-SP1 (blue), SP1-NC (green), NC-SP2 (orange), or SP2-p6 (purple) were totaled for one time point. (D) The present concentration of the final products MA (blue), CA (green), SP1 (orange), NC (purple), SP2 (yellow), and p6 (dark blue) or Gag-His (red) is calculated by the absence of all terminal cleavage sites of an individual subunit. The shown data points are derived as the mean value from triplicates, and the error bars indicate the standard deviation.

6.4 Processing of Gag

6.4.1 Gag in mono- and dimeric states

Until now, I tested only the processing of wild-type Gag with a non-physiological C-terminal His-tag. In a concentration of 27 μM for the processing experiment, Gag is present in the dimeric state at 70 %. In order to examine if these conditions influence the processing of Gag, other variants of this protein were introduced. Since this work aimed to analyze the impact of protein-protein interaction of Gag, among other factors, the Gag-His WM mutant (Datta, et al., 2007b) was also processed. While Gag-His WT

features a dissociation constant (K_d) of $8.34 \mu\text{M}$ (6.1), the introduction of the WM mutation in Gag disrupts the dimerization site and increases the dissociation constant to 0.53 mM (Datta, et al., 2007b). Thus, $27 \mu\text{M}$ of Gag-His WM would be 91 % monomeric. His-tags can induce an artificial dimerization of proteins (Wu, et al., 1999). In order to test the influence of the C-terminal His-tag on the processing of Gag-His WT, a protease cleavage site was introduced to create Gag-TEV-His. Upon cleavage by the TEV protease, the C-terminal His-tag was removed. This tool was used to compare the processing of Gag with and without His-tag. Other publications about the processing of recombinant purified Gag included $\Delta\text{MACANCSP2}$ (Ning, et al., 2016) and $\Delta\text{MACASP1NC}$ (Kucharska, et al., 2019). Since the processing of *in vitro* assembled had to be performed using $\Delta\text{MACANCSP2}$, and for a better comparison of this work with others (Ning, et al., 2016; Kucharska, et al., 2019), $\Delta\text{MACANCSP2}$ was also processed, as the last control. Thereby, the impact of His-tag could also be analyzed as well as the missing part of the MA domain. The buffers of all protein samples were changed by dialysis in PB and processed at $27 \mu\text{M}$ with $0.675 \mu\text{M}$ of recombinant PR in triplicate independent experiments.

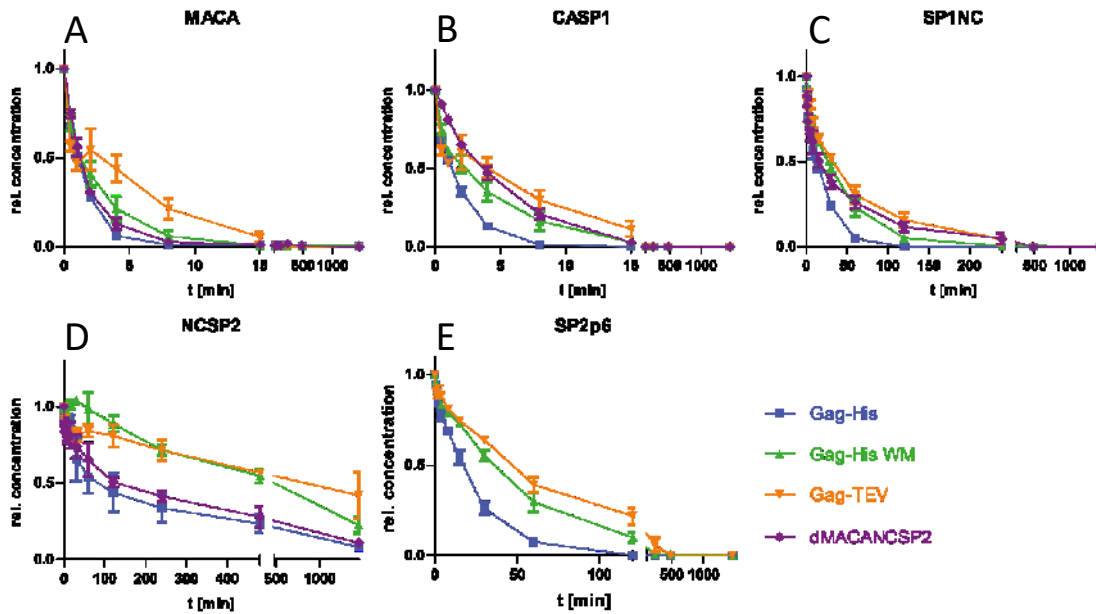


Figure 23: Time-course analysis of the Gag processing relating to a mono- or dimeric state. Coomassie G-250 stained Tricine-PAGEs were analyzed as described before (5.2.2.6.5 + 6.3.4), calculating concentrations of all existing products at each time point. Starting at a relative concentration (= 1), the amount of unprocessed CSs present in intermediates decreases over time. The summed concentration of products carrying unprocessed MA-CA (A), CA-SP1 (B), SP1-NC (C), NC-SP2 (D) or SP2-p6 (E) are plotted for triplicates of the proteolysis of unassembled Gag-His WT (blue), Gag-His WM (green), Gag-TEV (orange), and $\Delta\text{MACANCSP2}$ (purple). Error bars of the single figures indicate the standard deviation, and data points the mean values.

MA-CA was processed rapidly in the case of Gag-His WT with an apparent half-life of $\sim 1 \text{ min}$ (Figure 23 A blue line). Moreover, the processing of Gag-His WM and $\Delta\text{MACANCSP2}$ was comparable to the processing of Gag-His WT at MA-CA (Figure 23 A blue, green, and purple line). Gag-TEV, however, revealed a half-life of $\sim 1.8 \text{ min}$ (Figure 23 A orange line). In contrast, CA-SP1 was processed fastest in Gag-His WT with a half-life of $\sim 1.2 \text{ min}$ (Figure 23 B blue line), and the others were processed two- and three times slower

according to the half-lives. In the case of SP1-NC (Figure 23 C), Gag-His WT and Δ MACANCSP2 reveal a similar half-life of ~ 10 min, even though the processing in Gag-His WT is finished two times earlier than for all others. Δ MACANCSP2 and Gag-His WT were both cleaved at NC-SP2 with analogous decay rates and completely hydrolyzed within ~ 24 h. Gag-TEV and Gag-His WM, on the contrary, were not fully processed within the experimental time-frame (24h). The cleavage at the C-terminus at SP2-p6 was again finished first in Gag-His WT, while Gag-TEV and Gag-His WM were processed roughly two times slower, whereas Δ MACANCSP2 initially yielded no SP2-p6 CS.

Even though there were measurable differences in the processing at the single CSs of non-assembled Gag, there was no major impact on the processing of MA-CA, CA-SP1, and SP1-NC detectable when the WM mutation was introduced. Gag-TEV and Gag-His WM yielded comparable processing kinetics, meaning that the difference in the amount of dimers seems not to impact the processing of non-assembled Gag recognizable. On the other hand, Gag-His and Δ MACANCSP2 were also processed with similar half-lives except for the procession of CA-SP1. Because processing experiments of *in vitro* assembled particles could only be performed with Δ MACANCSP2 or viral particles, Gag-His was used without WM mutation in the following experiments, which included non-assembled protein.

6.4.2 Impact upon cleavage events by the structural arrangement of Gag

Gag is structurally highly ordered in the hexameric lattice of viral particles (Briggs, et al., 2009; Wright, et al., 2007; Schur, et al., 2015).; therefore, a question arises: which of the cleavage events are affected in the processing dynamics by the structural fixation and secondary structures? For example, this was proposed for the case of the helix at CA-SP1, which as a part of the helix bundle, is stabilized and thereby protected from processing by PR (Schur, et al., 2015; Mattei, et al., 2018). As described in 4.3.3, there were several approaches to analyze the processing of viral particles in a temporal manner, which either induced the processing of viral particles by stripping the membrane and addition of recombinant PR in the case of PR deficient particles (Konvalinka, et al., 1995) or by washing out PR inhibitors that prevented viral maturation (Mattei, et al., 2014). However, the analysis could only be done by immunoblots, which yields a low accuracy for protein quantitation.

Therefore, Gag-His WT was chosen for the processing system of the non-assembled protein and the *in vitro* assembled Δ MACANCSP2 WT as an alternative to viral particles in this thesis. To compare the processing, Δ MACANCSP2 WT was at first assembled at the storage concentration of 60 μ M with 4 % of the standard oligonucleotide for assembly (ss DNA of 68 nucleotides) in AB including 60 μ M IP6. Subsequently, the particles were dialyzed against PB and adjusted to 27 μ M Δ MACANCSP2, which was measured with a colorimetric protein quantitation assay. Subsequently, processing was initiated by the addition of 0.675 μ M PR dimer and incubated with gentle agitation at 37 °C. Gag-His was processed according to the protocol mentioned before (6.3.1).

Remarkably, the processing of non-assembled Gag-His WT (Figure 45 B in chapter 9) occurred in a different order compared to *in vitro* assembled Δ MACANCSP2 (Figure 24 A + B). In the case of the non-assembled protein, the first rapid processing occurred at MA-CA and CA-SP1 at comparable speed during the first

15 min with a half-life of ~ 1 min, releasing free MA and CA. The processing dynamics of SP1-NC and SP2-p6 were the second fastest finishing after 2 – 4 h with approximate half-lives of 10 and 15 min, respectively. During this, SP1 and p6-His were separated from processing intermediates. The slowest processing was at NC-SP2, which was not fully finished after 24 h. With this, the last connected domains SP2 and NC were separated.

In contrast, the proteolysis of *in vitro* assembled Δ MACANCSP2 started at Δ MA-CA and SP1-NC, which was completed during the first ~ 30 min. Until that point, only Δ MA was almost fully free. In the case of Δ MA-CA, the decay rate was four times slower in comparison to MA-CA of unassembled Gag-His WT; however, when in the case of SP1-NC, the decay was three times faster (Figure 24 A and B green lines) The next cleavage at CA-SP1 was completed after 60 min, at which point CA and SP1 were fully separated from other domains, which appeared roughly 14 times slower than for unassembled Gag-His WT (Figure 24 A and B blue lines). NC-SP2 was processed with the lowest rates; however, it finished after 4h releasing NC and SP2, which is ~ 6 -fold faster compared to unassembled Gag-His WT.

According to the decay rates of non-assembled Gag-His in the one-phase decay fit, the sites MA-CA and CA-SP1 were fully processed 50-fold, SP1-NC 5-fold, and SP2-p6 3.5-fold faster than NC-SP2. Furthermore, Δ MA-CA and SP1-NC of assembled Δ MACANCSP2 were 13.5- and 11-fold faster processed than NC-SP2, respectively. Whereas, the CA-SP1 was only processed with the 2-fold rates faster than NC-SP2.

In summary, the initial processing of the assembled Δ MACANCSP2 (SP1-NC) appeared slower, whereas the processing of the last CS (NC-SP2) was occurring earlier compared to the non-assembled Gag-His WT. The time to complete the processing of all CSs for non-assembled protein was ~ 1 d, whereas for the assembled protein, this time was less than ~ 4 h.

Additionally, the ordered release of mature processing products during the proteolysis was changed (Figure 24 C + D). MA and CA were released rapidly (within 15 min) for unassembled Gag-His WT, followed by the release of SP1 and p6 (~ 120 min). However, the NC-SP2 was not fully released even after 1 d. During the processing of assembled Δ MACANCSP2, Δ MA appeared to be released fully only after ~ 30 min, while CA and SP1 are almost 100 % separated from both flanking domains after 60 min. At last, SP2 and NC were released only after 480 min.

Because *in vitro* assembled Δ MACANCSP2 and non-assembled Gag-His WT displayed different processing dynamics, I wanted to compare the processing of assembled Δ MACANCSP2 also with that of virus-like particles (VLPs). In order to make sure that the processing results shown above are representative for the immature lattice in viral particles. Thus, HEK293T cells were transfected with a plasmid encoding a protease deficient virus genome (5.2.2.5), and the produced immature VLPs were pelleted from the cell culture supernatant via centrifugation over sucrose cushion (Figure 42 chapter 9). The viral pellets were resuspended in PBS, followed by the addition of 0.1 % TX-100 in order to remove the lipid membrane. The estimated Gag concentration by dot blot (Figure 42; 5.2.2.5) was ~ 15 μ M. Lastly, PR was added in a molar ratio to Gag of 1:40 in order to start the processing. Since there is a variety of different proteins that are encapsulated in virions or are can be co-purified, the samples were analyzed by immunoblots (Figure 44 in chapter 9), and the signals were evaluated as in the case of Coomassie-stained gels.

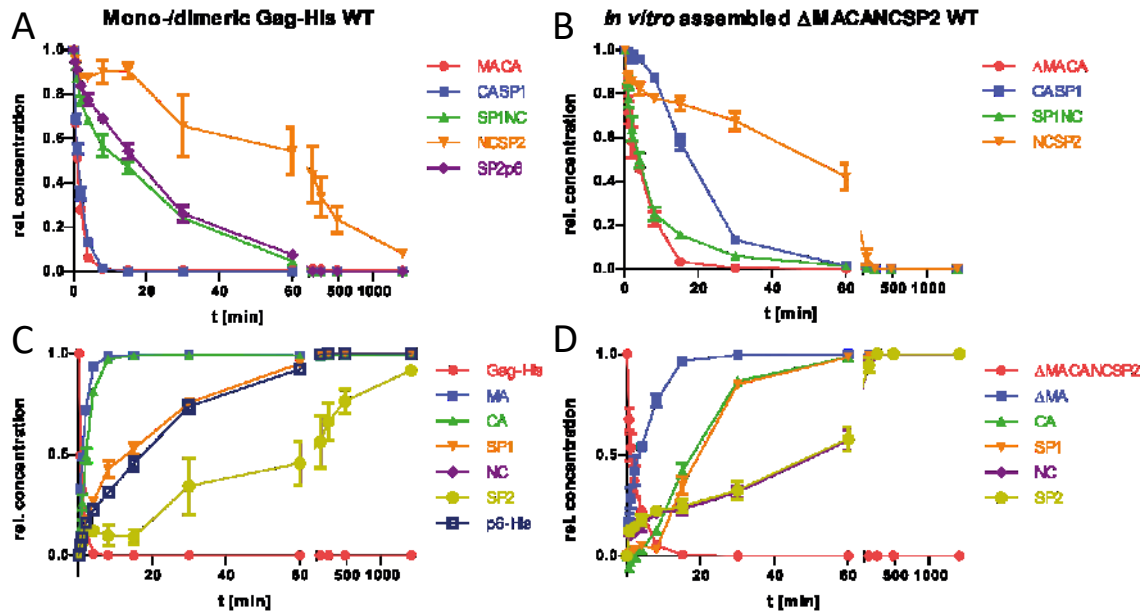


Figure 24: Cleavage site processing in an ordered sequence and decay of Gag and accumulation of processing products over time. Coomassie G-250 stained Tricine-PAGEs were analyzed by ImageJ and Ilastik as described in materials and method, calculating concentrations of all final products at each time point for non-assembled Gag-His WT (left) and *in vitro* assembled Δ MACANCSP2 WT (right). (A, B) The summed-up concentrations of products carrying unprocessed MA-CA/ Δ MA-CA (red), CA-SP1 (blue), SP1-NC (green), NC-SP2 (orange), or SP2-p6 (purple) are plotted. (C, D) The concentration of the final products was calculated by the absence of all terminal CSs of an individual subunit. Plotted are the starting Gag substrate (red) and the liberated subunits MA/ Δ MA (blue), CA (green), SP1 (orange), NC (purple), SP2 (yellow), and p6-His (dark blue). All processing experiments were performed in triplicate. Error bars indicate the standard deviation, and data points the mean values.

The processing in VLPs was indeed similar to the pattern derived from the *in vitro* assembled particles (Figure 25 red and blue lines). Δ MA-CA in the *in vitro* assembled Δ MACANCSP2 during processing had a half-life of 3 min, while in the VLPs cleavage at MA-CA was slightly slower with 4.2 min half-life. The most recognizable difference to non-assembled Gag-His WT (Figure 25 green line) appeared for CA-SP1, which was processed ~ 15.5 times slower for VLPs. However, SP1-NC and NC-SP2 were cleaved in VLPs with a two- and threefold higher decay rate, respectively, than for assembled Δ MACANCSP2. Because SP2-p6 is missing in Δ MACANCSP2, the processing in VLPs can only be set in contrast to non-assembled Gag-His WT. Here again, SP1-NC and NC-SP2 were processed faster for assembled Gag, with an almost three times higher decay rate than non-assembled Gag (Figure 25 E red and green line).

The results showed that *in vitro* assembled Δ MACANCSP2 could represent the processing of viral particles according to the condition mentioned above and setup, even though there were minor differences in some processing rates. This coincides with observations of other publications that lack the quantitative analysis of all processing events (Ning, et al., 2016). Nevertheless, *in vitro* assembled Δ MACANCSP2 displayed similar kinetic differences as the VLPs when compared to the non-assembled Gag-His WT. Therefore the *in vitro* assembled MACANCSP2 was used in the following experiments as the alternative to viral particles.

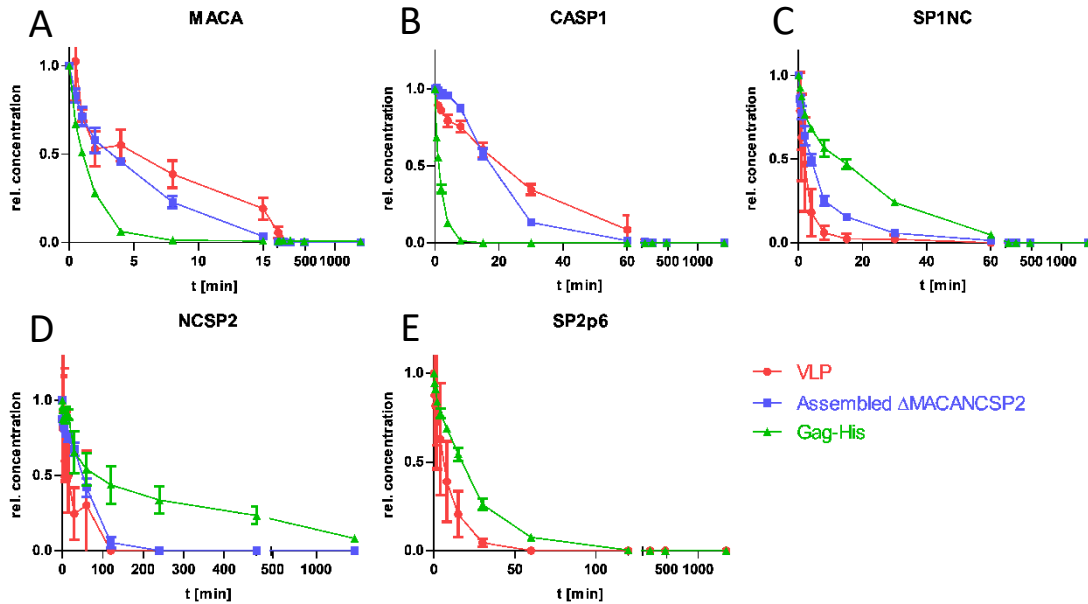


Figure 25: Time-course analysis of the processing of virus-like particles, assembled and non-assembled Gag WT. Coomassie G-250 stained Tricine-PAGEs were analyzed by ImageJ and Ilastik as described in materials and method, calculating concentrations of all existing products at each time point normalized to the starting concentration. The summed concentration of products carrying unprocessed MA-CA (A), CA-SP1 (B), SP1-NC (C), NC-SP2 (D) or SP2-p6 (E) are plotted for proteolysis of VLPs (red), *in vitro* assembled Δ MACANCSP2 (blue), and non-assembled Δ MACANCSP2 (green). All experiments had been performed as triplicates. Error bars of the single figures indicate the standard deviation of the measured data points.

According to the literature (Datta, et al., 2007), Gag forms a mono-/dimeric equilibrium, which in the presence of IP6 is altered to a mainly mono-/trimeric equilibrium. These trimers are thought to be a possible structural precursor for the assembly of the hexameric lattice. In the following experiment, I addressed whether the presence of IP6 is affecting the processing as well. Since Gag-His WT was shown to be precipitated in the presence of a high concentration of IP6 (6.2), Δ MACANCSP2 WT was used instead to monitor the processing of non-assembled protein. Therefore, 60 μ M Δ MACANCSP2 was dialyzed in PB with and without 60 μ M IP6 before processing and diluted afterward to 27 μ M Δ MACANCSP2.

The ratio of dimeric Δ MACANCSP2 without IP6 should be 70 %, according to the dissociation constant of $\sim 8.34 \mu$ M determined above (6.1). In the presence of IP6, the association constant (K_a) for trimeric Gag was determined to be $6.714 \times 10^9 \text{ M}^{-2}$ (Datta, et al., 2007). In conclusion, the Gag would be present at ~ 65 % as a trimer.

The cleavage of non-assembled Δ MACANCSP2 with and without IP6 proceeded with comparable dynamics (Figure 26). MA-CA, SP1-NC, and NC-SP2 were processed in both cases similar with half-lives of 1.2, 12, and 70 min, respectively. However, the apparent cleavage rate for CA-SP1 was ~ 20 % higher in the absence of IP6.

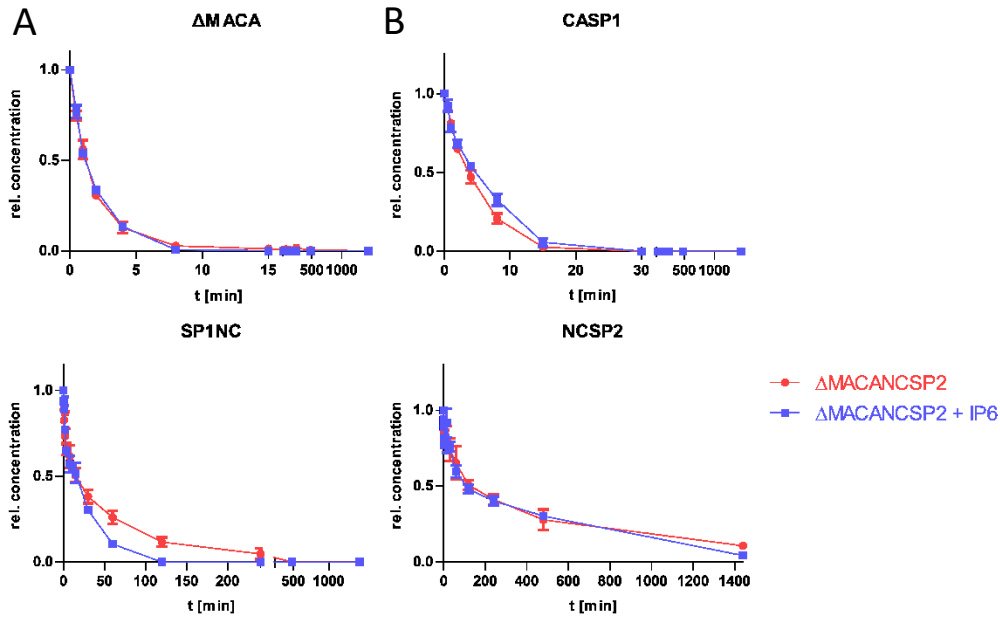


Figure 26: Time-course analysis of the processing of Δ MACANCSP2 in the presence and absence of IP6. Coomassie G-250 stained Tricine-PAGEs were analyzed by ImageJ and Ilastik as described in materials and method, calculating concentrations of all existing products at each time point. Starting at a relative concentration (= 1), the amount of unprocessed CSs present in intermediates decreases over time. The summed concentration of products carrying unprocessed Δ MA-CA (A), CA-SP1 (B), SP1-NC (C), or NC-SP2 (D) are plotted for proteolysis of 60 μ M non-assembled Δ MACANCSP2 without IP6 (red) with 27 μ M IP6 (blue). All experiments had been performed as triplicates. Error bars of the single figures indicate the standard deviation of the measured data points.

6.4.3 Maturation altering conditions

After the establishment of a processing protocol and a tool for quantitative analysis (6.3), the processing of non-assembled Gag-His WT and assembled Δ MACANCSP2 WT was achieved and revealed a considerable difference in the processing order and kinetics. In the following chapters, I tried to influence the processing of non-assembled and assembled protein by changing the conditions or introducing CS mutations. With this, the aim was to evaluate whether the processing of the single CSs is dependent on other cleavage events. Therefore, conditions as different pH values for the processing and usage of different types of NA for the assembly were tested. Additionally, mutations for the inhibition or alteration of certain cleavage events were introduced, and the maturation inhibitor bevirimat was also tested (the name, function, and source of specific mutations/ substances will be explained in the respective chapters).

Therefore, these mutants needed to be produced and purified as well. The purification protocol mentioned above (5.2.2.2) worked for all mutants of Gag-His and Δ MACANCSP2. In all cases, the final purity and concentration were in a comparable range (Figure 43 in chapter 9) with a total yield between 5 – 16 mg/L bacterial culture. The ratio of absorption at 260 nm and 280 nm was lower than 0.6 for all final protein samples, which implies no detectable traces of NA after the purification.

6.4.3.1 Impact of physiological vs. active protease pH

The pH optimum for HIV-1 PR has been determined to be 5.0 – 6.0 depending on the methods used for analysis (Tamburini, et al., 1990; Cheng, et al., 1990; Ido, et al., 1991), as described in chapter 4.4.1. For that reason, pH 6.0 was chosen for the processing experiments in this thesis. It is still unknown, at which pH value the maturation in viral particles takes place. However, because the physiological pH in human cells and blood is in the neutral range (7.0 – 7.4; reviewed in Diem, et al., 1970), this may affect the processing order and dynamics dramatically. Therefore, a series of different pH values, namely pH 6.0 (standard conditions), 6.5, and 7.0, was used to analyze the impact of pH in the acidic to neutral range on the processing of Gag in a non-assembled and assembled pattern. Gag-His WT was applied as the model for non-assembled protein processing and Δ MACANCSP2 WT for the processing of assembled protein (Figure 52 in chapter 9). The preparation of samples for processing was performed as before (5.2.2.5 and 5.2.2.4).

In order to control for the integrity of particles at the mentioned pH values, negative stain TEM was performed. At all three pH values, the particles after dialysis displayed the expected spherical shape with a diameter of \sim 90 nm (Figure 27). Measuring the centrifugable fraction after assembly proved that all three pH values yielded more than 80 % of Δ MACANCSP2 bound in the pelletable material. Based on this, the amount and quality of the particles matched that of the former experiments at pH 6.0 (6.2), and all assembled particles could be used for the processing experiments.

Surprisingly, Δ MA-CA in assembled Δ MACANCSP2 was processed at both higher pH values 30 % faster than at pH 6.0 (Figure 28 F). However, with an increasing pH, MA-CA in non-assembled Gag-His WT was processed 10 % slower (Figure 28 A). While an increased pH had only a minimal effect on the processing of SP1-NC in an assembled pattern (Figure 28 H), the non-assembled protein was processed slower at higher pH, delaying completion of processing from 120 to 480 min. SP1-NC of non-assembled Gag-His WT was hydrolyzed \sim 25 % slower at pH 6.5 than at pH 6.0; furthermore, the step from pH 6.5 to 7.0 reduced the apparent processing rate further to about 50 % more (Figure 28 C). As in the case of SP1-NC, the processing at SP2-p6 was delayed in the non-assembled protein (Figure 28 E) from 120 min to a bit more than 480 min at pH 7.0. The processing at pH 6.5 took 25 % longer than at pH 6.0 according to the decay rates, which increased by 50 % more with increasing the pH to 7.0.

NC-SP2 revealed the fastest processing in assembled Δ MACANCSP2 (Figure 28 I) at pH 6.0 within 120 min with a half-life of \sim 41 min. At pH 6.5, the processing was slightly delayed with a half-life of 44 min, and at pH 7.0 the site processing was not complete after 1440 min. In comparison, the amount of unprocessed NC-SP2 after 1440 min increased for non-assembled Gag-His WT from 8 % at pH 6.0 to 40 % at pH 6.5 and 64 % at pH 7.0 (Figure 28 D).

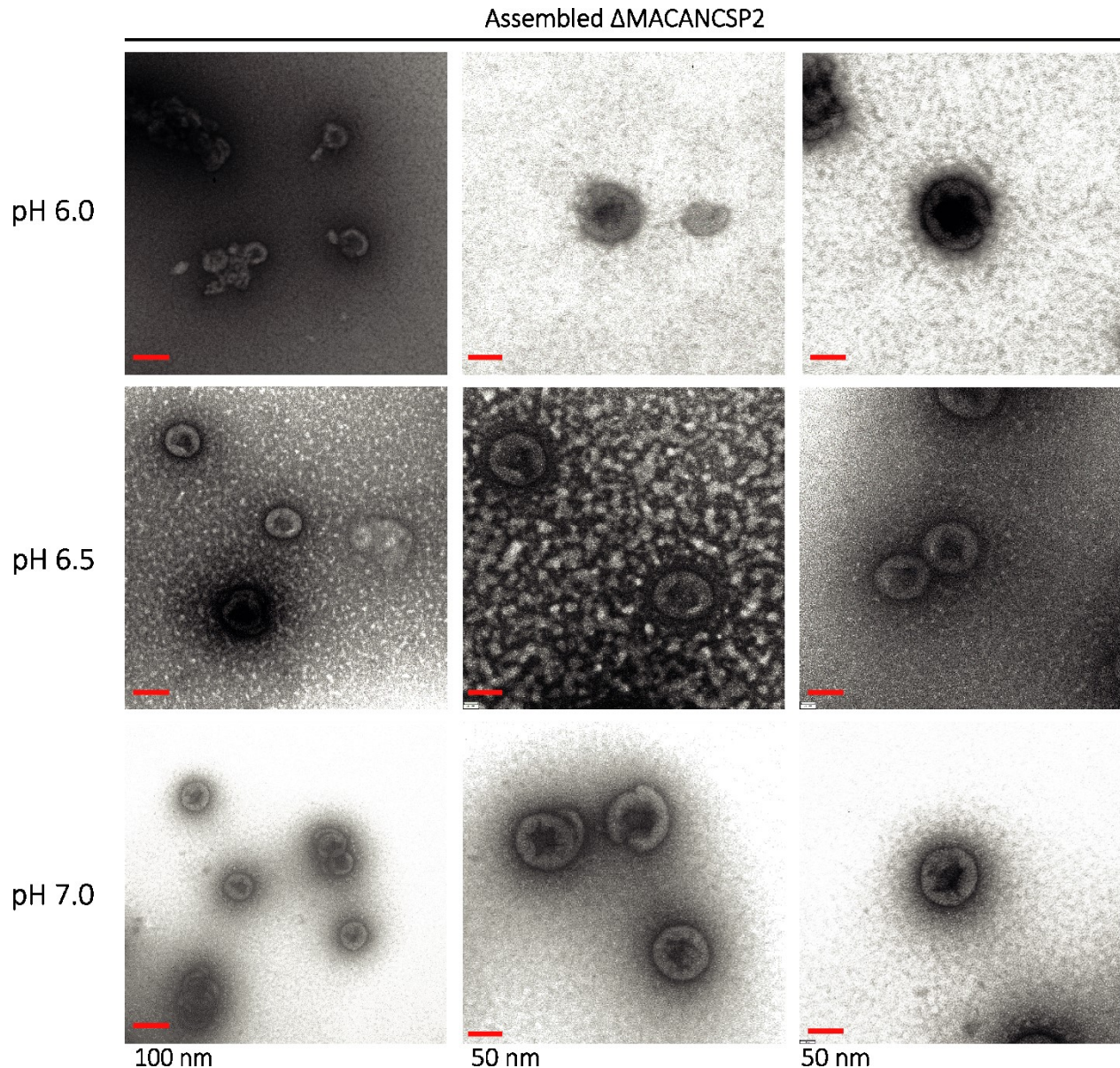


Figure 27: Morphological control of *in vitro* assembled Δ MACANCSP2 dialyzed at different pH values by TEM. Samples of recombinant purified Δ MACANCSP2 WT were assembled *in vitro* by dialysis in assembly buffer in the presence of 4 % standard oligonucleotide for assembly at 4 °C. Subsequently, the particle suspension was dialyzed for processing experiments in processing buffer (5.2.2.5) at pH 6.0, 6.5, or 7.0. Afterward, the resulting particles were analyzed by TEM with negative staining of 3 % uranyl acetate. Different magnifications show local and size distribution of assembled particles of MACANCSP2 MA-CA (top), CA-SP1 (upper-middle), SP1-NC (lower-middle), and NC-SP2 (bottom). The scale bars (red) indicate 100 and 50 nm.

CA-SP1 was fully processed in non assembled Gag-His WT withing 15 min yielding a half-life of 1.2 min. The processing was 3-4-times slower at pH 6.5, yielding a half-life of 3.7 min and full processing after 60 min, whereas at pH 7.0, completion of processing was delayed to 1440 min, which yielded a 5-times higher half-life of 19 min than at pH 6.5 (Figure 28 B). In the case of assembled Δ MACANCSP2, CA-SP1 was processed at pH 6.0 almost within 60 min yielding a half-life of \sim 17 min. At pH 6.5, CA-SP1 was totally processed after 120 min with a 2-fold lower decay rate than at a pH of 6.0 (Figure 28 G). \sim 50 % CA-SP1

remained unprocessed after 1440 min in the case of pH 7.0, preventing estimation of half-life or decay rate.

Since completion of processing at all sites was not achieved at the higher pH values, pH 6.0 was used in all further experiments.

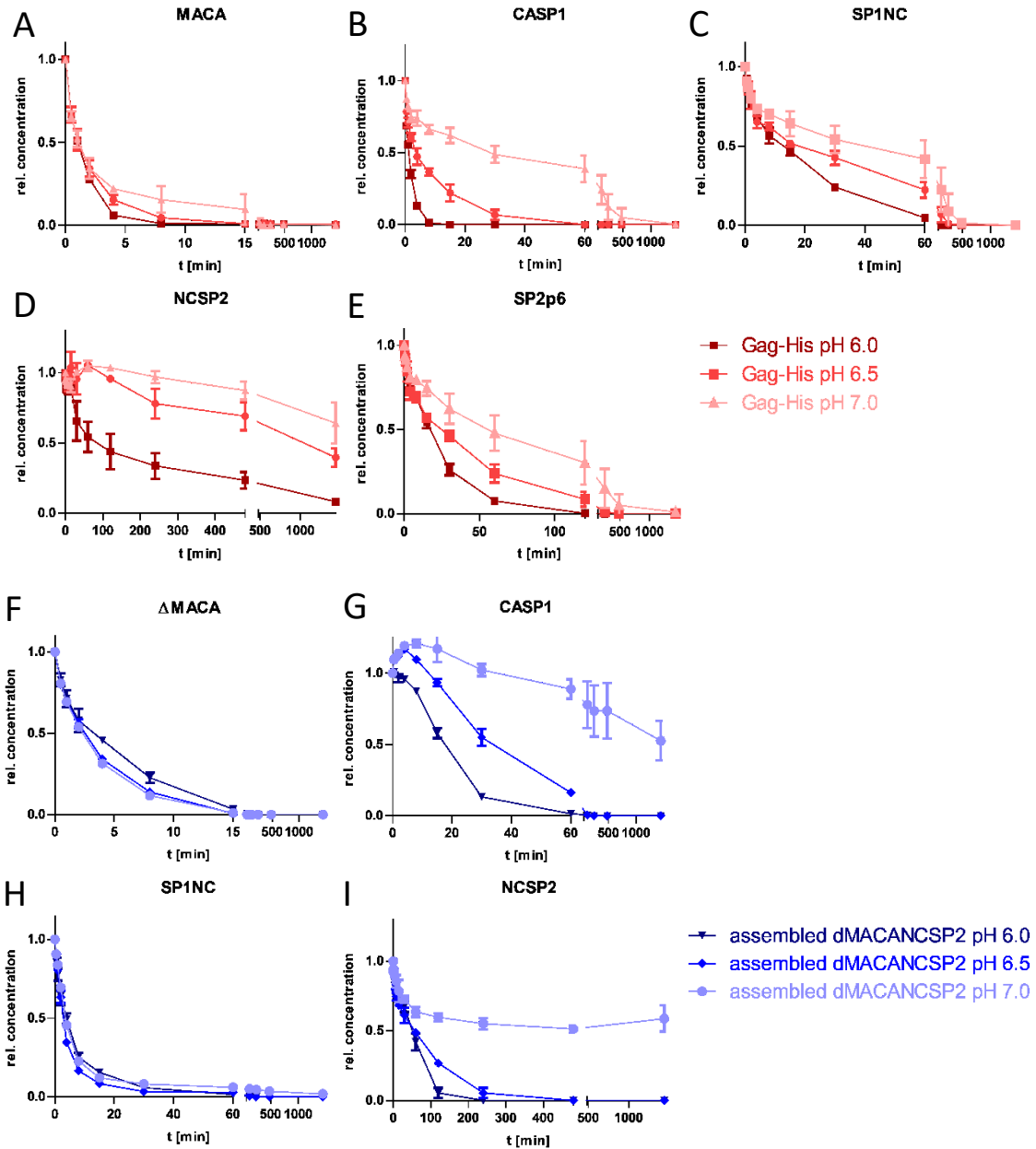


Figure 28: Time-course analysis of the processing of non-assembled Gag-His WT and *in vitro* assembled Δ MACANCSP2 WT at different pH values. Coomassie G-250 stained Tricine-PAGEs were analyzed by ImageJ and Ilastik as described in materials and method, calculating concentrations of all existing products at each time point. Starting at a relative concentration (= 1), the amount of unprocessed CSs present in intermediates decreases over time. The summed concentration of products carrying unprocessed Δ MA-CA/MA-CA (A, F), CA-SP1 (B, G), SP1-NC (C, H), NC-SP2 (D, I), or SP2-p6 (E) are plotted for proteolysis of unassembled Gag-His WT at pH 6.0 (dark-red), pH 6.5 (red), and pH 7.0 (bright red) or of *in vitro* assembled Δ MACANCSP2 at pH 6.0 (dark-blue), pH 6.5 (blue), and pH 7.0 (bright-blue). All experiments had been performed as triplicates. Error bars of the single figures indicate the standard deviation of the measured data points.

6.4.3.2 The effect of nucleic acid on Gag processing

The NC protein of Gag is, in principle, capable of binding to any NA independent of length and sequence. One NC is thought to bind to five bases of the NA strand (Fisher, et al., 1998; Stephen, et al., 2007). NA of at least 12 – 30 nucleotides are essential for a proper assembly (Chen, et al., 2017; Campbell, et al., 1999; reviewed in Rein, et al., 2011). In the *in vitro* based experiments, a clear correlation between the presence of ss NA and an enhanced processing of NC intermediates during maturation was shown (Mirambeau, et al., 2007; Sheng, et al., 1997; Deshmukh, et al., 2015; Potempa, et al., 2015).

In order to test the effect of NA length on the processing of assembled spherical particles with Gag, different experiments using varying oligonucleotides was performed. Oligonucleotides used for assembly were a 68mer (standard oligonucleotide for assembly) and the substantially longer MS2 RNA (3569 nt). I had demonstrated before that the assembly of Δ MACANCSP2 with the standard oligonucleotide for assembly enhanced the processing rates of CSs in SP1-NC-SP2 (6.4.2) compared to non-assembled protein. Whether this acceleration was caused by the binding of NC to NA or by the spatial concentration of substrate by several NC binding to one NA molecule was not yet clarified. Therefore, Δ MACANCSP2 was assembled prior to the processing in one experiment without NA and in another with a pentameric primer, which should only be bound to one NC at a time. As a control, non-assembled Gag-His WT was also processed under the same conditions.

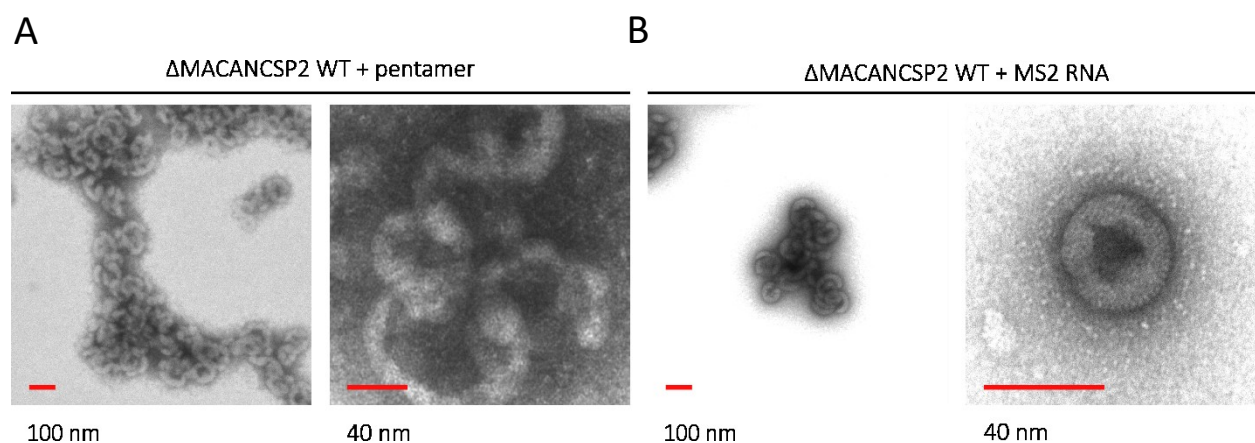


Figure 29: TEM images of *in vitro* assembled Δ MACANCSP2 with a pentameric oligonucleotide or with MS2 RNA. Sample of recombinant purified Δ MACANCSP2 WT was assembled *in vitro* by dialysis in assembly buffer (5.2.2.4) in the presence of 4 % a pentameric oligonucleotide (A) or MS2 RNA (B) at 4 °C. Subsequently, the particle suspension was dialyzed for processing experiments in processing buffer (5.2.2.5). The resulting particles were analyzed by negative stain TEM using 3 % uranyl acetate. Different magnifications show the local and size distribution of assembled particles of MACANCSP2. The scale bars are indicated in red.

27 μ M non-assembled Gag-His was incubated for 30 min at room temperature with the respective NA prior to the addition of PR. Afterward, there was no visible turbidity of the sample, which indicated that no major aggregation or assembly took place. In parallel, 60 μ M Δ MACANCSP2 were assembled and dialyzed with the respective NA, and the resulting particles were diluted to 27 μ M prior to the processing

and analyzed by negative stain TEM. The assembly in the presence of MS2 RNA (Figure 29 B) led to comparable particles regarding shape and size as those assembled in the presence of the standard oligonucleotide for assembly (Figure 13 E – H). The use of the pentameric oligonucleotide resulted in inefficient assembly. However, the major part of an assembled structures displayed similar morphologies as Δ MACANCSP2 assembled in the absence of NA (compare Figure 29 A and Figure 16 A).

According to the analysis of processing products (Figure 45 A + Figure 46 in chapter 9), NA had no major effect on the processing of non-assembled Gag-His WT. Cleavage at MA-CA, CA-SP1, and SP2-p6 revealed less than 10 % deviation between the different oligonucleotides (Figure 30 A, B, and E). In contrast, the pentameric nucleotide appeared to alter the processing (Figure 30 C and D). Due to the reduced PR activity at the later phases of the processing rates at SP1-NC and NC-SP2 (6.3.3) and the high standard deviation for the processing with the pentameric nucleotide (Figure 30 regular red lines), a clear quantitative comparison to the other conditions could not be achieved. At least, increased processing upon the addition of NA did not occur, however.

In presence of the pentameric nucleotide and absence of any NA, the cleavage rates at MA-CA of assembled Δ MACANCSP2 were ~ 33 % faster as for the other NA conditions (Figure 30 F), while processing of CA-SP1 was not affected by the presence of NA according to the decay rates (Figure 30 G). However, the processing of SP1-NC was ~ 50 % faster with the standard oligonucleotide for assembly than with the MS2 RNA for assembled Δ MACANCSP2 (Figure 30 H black and dark-blue lines). The processing at NC-SP2 occurred similarly for the two NA types (Figure 30 I black and dark-blue lines). In contrast, the processing at SP1-NC and NC-SP2 of assembled Δ MACANCSP2 in the absence of NA took place with similar rates as for non-assembled Gag-His (compare Figure 30 D + E and Figure 30 H + I bright-blue line). The use of the pentameric nucleotide slightly accelerated the processing (by 10 – 20 %) at these sites compared to assembled Δ MACANCSP2 in the absence of NA (Figure 30 H + I blue and bright-blue line), which was, however, still 20 % slower at the SP1-NC and 60 % at the NC-SP2 site compared to the assembly with MS2 RNA.

In summary, the presence of NA had no accelerating influence on the processing of non-assembled Gag-His. While MA-CA and CA-SP1 processing steps were also not majorly affected, assembled Δ MACANCSP2 with the pentameric nucleotide or in the absence of NA were processed at SP1-NC and NC-SP2 with comparable rates as the non-assembled protein, whereas the assembly with longer NA resulted in increased processing rates.

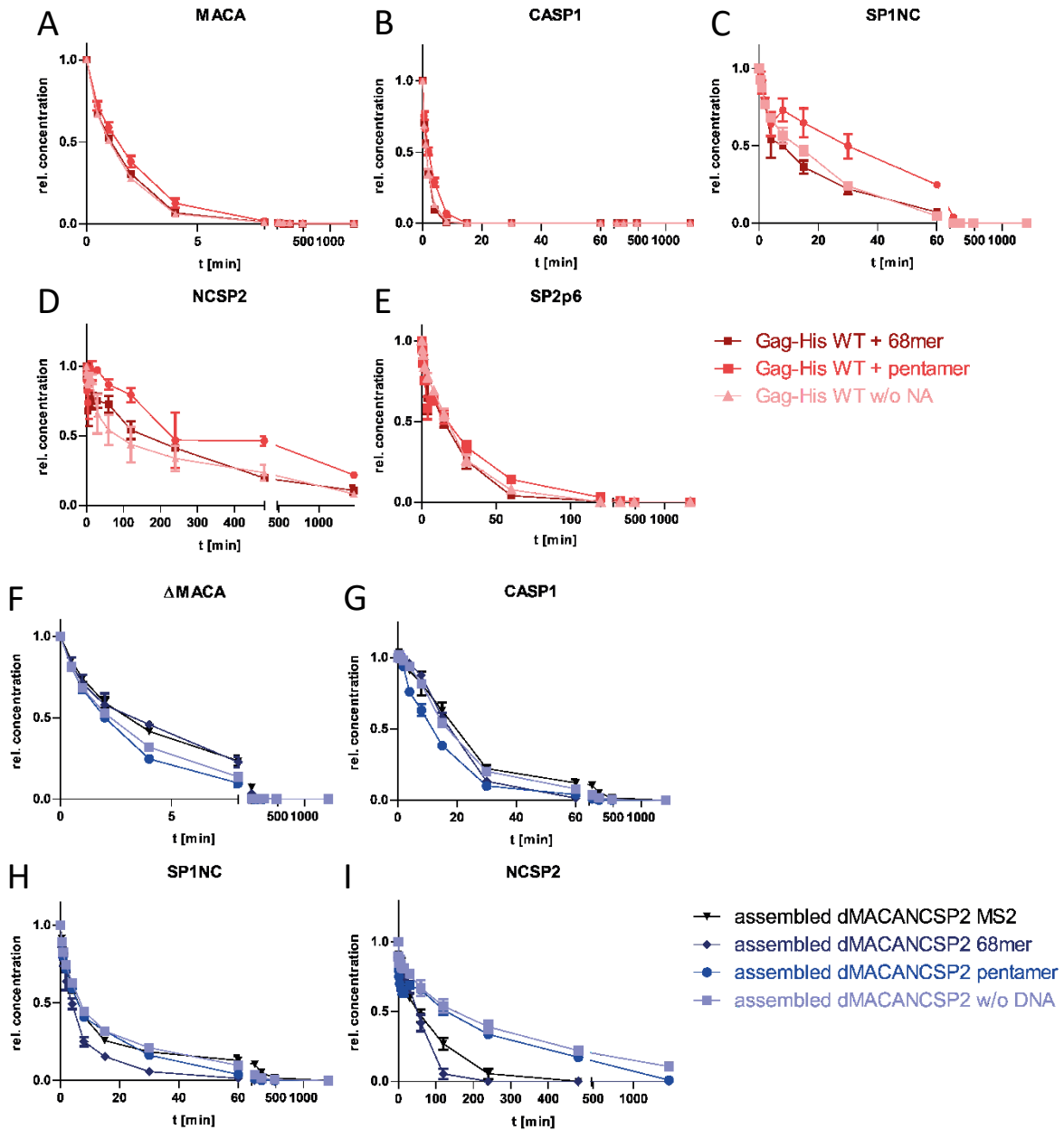


Figure 30: Time-course analysis of processing of assembled and non-assembled Gag WT in the absence or presence of different nucleic acid. Coomassie G-250 stained Tricine-PAGEs were analyzed by ImageJ and Ilastik as described in materials and method, calculating concentrations of all existing products at each time point. Starting at a relative concentration (= 1), the amount of unprocessed CSs present in intermediates decreases over time. The summed concentration of products carrying unprocessed Δ MA-CA/ MA-CA (A, F), CA-SP1 (B, G), SP1-NC (C, H), NC-SP2 (D, I), or SP2-p6 (E) are plotted for proteolysis of unassembled Gag-His WT (A – E) with 68mer oligonucleotide (dark-red), with a pentamer oligonucleotide (red), and without NA (bright-red), and assembled Δ MACANCSP2 (F – I) with MS2 RNA (black), with 68mer oligonucleotide (dark-blue), with a pentamer oligonucleotide (blue), and without NA (bright-blue). All experiments had been performed as triplicates. Error bars of the single figures indicate the standard deviation of the measured data points.

6.4.3.3 Inhibition of single cleavage events by point mutations

As described in chapter 4.3, maturation relies on sequential processing steps. How the impairment of cleavage at one site affects the processing rate of all other CS in the context of the assembled particles has yet not been quantified. Previously published results (Pettit, et al., 1994) indicate that inhibition of one CS for *in vitro* translated Gag had no or only minor effect on processing at other sites. Only due to the inhibition of SP1-NC, the CA-SP1 was processed with higher rates. However, as mentioned before, the experiments with *in vitro* translated Gag were not considering the state of oligomerization and could not achieve the analysis for all CS.

Therefore, mutations reported inhibiting processing (Figure 31) were introduced at individual CS of Gag-His as well as at Δ MACANCSP2 for the production of assembled particles. Mutations are referred to as Gag-His MA-CA, Δ MACANCSP2 MA-CA, Gag-His CA-SP1, etc.. The protein and particle samples were prepared according to the protocols described above (6.4.1 + 6.4.2). All versions of assembled Δ MACANCSP2 composing a CS inhibiting mutation were analyzed by TEM as before to exclude any aberrant morphological structures. Particle size and shape closely resembled that of the WT protein of Δ MACANCSP2. Particles were dispersed and roughly 90 – 100 nm in diameter (Figure 32), which indicates that the introduced mutations had no vital impact on the assembly of Δ MACANCSP2 or their biochemical properties.

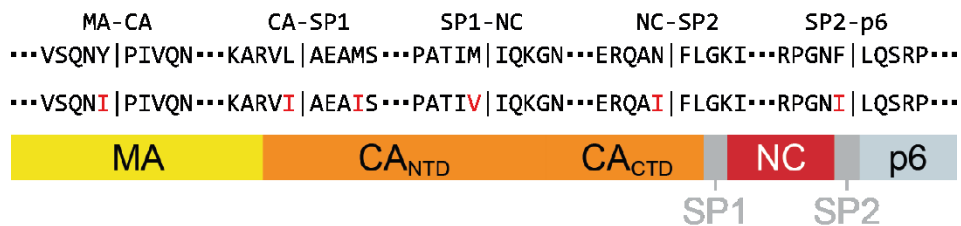


Figure 31: Gag sequences at protease cleavage sites and their cleavage inhibiting mutations. The prequel and sequel amino acid sequences of all cleavage sites can be blocked by single and double mutations (red letters). While MA-CA, SP1-NC, NC-SP2, and SP2-p6 are affected by substitution of the first amino acids upstream of the CS by isoleucine (Wyma, et al., 2004) or valine in the case of SP1-NC (Wiegiers, et al., 1998), CA-SP1 needs another substitution by isoleucine the fourth amino acids downstream of the cleavage site to prevent processing at another cryptic cleavage site (Wiegiers, et al., 1998).

Non-assembled Gag-His and assembled Δ MACANCSP2 carrying the mutations shown in Figure 31 were processed according to the protocol described in the previous chapters (6.3.1 + 6.4.2) and analyzed with the help of Coomassie-stained Tricine-PAGEs (Figure 49, and Figure 47 in chapter 9). The mutation at the MA-CA CS inhibited the cleavage at this site for non-assembled and assembled protein, while other mutations were processed only with minor differences from the WT (Figure 33 A + F). Inhibiting mutations of MA-CA, NC-SP2, and SP2-p6 had no relevant impact on the processing, but the mutation of CA-SP1 inhibited the processing fully (Figure 33 B + G). When the cleavage at the SP1-NC site was inhibited of

assembled Δ MACANCSP2, the CA-SP1 site was processed $\sim 40\%$ slower in relation to Δ MACANCSP2 WT (Figure 33 G red and orange line). This result is contrary to previously described observation that inhibition of SP1-NC enhances the processing of CA-SP1 (Pettit, et al., 1994) obtained using *in vitro* translated Gag.

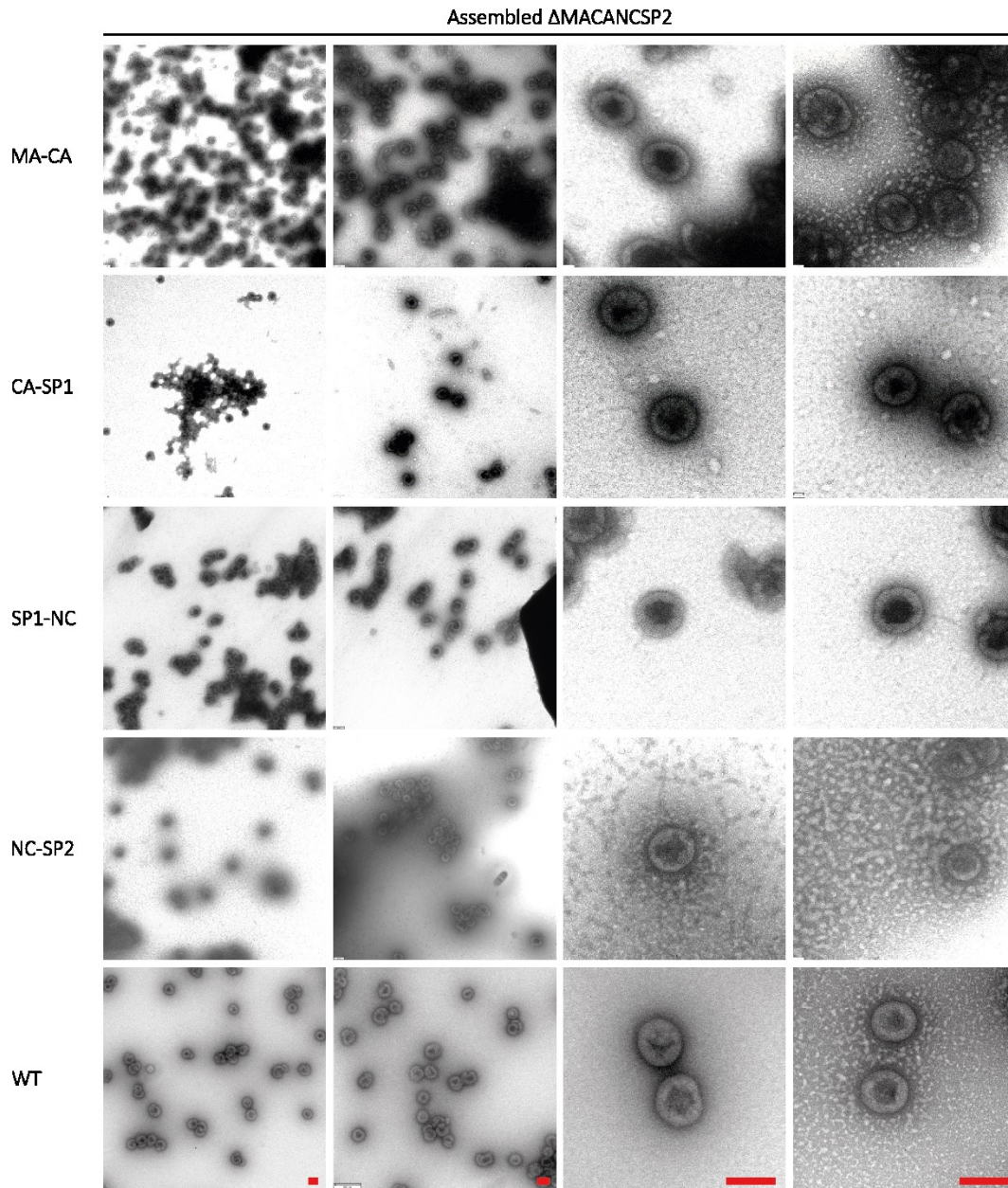


Figure 32: Morphology of *in vitro* assembled Δ MACANCSP2 particles carrying cleavage site mutations. Sample of recombinant purified Δ MACANCSP2 for all four versions with an inhibited CSs mutation and wild-type were assembled, respectively, *in vitro* by dialysis in assembly buffer (5.2.2.4) in the presence of 4 % standard oligonucleotide for assembly (5.1.7) at 4 °C. Subsequently, the particle suspension was dialyzed for processing experiments in processing buffer (5.2.2.5). The resulting particles were analyzed by TEM with negative staining of 3 % uranyl acetate. Different magnifications show local and size distribution of assembled particles of MACANCSP2 MA-CA (top), CA-SP1 (upper-middle), SP1-NC (middle), NC-SP2 (lower-middle), and WT (bottom). The scale bars (red) indicates 100 nm.

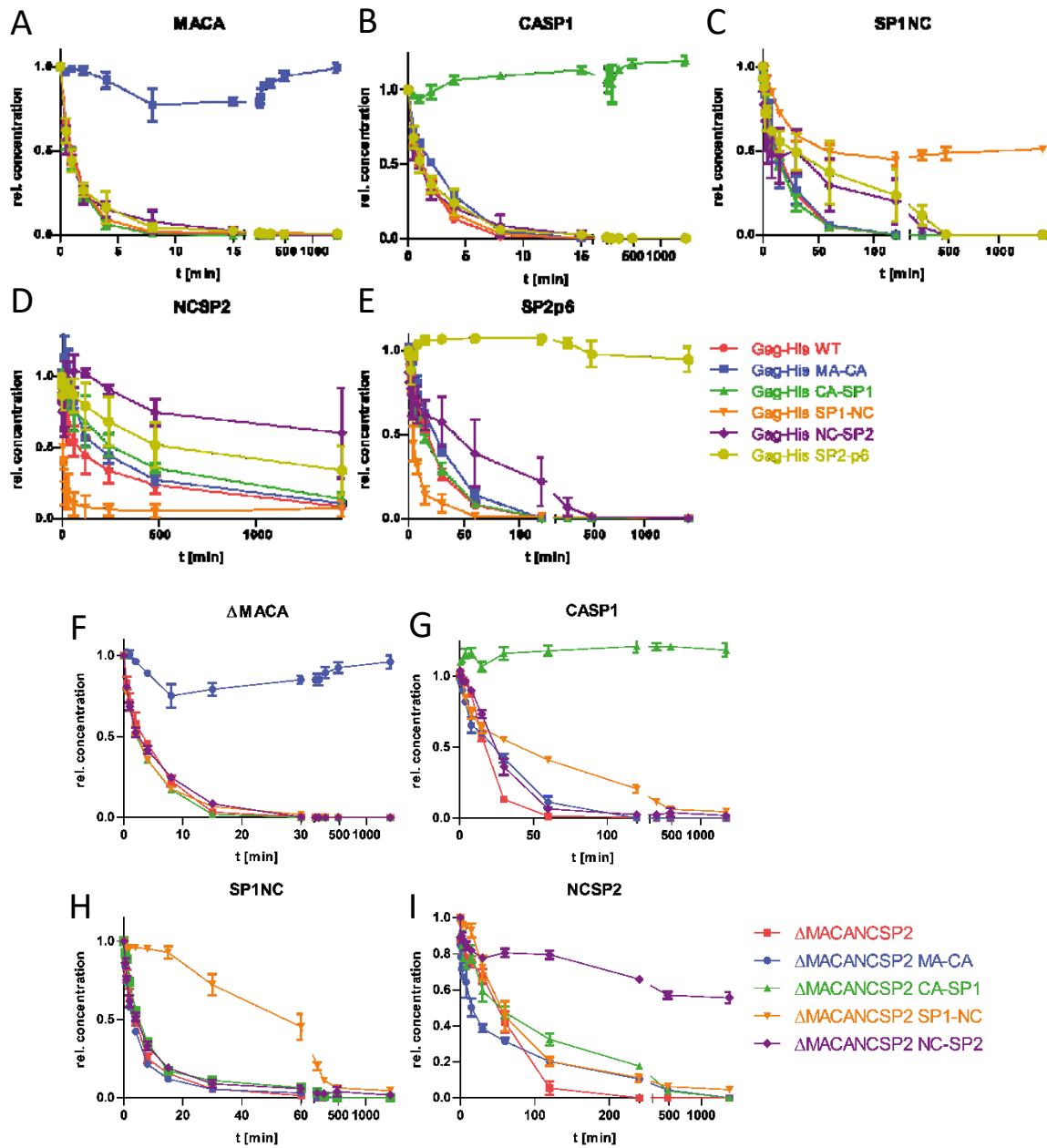


Figure 33: Time-course analysis of non-assembled Gag-His and *in vitro* assembled Δ MACANCSP2 containing cleavage inhibiting mutations. Coomassie G-250 stained Tricine-PAGEs were analyzed by ImageJ and Ilastik as described in materials and method, calculating concentrations of all existing products at each time point. Starting at a relative concentration (= 1), the amount of unprocessed CSs present in intermediates decreases over time. The summed concentration of products carrying unprocessed Δ MA-CA/MA-CA, CA-SP1, SP1-NC, or NC-SP2 are plotted for proteolysis of (A, B, C, D, E) unassembled Gag-His WT (red), Gag-His MA-CA (blue), Gag-His CA-SP1 (green), Gag-His SP1-NC (orange), and Gag-His NC-SP2 (purple) and *in vitro* assembled (F, G, H, I) Δ MACANCSP2 WT (red), MA-CA (blue), CA-SP1 (green), SP1-NC (orange), and NC-SP2 (purple). All experiments had been performed as triplicates. Error bars of the single figures indicate the standard deviation of the measured data points.

Inhibition of SP1-NC, non-assembled and assembled, lead to slower processing at this site (Figure 33 C + H). Since SP1-NC was not detectable by Coomassie-stained Tricine-PAGE, the concentration of unprocessed SP1-NC CS shown here may be underestimated. For the other inhibiting mutations depart

from the site of SP1-NC, only the mutation at NC-SP2 caused a substantial alteration of more than 15 % in the processing rate of SP1-NC. The processing at SP1-NC appeared to be ~ 2-fold higher than for the WT protein in the case of non-assembled Gag-His (Figure 33 C red and orange lines). Since NC-SP2 is processed last in the late phases of the experiments, when the PR activity is diminishing (6.3.3), the fitting by the one-phase decay fitting cannot be applied properly.

Albeit the mutation at NC-SP2 did not inhibit processing, it reduced the processing rate for non-assembled and assembled protein (Figure 33 D + I). SP2-p6 processing was inhibited fully upon the mutation at this site for non-assembled Gag-His (Figure 33 E yellow line), while the mutation at SP1-NC led to 4-fold increased processing of SP2-p6 (Figure 33 E orange line). Other mutations had no relevant impact on the processing of SP2-p6.

In summary, the processing at MA-CA, CA-SP1, or SP2-p6 was inhibited by the respective mutation independent of the oligomerization state of Gag. Additionally, introducing an inhibiting mutation had no impact on the processing of other CSs, except in the case of SP1-NC.

However, in the case of the mutation of MA-CA, an aberrant cleavage was observed. The main product MA-CA appeared to be slowly cleaved within CA slowly over time (Figure 49 A in chapter 9). This effect was stronger for non-assembled Gag-His WT than for assembled Δ MACANCSP2. The determination of this aberrant CS is described in the following chapter (6.4.3.3.1).

As already described, the assembly of the N-terminal region of Gag (SP1-NC-SP2-p6) with NA accelerates the processing at the contained CSs (Pettit, et al., 1998; Sheng, et al., 1997; Mirambeau, et al., 2010). In order to test whether the increased processing at CA-SP1 in the case of impaired cleavage at SP1-NC was dependent on assembly alone or on NC bound to NA, a second experiment was performed. Because the assembly without NA represents an intermediate state between non-assembled and assembled protein, Δ MACANCSP2 SP1-NC was assembled without NA and processed according to the protocol (6.4.2).

As shown in Figure 34 B, the processing rates at CA-SP1 were similar for both assembly states and notably slower than for the assembled WT protein with NA. Even though the processing at SP1-NC of Δ MACANCSP2 WT assembled without NA was 2-fold slower than with NA, the inhibition decreased the processing at this site 10-times more (Figure 34 C). The reducing effect on the processing of NC-SP2 by inhibition of SP1-NC was similar for assembly with and without NA. However, the processing was ~ 37 % faster than for Δ MACANCSP2 WT assembled without NA (Figure 34 D blue and orange line). The cleavage at MA-CA was not affected (Figure 34 A). Consequently, the decreased processing at the CA-SP1 site is not dependent on the binding of NA to NC but the assembly state.

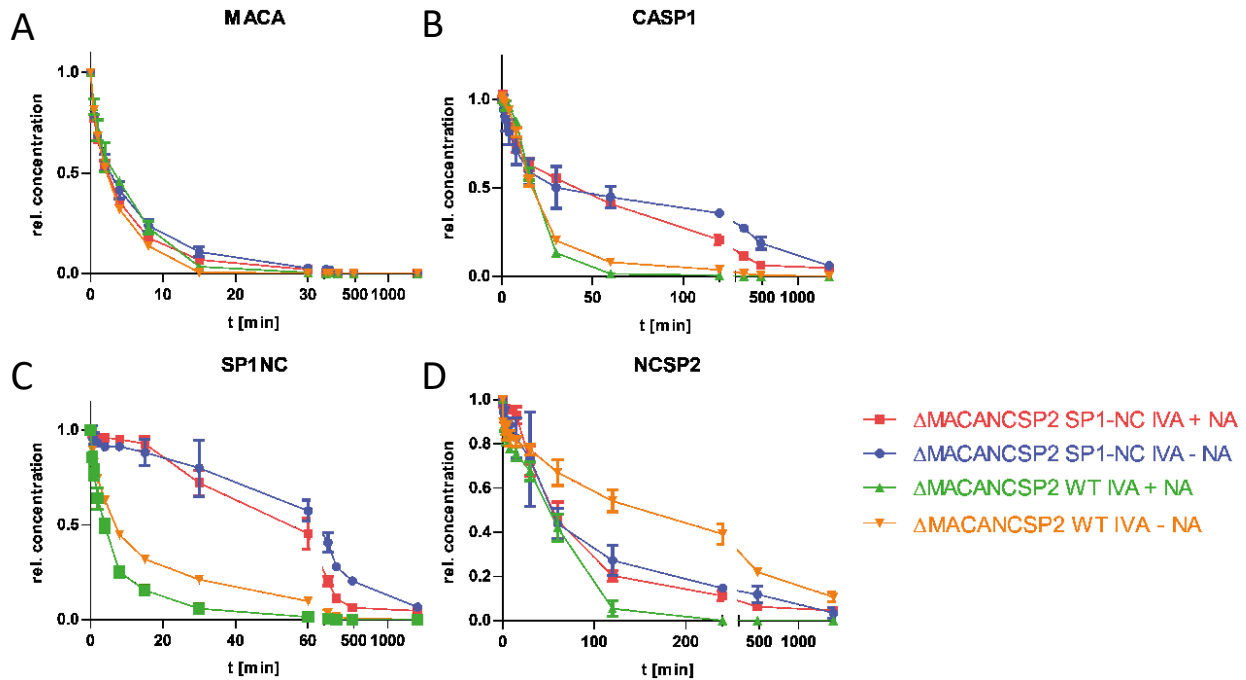


Figure 34: Time-course analysis of *in vitro* assembled Δ MACANCSP2 WT and SP1-NC with and without nucleic acid. Coomassie G-250 stained Tricine-PAGEs were analyzed by ImageJ and Ilastik as described in materials and method, calculating concentrations of all existing products at each time point. Starting at a relative concentration (= 1), the amount of unprocessed CSs present in intermediates decreases over time. The summed concentration of products carrying unprocessed MA-CA (A), CA-SP1 (B), SP1-NC (C), or NC-SP2 (D) are plotted for proteolysis of *in vitro* assembled Δ MACANCSP2 SP1-NC with (red) and without nucleic (blue), and Δ MACANCSP2 WT with (green) and without NA (orange). All experiments had been performed as triplicates. Error bars of the single figures indicate the standard deviation of the measured data points.

6.4.3.3.1 MA-CA inhibition induced aberrant cleavage inside CA

Upon processing of Gag with the inhibited CS mutant at the MA-CA CS (Figure 47 A), two previously not observed bands occurred after ~ 30 min, one of higher electrophoretic mobility than CA (at ~ 22 kDa) and one of lower electrophoretic mobility than MA (at ~ 17 kDa; Figure 35). To test whether the processing at this site was caused by HIV-1 PR rather than by degradation, non-assembled Gag-His MA-CA ($30 \mu\text{M}$) and Gag-His WT ($5.5 \mu\text{M}$) were processed for 24 h. For analysis, the following samples were taken before processing as well as after 2 h and 24 h of incubation:

1. Samples incubated according to the standard processing protocol
2. Samples pre-treated before processing with $20 \mu\text{M}$ tipranavir (TPV) to block HIV-1 PR
3. Samples treated after 2 h with $20 \mu\text{M}$ TPV to inhibit further processing by PR

Samples from all reactions were applied to Coomassie-stained Tricine-PAGE and immunoblot using primary antibodies raised against CA and MA.

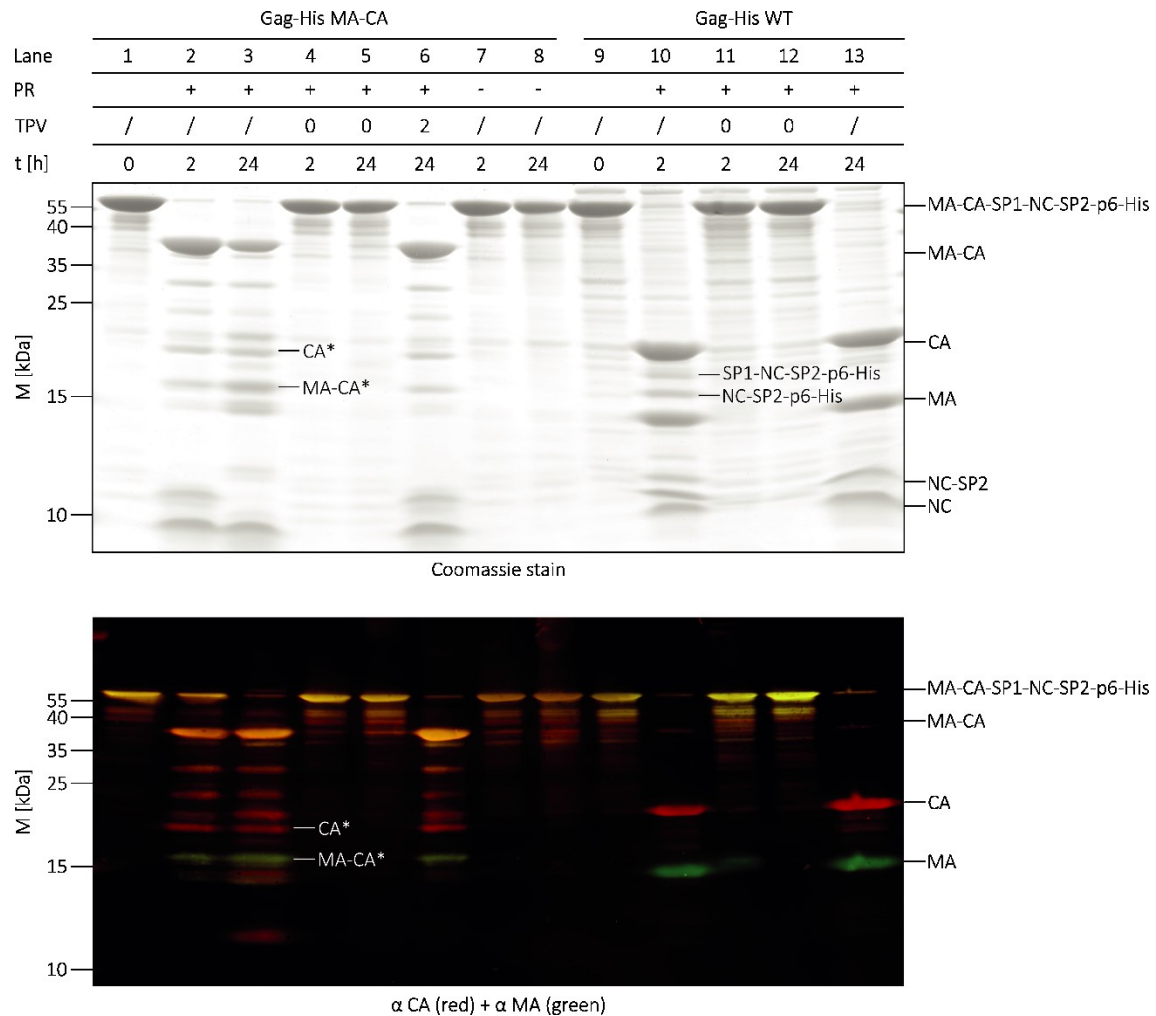


Figure 35: Aberrant cleavage in case of an inhibited MA-CA cleavage site in Gag. Gag-His WT and Gag-His MA-CA were incubated with and without recombinant HIV-1 PR according to the standard protocol (5.2.2.5). Processing was analyzed in the absence of tipranavir (TPV) or after the addition of PR inhibitor TPV at 0 or 2 h. Samples for analysis were taken after 0, 2, or 24 h analyzed by SDS-PAGE (17.5 % PAA, 1:200 AA/BAA) followed by (top) Coomassie G-250 staining or (bottom) immunoblot using polyclonal antisera raised against CA (red) and MA (green). The positions of molecular mass standards marker are shown left, and the position of the Gag-His variants is indicated at the right.

According to the immunoblot (Figure 35), the processing of the wild-type protein was as described before. Already after 2 h, mature MA and CA were detected (Figure 35 lane 10 and 13). The addition of TPV completely inhibited the processing of Gag-His WT (Figure 35 lane 11 and 12). In the case of Gag-His MA-CA processing without TPV, the two unidentified bands were visible after 2 h and even more prominent after 24 h (Figure 35 lane 2 and 3), when mature MA and CA were also present. The higher new band of the two new bands was only recognized by the CA antiserum, while the lower band reacted with MA and CA antisera. This observation suggested that inhibited cleavage of MA-CA lead to processing within CA, providing a shortened version of CA (= CA*) and MA attached to a small part of CA (= MA-CA*). No processing was observed when TPV was added at t = 0 (Figure 35 lane 4 and 5) or in the absence of PR (Figure 35 lane 7 and 8). Furthermore, processing at the aberrant site was stopped entirely when TPV was

added after 2 h (Figure 35 lane 6). These results showed, that the aberrant cleavage within CA is derived by the HIV-1 PR and not by the degradation of Gag.

To analyze where the aberrant cleavage occurred exactly, 30 μ M Gag-His MA-CA was processed according to the protocol (6.3.1) for 36 h, and 500 μ L sample was applied to a Superdex 75 10/300 column (Figure 36 C) to segregate the proteins for intact protein mass spectrometry as done before (6.3.2). Several samples from five elution peaks according to the absorbance at 280 nm were applied for examination to a Tricine-PAGE and stained by Coomassie (Figure 36 B). Peak 1 comprised almost no protein visible in the detection range of Coomassie staining, peak 2 contained mainly MA-CA, peak 3 CA, CA*, MA-CA* and MA, and mainly peak 4 NC. Peak 5 comprised no detectable protein content.

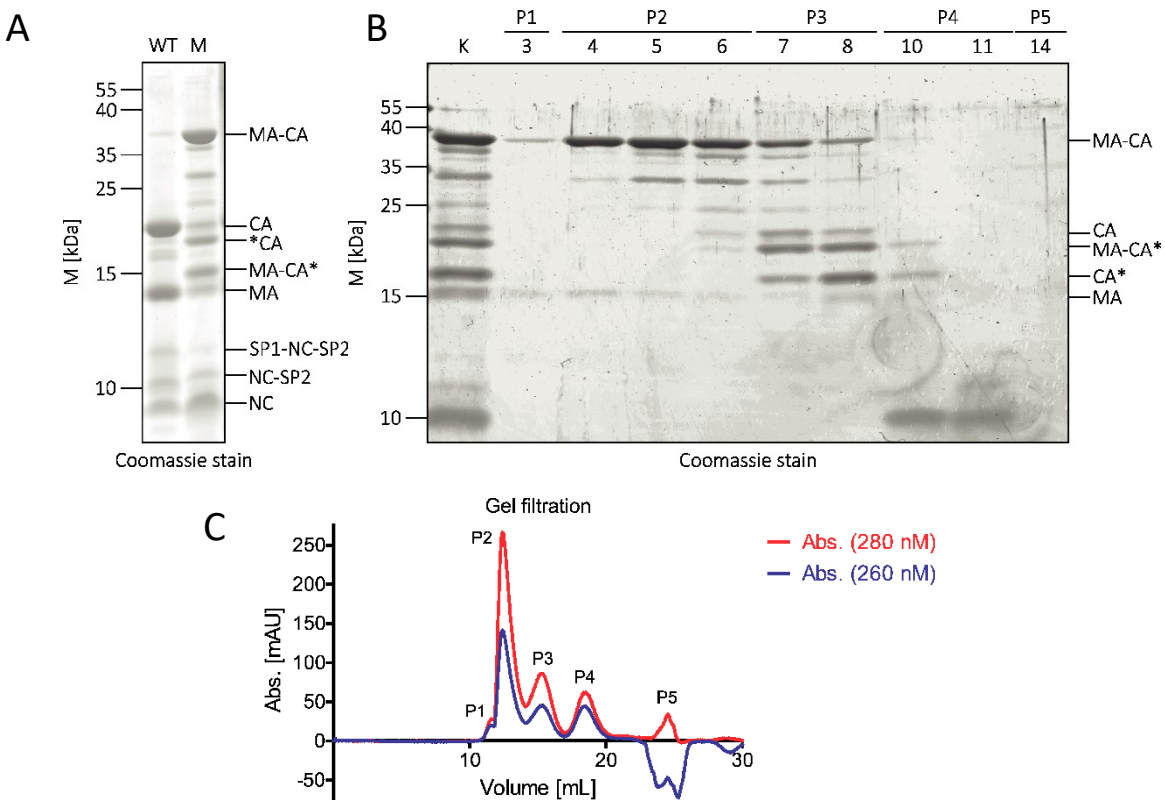


Figure 36: Gel filtration analysis of Gag-His MA-CA processing products. 31 μ M recombinant Gag-His MA-CA was processed according to material and methods with 1 μ M recombinant protease in 750 μ L for 36 h. (A) After processing the processing pattern of products of Gag-His WT (WT) and Gag-His MA-CA (M) showed a recognizable difference in the analysis by Tricine-PAGE (16 % PAA, crosslinking ratio 1:32 BAA/AA and 9.6 % PAA, 1:32 BAA/AA) stained by Coomassie G-250 staining. (B) The resulting sample was loaded on a Superdex 75 10/300, and absorption was measured at 280 nm (red) and 260 nm (blue). (C) Fractions of the gel filtration (3 – 14, Peak 1 – 5) and an unprocessed control sample (K) were analyzed by Tricine-PAGE stained by Coomassie G-250 staining. The position of molecular mass standards marker is shown left, and the position of the Gag-His and processing products are indicated at the right. Fractions 4 and 8 were used for later intact mass spectrometry.

Samples from fraction 4 in peak 2 and fraction 8 in peak 3 were analyzed by intact protein mass spectrometry (5.2.2.6.4). According to the results, mainly a protein of 40245.2 Da was measured in fraction

4 (Figure 48 C), which was identified as MA-CA without the N-terminal methionine (= 40245.9 Da). In the fraction 8 of peak 2, prominent proteins had a mass of 14661.2, 17058.7, 23204.0, and 25602.1 Da (Figure 48 A, B, and C). The smallest protein was identified as MA (= 14661.6 Da) and the largest as CA (= 25602.4 Da), which were less present in the sample according to the detection signal of the mass spectrometry. The combined mass of the two remaining signals was in 40262.7 Da, which is close to the mass of unprocessed MA-CA protein (= 40245.9 Da) plus water (= 18 Da) from the hydrolyzation reaction. Additionally, their signal intensity in the mass spectrometry measurement correlates roughly with the amounts of the aberrant cleaved MA-CA* and CA* relative to the correctly cleaved MA and CA (Figure 48 + Figure 37 A). Calculation of possible polypeptide sequences from the full-length Gag fitting to the two measured masses using ProteinCalculator v3.4 (<http://protcalc.sourceforge.net/>) gave one compatible result for each protein. The suggested fragments were consecutive in the Gag sequence. The first peptide for 17058.7 Da starts at the first amino acid of MA and stops inside CA at the sequence RTLNA at position 154 of Gag. The second polypeptide of 23204.0 Da starts at the position of 155 at the sequence WVKVV and ends at the C-terminus of CA (KARVL). Thus, the aberrant CS was identified as WVKVV|RTLNA within the helix 1 of CA.

6.4.3.4 Analysis of protease inhibitor resistance conveying and cleavage rate altering mutations of Gag

Due to the high mutation rate of HIV-1, it can adapt to certain limiting or critical conditions during infection and replication. As a result of PI treatment of infected patients, mutations occur in the HIV-1 genome as a compensatory mechanism to rescue viral replication and infectivity. Primary mutations are found in the sequence of PR, which reduces the binding affinity of PI to the PR (reviewed in Wensing, et al., 2010). Secondary or accessory mutations of PR enhance the effect of primary mutations or compensate for a reduction of PR activity due to the primary mutations (Callebaut, et al., 2011; van Maarseveen, et al., 2007). However, these mutations are often found in combination with mutations at Gag located primarily at the CSs (reviewed in Shafer, et al., 2008). Recent publications revealed that mutations in the region of NC-SP2-p6 contribute to PI resistance even without mutations in PR confirmed by clinical observations (Dam, et al., 2009) and cell culture experiments (Nijhuis, et al., 2007), albeit the actual mechanism is not yet fully understood.

To complement to the clinical and *in vivo* data for obtained Gag mutations conveying PI resistance, I wanted to study the effect of mutations on the processing of non-assembled Gag yielding one of the mentioned mutations processed by recombinant wild-type PR as before, what could help to understand the mechanism better how the mutations contribute to PR resistance. Here, I focused on two previously described mutations (A431V and I437V) at NC-SP2 of Gag. Both were shown to contribute strongly to the resistance of the virus to PI, even though their effect on the replicative capacity was negligible (Dam, et al., 2009). Processing and data analysis (Figure 50 in chapter 9) were performed as described above.

In the case of Gag-His I437V, the processing of MA-CA, CA-SP1, and SP2-p6 appeared to be of less than 15 % different in comparison to the rates determined for Gag-His WT (Figure 37 A, B, and E green and red

lines). However, cleavage at SP1-NC occurred 20 % slower, which is also the case of Gag-His A431V (Figure 37 C). The cleavage of NC-SP2 was affected most, as A431V and I437V seemed to decrease the processing (Figure 37 D). For MA-CA and CA-SP1, the mutation A431V may indicate a decreased processing. However, as the standard deviation was relatively high in the data set of A431V, the differences to other experiments remain unclear. Nevertheless, the introduction of the mutations of A431V or I437V yielded especially for NC-SP2 no notable difference.

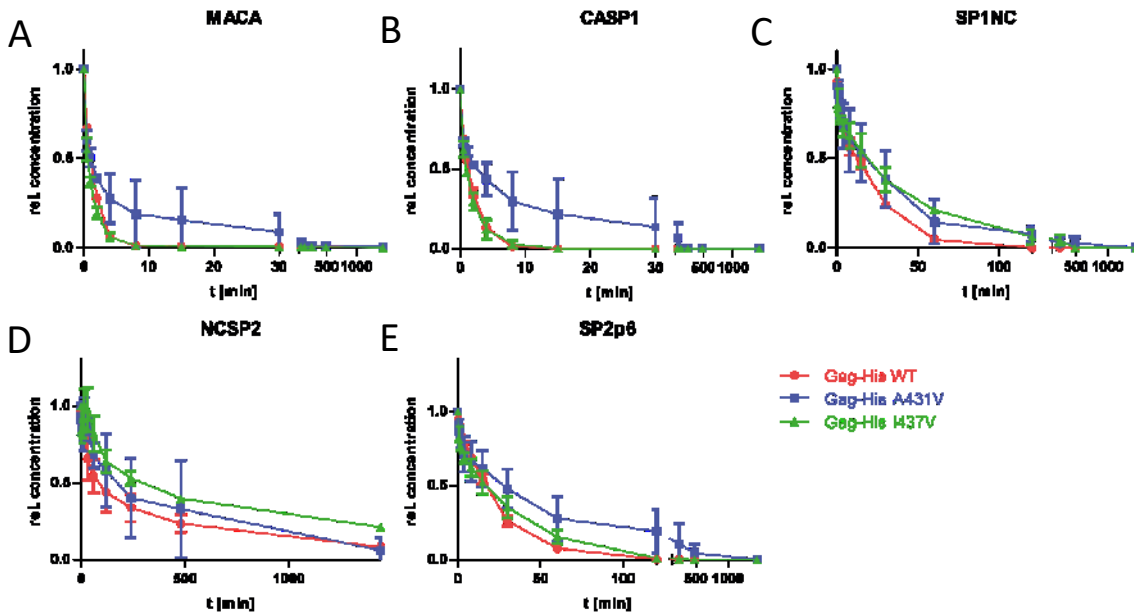


Figure 37: Similar processing of Gag-His WT and with Gag mutations enabling protease inhibitor resistance. Coomassie G-250 stained Tricine-PAGEs were analyzed by ImageJ and Ilastik as described in materials and method, calculating concentrations of all existing products at each time point. Starting at a relative concentration (= 1), the amount of unprocessed CSs present in intermediates decreases over time. The summed concentration of products carrying unprocessed MA-CA (A), CA-SP1 (B), SP1-NC (C), NC-SP2 (D) or SP2-p6 (E) are plotted for proteolysis of unassembled Gag-His WT (red), Gag-His A431V (blue), and Gag-His I437V (green). All experiments had been performed as triplicates. Error bars of the single figures indicate the standard deviation of the measured data points.

I further analyzed Gag carrying mutations designed to alter the speed of processing at the sites flanking SP2. Cleavage at the CSs in the region of NC-SP2-p6 was shown to be relevant for viral infectivity and core formation (de Marco, et al., 2012; Coren, et al., 2007; Müller, et al., 2009). The inhibition of cleavage at SP2-p6 severely abolished viral infectivity and led to majorly deformed viral cores. Inhibition of NC-SP2 or complete deletion of SP2, however, had a mild effect on viral infectivity and core formation (de Marco, et al., 2012). Thus, it was concluded that at one fast CS downstream of NC may be important for maturation in viral particles (de Marco, et al., 2012). Why and how both mutations participate to ensure the correct formation of viral cores remains yet not fully understood and, as these observations were yet not compared to kinetic data of Gag processing, this could give more insight about the dependencies of the temporal release of NC-SP2 and SP2-p6 during proteolytic maturation.

Previous research by (Pettit, et al., 2002) identified several CS mutations that alter the processing rates at individual sites of *in vitro* translated Gag. Since the experiments with *in vitro* translated Gag were not considering the oligomerization state of Gag and because these mutations are only analyzed regarding the processing rate at the respective mutated site, I decided to apply the improved analysis tool for Gag processing to the mutations N432L and F448M. While the former was described as an enhancer for 30-fold processing rates at the slow CS NC-SP2, the latter reduces the cleavage rate at the fast CS SP2-p6 about 7-fold (Pettit, et al., 2002), so both in combination should potentially enable full processing of Gag and change the order of processing regarding of these sites (Pettit, et al., 2002). As the Δ MACANCS2 does not comprise an SP2-p6 CS, the processing of the assembled protein was excluded from this experiment. Therefore, 27 μ M non-assembled Gag-His comprising single mutations solely (N432L or F448M) or both in combination (Figure 51 in chapter 9) was processed according to the mentioned protocol (6.3.1),.

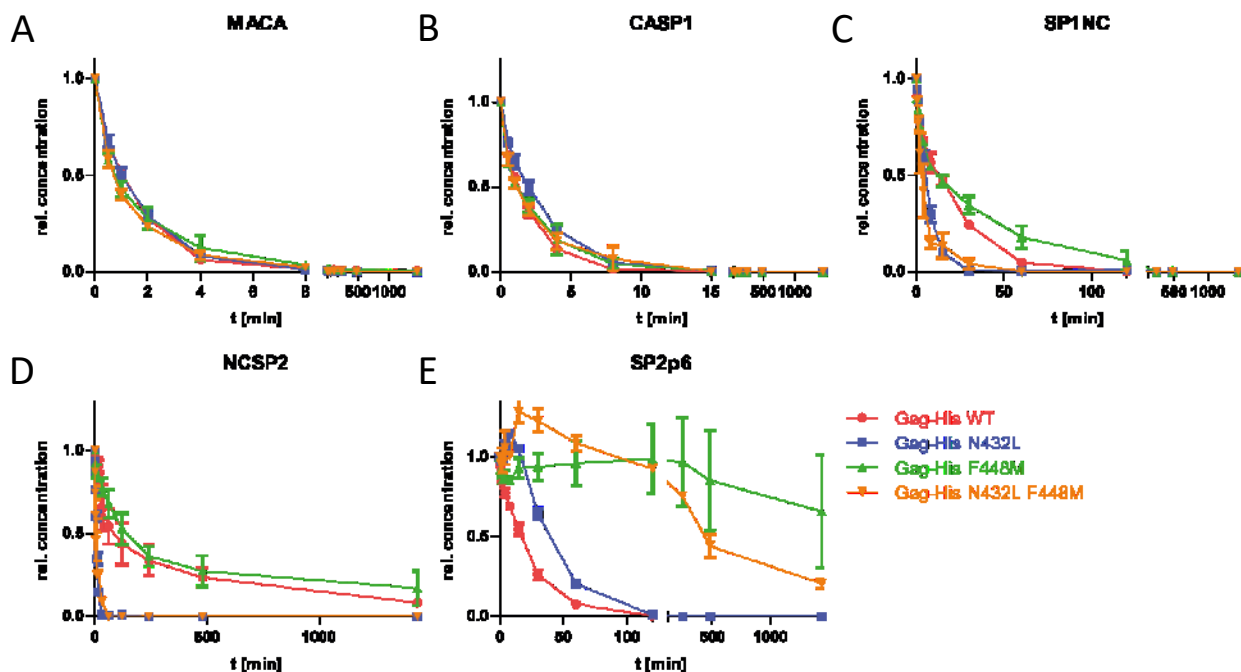


Figure 38: Time-course analysis of the processing of non-assembled Gag-His containing cleavage rate altering mutations. Coomassie G-250 stained Tricine-PAGEs were analyzed by ImageJ and Ilastik as described in materials and method, calculating concentrations of all existing products at each time point. Starting at a relative concentration (= 1), the amount of unprocessed CSs present in intermediates decreases over time. The summed concentration of products carrying unprocessed MA-CA (A), CA-SP1 (B), SP1-NC (C), NC-SP2 (D) or SP2-p6 (E) are plotted for proteolysis of unassembled Gag-His WT (red), Gag-His N432L (blue), Gag-His F448M (green), and Gag-His N432L F448M (orange). All experiments had been performed as triplicates. Error bars of the single figures indicate the standard deviation of the measured data points.

None of the three mentioned mutants displayed altered processing rates at the CSs MA-CA and CA-SP1 (Figure 38 A + B). In all the cases, the processing had a similar pattern compared to the wild-type. Interestingly, the processing at SP1-NC was 60 – 70 % faster for N432L mutant independent of the second mutation at SP2-p6 (Figure 38 C red and green line), while F448M had no effect. Additionally, N432L in both mutants increased the processing rate at NC-SP2 massively around 10 – 15-fold (Figure 38 D red and

green line). On the other hand, F448M strongly reduced (~ 40 -fold) the processing at SP2-p6 with or without the second mutation N432L (Figure 38 E green and orange line), so that it was not fully processed after 24 h. These results, regarding the processing of NC-SP2 and SP2-p6, are almost precisely covering the previously mentioned published results (Pettit, et al., 2002). However, both mutations appeared to have no impact on other cleavage sites in the non-assembled state, with the notable exception of SP1-NC in the case of the N432L mutation.

6.4.3.5 Influence of the maturation inhibitor bevirimat on Gag processing

Bevirimat (BVM; Li, et al., 2003) is an HIV-1 maturation inhibitor, which has been found to specifically impair processing at the CA-SP1 site (Zhou, et al., 2004; Li, et al., 2003). Cryo-electron tomography indicated that it binds to and stabilizes the region of CA-SP1 in viral particles (chapter 4.4.4; Schur, et al., 2016; Keller, et al., 2011). The processing of CA-SP1 is reduced in the presence of BVM (Li, et al., 2003; Zhou, et al., 2004). The impact of BVM on the overall proteolytic maturation was only analyzed in a few time steps and mainly for a few CSs. Exemption of this are several published data derived from cell culture-based experiments without dynamical analysis (Adamson, et al., 2010; Zhou, et al., 2004), and another study which targeted the impact of CA-SP1 *in vitro* with a temporal resolution (Ning, et al., 2016). These publications included only assembled Gag and the processing analysis at the CA-SP1 cleavage site exclusively. Furthermore, they covered a smaller time frame (180 min; Ning, et al., 2016) with fewer time steps (6; Kucharska, et al., 2019) for the analysis than this thesis.

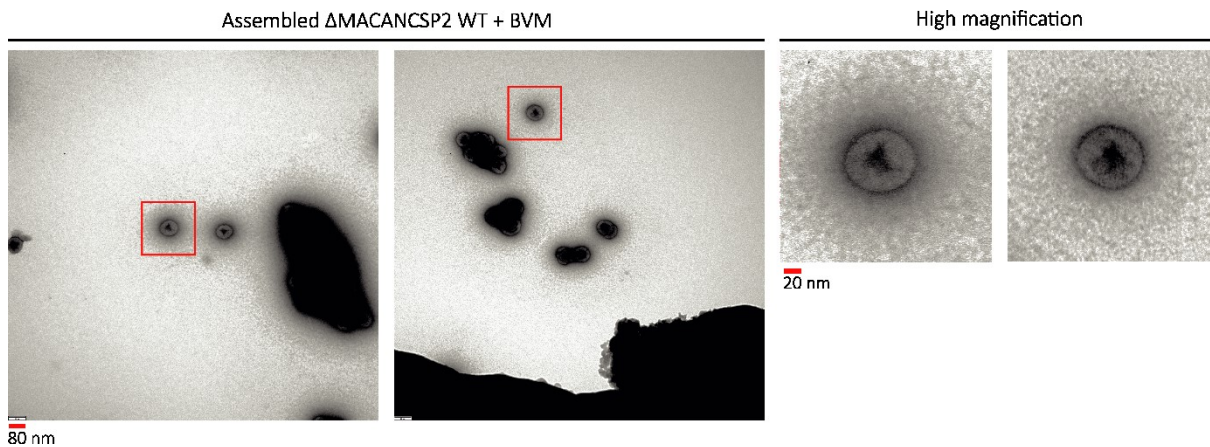


Figure 39: Morphological control of *in vitro* assembled Δ MACANCSP2 WT in the presence of maturation inhibitor bevirimat by TEM. 27 μ M recombinant purified Δ MACANCSP2 WT was assembled *in vitro* by dialysis in assembly buffer (5.2.2.4) in the presence of 4 % standard oligonucleotide for assembly (5.1.7) at 4 °C. Subsequently, the particle suspension was dialyzed for processing experiments in processing buffer (5.2.2.5). Subsequently, the resulting particles were carefully agitated for 30 min at roomtemperature with BVM and analyzed by TEM with negative staining by 3 % uranyl acetate. Different magnifications show the size distribution of assembled. The scale bars (red) indicates 80 and 20 nm.

Here, non-assembled Gag-His WT and assembled Δ MACANCSP2 WT were processed according to the protocol (5.2.2.5) in the presence or absence of 100 μ M BVM (molar excess over Gag of 4:1). Negative-

stain TEM analysis (Figure 39) showed correct spherical particles after incubation with BVM with a size of roughly 90 – 100 nm in diameter. The amount of pelletable Δ MACANCSP2 was not affected by BVM; thus, BVM displayed no disassembling properties, and the processing conditions of assembled Δ MACANCSP2 were the same apart from the presence of BVM.

The processing of non-assembled Gag-His WT at all five CSs (Figure 53 in chapter 9) remained mainly unchanged upon the addition of BVM. MA-CA, SP1-NC, and SP2-p6 were cleaved with less than 10 % difference in the decay rates with and without BVM (Figure 40 A, C, and E red lines). The most prominent change was observed at the NC-SP2 site (Figure 40 D red lines). Estimation of the processing rate was not possible since the CS was processed in the late phase when PR activity is severely diminished (6.3.3). In the case of CA-SP1, the processing rates at non-assembled protein were slightly reduced ($\sim 25\%$) in the presence of 100 μ M BVM (Figure 40 A-E).

In contrast, assembled Δ MACANCSP2 displayed substantially delayed processing at the CS of CA-SP1 (Figure 40 B blue lines). Without BVM, the processing at CA-SP1 of assembled Δ MACANCSP2 occurred 90 % slower compared to non-assembled protein, as it was already described in 6.4. Upon the addition of BVM, processing at the CA-SP1 site was completed after 480 min instead of 60 min. BVM reduced the apparent decay rates at CA-SP1 for assembled Δ MACANCSP2 about 86 %. However, MA-CA, SP1-NC, and NC-SP2 were only slightly affected with less than 10 % difference (Figure 40 A, C, and D blue lines).

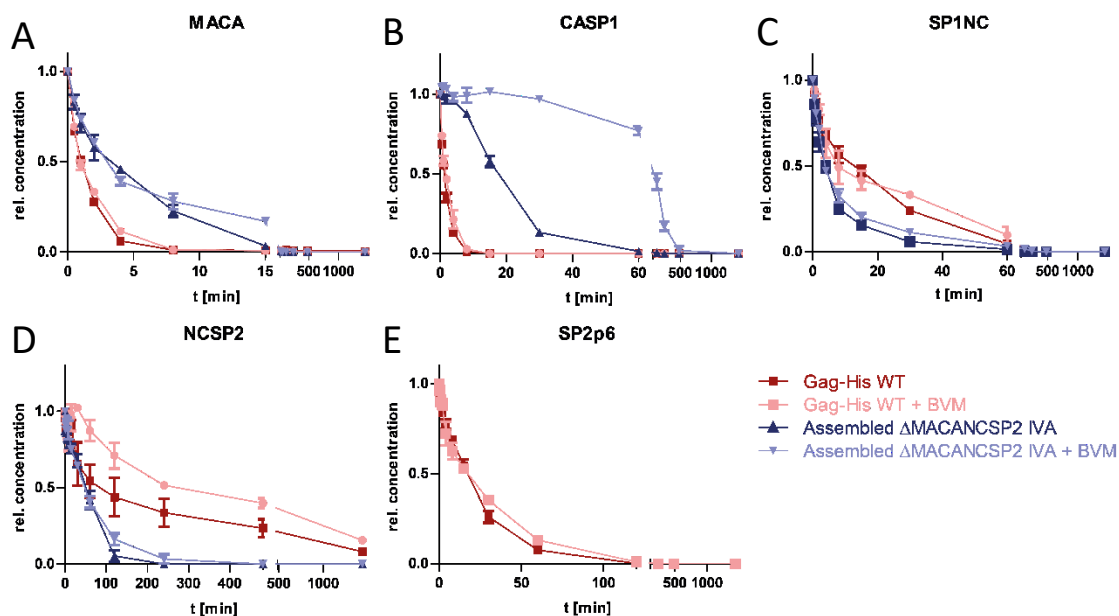


Figure 40: Time-course analysis of the processing of non-assembled Gag-His WT and *in vitro* assembled Δ MACANCSP2 WT in the absence and presence of maturation inhibitor bevirimat. Coomassie G-250 stained Tricine-PAGEs were analyzed by ImageJ and Ilastik as described in materials and method, calculating concentrations of all existing products at each time point. Starting at a relative concentration (= 1), the amount of unprocessed CSs present in intermediates decreases over time. The summed concentration of products carrying unprocessed Δ MA-CA/MA-CA (A), CA-SP1 (B), SP1-NC (C), NC-SP2 (D), or SP2-p6 are plotted for proteolysis of unassembled Gag-His WT (red) and assembled Δ MACANCSP2 (blue) in case of absent (light color) and present (bright color) maturation inhibitor bevirimat (BVM). All experiments had been performed as triplicates. Error bars of the single figures indicate the standard deviation of the measured data points.

7 Discussion

7.1 Non-assembled Gag reveals an altered sequential processing independent of the oligomerization state

One of the first parts of this thesis was to compare the processing of Gag in a non-assembled and assembled state, to determine the structural impact of assembly on maturation. So far, the main published work about this topic in a quantitative manner included *in vitro* translated Gag (Erickson-Viitanen, et al., 1989; Pettit, et al., 1994) or synthetic peptides of Gag CSs (Fehér, et al., 2002; Tözsér, et al., 1991); however, the processing rates of the different CSs differed considerably in those two setups. The commonly propagated processing sequence is (Pettit, et al., 1994): Rapid (SP1-NC); intermediate (MA-CA, SP2-p6); slow (CA-SP1, NC-Sp2).

The *in vitro* assembled Δ MACANCSP2 in this work was processed with analogous kinetics as purified VLPs and in a similar order as proposed for proteolytic maturation (Pettit, et al., 1994; reviewed in Sundquist and Kräusslich, 2012). Contrary, non-assembled Gag-His revealed an altered processing order, which was independent if Gag was majorly mono- or dimeric: Rapid (MA-CA, CA-SP1); intermediate (SP1-NC; SP2-p6); slow (NC-SP2). Consequently, I can conclude that the assembly of viral particles is crucial for the correct proteolytic and morphological maturation.

As long as Gag is not assembled, it presumably does not yield the helical structure at CA-SP1 of the hexameric bundle in an immature lattice or other intermolecular interactions in the region of MA and CA. It is proposed that the immature lattice shields certain regions of Gag, especially CA-SP1 (Schur, et al., 2016; Mattei, et al., 2018); non-assembled Gag needs no decomposition of the helix structure or other hindering structures. PR obtains direct access to the CSs, facilitating a mainly amino acid (aa)-sequence based and rapid processing of MA-CA and CA-SP1.

C-terminal CSs, SP1-NC, NC-SP2, and SP2-p6, are processed notably slower in the case of non-assembled Gag, which is not derived by the missing assembly solely, but also the absence of NA. It was shown that NA bound to NC in assembled Gag or various other processing intermediates containing NC accelerates PR activity. While this effect was observed quite early (Pettit, et al., 1998; Sheng, et al., 1997), recent research proved that NC containing proteins of HIV are organizing with bound NA *in vitro* into quaternary structures on their own (Mirambeau, et al., 2007; Lyonnais, et al., 2019). Active HIV-1 PR gets sequestered by scaffold-like structures and is brought in close proximity to uncleaved CSs, which is predicted to be one of the main causatives for enhanced processing (Lyonnais, et al., 2019). In addition to this, interactions of RNA and PR also boost the enzymatic activity (Potempa, et al., 2015). Since the C-terminal part of Gag is not known to form specific lattices as MA-CA-SP1 by intermolecular interactions, SP1-NC, NC-SP2, and SP2-p6 are presumably also processed based on their CS sequence in the case of non-assembled Gag.

Several publications solidify the argument that processing of non-assembled Gag-His is mainly based on the CS sequences: The processing of synthetic peptides (Tözsér, et al., 1991; Fehér, et al., 2002; Fehér, et al., 2006) deliver the same theoretical processing “order” regarding their processing rates compared to non-assembled Gag-His. However, to directly compare the processing of the different CSs, the kinetic values as k_{cat}/K_M would be needed, which can be judged as a comparator of the catalytic efficiency for

enzymatic efficiency of a specific substrate (Eisenthal, et al., 2007). While the CSs in Gag compete for the binding to PR, synthetic CSs are processed without competition. Thus, the data of my work and the processing of *in vitro* translated Gag cannot be fitted by a one-phase decay in order to get k_{cat}/K_M . In order to compare the results in a semi-quantitative way and get insight into the differences in the processing of assembled and non assembled Gag, the processing rates were normalized by the rate of SP1-NC of the individual experiment (Table 22).

Table 22: Normalized processing rates of Gag CSs derived from different sources. The processing rates of the processing experiments of this work (pH 6.0), including non-assembled Gag-His and *in vitro* assembled Δ MACANCSP2 were calculated with a one-phase decay rate fitting. Data for processing of *in vitro* translated Gag (pH 5.0) (Pettit, et al., 1994) and synthetic peptides (pH 5.6) (Tözsér, et al., 1991; Fehér, et al., 2002) of the CSs were obtained from different publications. To compare the experimental values, all processing rates were normalized by the respective value for SP1-NC. Additionally, the ratios between assembled Δ MACANCSP2 and non-assembled Gag-His as well as *in vitro* translated Gag and the synthetic CS peptides were calculated.

Source	Biochemical state	MA-CA	CA-SP1	SP1-NC	NC-SP2	SP2-p6	pH
This work	<i>In vitro</i> assembled	1.2	1/5	1	0.89	-	6.0
This work	Non-assembled	11	9	1	1/5	0.73	6.0
Pettit, et al., 1994	<i>In vitro</i> translated	1/14	1/400	1	1/350	1/9	5.0
Tözsér, et al., 1991 Fehér, et al., 2002	Synthetic peptides	0.6	1.2	1	1/74	1/93	5.6
	Ratio 2:1	9.16	43	1	2.35	-	
	Ratio 4:3	8.45	480	1	4.6	1/10	

The conditions used in these experiments differ partially (e.g., pH). Even though pH affects processing (discussed later), especially at higher values than 6.0, the normalized cleavage rates allow some evidence: Processing of non-assembled Gag-His appears closer to synthetic CS peptides and *in vitro* assembled Gag to *in vitro* translated Gag regarding the cleavage rate ratios (Table 22 Ratio 2:1, 4:3). Based on this, I suggest that the CSs of non-assembled Gag are processed according to their aa-sequence. In contrast, assembled Gag is processed slower at Δ MA-CA and CA-SP1, because of the intra- and intermolecular interactions of Gag, and faster at SP1-NC as well as NC-SP2 because of bound NA. The extensive difference of the CA-SP1 processing of *in vitro* translated Gag and synthetic CS peptides again attests to the importance of processing conditions and Gag structures, in particular of CA-SP1.

Besides the fact that preliminary active PR dimers yields a low activity (Tamburini, et al., 1990; Kräusslich, et al., 1989; Szeltner, et al., 1996; Cheng, et al., 1990; Ido, et al., 1991) in the pH (7.0 – 7.2) of the cytoplasm (reviewed in Diem, et al., 1970), it is customary that subunits of preliminary processed Gag are found in HIV-1 infected cells. I propose that the altered processing sequence of non-assembled Gag facilitates a protective function for HIV-1 assembly and budding. Preliminary active PR in the cytoplasm would process the non-assembled Gag according to my data first at MA-CA and CA-SP1, which consequently prevents

preliminary cut Gag from taking part in viral assembly. In parallel, the reduced processing in the region SP1-p6 protects these CS from being processed before assembly and binding of vRNA.

As mentioned, it needs to be noted that the processing rates discussed in this chapter were all based on experimental setups at pH 6.0 or lower. Yet it is not known which pH is prevalently given during maturation, although it plays an essential role for intermolecular interactions and the formation of the CA-SP1 helix. The impact of other pH values upon processing will be discussed in chapter 7.2. Furthermore, I could only discuss the cleavage rates derived by the fitting of a one-phase decay normalized to SP1-NC. The actual values like k_{cat}/K_M could not be discussed and would give an even more precise insight. However, the modeling of my processing results in this work is planned and will be described in chapter 7.7.

7.2 IP6 and pH: Assembly stabilizer and maturation accelerator

In order to compare the processing of non-assembled with assembled Gag, a high yield of stable particles needed to be generated in first place efficiently with high stability. The cellular compound IP6 is known to induce in a variety of lentiviral Gag proteins assembly (mainly Δ MA truncated) (Dick, et al., 2020) and features a high assembly efficiency and kinetic (Dick, et al., 2018; Kucharska, et al., 2019). The assembly of Gag Δ p6 was achieved as small particles of 25 – 30 nm (Campbell, et al., 2001) and 20 nm for Gag-His (McKinstry, et al., 2014) in the absence of IP6. While the former can arrange in the presence of 2 μ M IP6 as standard-sized particles (Datta, et al., 2007a; Campbell, et al., 2001) as Δ MACANCSP2 (~90 – 140 nm) with IP6, the latter was yet not able to be properly assembled in the presence of IP6.

Even though Gag-His was assembled in this work with low efficiency and missing reproducibility, the addition of 0.3 μ M IP6 induced Gag-His to assemble in two different populations. One fraction displayed the same diameter as assembled Δ MACANCSP2 (90 – 100 nm), and the other population contained smaller particles (~ 60 nm). The population of the bigger particles could represent the assembly of Gag-His with an IP6 saturation; the population of the smaller particles would then yield no IP6 or only a partial saturation, as they are bigger as it was shown for the complete absence of IP6 (20 nm) (McKinstry, et al., 2014).

The binding of IP6 to Gag forms the mono-trimeric equilibrium (Datta, et al., 2007b), which is thought to be the precursor for the assembly into the hexameric lattice, and increases, as a result, the assembly rates (Kucharska, et al., 2019). Based on this, I propose that Gag molecules attached with IP6 would interact with other Gag-IP6 complexes first, leading to the formation of bigger particles, and remaining Gag in a mono-dimeric equilibrium would assemble slower and into the smaller particles. This hypothesis explains why two populations during assembly appear and could be easily verified by the determination of the IP6 content in both populations. In the case of my hypothesis, the IP6 saturation of non-assembled Gag acts as a regulator for particle size, and the smaller particles in my work (60 nm) represent an intermediate state of particles with high (90 – 100 nm) IP6 saturation and no IP6 (20 -30 nm) (McKinstry, et al., 2014).

According to my results, the presence of IP6 is indispensable for the correct formation and high stability of full-length Gag, which covers the observation that VLPs contain IP6, and the depletion of IP6 leads to a severe reduction of VLP production and infectivity (Mallery, et al., 2019). Besides the assembly accelerating effect of IP6, the cleavage at CA-SP1 is also reduced (Kucharska, et al., 2019) where IP6 is

bound during assembly (Dick, et al., 2018). All this is in line with my results that IP6 was vital for assembled Δ MACANCSP2 to be stable at pH 6.0. Non-assembled Δ MACANCSP2, however, revealed no altered processing in the presence of IP6. Even though it enables the mono-trimeric equilibrium of Gag, it presumably does not stabilize or induced any precursor for the helix bundle in the region of CA-SP1, and only the fully assembled Δ MACANCSP2 is protected by IP6. Thus, IP6 should be included in all *in vitro* processing experiments for the precise imitation of the proteolytic maturation *in vitro*.

Analogical to IP6, pH also plays an essential role in the assembly and PR activity. While high pH (8.0) favors the immature assembly of CA, low pH (6.0) provides mature assembled CA (Gross, et al., 2000) and maximizes PR activity (Tamburini, et al., 1990; Kräusslich, et al., 1989; Szeltner, et al., 1996; Cheng, et al., 1990; Ido, et al., 1991). The pH of the human cytoplasm lies around 7.0 – 7.2 (Diem, et al., 1970). However, the given pH during maturation of HIV-1 could not be tracked yet, and there is no defined mechanism known for HIV-1 to generate a pH reduction or local gradient in viral particles.

In my experiments, the processing of CA-SP1 and NC-SP2 was affected most by the pH change for both, assembled and non-assembled protein. Except for the non-assembled CA-SP1, the processing at these CS was occurring last at all tested pH values (6.0, 6.5, and 7.0) and was slower with an increasing pH. While the PR activity is reduced at higher pH, another important fact could be the presence of ionic aas in the CS sequences of the used Gag gene in this work. It was earlier proposed that the processing acceleration at CA-SP1 is caused at lower pH by a sequence-based mechanism instead of a conformational or spatial effect (Pettit, et al., 1994).

In both cases, CA-SP1 and NC-SP2, the CS sequences of five aas up- and downstream yield two basic and one acidic aas, while all others contain no acidic and except for SP2-p6 less basic aas. The theoretical charge of these aas in the CS region is reflected in the isoelectric point (IEP) of theoretical synthetic CS peptides. According to a standard calculation software (Gasteiger, et al., 2003), the IEP is 5.5 for MA-CA, 9.2 for SP1-NC, and 12.0 for SP2-p6. However, the IEP of CA-SP1 and NC-SP2 are at 8.8, which enables a more significant percentage of charged aas residues at a pH of, e.g., 7.0. These ionic residues can enable intra- or intermolecular Gag-Gag interaction or may influence the accessibility of the PR to the CSs. As CA-SP1 forms helical structures for the immature lattice at higher pH but not at lower, the presence of ionic aas may be of importance for immature assembly. The importance of those charged aa is covering with the low mutation rates at the positions of ionic aas at NC-SP2 and CA-SP1 (Ghosn, et al., 2011; Li, et al., 2013), even though the sequences of CSs in Gag reveal relatively high conservation generally. If ionic aas play an essential role in the processing could be easily tested with point mutations in non-assembled Gag-His, which would be preferred instead of assembled protein since mutations of, e.g., CA-SP1 likely prevent assembly (Wagner, et al., 2016).

In summary, pH could function as a restrainer for the full completion of proteolytic maturation. As the processing of CA-SP1 and NC-SP2 are both affected analogous by the pH change, this could enable that under different conditions, these two cleavage events are always timed for the following morphological assembly. Nevertheless, the effect of the delayed processing at CA-SP1 and NC-SP2 may appear even stronger due to the loss of PR activity over time (Figure 21 chapter 6.3.3) in this work.

Combining the knowledge about assembly and maturation from this and other works:

1. Immature *in vitro* assembly is preferred at pH 8.0 (Gross, et al., 2000), almost in the range of cytoplasm or blood (Diem, et al., 1970)

2. Mature assembly of CA prefers low pH of ~ 6.0 (Gross, et al., 2000)
3. High PR activity at pH 5.0 – 6.0 (Tamburini, et al., 1990; Kräusslich, et al., 1989; Szeltner, et al., 1996; Cheng, et al., 1990; Ido, et al., 1991)
4. High stability of assembled Gag at pH 6.0 in the presence of IP6 (this work)
5. Increased processing at lower pH (6.0) of *in vitro* assembled Δ MACANCSP2 suits better the expected time frame for maturation in viral particles than higher pH, as freshly assembled particles majorly contain already condensed RNPs (Dussupt, et al., 2011); and it is predicted that the initialization of maturation takes place shortly before or during budding (Kräusslich, et al., 1991; reviewed in Vogt, 1997; reviewed in Sundquist and Kräusslich, 2012), while viral particles are released ~ 25 min after the start of assembly (Ivanenko, et al., 2009)

Because the pH in viral particles during maturation could not be tracked yet, I suggest, therefore, the following mechanisms for HIV-1 assembly and maturation:

1. Assembly of Gag occurs at the plasma membrane of host cells at the pH of the cytoplasm for immature lattice
2. Initiation of maturation or proceeding of proteolytic maturation is driven by a lower pH

The addition of one proton (H^+) into the volume of one viral particle with a diameter of 150 nm changes the pH of an unbuffered neutral solution from 7.0 to ~ 3.0 . As viral particles contain several buffering agents (e.g., proteins, remaining cytoplasm), the addition of several protons could consequently reduce the pH in viral particles from 7.0 – 7.2 to ~ 6.0 for an accelerated proceeding of maturation. If a low pH is not present during initialization of maturation, it could also be generated during the first steps of maturation, as the cleavage of several thousand CSs of Gag and GagProPol by HIV-1 PR sets additional carboxyl and amino groups free at the protein termini, which in average yield a pH ~ 6.0 .

If in the future, the maturation of HIV-1 could be tracked more precisely regarding its total timeframe, the comparison to *in vitro* processing at different pH values could give insight into the given pH during maturation of viral particles. However, *in vitro* processing excludes several factors that may also influence the maturation kinetics in viral particles, consequently the *in vitro* processing at different pH values should not be compared par for par with the viral maturation.

7.3 Assembly and nucleic acid: Structural agents and proteolytic maturation modulators?

The main aim of my work was to define the impact of assembly on processing. As described, the sequential processing of assembled and non-assembled Gag differed. Recently, the assembly of Δ MACASP1NC to immature particles in the absence of NA, but the presence of tartrate was achieved (Wagner, et al., 2016), which clarified that no recruiting by NA for assembly is necessary. As this approach led also to spherical particles, it seems likely that the metal ion complexing of tartrate (Gácsi, et al., 2016; Peters, et al., 1988)

or its protein precipitating influence could affect Gag to assemble. However, the processing of assembled Gag variants without NA was not yet performed.

In my work, the presence of 20 % methanol but absence NA during assembly also led to assembled structures. Instead of spherical particles, filament-like structures were built, which is a novelty. Similar to tartrate, methanol is capable of precipitating proteins. For the assembly of Δ MACANCSP2, methanol presumably stabilizes the correct folding of hydrophobic regions of Gag, which is not the case in a complete aqueous environment without a lipid bilayer.

The processing of those filamentous particles revealed that Δ MA-CA and CA-SP1 are processed as in assembled Δ MACANCSP2 with NA, and the remaining CSs were processed as in non-assembled Gag-His. This covers the results that the presence of NA increases upon assembly processing of CSs within SP1-p6 (Lyonnais, et al., 2019). Furthermore, this indicates, on the one hand, that assembly without NA leads to an immature assembly for the two N-terminal CSs, and those filaments contain an immature hexameric lattice. For verification, the structural analysis by Cryo-EM is planned.

On the other hand, NA is responsible for the correct particle curvature and proper assembly of the C-terminal CSs, which is, however, only the case if assembly at MA-SP1 took place in advance, as the processing of non-assembled Gag-His with and without NA appeared to be the same. Based on this, I propose that the initial switch from solubilized and unstructured Gag to the assembled lattice is primarily driven by the structuring of CA-SP1 into the hexameric lattice, while NA and its potential interaction with NC enable the curvature of the hexameric lattice. As it is suggested (Kucharska, et al., 2019), Gag on its own delivers all necessary prerequisites for assembly and NA as well as IP6 function only as optional modulators.

Nevertheless, the presence of the immature lattice needs to be proven in the filaments, and the processing would need to be performed with full-length Gag as well to prove for processing of the non-truncated region of MA-CA in the assembled pattern. Additionally, the impact of the lipid membrane is excluded from the experiments, which plays at least intracellularly an important role for assembly, as the depletion of the membrane-bound PIP2 prevents Gag assembly (Mücksch, et al., 2018). The membrane binding or the display of the myristoyl group is a prerequisite for Gag assembly in particles (4.2) and should be taken at least theoretically into account.

Besides the processing analysis without NA, I could show that pentameric NA did not accelerate the processing of SP1-NC-SP2 in Δ MACANCSP2, which is in line with the results of Lyonais, et al., (2019) that short oligonucleotides cannot induce increased processing. It is proposed that Gag needs to be connected via NA to a minimum of three neighboring Gag molecules to ensure a formation of a two-dimensional superstructure at the C-terminal region (Zhao, et al., 2019). Above the a minimum length of the oligonucleotides the length seems, however, not to be of importance in my experimental setup, as the processing with MS2 RNA (3569 nt) appeared with similar or even lower rates than the shorter standard oligonucleotide for assembly (68 nt), which is contrary to the observations of Lyonais, et al., (2019). In their work, SP1-NC-SP2-p6 was assembled and processed with NA, which is lacking the important and primary part for the structural arrangement of Gag in the immature lattice, namely MA and CA.

If the type of NA may be crucial for the processing was yet not tackled. Specific sequences of the viral RNA genome of HIV-1 described as Ψ RNA are essential for the incorporation of the genome into assembling particles. The Ψ RNA binds with a higher affinity to NC and could influence the processing of Gag by PR.

The actual RNA genome of HIV-1 would be preferably used to mimic the proteolytic maturation closer to the “natural” state.

Summarizing the key results of assembly as well as NA and their impact on Gag processing, MA-CA and CA-SP1 are processed differently in non-assembled and assembled protein. CSs in SP1-NC-SP2-p6 are processed slowly in a non-assembled state. Their cleavage rates are accelerated when Gag is assembled in the presence of NA. According to literature, the commonly accepted classification of Gag CSs is according to their processing dynamics (Pettit, et al., 1994). Nevertheless, this classification is limited as the processing of Gag *in vitro* is altered. Important co-factors are excluded and the pH value of viral maturation is not known. Both have a notable impact on the processing at individual sites. Taking my results into account, I suggest a classification of the Gag CSs according to their biochemical properties in correlation to maturation:

1. Delayed processing due to assembly and structural dependent cleavage rates (MA-CA, CA-SP1)
2. Increased processing due to assembly as well as the presence of NA and CS sequence-dependent cleavage rates (SP1-NC, NC-SP2, and SP2-p6)

7.4 Synchronized but independent cleavage events

For the CSs in Gag, point mutations are known to inhibit the processing at a certain CS in viral particles. These inhibitions impair the infectivity and morphology of mature particles. The actual impact on the processing of other CSs than the mutated one was not clarified yet. According to my results, these mutations left the cleavage rates of other CSs majorly unchanged for non-assembled and assembled Gag, as did the application of BVM for the inhibition at CA-SP1. The fact that cleavage events occur mostly independent of the cleavage of other CSs leads to the conclusion that the sequence of the processing events is mainly predetermined by the processing dynamics of the single CSs on their own instead of an interactive mechanism during maturation. This conclusion also covers the results of chapter 6.4.3.4 about introducing cleavage altering mutants, and former publications with the processing of *in vitro* translated Gag (Pettit, et al., 1994), where inhibited CS mutations had mostly no impact on other cleavage events. Additionally, it correlates with the observation of publications in which BVM stabilizes CA-SP1 and reduces the processing rate at these sites but no others (Ning, et al., 2016; Keller, et al., 2011). Consequently, as the cleavage events are not influencing each other, slight delays in processing speeds at singular sites change the sequential release of Gag subunits and prevent correct maturation. Interestingly, while the increased processing of SP2-p6 with the introduction of F448M also had no other effect on other cleavage events, N432L in NC-SP2 increased the processing at SP1-NC, which could indicate that only increased processing instead of decreased or inhibited may affect other cleavage events.

The only cleavage event to affect others was the inhibition of SP1-NC, which also delayed the processing at CA-SP1 for assembled Δ MACANCSP2. This is in line with the accumulation of CA-SP1-NC in viral particles upon inhibition of SP1-NC (Wieggers, et al., 1998); contrary, *in vitro* translated Gag was processed more rapidly at CA-SP1 (Pettit, et al., 1994). Because the delayed processing is also occurring upon assembly of

Δ MACANCSP2 SP1-NC without NA, I propose that interactions of NC or SP1-NC may enforce the stability of the CA-SP1 bundle.

The concentration of Gag applied in the experiments of this work ranged from 20 – 80 μ M, which is lower than the concentration of Gag \sim 3.5 mM in enveloped viral particles (Briggs, et al., 2003). A dense structure of Gag and reduced space for PR to interact with CSs restricted to a small volume may have additional impacts on the processing, so a dependency of a cleavage event on others may be given.

7.5 Aberrant cleavage of MA-CA: Biological compensation or possible target in HIV-1 replication?

The inhibition of MA-CA severely impairs the infectivity of HIV-1 at even a low percental amount (Müller, et al., 2009). In this work, I found a new cryptic cleavage site inside CA, which occurs upon inhibition of MA-CA independent of the assembly state of Gag. The CS lies between A154 and W155 of CA, which is downstream of the binding domain for IP6 of mature CA (Dick, et al., 2018; reviewed in Pornillos, et al., 2019). As a result of cleavage, the binding site for IP6 in mature CA would be removed. Also, the aberrant CS is part of helix 1 of CA, the homodimerization of CA-NTD in the hexameric lattice (Schur, et al., 2015). Even though the deletion of CA-NTD leads to the production of VLPs (Borsetti, et al., 1998), mutations inside the sequence of helix 1 lead to defective mature assembly (López, et al., 2013), arguing that an intact N-terminal part is vital for the proper mature assembly of CA. Thus, a biological function of this aberrant cleavage seems not to be given. If the aberrant cleavage also occurs in other publications (Müller, et al., 2009; Mattei, et al., 2018; Pettit, et al., 1994) is not comprehensible as they were not aimed to detect this processing. Additionally, the processing in assembled particles is slower, and the size differences to correctly processed CA and MA are small and can be easily overseen.

Nevertheless, the aberrant cleavage in CA may not lead to infectious or mature particles, but the aberrant cleavage at this site upon MA-CA inhibition should be investigated as a possible target in HIV-1 infection treatment. As mentioned, the aberrant cleavage is occurring in the helix 1 region of CA-NTD, which is vital for mature capsid interactions and is highly conserved. Consequently, an adaption of HIV-1 due to mutation would be significantly reduced. A theoretical maturation inhibitor that prevents cleavage at MA-CA would delay, on the one hand, the release of CA for the core assembly and lead, on the other hand, partially to aberrantly cut CA, which may also impact the formation of capsid core negatively.

If the shortened CA is capable of assembling or if it impairs the assembly of full-length CA should be tested. Therefore, the capability of aberrantly processed CA should be analyzed with *in vitro* assembly, maybe in mixture with correctly processed CA. Furthermore, the infectivity and morphology of viral particles yielding the mutation for MA-CA inhibition at a certain ratio should be tracked over time, considering that maturation could take longer than for WT particles.

7.6 Gag mutations for PI resistance without accelerating effect on processing

Upon treatment with PIs of HIV-1 infection, patients can develop compensatory mutations in PR and Gag. While PR mutations are classified according to their PI affinity or processing altering effect (4.4.3), the Gag mutations are yet only poorly understood. It was shown that the introduction of I437V and A431V rescue the replicative capacity of HIV-1 and induce PI resistance regarding the cleavage at NC-SP2. Viral particles yielding one of these mutations had a higher extent of NC cleaved at both terminal sites than WT Gag in the presence of PIs (Dam, et al., 2009).

In order to counteract the effect of PIs, there are two distinct main mechanisms caused by mutations in Gag. The first would be to increase the catalytic activity at a particular site, and the second would be to increase the affinity of Gag to PR by binding better or at a slightly altered region of PR (Dam, et al., 2009; Prabu-Jeyabalan, et al., 2004). Because introducing the mutations A431V or I437V to non-assembled Gag-His left the processing unchanged, the latter seems more likely. The main area for mutations at Gag upon PI treatment is appearing mainly at the N-terminal CSs. Based on the suggestion of chapter 7.3, the processing of SP1-NC, NC-SP2 and SP2-p6 are less structure- but more sequence-dependent regarding their turnover rates, and MA-CA and CA-SP1 reveal processing after unwrapping of structural elements of Gag (Mattei, et al., 2018). Consequently, delayed processing in the presence of PIs would have the biggest impact on those cleavage sites with a low turnover rate according to their aa sequence. These arguments are consistent with data of patient-derived viral sequences showing that mainly the interplay of Gag mutations at the C-terminal CSs with mutations at PR are enabling high replicative capacity and PI resistance (Dam, et al., 2009)

These Gag mutations are often appearing in patient-derived sequences combined with the mutations L76V or V82A in the PR. Their capability of processing Gag-His A431V or I437V should be also tested in the future. Especially the combination of several mutations in Gag plus mutations in PR could reveal the mechanism to overcome the effect of PIs.

7.7 Kinetic modeling of maturation

An experimental approach to imitate maturation as a viral or *in vitro* system is always restricted in its number of analyzable timepoints or interpretable signals. The results of this work are also representing maturation in a limited time frame with snapshots of the proteolytic maturation. Therefore, there is plenty of publications about mimicking the dynamics and processes of maturation *in silico* (Könnnyú, et al., 2013; Lyonnais, et al., 2019; Sadiq, et al., 2011; Sadiq, et al., 2012). However, these techniques can always only be based on *in vitro* or *in vivo* derived data, which were yet incomplete, inaccurate, or nonrepresentative for the proteolytic maturation. A highly quantitative and precise analysis tool for the processing of Gag is consequently needed to generate a training data set for bioinformatic modeling. The experiments of this work delivered a bunch of reliable and reproducible results regarding the processing of CSs of non-assembled and assembled Gag.

In collaboration with Dr. Kashif Sadiq of the Heidelberg Institute for Theoretical Studies HITS gGmbH, we started a project to calculate the actual kinetic data from my results in order to get precise values to point out the interactions during maturation more closely. Initially, this collaboration will be mainly focused on

the evaluation of the generated data on a modeling level. Based on Michaelis-Menten kinetic of heteropolymeric processing (Sadiq, et al., 2011), results as the ratio k_{cat}/K_M can be calculated from my data. Yet the software code is finished in its alpha version and was capable to present certain values for k_{cat}/K_M of single CSs. Due to the high values of the calculated error rates for the fitting of the heteropolymeric processing, the code for the fitting still needs to be improved. Additionally, the previously described loss of PR activity (chapter 6.3.3) was not included yet.

In the long term, the so calculated data are planned to be applied to coarse-grained modeling of the maturation (Sadiq, 2016). Implementing an *in silico* system for maturation could give a better understanding of the relationship between proteolytic and morphologic maturation, and enhance the speed in the search for possible targets in maturation to treat HIV-1 infection.

8 Abbreviations

(NH ₄) ₂ SO ₄	ammonium sulfate
° C	degrees Celsius
µg	microgram
µL	microliter
µM	micromolar
A	adenosine
a.u./ AU	arbitrary units
aa	amino acid
AA	acrylamide
AB	assembly buffer
Abs.	absorption
AIDS	acquired immune deficiency syndrome
ALIX	apoptosis-linked gene-2 interacting protein 1/X
APS	ammonium persulphate
APV	amprenavir
ART	antiretroviral therapy
ATV	atazanavir
AZT	azidothymidine
BAA	bis acrylamide
bp	base pairs
BSA	bovine serum albumin
BVM	bevirimat
C	cytosine
CA	capsid protein
CA*	capsid protein with aberrant cleavage
CaCl ₂	calcium chloride
CA-CTD	C-terminal domain of capsid protein
CA-NTD	N-terminal domain of capsid protein
CCHC	Cys-Cys-His-Cys; type of zinc finger motif
CCR5	CC chemokine receptor 5 – HIV-1 coreceptor
CD4 ⁺ T cell	T cell positive for CD4
Cryo-ET	cryo-electron tomography
CS	cleavage site
CXCR4	CXC chemokine type 4 receptor – HIV-1 coreceptor
d	days
DMEM	Dulbecco's modified Eagle's serum
DMSO	dimethyl sulphoxide
DNA	deoxyribonucleic acid
dNTP	deoxynucleoside triphosphate
DRV	darunavir
DTT	dithiothreitol
EDTA	ethylenediaminetetraacetic acid
EM	electron microscopy
Env	envelope protein
ER	endoplasmatic reticulum
ESCRT	endosomal sorting complex required for transport

EtOH	ethanol
FCS	fetal calf serum
FPLC	fast protein liquid chromatography
G	guanine
Gag	group specific antigen
gp120	glycoprotein 120 (kDa size)
gp160	glycoprotein 160 (kDa size)
gp41	glycoprotein 41 (kDa size)
h	hour
H ₂ O	water
cART	combined antiretroviral therapy
HBR	highly basic region
HEPES	4-(2-hydroxyethyl)-1-piperazineethanesulfonic acid
His-tag	hexahistidine tag
HIV	human immunodeficiency virus
HTLV	human T-lymphotropic virus
IDV	indinavir
IEP	isoelectric point
IN	integrase
IP6	inositol hexakisphosphate
K	kanamycin
K ₂ HPO ₄	dipotassium phosphate
kb	kilobases
KCl	potassium chloride
K _d	dissociation constant
kDa	kilodalton
KH ₂ PO ₄	monopotassium phosphate
kV	kilovolt
L	liter
LB	lysogeny broth
LPV	lopinavir
LTR	long terminal repeat
MA	matrix protein
mA	milliampere
MeOH	methanol
MES	2-(N-morpholino)ethanesulfonic acid
mg	milligram
MgCl ₂	magnesium chloride
MHR	major homology region
MI	maturation inhibitor
min	minutes
mL	milliliter
mM	millimolar
mRNA	messenger RNA
MS	mass spectrometry
MWCO	molecular weight cut-off
n	number
NA	nucleic acid
NaCl	sodium chloride

NC	nucleocapsid protein
Nef	negative factor
NFV	nelfinavir
nM	nanomolar
nm	nanometer
OD	optical density
ON	overnight
ORF	open reading frame
p6	protein 6 (kDa size)
PAGE	polyacrylamide gel electrophoresis
PB	processing buffer
PBS	phosphate-buffered saline
PCR	polymerase chain reaction
PEI	polyethyleneimine
PI(4,5)P2	phosphatidylinositol-4,5-bisphosphate
PIC	pre-integration complex
PM	plasma membrane
POI	protein of interest
Pol	polymerase
PR	protease
R ²	coefficient of determination
RCF	relative centrifugal force
Rev	regulator of expression of viral proteins
RNA	ribonucleic acid
rpm	revolutions per minutes
RRE	Rev-response element
RT	reverse transcriptase
RTC	reverse transcribing complex
RTV	ritonavir
s	seconds
sdm	site-directed mutagenesis
SDS	sodium dodecyl sulfate
SP1	spacer peptide 1
SP2	spacer peptide 2
SQV	saquinavir
ss	single-stranded
STEM	scanning transmission electron microscopy
t	time
T	tyrosine
TAR	trans-activation response element
Tat	trans-activator of transcription
TBST	tris-buffered saline – Tween 20
TCEP	tris(2-carboxymethyl)phosphine
TEM	transmission electron microscopy
TEMED	tetramethylethylenediamine
TEV	TEV cleavage site
TPV	tipranavir
TRIS	tris(hydroxymethyl)-aminomethan
TX-100	tritonX-100

U	units
V	volt
v/v	volume per volume
Vif	viral infectivity factor
VLP	virus-like particle
Vpr	viral protein r
Vpu	viral protein u
vRNA	viral genomic RNA
w/v	weight per volume
WM	W184A M185A mutation of Gag/ CA
WT	wild type
ZnCl ₂	zinc chloride

9 Appendix

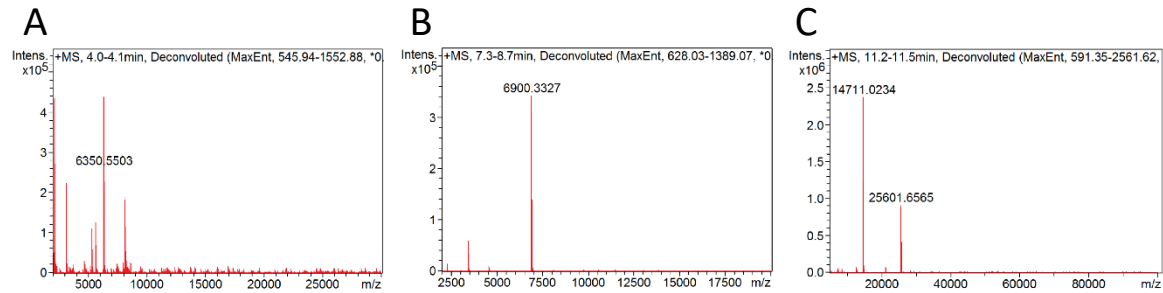


Figure 41: Intact protein mass spectrometry of Gag-His WT processing products. 22 μ M Gag-His WT was processed according to the processing protocol for 40 h by the HIV-1 PR. Afterward the proteins were separated by size via a superdex 75 10/300 column. The fraction of this purification was measured by intact protein mass spectrometry. Therefore, the sample was applied to a POROS 10R1 column equilibrated in 0.3 % formic acid and eluted with an isocratic gradient to 50 % of a buffer, containing 80 % isopropanol, 10 % acetonitrile and 0.3 % formic acid. Eluted proteins were immediately measured in a maXis mass spectrometer. The calculation was performed with Data Analysis 4.2 (Bruker) and ESI Compass 1.3 Maximum Entropy Deconvolution Option. Here are the mass spectrometry data shown for peak 3 of Figure 20. Proteins eluted after \sim 4 min contained prominently proteins of 6350.55 Da (A), after 7.3 – 8.7 min 6900.3327 (B), and after 11.2 – 11.5 min 14711.02 as well as 25601.66 Da (C).

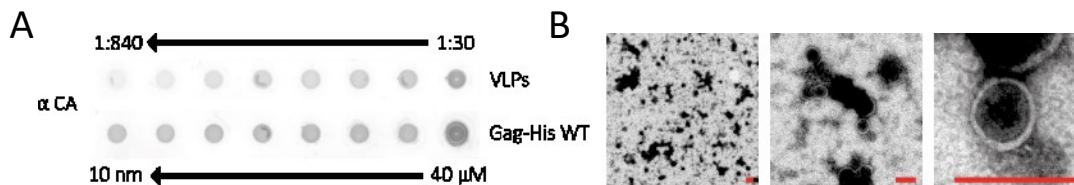


Figure 42: Concentration determination of purified VLPs and EM analysis. Protease deficient HIV-1 (D25N) was produced in 293T cells after transfection (5.2.2.4). The VLPs were purified by sucrose cushion and resuspended in processing buffer and stripped for 5 min with 0.1 % TX-100. (A) For fast concentration determination, a dot blot with primary antibody was performed with a dilution series of the VLPs and Gag-His WT as a control. According to the known concentration of Gag-His WT and dilution of the VLPs, the concentration of intrinsic Gag was calculated ($= 22.7 \mu$ M). (B) The purified VLPs were stained negatively for the usage of EM. The scale bar (red) shows a size of 200 nm.

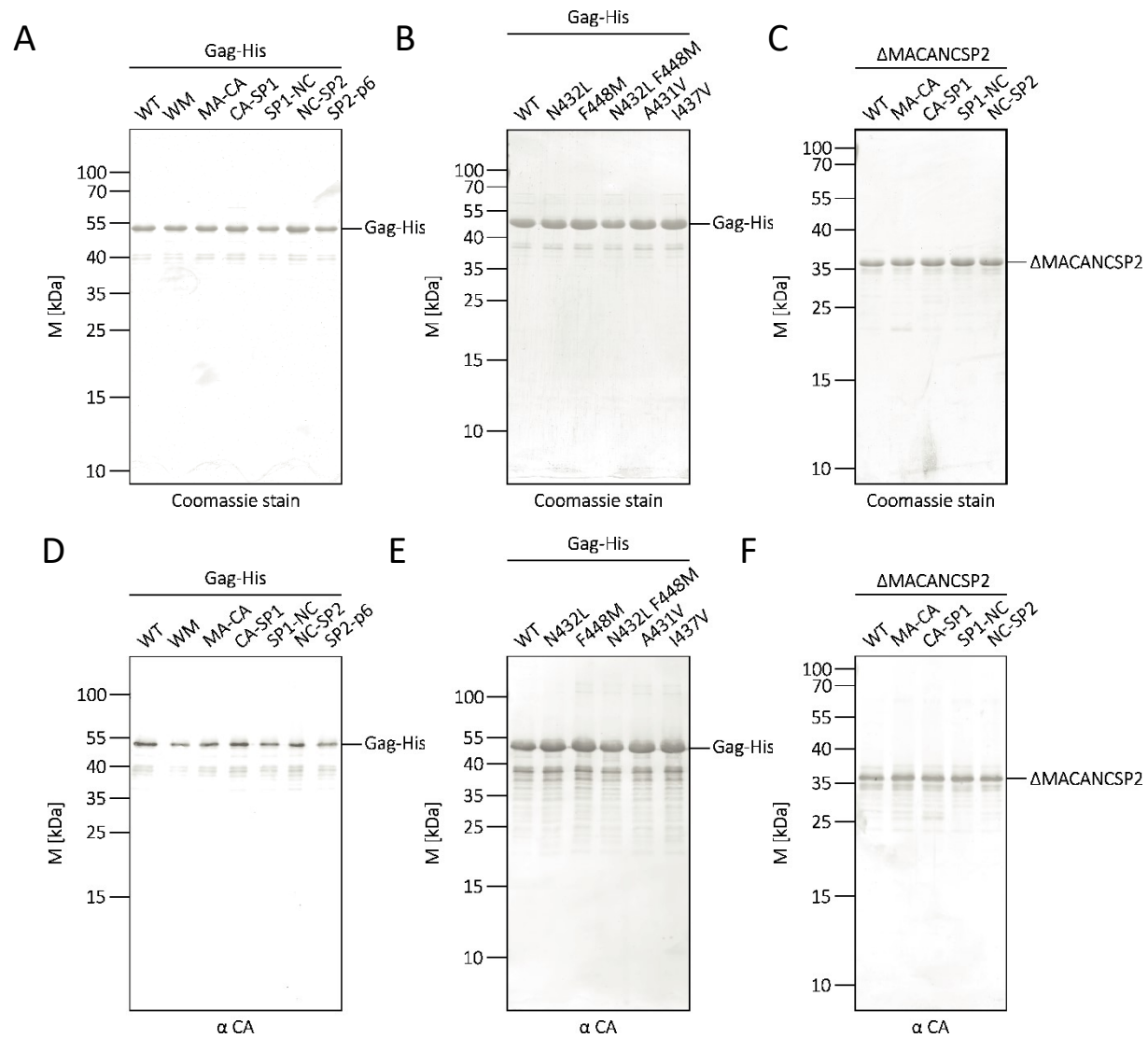


Figure 43: Analysis of purified Gag-His variants. The proteins were purified after production in *E. coli* BL21 (DE3) by $(\text{NH}_4)_2\text{SO}_4$ -precipitation and Ni-NTA-chromatography. (A, D) Resulting samples are from Gag-His WT, Gag-His WM, Gag-His MA-CA, Gag-His CA-SP1, Gag-His SP1-NC, Gag-His NC-SP2, and Gag-His SP2-p6 and (C, E) from Gag-His WT, Gag-His N432L, Gag-His F448M, Gag-His N432L F448M, Gag-His A431V, and Gag-His I437V and (E, F) from Δ MACANCSP2 WT, Δ MACANCSP2 MA-CA, Δ MACANCSP2 CA-SP1, Δ MACANCSP2 SP1-NC, and Δ MACANCSP2 NC-SP2. Proteins were equimolarly analyzed by SDS-PAGE (17.5 % PAA, 1:200 AA/BAA) followed by Coomassie G-250 staining (top) or immunoblot using polyclonal antiserum raised against CA (bottom). The positions of molecular mass standards marker are shown left, and the position of the Gag-His variants is indicated at the right.

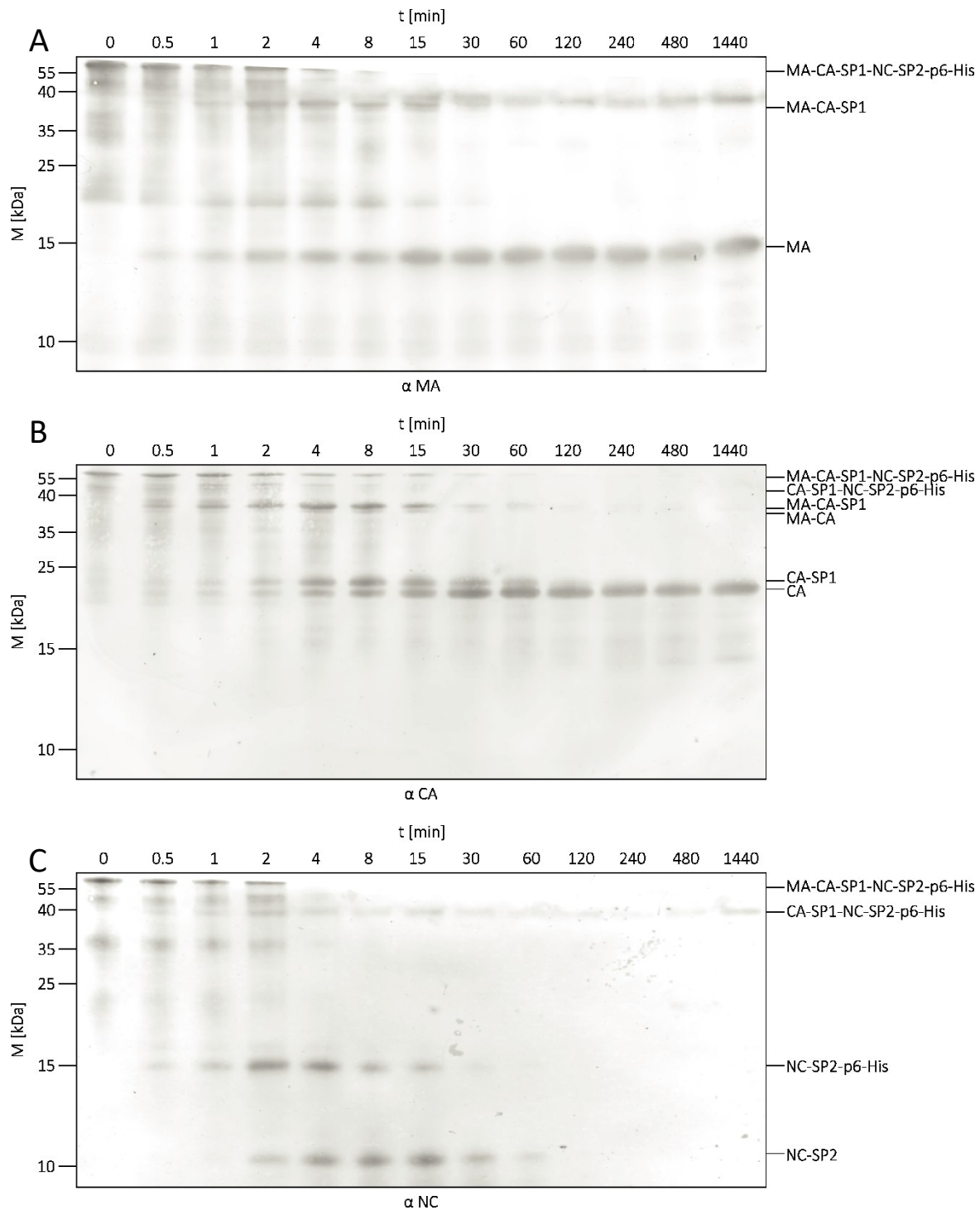


Figure 44: Time course of VLP processing analyzed by immunoblots of Tricine-PAGEs. Protease deficient particles of HIV-1 (D25N) were purified after the transfection of 293T cells by sucrose cushion. After resuspension in processing buffer and membrane stripping with TX-100, the VLPs were processed with recombinant protease over 24 h (= 1440 min) at 37 °C and 450 rpm. After successive increasing time steps (0 – 1440 min) were taken for analysis by immunoblot of Tricine-PAGEs (16 % PAA, crosslinking ratio 1:32 BAA/AA and 9.6 % PAA, 1:32 BAA/AA) using a polyclonal antiserum raised against MA (A), CA (B), and NC (C). Positions of molecular mass standards marker are shown at the left, and the position of Gag-His and processing products are indicated at the right.

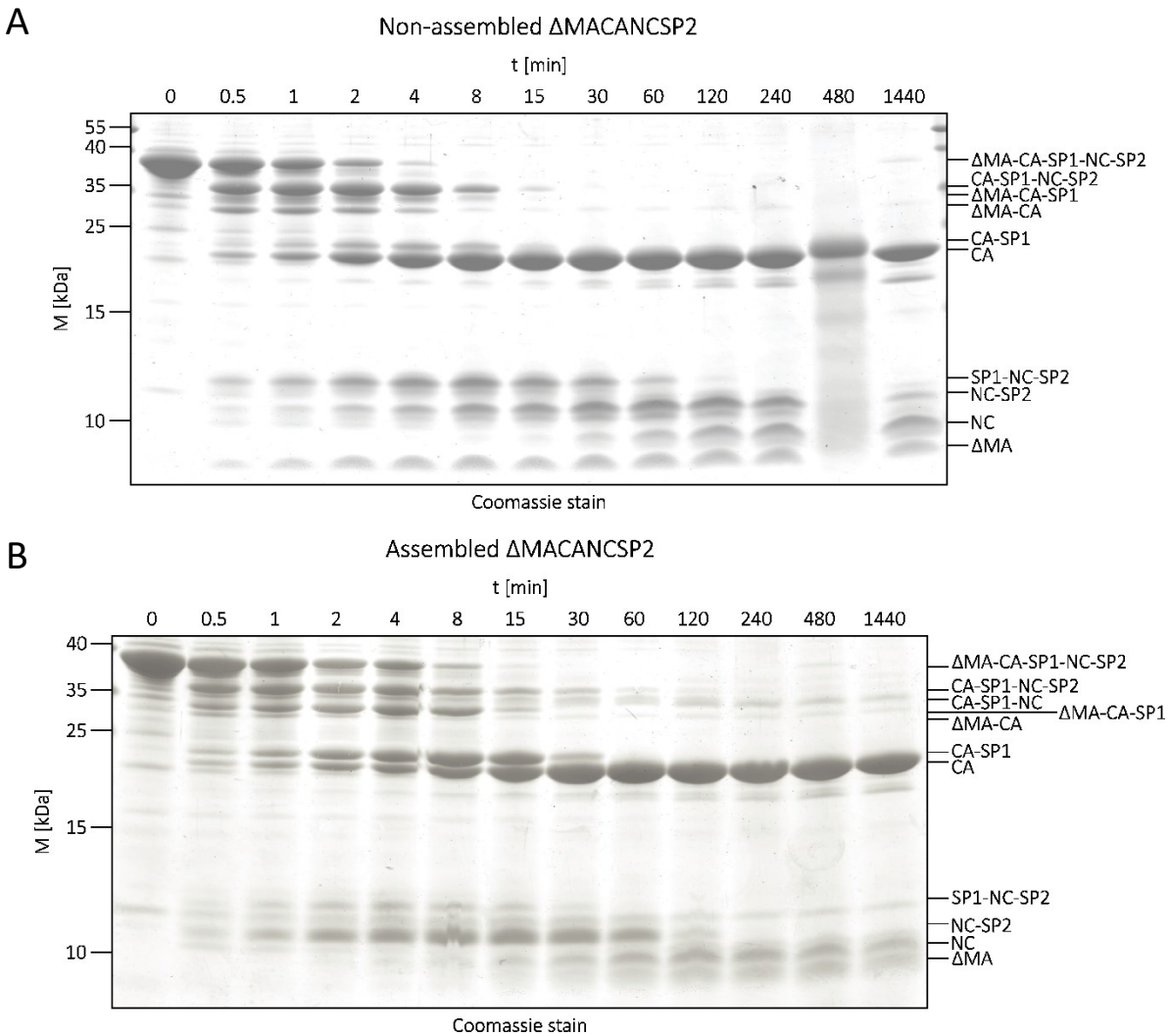
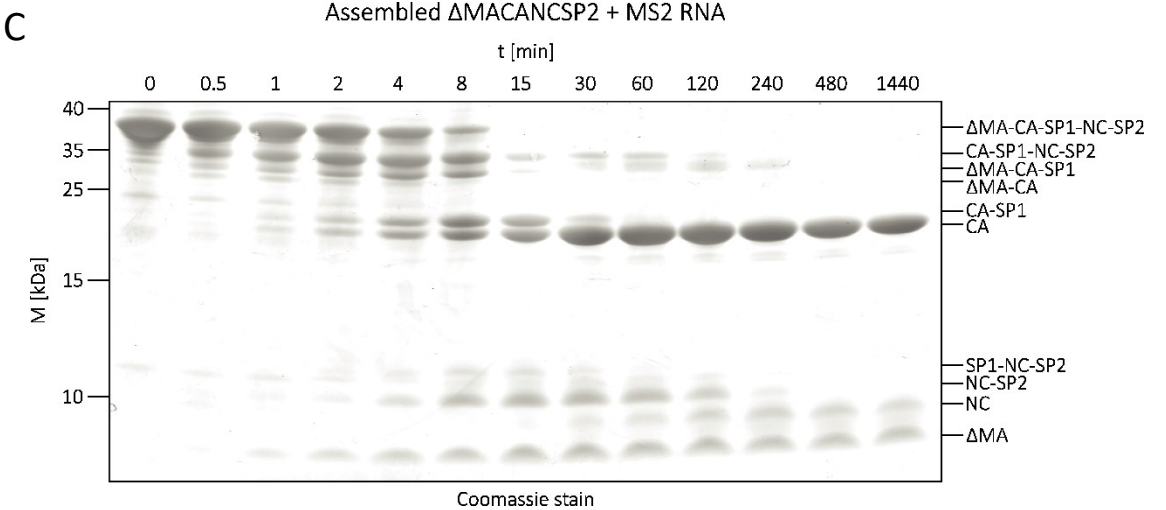
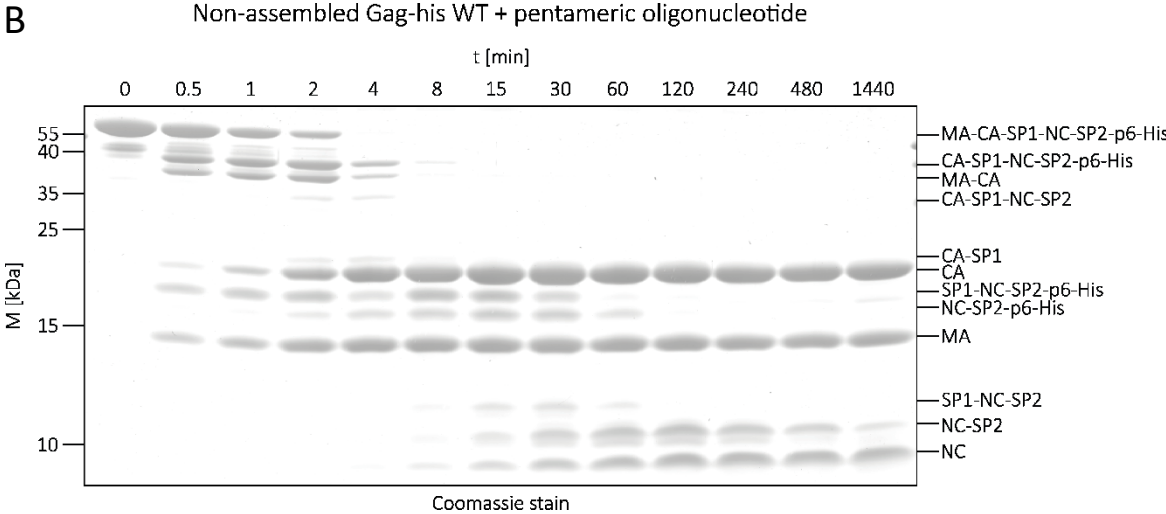
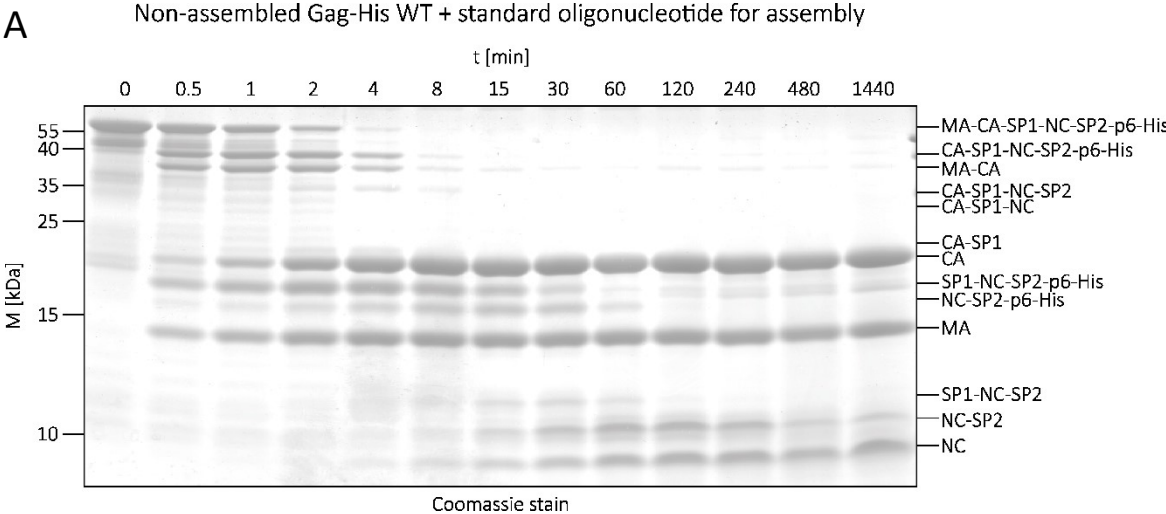


Figure 45: Time course of Δ MACANCSP2 processing in a non-assembled state and *in vitro* assembled analyzed by Tricine-PAGE. Recombinant purified protein of Δ MACANCSP2 was directly dialyzed for non-assembled processing (A) or first assembled according to standard protocol (5.2.2.4) and afterward dialyzed against processing buffer for *in vitro* assembled particles (B). Subsequently, the samples were processed *in vitro* by the addition of recombinant purified HIV-1 PR over 24 h (= 1440 min) at 37 °C and 450 rpm. After successive increasing time steps (0 – 1440 min), samples were taken for analysis by Coomassie G-250 stained Tricine-PAGEs (16 % PAA, crosslinking ratio 1:32 BAA/AA and 9.6 % PAA, 1:32 BAA/AA). Positions of molecular mass standards marker are shown at the left, and the position of Gag-His and processing products are indicated at the right.



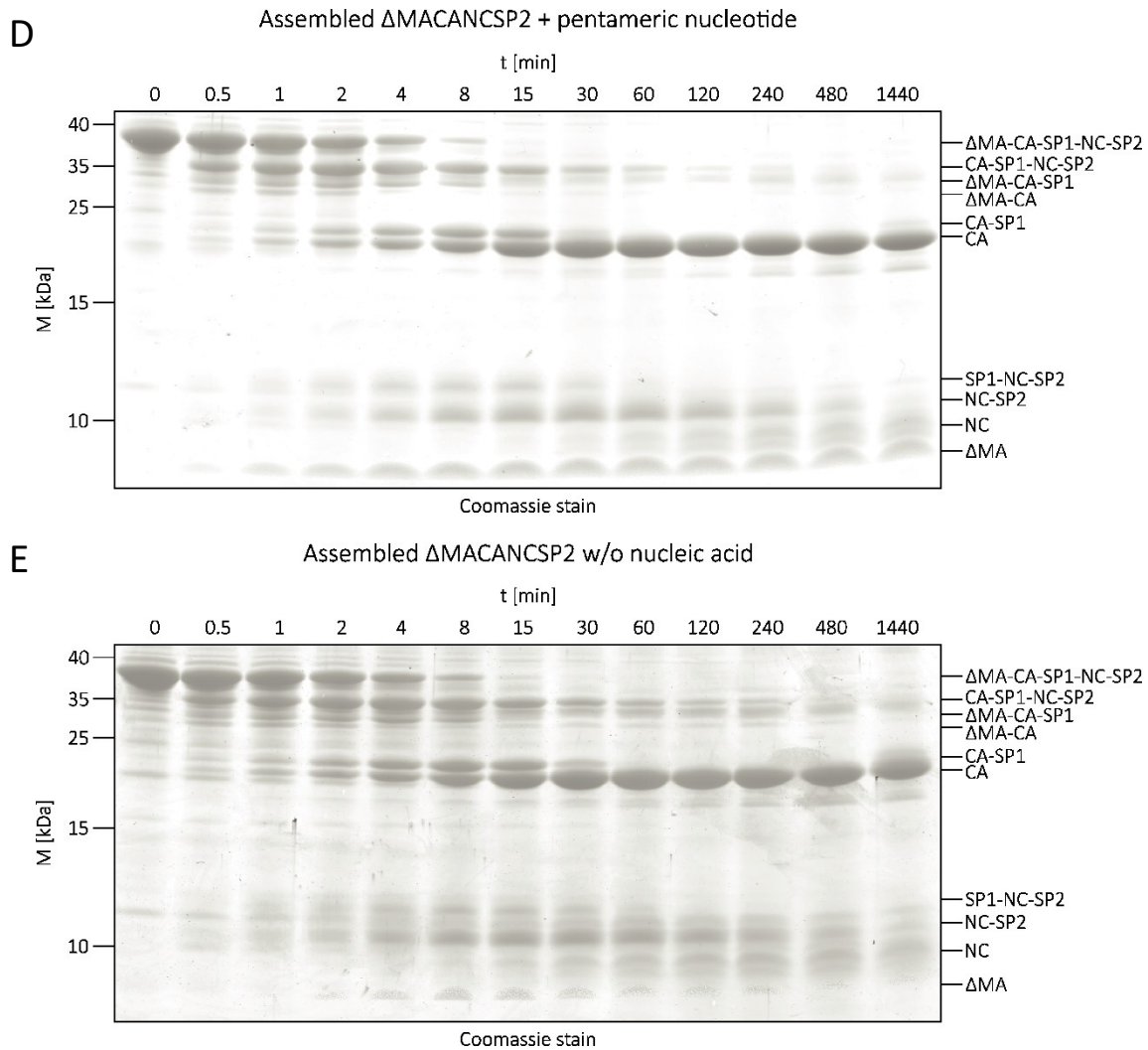
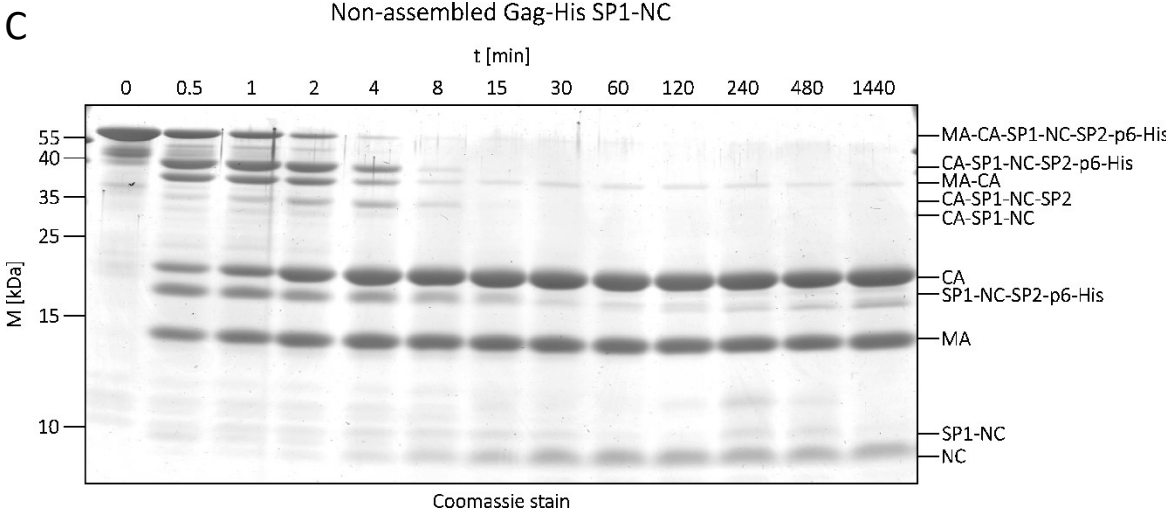
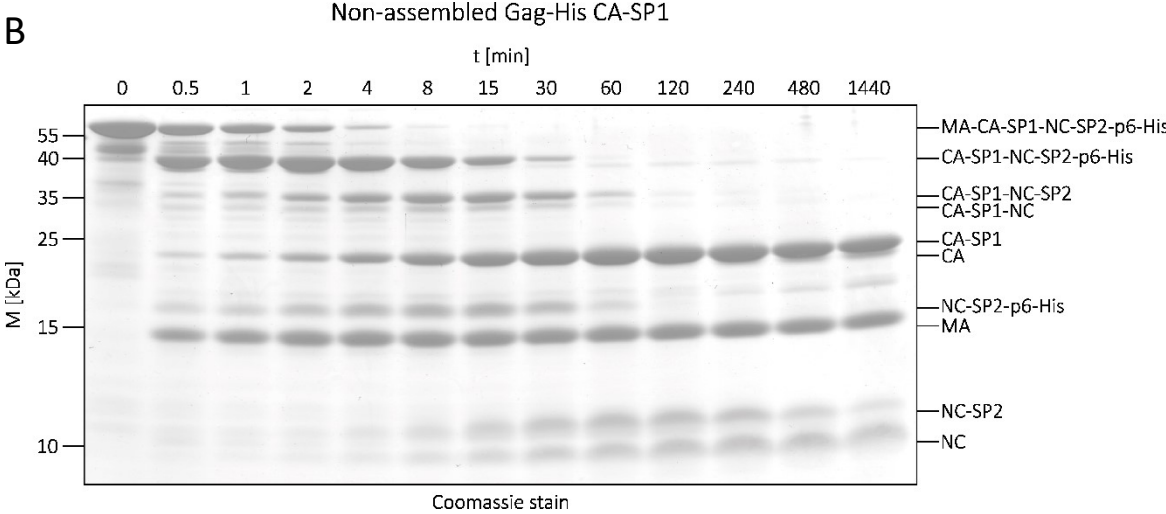
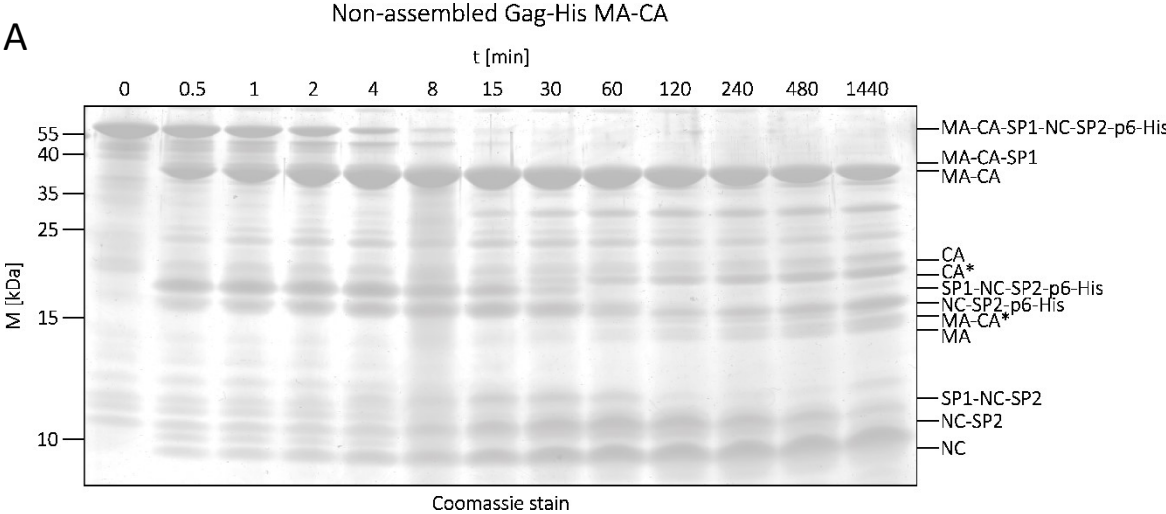


Figure 46: Nucleic acid-dependent processing of non-assembled Gag-His WT or assembled Δ MACANCSP2 WT analyzed in time course manner with Tricine-PAGE. Recombinant purified protein Gag-His WT was processed in non-assembled in the presence of the assembly oligonucleotide (A), the pentameric oligonucleotide (B), and without nucleic acid (Figure 17). Δ MACANCSP2 WT was processed after assembly with MS2 RNA (C), the standard assembly oligonucleotide (5.2.2.4), the pentameric oligonucleotide (D), and without nucleic acid (E). Samples were processed *in vitro* by the addition of recombinant purified HIV-1 PR over 24 h (= 1440 min) at 37 °C and 450 rpm. After successive increasing time steps (0 – 1440 min), samples were taken for analysis by Coomassie G-250 stained Tricine-PAGEs (16 % PAA, crosslinking ratio 1:32 BAA/AA and 9.6 % PAA, 1:32 BAA/AA). Positions of molecular mass standards marker are shown at the left, and the position of Gag-His and processing products are indicated at the right.



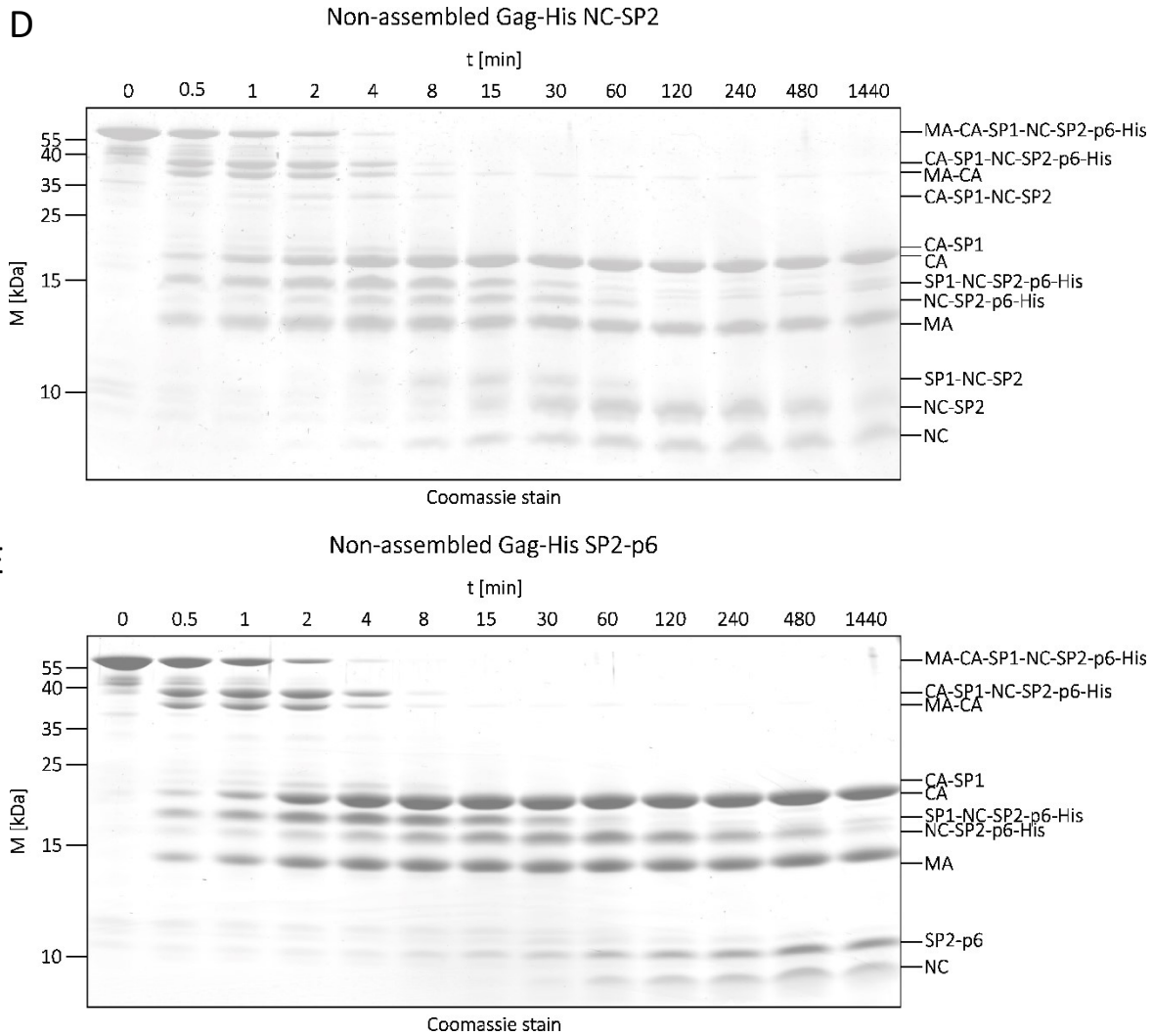


Figure 47: Time course of Gag-His with inhibiting mutations processing analyzed by Tricine-PAGE. Recombinant purified protein of Gag-His MA-CA (A), CA-SP1 (B), SP1-NC (C), NC-SP2 (D) or SP2-p6 (E) were dialyzed against processing buffer and processed *in vitro* by addition of recombinant purified HIV-1 PR over 24 h (= 1440 min) at 37 °C and 450 rpm. After successive increasing time steps (0 – 1440 min), samples were taken for analysis by Coomassie G-250 stained Tricine-PAGEs (16 % PAA, crosslinking ratio 1:32 BAA/AA and 9.6 % PAA, 1:32 BAA/AA). Positions of molecular mass standards marker are shown at the left, and the position of Gag-His and processing products are indicated at the right.

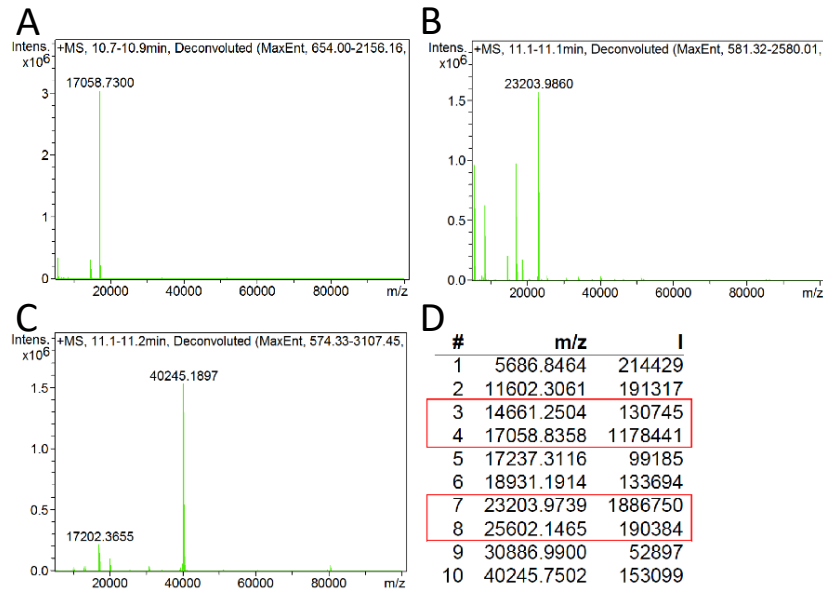
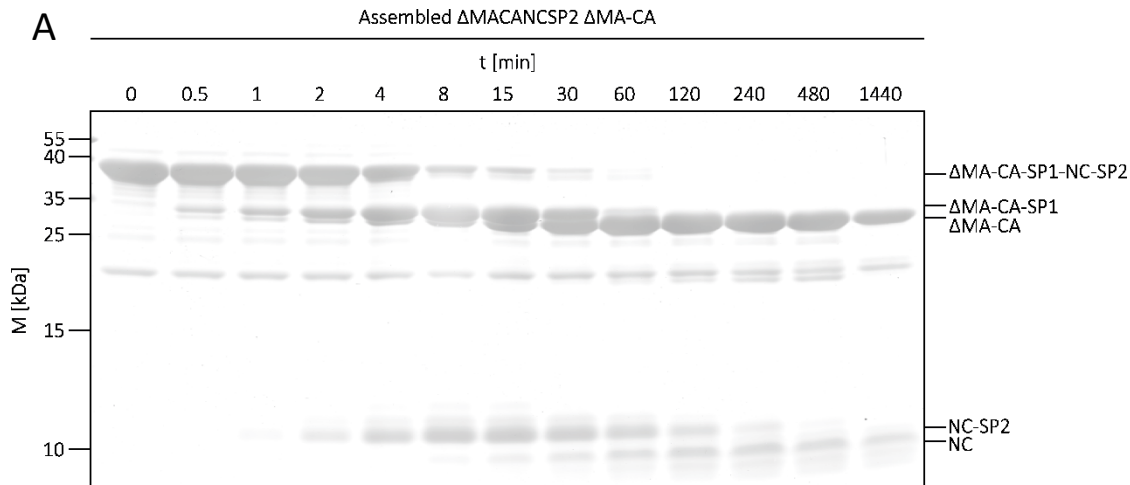
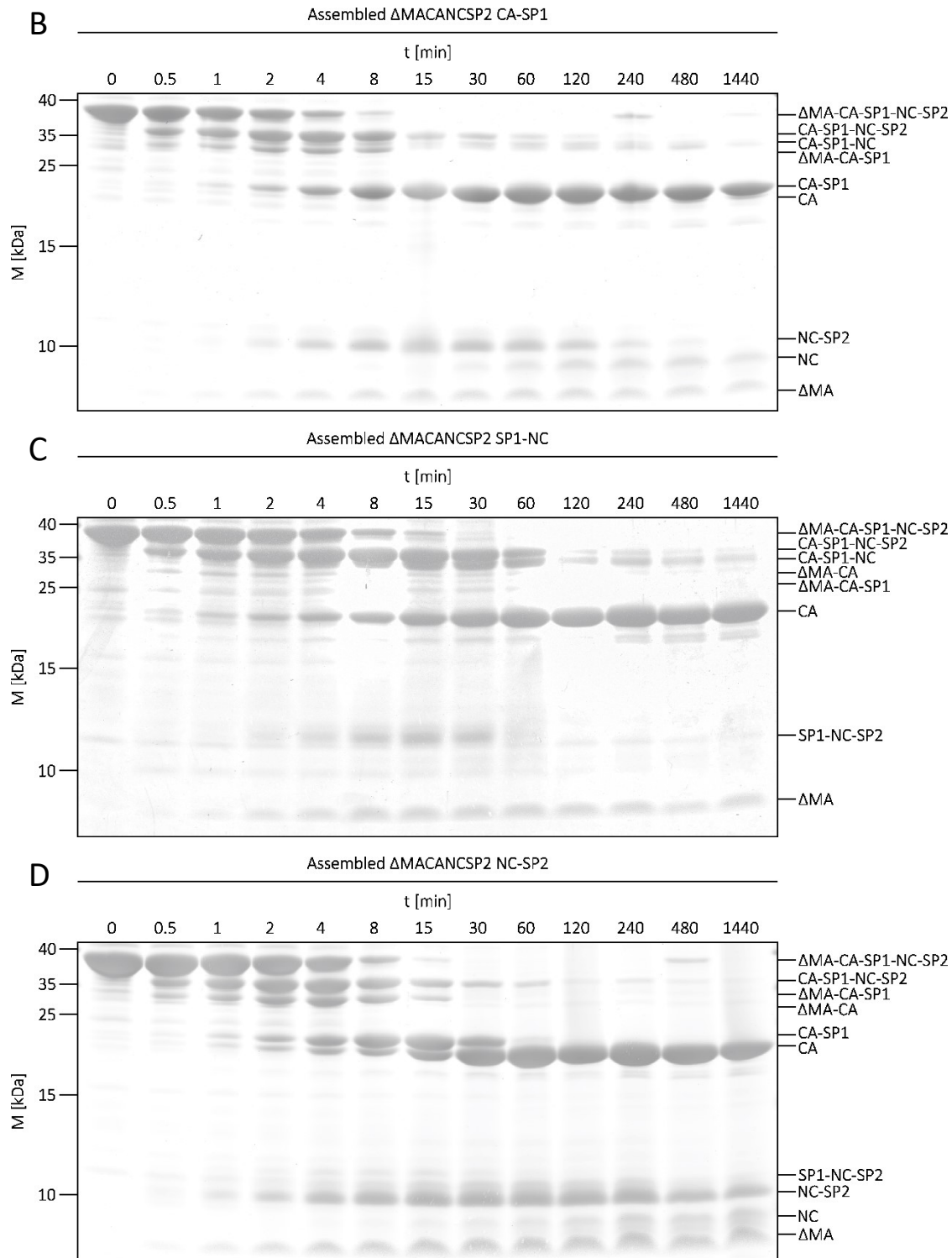


Figure 48: Intact protein mass spectrometry of Gag-His MA-CA processing products. 31 μ M Gag-His MA-CA was processed according to the processing protocol for 36 h by the HIV-1 PR. Afterward the proteins of 500 μ L sample were separated by size via a superdex 75 10/300 column (Figure 36 B + C). The fraction 4 and 8 of this purification were measured by intact protein mass spectrometry. Therefore, the sample was applied to a POROS 10R1 column equilibrated in 0.3 % formic acid and eluted with an isocratic gradient to 50 % of a buffer, containing 80 % isopropanol, 10 % acetonitrile and 0.3 % formic acid. Eluted proteins were immediately measured in a mAxis mass spectrometer. The calculation was performed with Data Analysis 4.2 (Bruker) and ESI Compass 1.3 Maximum Entropy Deconvolution Option. Proteins from fraction 8 eluted after \sim 10.7 – 10.9 min contained prominently proteins of 17058.7 Da (A) and after 11.1 min of 14661.3 Da, 17058.8 Da, 23204.0 Da, and 25602.1 Da (B), as indicated in the red boxes of the signal list of figure B (D). Proteins from fraction 4 eluted after 11.1 – 11.2 min contained prominently proteins of 40245.2 Da (C).





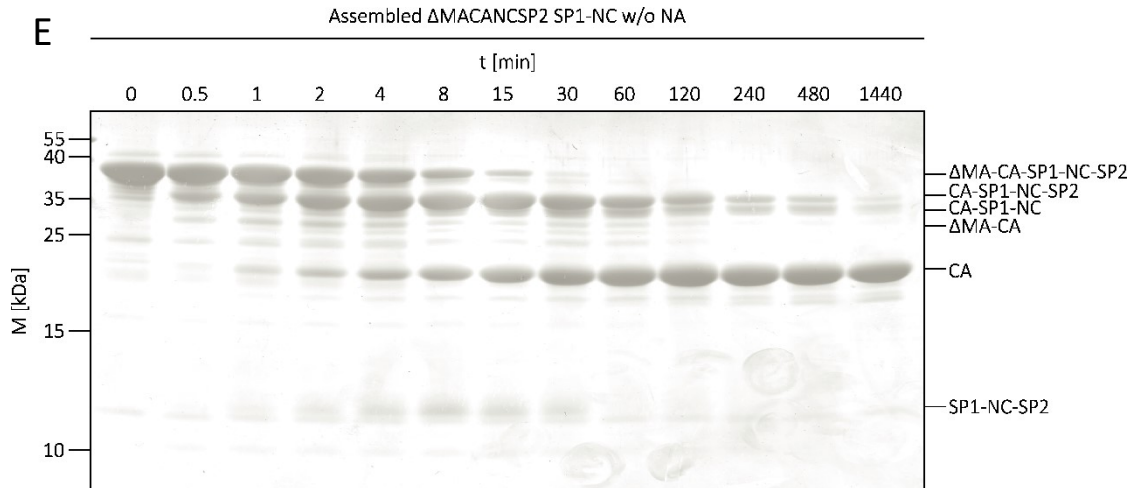
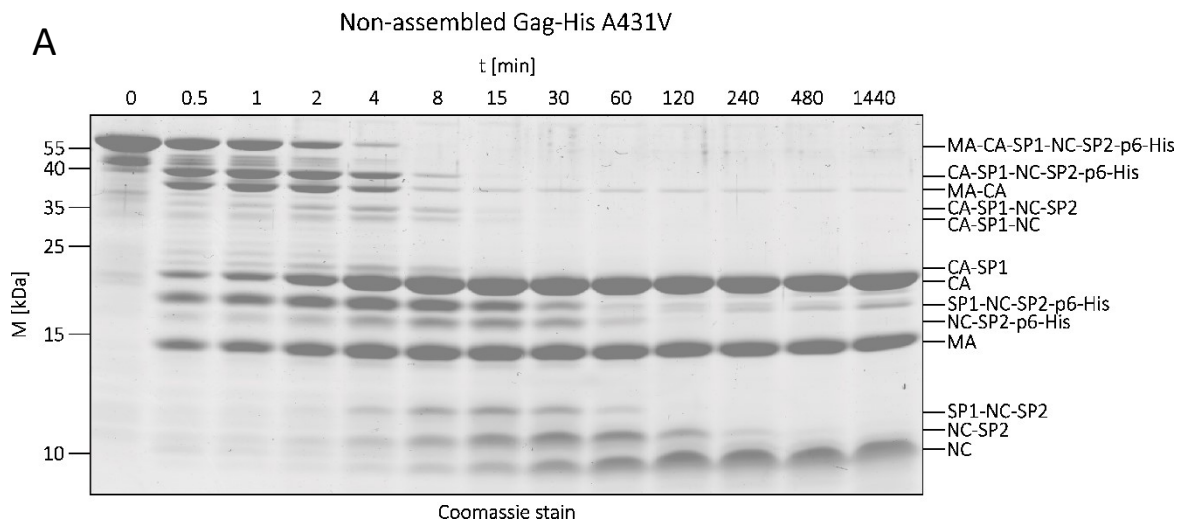


Figure 49: Time course assembled Δ MACANCSP2 with inhibiting mutations processing analyzed by Tricine-PAGE. Recombinant purified Δ MACANCSP2 MA-CA (A), CA-SP1 (B), SP1-NC (C), or NC-SP2 (D) was dialyzed after assembly with the standard oligonucleotide for assembly or without NA in a case of Δ MACANCSP2 SP1-NC (E) in processing buffer and processed *in vitro* by addition of recombinant purified HIV-1 PR over 24 h (= 1440 min) at 37 °C and 1000 rpm. After successive increasing time steps (0 – 1440 min), samples were taken for analysis by Coomassie G-250 stained Tricine-PAGEs (16 % PAA, crosslinking ratio 1:32 BAA/AA and 9.6 % PAA, 1:32 BAA/AA). Positions of molecular mass standards marker are shown at the left, and the position of Gag-His and processing products are indicated at the right.



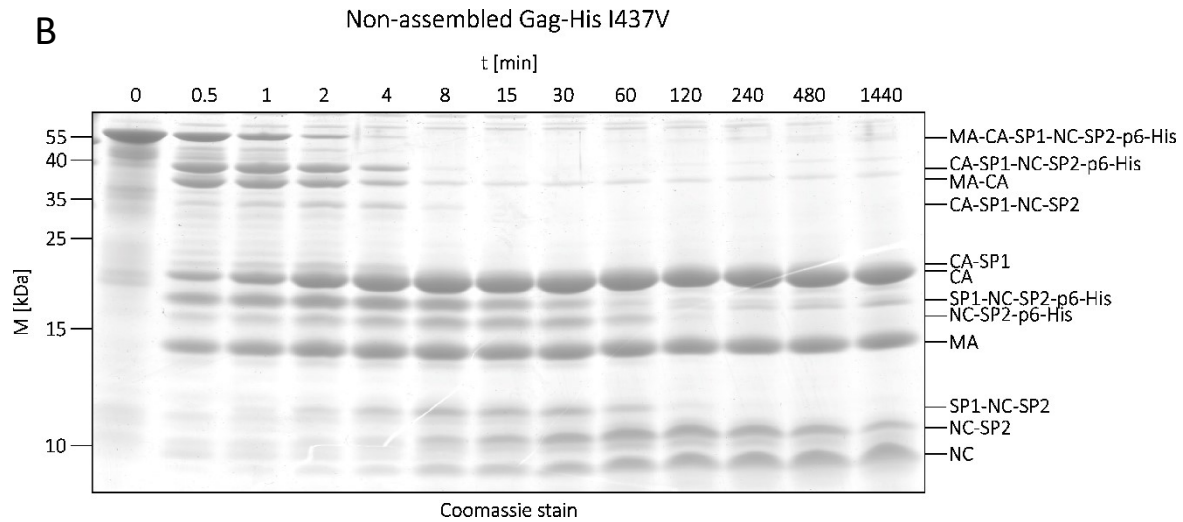
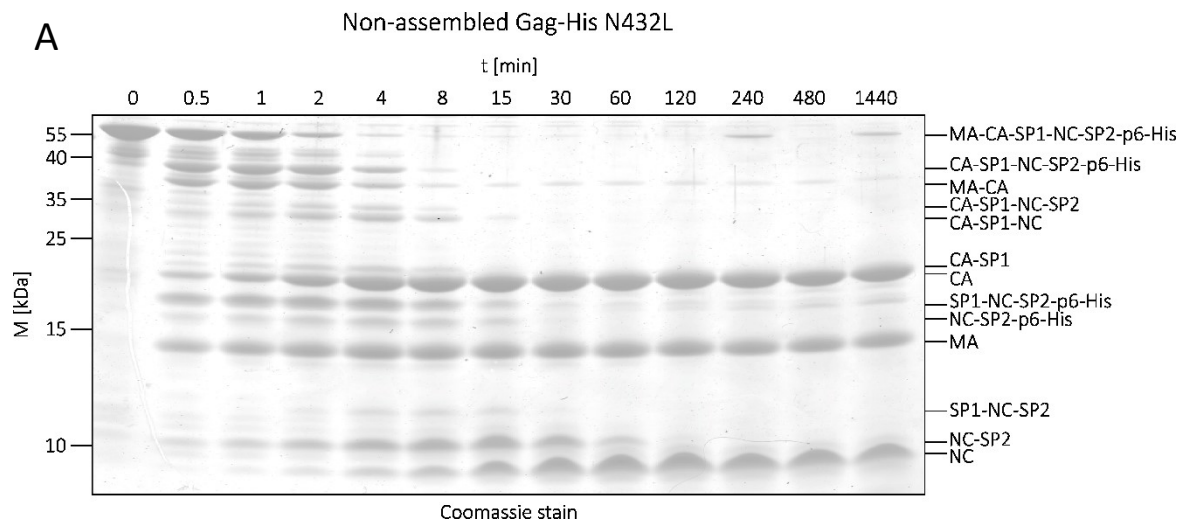


Figure 50: Time course of Gag-His processing containing PR resistance enabling mutations analyzed by Tricine-PAGE. Recombinant purified protein of Gag-His A431V (A) and I437V (B) were dialyzed against processing buffer and processed *in vitro* by the addition of recombinant purified HIV-1 PR over 24 h (= 1440 min) at 37 °C and 450 rpm. After successive increasing time steps (0 – 1440 min), samples were taken for analysis by Coomassie G-250 stained Tricine-PAGEs (16 % PAA, crosslinking ratio 1:32 BAA/AA and 9.6 % PAA, 1:32 BAA/AA). Positions of molecular mass standards marker are shown at the left, and the position of Gag-His and processing products are indicated at the right.



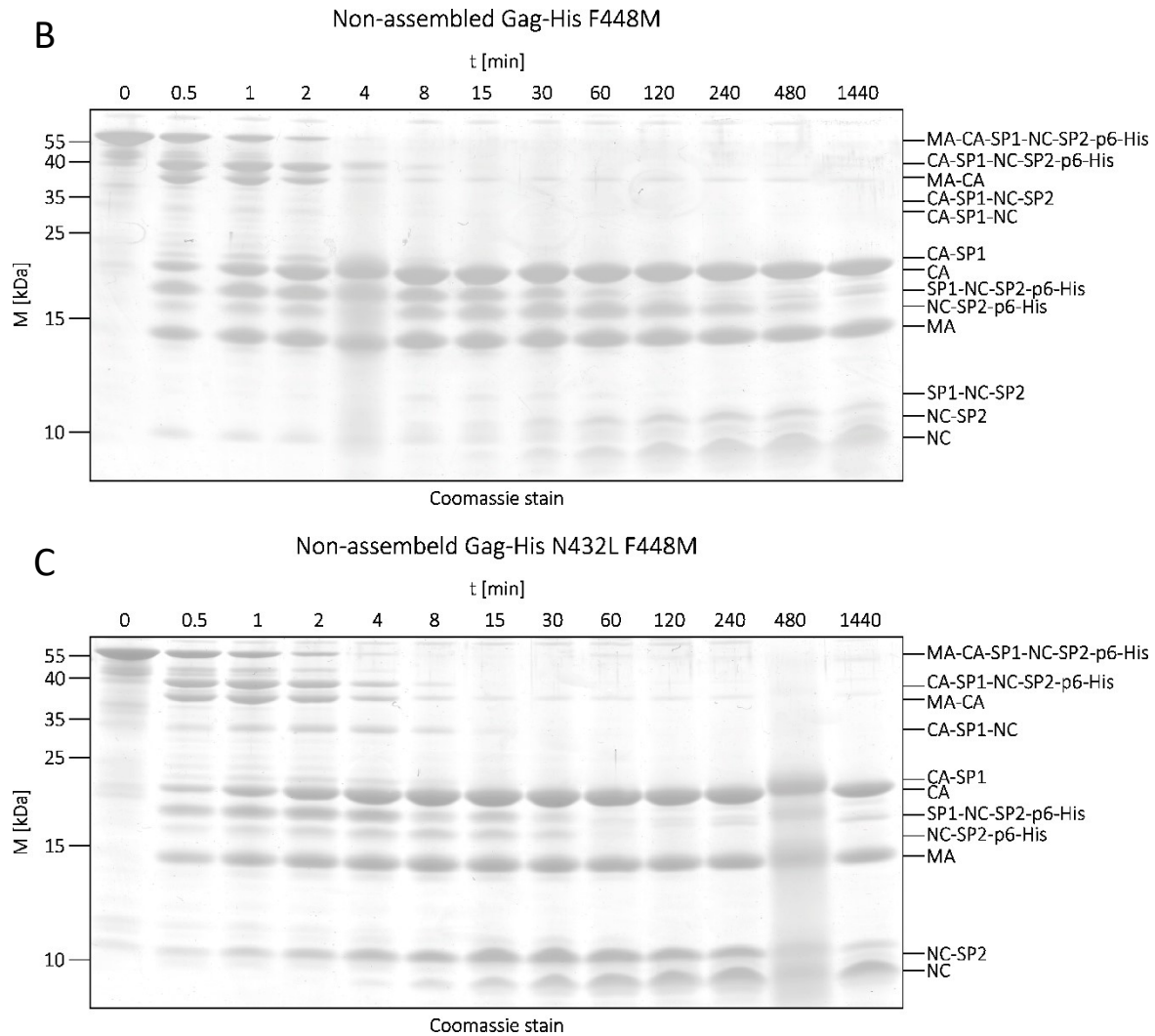
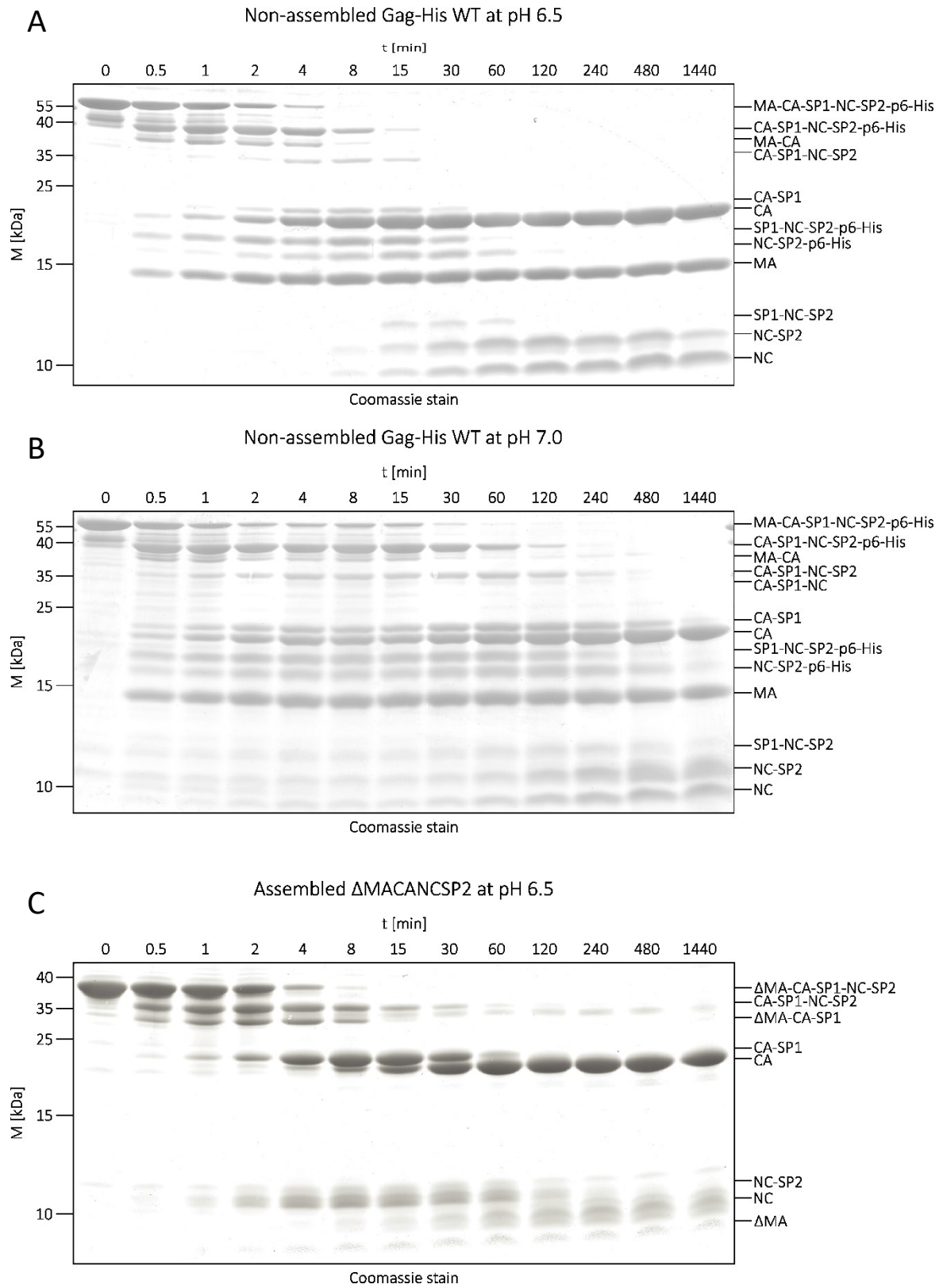


Figure 51: Time course of Gag-His processing containing cleavage rate altering mutations analyzed by Tricine-PAGE. Recombinant purified protein of Gag-His N432L (A), F448M (B), and N432L F448M (C) were dialyzed against processing buffer and processed *in vitro* by addition of recombinant purified HIV-1 PR over 24 h (= 1440 min) at 37 °C and 450 rpm. After successive increasing time steps (0 – 1440 min), samples were taken for analysis by Coomassie G-250 stained Tricine-PAGEs (16 % PAA, crosslinking ratio 1:32 BAA/AA and 9.6 % PAA, 1:32 BAA/AA). Positions of molecular mass standards marker are shown at the left, and the position of Gag-His and processing products are indicated at the right.



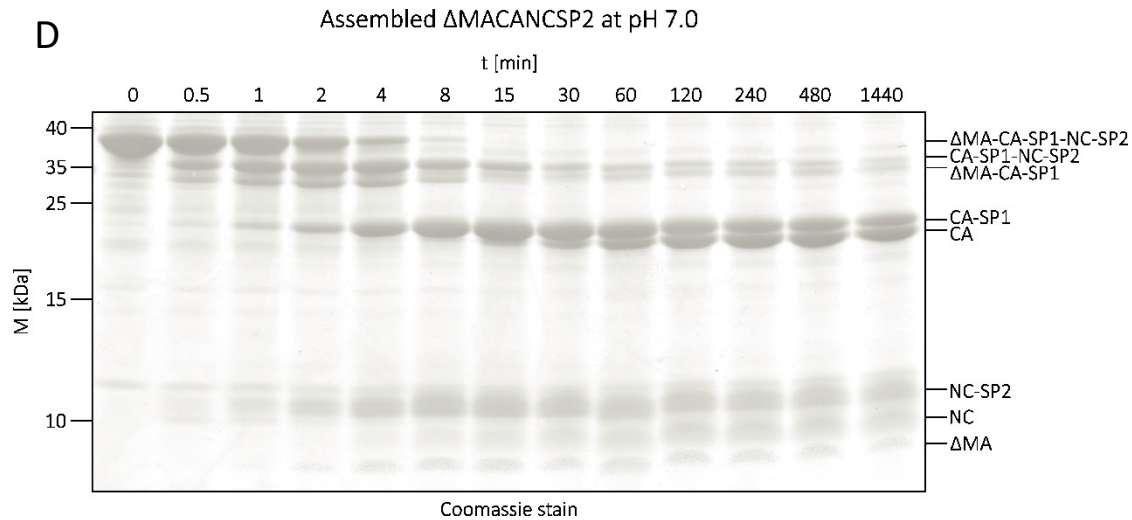


Figure 52: Impact of pH on the processing of non-assembled Gag-His and *in vitro* assembled Δ MACANCSP2 analyzed by Tricine-PAGE. At pH of 6.0 (Figure 17), 6.5 (A, C), and 7.0 (B, D) recombinant purified protein of Gag-His WT was directly dialyzed for non-assembled processing (A, B) and Δ MACANCSP2 was first assembled according to standard protocol (5.2.2.4) and afterward dialyzed against processing buffer of the respective pH for *in vitro* assembled particles (C, D). Subsequently, the samples were processed *in vitro* by the addition of recombinant purified HIV-1 PR over 24 h (= 1440 min) at 37 °C and 450 rpm. After successive increasing time steps (0 – 1440 min), samples were taken for analysis by Coomassie G-250 stained Tricine-PAGEs (16 % PAA, crosslinking ratio 1:32 BAA/AA and 9.6 % PAA, 1:32 BAA/AA). Positions of molecular mass standards marker are shown at the left, and the position of Gag-His and processing products are indicated at the right.

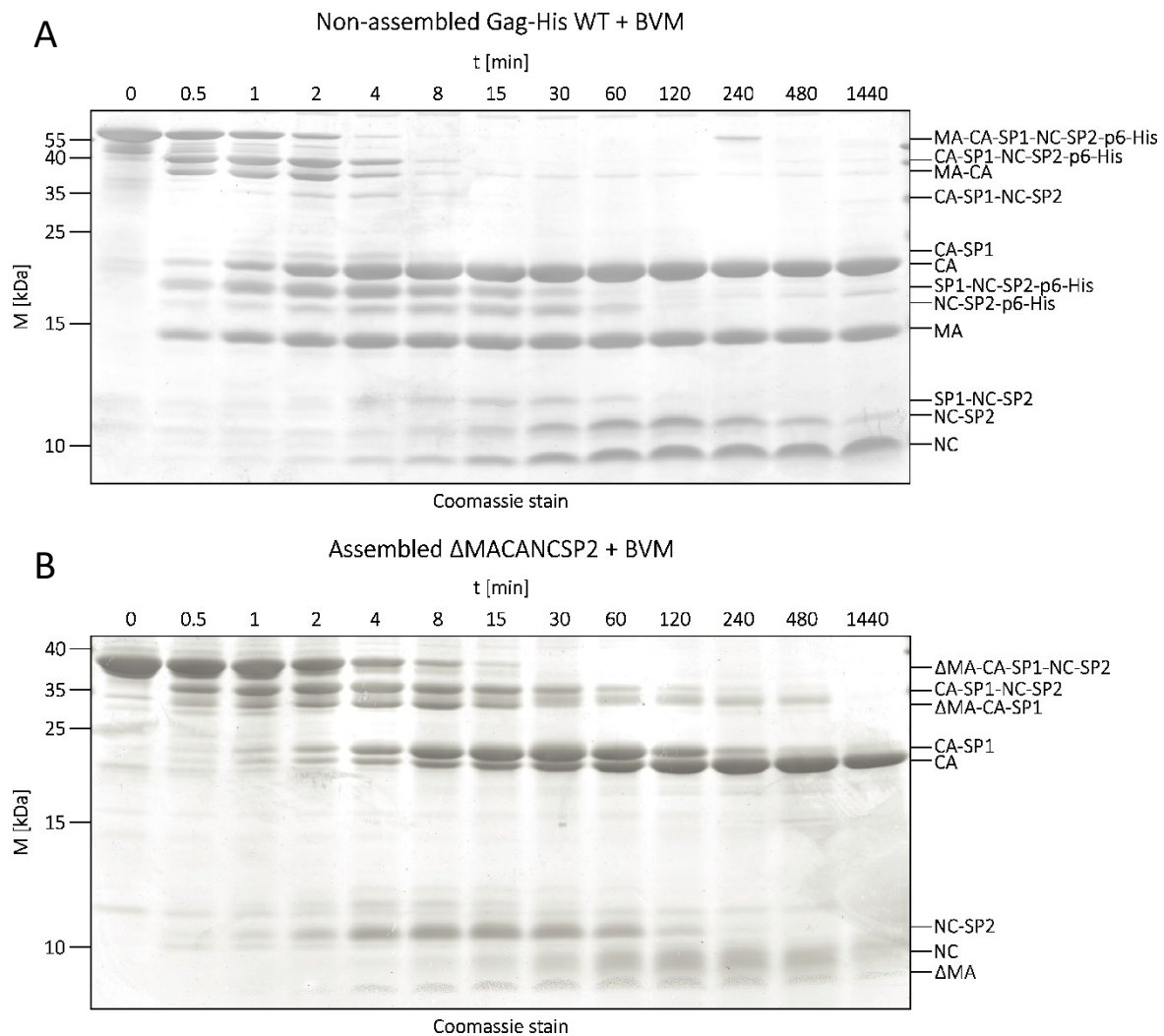


Figure 53: Impact of bevirimat (BVM) on the processing of non-assembled Gag-His and *in vitro* assembled Δ MACANCSP2 analyzed by Tricine-PAGE. In the presence of 100 μ M BVM, the recombinant purified protein of Gag-His WT was directly dialyzed for non-assembled processing(A) and Δ MACANCSP2 was first assembled according to standard protocol (5.2.2.4) and afterward dialyzed against processing buffer for *in vitro* assembled particles (B). Subsequently, the samples were processed *in vitro* by the addition of recombinant purified HIV-1 PR over 24 h (= 1440 min) at 37 °C and 450 rpm. After successive increasing time steps (0 – 1440 min), samples were taken for analysis by Coomassie G-250 stained Tricine-PAGEs (16 % PAA, crosslinking ratio 1:32 BAA/AA and 9.6 % PAA, 1:32 BAA/AA). Positions of molecular mass standards marker are shown at the left, and the position of Gag-His and processing products are indicated at the right.

10 Index

Figure 1: Organization of the HIV-1 genome.	2
Figure 2: Schematic monomeric structures of Gag.....	3
Figure 3: Schematic assembled Gag structures of immature and mature HIV-1 in comparison to tomograms made by cryo-EM.	6
Figure 4: Schematic illustration of assembly, budding, and maturation of HIV-1 particles.	8
Figure 5: Gag sequences at protease cleavage sites and schematic depiction of sequential proteolysis of Gag during maturation.	9
Figure 6: HIV-1 Gag derivatives and <i>in vitro</i> assembly systems.....	12
Figure 7: Cloning scheme of ordered synthetic DNA constructs of Gag.	32
Figure 8: Pierce 660 nm protein assay calibration.....	41
Figure 9: Gel filtration calibration.	43
Figure 10: Simplified schedule of the quantitative analysis of processing samples with Coomassie-stained Tricine-PAGEs.....	45
Figure 11: Production and IMAC-purification of Gag-His.	48
Figure 12: Analysis of Gag dimerization by gel filtration.	50
Figure 13: Visualization of <i>in vitro</i> assembled Gag-His WT and Δ MACANCSP2 WT by TEM.....	53
Figure 14: Capto Core purification of <i>in vitro</i> assembled Δ MACANCSP2.	56
Figure 15: Long-term stability of assembled particles and aberrant assembly induced in the absence of nucleic acid.....	58
Figure 16: Morphological analysis of elongated filament-like assemblate of Δ MACANCSP2.	59
Figure 17: Time course of Gag-His WT processing analyzed by Tricine-PAGE.....	60
Figure 18: Affinity chromatography of polyclonal antibodies against SP1 and SP2.	63
Figure 19: Intermediate and product identification of Gag-His WT processing analyzed by immunoblotting.....	65
Figure 20: Gel filtration analysis of non-assembled Gag-His WT processing products.....	67
Figure 21: Gag-His and PR stability under processing conditions.	68
Figure 22: Different representations of the quantitative analysis for Gag-His processing.....	70
Figure 23: Time-course analysis of the Gag processing relating to a mono- or dimeric state.	71
Figure 24: Cleavage site processing in an ordered sequence and decay of Gag and accumulation of processing products over time.	74
Figure 25: Time-course analysis of the processing of virus-like particles, assembled and non-assembled Gag WT.....	75
Figure 26: Time-course analysis of the processing of Δ MACANCSP2 in the presence and absence of IP6.	76
Figure 27: Morphological control of <i>in vitro</i> assembled Δ MACANCSP2 dialyzed at different pH values by TEM.	78
Figure 28: Time-course analysis of the processing of non-assembled Gag-His WT and <i>in vitro</i> assembled Δ MACANCSP2 WT at different pH values.	79
Figure 29: TEM images of <i>in vitro</i> assembled Δ MACANCSP2 with a pentameric oligonucleotide or with MS2 RNA.	80
Figure 30: Time-course analysis of processing of assembled and non-assembled Gag WT in the absence or presence of different nucleic acid. C	82

Figure 31: Gag sequences at protease cleavage sites and their cleavage inhibiting mutations.	83
Figure 32: Morphology of <i>in vitro</i> assembled ΔMACANCSP2 particles carrying cleavage site mutations.	84
Figure 33: Time-course analysis of non-assembled Gag-His and <i>in vitro</i> assembled ΔMACANCSP2 containing cleavage inhibiting mutations.	85
Figure 34: Time-course analysis of <i>in vitro</i> assembled ΔMACANCSP2 WT and SP1-NC with and without nucleic acid.	87
Figure 35: Aberrant cleavage in case of an inhibited MA-CA cleavage site in Gag.	88
Figure 36: Gel filtration analysis of Gag-His MA-CA processing products.	89
Figure 37: Similar processing of Gag-His WT and with Gag mutations enabling protease inhibitor resistance.	91
Figure 38: Time-course analysis of the processing of non-assembled Gag-His containing cleavage rate altering mutations.	92
Figure 39: Morphological control of <i>in vitro</i> assembled ΔMACANCSP2 WT in the presence of maturation inhibitor bevirimat by TEM.	93
Figure 40: Time-course analysis of the processing of non-assembled Gag-His WT and <i>in vitro</i> assembled ΔMACANCSP2 WT in the absence and presence of maturation inhibitor bevirimat.	94
Figure 41: Intact protein mass spectrometry of Gag-His WT processing products.	109
Figure 42: Concentration determination of purified VLPs and EM analysis.	109
Figure 43: Analysis of purified Gag-His variants.	110
Figure 44: Time course of VLP processing analyzed by immunoblots of Tricine-PAGEs.	111
Figure 45: Time course of ΔMACANCSP2 processing in a non-assembled state and <i>in vitro</i> assembled analyzed by Tricine-PAGE.	112
Figure 46: Nucleic acid-dependent processing of non-assembled Gag-His WT or assembled ΔMACANCSP2 WT analyzed in time course manner with Tricine-PAGE.	114
Figure 47: Time course of Gag-His with inhibiting mutations processing analyzed by Tricine-PAGE. ..	116
Figure 48: Intact protein mass spectrometry of Gag-His MA-CA processing products.	117
Figure 49: Time course assembled ΔMACANCSP2 with inhibiting mutations processing analyzed by Tricine-PAGE.	119
Figure 50: Time course of Gag-His processing containing PR resistance enabling mutations analyzed by Tricine-PAGE.	120
Figure 51: Time course of Gag-His processing containing cleavage rate altering mutations analyzed by Tricine-PAGE.	121
Figure 52: Impact of pH on the processing of non-assembled Gag-His and <i>in vitro</i> assembled ΔMACANCSP2 analyzed by Tricine-PAGE.	123
Figure 53: Impact of bevirimat (BVM) on the processing of non-assembled Gag-His and <i>in vitro</i> assembled ΔMACANCSP2 analyzed by Tricine-PAGE.	124

11 Acknowledgments

During the time of my PhD, I met a plethora of interesting, helpful, and guiding people. All of those who did take part in my work, if by a helping hand or just by a word of encouragement, I would like to thank very dearly. Following, I would like to thank individual and important people for me in no particular order.

First of all, I would like to thank Prof. Dr. Barbara Müller for her supervision and the opportunity for me to work in her group. I am grateful for the trust and space given to me during my PhD, even though I needed from time to time a push in the correct way. Scientifically, I learned a lot and was able to develop many abilities I was lacking before. Thank you for all the corrections, support, and understanding during the last three years.

Also, I acknowledge Prof. Dr. Kräusslich for a lot of valuable scientific input, his supervision, and providing a focus on the really essential parts of my work. Thank you for examining my thesis and being part of my TAC and defense committee.

Additionally, I would like to thank the rest of my TAC, Prof. Dr. Stephan Urban and PD Dr. Joachim Reinstein, for their technical advice and giving me helpful feedback.

I acknowledge Dr. Kashif Sadiq for a highly interesting collaboration. Although Kashif's work was always of a complex nature, he could make it easily understandable for me.

I want to acknowledge Stefan Hilmer and Charlotta Funaya of the electron microscopy core facility at the Heidelberg University for providing me access to their instruments and a lot of lessons to improve my microscopy skills.

Additionally I acknowledge Prof. Dr. Frauke Melchior and Heidi Ehret for providing me unrestricted access to their cell disruptor.

Thanks go to Jiri Schirmer for sending over and over again recombinant protease after I was, unfortunately, unable to produce it on my own.

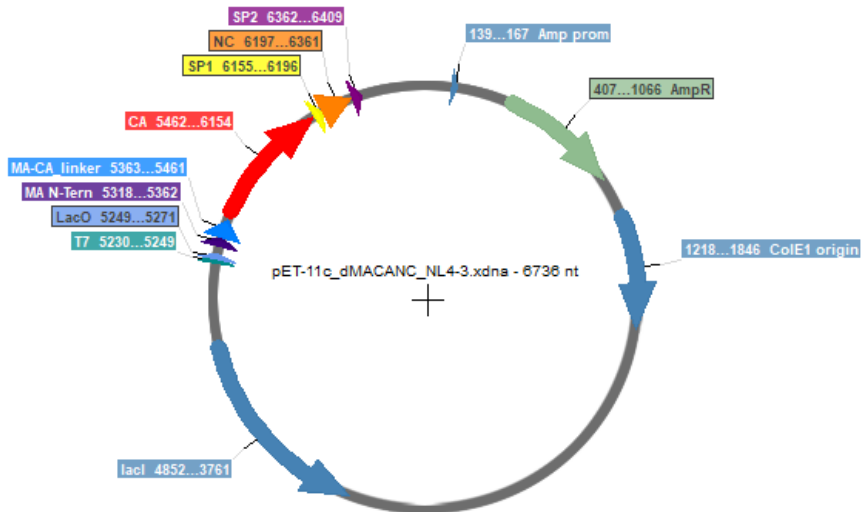
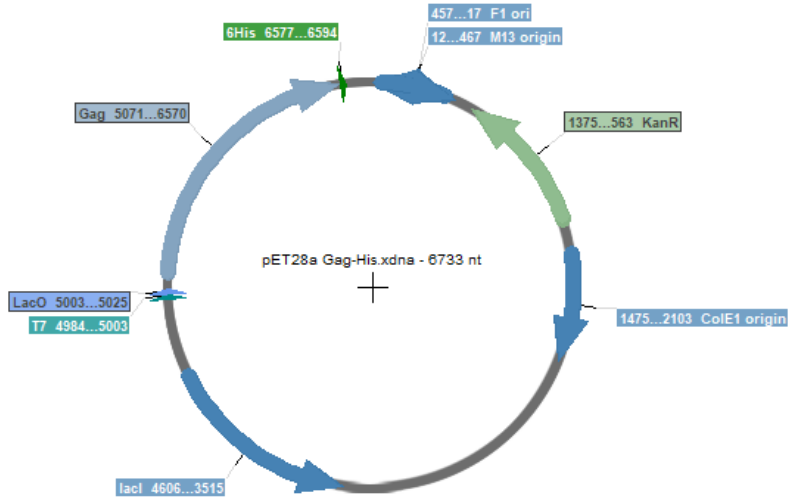
Furthermore, I also would like to heartily thank Maria for excellent technical assistance and Annica, Sandra, Volkan Sakin, Afrodite and Stephanie. Thank you for all the fun time, breakfasts and philosophical excursions. I will miss you all.

I also thank all other members of the Center for Integrative Infectious Diseases, with whom I had a great and fascinating time during my PhD. I am happy that I found some good friends among you. Special thanks go to Anke, Bärbel, Vera, Thorsten, Tamara, Robin, Vojtech, Daniel, and Martin for the help with cells, scientific issues electron microscopy.

I want to express my gratitude to my parents who always took care of me and enabled my road of life so far. Thank you for providing me assistance of any type at any time. Without you I would have never passed my long-time dream of getting a doctoral degree.

At the end I especially thank my wife, Carmen, who supported me intensively during the last three years, always kept me calm, and focused and encouraged me to live my dreams. Thank you for all your time, power and understanding when I was about to turn crazy.

12 Plasmid maps



13 References

- Abraham, L. und Fackler, O. T. 2012.** *HIV-1 Nef: a multifaceted modulator of T cell receptor signaling.* s.l. : Cell Commun Signal, 2012. Bd. 10, 1, S. 39.
- Accola, M. A., Höglund, S. and Göttlinger, H. G. 1998.** *A putative alpha-helical structure which overlaps the capsid-p2 boundary in the human immunodeficiency virus type 1 Gag precursor is crucial for viral particle assembly.* s.l. : J Virol, 1998. Vol. 72, 3, pp. 2072-2078.
- Adamson, C. S., et al. 2010.** *Polymorphisms in Gag spacer peptide 1 confer varying levels of resistance to the HIV-1 maturation inhibitor bevirimat.* s.l. : Retrovirology, 2010. Bd. 7:36, doi: 10.1186, S. 1742-4690-7-36.
- Alfadhli, A., Barklis, R. L. und Barklis, E. 2009.** *HIV-1 matrix organizes as a hexamer of trimers on membranes containing phosphatidylinositol-(4,5)-bisphosphate.* s.l. : Virology, 2009. Bd. 387, 2, S. 466-472.
- Alfadhli, A., et al. 2011.** *HIV-1 matrix protein binding to RNA.* s.l. : J Mol Biol, 2011. Bd. 410, 4, S. 653-666.
- Anderson, J. und Hope, T. J. 2004.** *HIV accessory proteins and surviving the host cell.* s.l. : Curr HIV/AIDS Rep, 2004. Bd. 1, 1, S. 47-53.
- Arnold, E. und Sarafianos, S. 2008.** *An HIV secret uncovered.* 2008. Bd. 453, S. 169-170.
- Baltimore, D. 1971.** *Expression of animal virus genomes.* s.l. : Bacteriol Rev., 1971. Bd. 35, 5, S. 235-241.
- Barré-Sinoussi, F., et al. 1983.** *Isolation of a T-lymphotropic retrovirus from a patient at risk for acquired immune deficiency syndrome (AIDS).* s.l. : Science, 1983. Bd. 220, 4599, S. 868-871.
- Bayro, M. J., et al. 2016.** *Helical Conformation in the CA-SP1 Junction of the Immature HIV-1 Lattice Determined from Solid-State NMR of Virus-like Particles.* s.l. : J Am Chem Soc, 2016. Bd. 138, 37, S. 12029-12032.
- Bejarano, D. A., et al. 2019.** *HIV-1 nuclear import in macrophages is regulated by CPSF6-capsid interactions at the nuclear pore complex.* s.l. : Elife, 2019. Bd. 8, pii: e41800.
- Berger, E. A. 1997.** *HIV entry and tropism: the chemokine receptor connection.* s.l. : AIDS, 1997. Bd. 11, S. 3-16.
- Bewley, M. C., et al. 2017.** *A non-cleavable hexahistidine affinity tag at the carboxyl-terminus of the HIV-1 Pr55Gag polyprotein alters nucleic acid binding properties.* s.l. : Protein Expr Purif, 2017. Bd. 130, S. 137-145.
- Bharat, T. A., et al. 2012.** *Structure of the immature retroviral capsid at 8 Å resolution by cryo-electron microscopy.* s.l. : Nature, 2012. Bd. 487, 7407, S. 385-389.
- Bharat, T. A., et al. 2014.** *Cryo-electron microscopy of tubular arrays of HIV-1 Gag resolves structures essential for immature virus assembly.* s.l. : Proc Natl Acad Sci U S A, 2014. Bd. 111, 22, S. 8233-8238.
- Blundell, T. L., et al. 1998.** *The aspartic proteinases. An historical overview.* s.l. : Adv Exp Med Biol, 1998. Bd. 436, S. 1-13.
- Borsetti, A., Ohagen, A. und Göttlinger, H. G. 1998.** *The C-terminal half of the human immunodeficiency virus type 1 Gag precursor is sufficient for efficient particle assembly.* s.l. : J Virol, 1998. Bd. 72, 11, S. 9313-9317.
- Briggs, J. A. G., et al. 2003.** *Structural organization of authentic, mature HIV-1 virions and cores.* s.l. : EMBO J, 2003. Bd. 22, 7, S. 1707-1715.

- Briggs, J. A. G., et al. 2009.** *Structure and assembly of immature HIV.* s.l. : Proc Natl Acad Sci U S A, 2009. Bd. 106, 27, S. 11090-11095.
- Briggs, J. A. G., et al. 2006.** *The mechanism of HIV-1 core assembly: insights from three-dimensional reconstructions of authentic virions.* s.l. : Structure, 2006. Bd. 14, 1, S. 15-20.
- Briggs, J. A. G., et al. 2004.** *The stoichiometry of Gag protein in HIV-1.* s.l. : Nat Struct Mol Biol, 2004. Bd. 11, 7, S. 672-675.
- Briggs, J. A. und Kräusslich, H. G. 2011.** *The molecular architecture of HIV.* s.l. : J Mol Biol, 2011. Bd. 410, 4, S. 491-500.
- Bunce, C. M., et al. 1993.** *Comparison of the levels of inositol metabolites in transformed haemopoietic cells and their normal counterparts.* s.l. : Biochem J, 1993. Bd. 289, 3, S. 667-673.
- Bushman, F. D., Fujiwara, T. und Craigie, R. 1990.** *Retroviral DNA integration directed by HIV integration protein in vitro.* s.l. : Science, 1990. Bd. 249, 4976, S. 1555-1558.
- Butt, R. H. und Coorsen, J. R. 2013.** *Coomassie blue as a near-infrared fluorescent stain: a systematic comparison with Sypro Ruby for in-gel protein detection.* s.l. : Mol Cell Proteomics, 2013. Bd. 12, 12, S. 3834-3850.
- Callebaut, C., et al. 2011.** *In vitro characterization of GS-8374, a novel phosphonate-containing inhibitor of HIV-1 protease with a favorable resistance profile.* s.l. : Antimicrob Agents Chemother, 2011. Bd. 55, 4, S. 1366-13676.
- Campbell, E. M. und Hope, T. J. 2015.** *HIV-1 capsid: the multifaceted key player in HIV-1 infection.* s.l. : Nat Rev Microbiol, 2015. Bd. 13, 8, S. 471-483.
- Campbell, S. und Rein, A. 1999.** *In vitro assembly properties of human immunodeficiency virus type 1 Gag protein lacking the p6 domain.* s.l. : J Virol, 1999. Bd. 73, 3, S. 2270-2279.
- Campbell, S., et al. 2001.** *Modulation of HIV-like particle assembly in vitro by inositol phosphates.* s.l. : Proc Natl Acad Sci U S A, 2001. Bd. 98, 19, S. 10875-10879.
- Campbell-Yesufu, O. T. und Gandhi, R. T. 2011.** *Update on human immunodeficiency virus (HIV)-2 infection.* s.l. : Clin Infect Dis., 2011. Bd. 52, 6, S. 780-787.
- Capon, D. J. und Ward, R. H. 1991.** *The CD4-gp120 interaction and AIDS pathogenesis.* s.l. : Annu Rev Immunol, 1991. Bd. 9, S. 649-678.
- Carlson, L. A., et al. 2008.** *Three-dimensional analysis of budding sites and released virus suggests a revised model for HIV-1 morphogenesis.* s.l. : Cell Host Microbe, 2008. Vol. 4, 6, pp. 592-599.
- Carlson, L. A., et al. 2010.** *Cryo electron tomography of native HIV-1 budding sites.* s.l. : PLoS Pathog, 2010. Bd. 6, 11, S. e1001173.
- CDC, Centers for Disease Control. 1981.** *Pneumocystis pneumonia--Los Angeles.* s.l. : MMWR Morb Mortal Wkly Rep, 1981. Bd. 30, 21, S. 250-252.
- Center, R. J., et al. 2002.** *Oligomeric structure of the human immunodeficiency virus type 1 envelope protein on the virion surface.* s.l. : J Virol, 2002. Bd. 76, 15, S. 7863-7867.
- Chan, D. C., et al. 1997.** *Core structure of gp41 from the HIV envelope glycoprotein.* s.l. : Cell, 1997. Bd. 89, 2, S. 263-273.
- Checkley, M. A., et al. 2010.** *The capsid-spacer peptide 1 Gag processing intermediate is a dominant-negative inhibitor of HIV-1 maturation.* s.l. : Virology, 2010. Bd. 400, 1, S. 137-144.
- Checkley, M. A., Luttge, B. G. und Freed, E. O. 2011.** *HIV-1 envelope glycoprotein biosynthesis, trafficking, and incorporation.* s.l. : J Mol Biol, 2011. Bd. 410, 4, S. 582-608.

- Chen, L., et al. 2009.** *Structural Basis of Immune Evasion at the Site of CD4 Attachment on HIV-1 gp120.* s.l. : Science, 2009. Bd. 326, 5956, S. 1123-1127.
- Chen, Z. und Cheng, W. 2017.** *Reversible aggregation of HIV-1 Gag proteins mediated by nucleic acids.* s.l. : Biochem Biophys Res Commun, 2017. Bd. 482, 4, S. 1437-1442.
- Cheng, Y. S., et al. 1990.** *Stability and activity of human immunodeficiency virus protease: comparison of the natural dimer with a homologous, single-chain tethered dimer.* s.l. : PNAS, 1990. Bd. 87, 24, S. 9660-9664.
- Chertova, E., et al. 2002.** *Envelope glycoprotein incorporation, not shedding of surface envelope glycoprotein (gp120/SU), is the primary determinant of SU content of purified human immunodeficiency virus type 1 and simian immunodeficiency virus.* s.l. : J Virol, 2002. Bd. 76, 11, S. 5315- 5325.
- Chojnacki, J., et al. 2017.** *Envelope glycoprotein mobility on HIV-1 particles depends on the virus maturation state.* s.l. : Nat Commun, 2017. Bd. 8, 1, S. 545.
- Chukkapalli, V1., et al. 2008.** *Interaction between the human immunodeficiency virus type 1 Gag matrix domain and phosphatidylinositol-(4,5)-bisphosphate is essential for efficient gag membrane binding.* s.l. : J Virol, 2008. Bd. 82, 5, S. 2405-2417.
- Coffin, J.M. 1992.** *Structure and Classification of Retroviruses.* [Buchverf.] Levy J.A. *The Retroviridae. The Viruses.* s.l. : Springer, Boston, MA, 1992.
- Coren, L. V., et al. 2007.** *Mutational analysis of the C-terminal gag cleavage sites in human immunodeficiency virus type 1.* s.l. : J Virol, 2007. Bd. 81, 18, S. 10047-10054.
- Dam, E., et al. 2009.** *Gag mutations strongly contribute to HIV-1 resistance to protease inhibitors in highly drug-experienced patients besides compensating for fitness loss.* s.l. : PLoS Pathog, 2009. Bd. 5, 3, S. e1000345.
- Darke, P. L., et al. 1988.** *HIV-1 protease specificity of peptide cleavage is sufficient for processing of gag and pol polyproteins.* s.l. : Biochem Biophys Res Commun, 1988. Bd. 156, 1, S. 297-303.
- Datta, S. A. K., et al. 2007a.** *365 Interactions between HIV-1 Gag Molecules in Solution: An Inositol Phosphate-mediated Switch.* s.l. : Journal of Molecular Biology, 2007a. S. 799–811.
- Datta, S. A. und Rein, A. 2017.** *Preparation of recombinant HIV-1 gag protein and assembly of virus-like particles in vitro.* s.l. : Methods Mol Biol, 2017. Bd. 485, S. 197-208.
- Datta, S. A., et al. 2011.** *HIV-1 Gag extension: conformational changes require simultaneous interaction with membrane and nucleic acid.* s.l. : J Mol Biol, 2011. Bd. 406, 2, S. 205-214.
- Datta, S. A., et al. 2007b.** *Conformation of the HIV-1 Gag Protein in Solution.* s.l. : J Mol Biol, 2007b. Bd. 365, 3, S. 812-824.
- De Guzman, N. R., et al. 1998.** *Structure of the HIV-1 nucleocapsid protein bound to the SL3 psi-RNA recognition element.* s.l. : Science, 1998. Bd. 279, 5349, S. 384-388.
- de Marco, A., et al. 2010.** *Structural analysis of HIV-1 maturation using cryo-electron tomography.* s.l. : PLoS Pathog, 2010. Bd. 6, 11, S. e1001215.
- de Marco, A., et al. 2012.** *Role of the SP2 domain and its proteolytic cleavage in HIV-1 structural maturation and infectivity.* s.l. : J Virol, 2012. Bd. 86, 24, S. 13708-13716.
- de Moreno, M. R., Smith, J. F. und Smith, R. V. 1986.** *Mechanism studies of coomassie blue and silver staining of proteins.* s.l. : Journal of Pharmaceutical Sciences, 1986. Bd. 75, 9, S. 907-911.
- Deshmukh, L., Ghirlando, R. und Clore, G. M. 2015.** *Conformation and dynamics of the Gag polyprotein of the human immunodeficiency virus 1 studied by NMR spectroscopy.* s.l. : Proc Natl Acad Sci U S A, 2015. Bd. 112, 11, S. 3374-3379.

- Deutsche AIDS-Gesellschaft. 2019.** *Deutsch-Österreichische Leitlinien zur antiretroviralen Therapie der HIV-1-Infektion.* s.l. : Deutsche AIDS-Gesellschaft e.V., 2019.
- Di Nunzio, F. 2013.** *New insights in the role of nucleoporins: a bridge leading to concerted steps from HIV-1 nuclear entry until integration.* s.l. : Virus Res, 2013. Bd. 178, 2, S. 187-196.
- Dick, R. A., et al. 2012.** *HIV-1 Gag protein can sense the cholesterol and acyl chain environment in model membranes.* s.l. : Proc Natl Acad Sci U S A, 2012. Bd. 109, 46, S. 18761-18766.
- Dick, R. A., et al. 2018.** *Inositol phosphates are assembly co-factors for HIV-1.* s.l. : Nature, 2018. Bd. 560, 7719, S. 509-512.
- Dick, R. A., et al. 2020.** *Structures of immature EIAV Gag lattices reveal a conserved role for IP6 in lentivirus assembly.* s.l. : PLoS Pathog, 2020. Bd. 16, 1, S. e1008277.
- Diem, K. und Lentner, C. 1970.** *Scientific Tables, Excerpts from the Seventh Edition.* s.l. : Ardsley NY Geigy Pharmaceuticals C, 1970.
- Dorfman, T., et al. 1994.** *Role of the matrix protein in the virion association of the human immunodeficiency virus type 1 envelope glycoprotein.* s.l. : J Virol, 1994. Bd. 68, 3.
- Dumetz, A. C., Snellinger-O'Brien, A. M. und Lenhoff, A. M. 2007.** *Patterns of protein-protein interactions in salt solutions and implications for protein crystallization.* s.l. : Protein Science, 2007. Bd. 16, 9, S. 1867-1877.
- Dussupt, V., et al. 2011.** *Basic residues in the nucleocapsid domain of Gag are critical for late events of HIV-1 budding.* s.l. : J Virol, 2011. Bd. 85, 5, S. 2304-2315.
- Dyballa, N. und Metzger, S. 2009.** *Fast and sensitive colloidal coomassie G-250 staining for proteins in polyacrylamide gels.* s.l. : J Vis Exp, 2009. Bd. 30, 1431.
- Eisenthal, R., Danson, M. J. und Hough, D. W. 2007.** *Catalytic efficiency and kcat/KM: a useful comparator?* s.l. : Trends Biotechnol, 2007. Bd. 25, 6, S. 247-249.
- Engelman, A. 2010.** Reverse transcription and integration. [Buchverf.] R. Kurth und N. Bannert. *Retroviruses: Molecular Biology, Genomics and Pathogenesis.* s.l. : Norfolk, UK: Caister Academic Press, 2010, S. 129-159.
- Erickson-Viitanen, S., et al. 1989.** *Cleavage of HIV-1 gag polyprotein synthesized in vitro: sequential cleavage by the viral protease.* s.l. : AIDS Res Hum Retroviruses, 1989. Bd. 5, 6, S. 577-591.
- Fabryova, H. und Strebel, K. 2019.** *Vpr and Its Cellular Interaction Partners: R We There Yet?* s.l. : Cells, 2019. Bd. 8, 11, S. pii: E1310.
- Faria, N. R., et al. 2014.** *HIV epidemiology. The early spread and epidemic ignition of HIV-1 in human populations.* s.l. : Science, 2014. Bd. 346, 6205, S. 56-61.
- Fassati, A. und Goff, S. P. 2001.** *Characterization of intracellular reverse transcription complexes of human immunodeficiency virus type 1.* s.l. : J Virol, 2001. Bd. 75, 8, S. 3626-3635.
- Fehér, A., et al. 2002.** *Effect of sequence polymorphism and drug resistance on two HIV-1 Gag processing sites.* s.l. : Eur J Biochem, 2002. Bd. 296, 12, S. 4114-4120.
- Fehér, A., et al. 2006.** *Characterization of the murine leukemia virus protease and its comparison with the human immunodeficiency virus type 1 protease.* s.l. : J Gen Virol, 2006. Bd. 87, 5, S. 1321-1330.
- Feinberg, M. B., Baltimore, D. und Frankel, A. D. 1991.** *The role of Tat in the human immunodeficiency virus life cycle indicates a primary effect on transcriptional elongation.* s.l. : Proc Natl Acad Sci U S A, 1991. Bd. 88, 9, S. 4045-4049.
- Feng, S. und Holland, E. C. 1988.** *HIV-1 tat trans-activation requires the loop sequence within tar.* s.l. : Nature, 1988. Bd. 334, 6178, S. 165-167.

- Fisher, R., et al. 1998.** *Sequence-specific binding of human immunodeficiency virus type 1 nucleocapsid protein to short oligonucleotides.* s.l. : J Virol, 1998. Bd. 72, 3, S. 1902-1909.
- Fogarty, K. H., et al. 2014.** *Interrelationship between cytoplasmic retroviral Gag concentration and Gag-membrane association.* s.l. : J Mol Biol, 2014. Bd. 426, 7, S. 1611-1624.
- Frank, G. A., et al. 2015.** *Maturation of the HIV-1 core by a non-diffusional phase transition.* s.l. : Nat Commun, 2015. S. 6:5854.
- Gaber, R., et al. 2013.** *Noninvasive high-throughput single-cell analysis of HIV protease activity using ratiometric flow cytometry.* s.l. : Sensors (Basel), 2013. Bd. 13, 12, S. 16330-16346.
- Gácsi, A., et al. 2016.** *Calcium l-tartrate complex formation in neutral and in hyperalkaline aqueous solutions.* s.l. : Dalton Trans, 2016. Bd. 45, 43, S. 17296-17303.
- Gallo, R. C., et al. 1983.** *Isolation of human T-cell leukemia virus in acquired immune deficiency syndrome (AIDS).* s.l. : Science, 1983. Bd. 220, 4599, S. 865-867.
- Gamble, T. R., et al. 1997.** *Structure of the carboxyl-terminal dimerization domain of the HIV-1 capsid protein.* s.l. : Science, 1997. Bd. 278, 5339, S. 849-853.
- Ganser, B. K., et al. 1999.** *Assembly and analysis of conical models for the HIV-1 core.* s.l. : Science, 1999. Bd. 283, 5398, S. 80-83.
- Ganser-Pornillos, B. K., Yeager, M. und Sundquist, W. I. 2008.** *The structural biology of HIV assembly.* s.l. : Curr Opin Struct Biol, 2008. Bd. 18, 2, S. 203-217.
- Gasteiger, E., et al. 2003.** *ExpASY: The proteomics server for in-depth protein knowledge and analysis.* s.l. : Nucleic Acids Res, 2003. Bd. 31, 13, S. 3784-3788.
- Gaudin, R., et al. 2013.** *HIV trafficking in host cells: motors wanted!* s.l. : Trends Cell Biol, 2013. Bd. 23, 12, S. 652-662.
- Gendusa, R., et al. 2014.** *Elution of High-affinity (>10⁻⁹ KD) Antibodies from Tissue Sections: Clues to the Molecular Mechanism and Use in Sequential Immunostaining.* s.l. : J Histochem Cytochem, 2014. Bd. 62, 7, S. 519-531.
- Gheysen, D., et al. 1989.** *Assembly and release of HIV-1 precursor Pr55gag virus-like particles from recombinant baculovirus-infected insect cells.* s.l. : Cell, 1989. Bd. 59, 1, S. 103-112.
- Ghosn, J., et al. 2011.** *Polymorphism in Gag gene cleavage sites of HIV-1 non-B subtype and virological outcome of a first-line lopinavir/ritonavir single drug regimen.* s.l. : PLoS One, 2011. Bd. 6, 9, S. e24798.
- GLOBAL HIV STATISTICS . 2019.** *GLOBAL HIV STATISTICS.* s.l. : UNAIDS, 2019.
- Göttlinger, H. G., Dorfman, T., Sodroski, J. G. und Haseltine, W. A. 1991.** *Effect of mutations affecting the p6 gag protein on human immunodeficiency virus particle release.* s.l. : Proc Natl Acad Sci U S A, 1991. Bd. 88, 8, S. 3195-3199.
- Grant, S. G., et al. 1990.** *Differential plasmid rescue from transgenic mouse DNAs into Escherichia coli methylation-restriction mutants.* s.l. : Proc Natl Acad Sci U S A, 1990. Bd. 87, 12, S. 4645-4649.
- Gross, I., et al. 2000.** *A conformational switch controlling HIV-1 morphogenesis.* s.l. : EMBO J, 2000. Bd. 19, 1, S. 103-113.
- Grove, H., et al. 2009.** *Improved dynamic range of protein quantification in silver-stained gels by modelling gel images over time.* s.l. : Electrophoresis, 2009. Bd. 30, 11, S. 1856-1862.
- Gulnik, S. V., et al. 1995.** *Kinetic characterization and cross-resistance patterns of HIV-1 protease mutants selected under drug pressure.* s.l. : Biochemistry, 1995. Bd. 34, 29, S. 9282-9287.
- Hallenberger, S., et al. 1992.** *Inhibition of furin-mediated cleavage activation of HIV-1 glycoprotein gp160.* s.l. : Nature, 1992. Bd. 360, 6402, S. 358-361.

- Hanne, J., et al. 2016.** *Stimulated Emission Depletion Nanoscopy Reveals Time-Course of Human Immunodeficiency Virus Proteolytic Maturation.* s.l. : ACS Nano, 2016. Bd. 10, 9, S. 8215-8222.
- Henderson, L. E., et al. 1992.** *Gag proteins of the highly replicative MN strain of human immunodeficiency virus type 1: posttranslational modifications, proteolytic processings, and complete amino acid sequences.* s.l. : Journal of Virology, 1992. Bd. 66, 4, S. 1856-1865.
- Henderson, L. E., et al. 1990.** *Gag precursors of HIV and SIV are cleaved into six proteins found in the mature virions.* s.l. : J Med Primatol, 1990. Bd. 19, 3-4, S. 411-419.
- Hope, T. J. 1999.** *The ins and outs of HIV Rev.* s.l. : Arch Biochem Biophys, 1999. Bd. 365, 2, S. 186-191.
- Ido, E., et al. 1991.** *Kinetic studies of human immunodeficiency virus type 1 protease and its active-site hydrogen bond mutant A28S.* s.l. : J Biol Chem, 1991. Bd. 266, 36, S. 24359-66.
- Iordanskiy, S., et al. 2006.** *Intracytoplasmic maturation of the human immunodeficiency virus type 1 reverse transcription complexes determines their capacity to integrate into chromatin.* s.l. : Retrovirology, 2006. Bd. 3, 4.
- Ivanchenko, S., et al. 2009.** *Dynamics of HIV-1 assembly and release.* s.l. : PLoS Pathog, 2009. Bd. 5, 11, S. e1000652.
- Jacks, T., et al. 1988.** *Characterization of ribosomal frameshifting in HIV-1 gag-pol expression.* s.l. : Nature, 1988. Bd. 331, 6153, S. 280-283.
- Jacobs, E., et al. 1989.** *The HIV-1 Gag precursor Pr55gag synthesized in yeast is myristoylated and targeted to the plasma membrane.* s.l. : Gene, 1989. Bd. 79, 1, S. 71-81.
- James, J. S. 1995.** *Saquinavir (Invirase): first protease inhibitor approved--reimbursement, information hotline numbers.* s.l. : AIDS Treat News, 1995. Bd. 237, S. 1-2.
- Kao, S. Y., et al. 1987.** *Anti-termination of transcription within the long terminal repeat of HIV-1 by tat gene product.* s.l. : Nature, 1987. Bd. 330, 6147, S. 489-493.
- Karacostas, V., et al. 1989.** *Human immunodeficiency virus-like particles produced by a vaccinia virus expression vector.* s.l. : Proc Natl Acad Sci U S A, 1989. Bd. 86, 22, S. 8964-8967.
- Keele, B. F., et al. 2006.** *Chimpanzee reservoirs of pandemic and nonpandemic HIV-1.* s.l. : Science, 2006. Bd. 313, 5786, S. 523-526.
- Keller, P. W., et al. 2013.** *A two-pronged structural analysis of retroviral maturation indicates that core formation proceeds by a disassembly-reassembly pathway rather than a displacive transition.* s.l. : J Virol, 2013. Bd. 87, 24, S. 13655-13664.
- Keller, P. W., et al. 2011.** *HIV-1 maturation inhibitor bevirimat stabilizes the immature Gag lattice.* s.l. : J Virol, 2011. Bd. 85, 4, S. 1420-1428.
- Könnyű, B., et al. 2013.** *Gag-Pol processing during HIV-1 virion maturation: a systems biology approach.* s.l. : PLoS Comput Biol, 2013. Bd. 9, 6, S. e1003103.
- Konvalinka, J., et al. 1995.** *Proteolytic processing of particle-associated retroviral polyproteins by homologous and heterologous viral proteinases.* s.l. : Eur J Biochem, 1995. Bd. 228, 1, S. 191-198.
- Kräusslich, H. G., et al. 1995.** *The spacer peptide between human immunodeficiency virus capsid and nucleocapsid proteins is essential for ordered assembly and viral infectivity.* s.l. : J Virol, 1995. Bd. 69, 6, S. 3404-3419.
- Kräusslich, H. G., et al. 1989.** *Activity of purified biosynthetic proteinase of human immunodeficiency virus on natural substrates and synthetic peptides.* s.l. : Proc Natl Acad Sci U S A, 1989. Bd. 86, 3, S. 807-811.

- Kräusslich, H. G., Traenckner, A. M. und Rippmann, F. 1991.** *Expression and characterization of genetically linked homo- and hetero-dimers of HIV proteinase.* s.l. : Adv Exp Med Biol, 1991. Bd. 306, S. 417-428.
- Krishnan, L., et al. 2010.** *Structure-based modeling of the functional HIV-1 intasome and its inhibition.* s.l. : Proc Natl Acad Sci U S A, 2010. Bd. 107, 36, S. 15910-15915.
- Kucharska, I., et al. 2019.** *Biochemical reconstitution of HIV-1 assembly and maturation.* s.l. : J Virol, 2019. Bde. JVI.01844-19.
- Kutluay, S. B. und Bieniasz, P. D. 2010.** *Analysis of the initiating events in HIV-1 particle assembly and genome packaging.* s.l. : PLoS Pathog, 2010. Bd. 6, 11.
- Kutluay, S. B., et al. 2014.** *Global changes in the RNA binding specificity of HIV-1 gag regulate virion genesis.* s.l. : Cell, 2014. Bd. 159, 5, S. 1096-1109.
- Kwong, P. D., et al. 1998.** *Structure of an HIV gp120 envelope glycoprotein in complex with the CD4 receptor and a neutralizing human antibody.* s.l. : Nature, 1998. Bd. 393, 6686, S. 648-659.
- Lacy, M. K. und Abriola, K. P. 1996.** *Indinavir: a pharmacologic and clinical review of a new HIV protease inhibitor.* s.l. : Conn Med, 1996. Bd. 60, 12, S. 723-727.
- Lambert-Niclot, S., et al. 2008.** *Impact of gag mutations on selection of darunavir resistance mutations in HIV-1 protease.* s.l. : J Antimicrob Chemother, 2008. Bd. 62, 5, S. 905-908.
- Laughrea, M. und Jetté, L. 1994.** *A 19-nucleotide sequence upstream of the 5' major splice donor is part of the dimerization domain of human immunodeficiency virus 1 genomic RNA.* s.l. : Biochemistry, 1994. Bd. 33, 45, S. 13464-13474.
- Lee, S. K., et al. 2012.** *Context surrounding processing sites is crucial in determining cleavage rate of a subset of processing sites in HIV-1 Gag and Gag-Pro-Pol polyprotein precursors by viral protease.* s.l. : J Biol Chem, 2012. Bd. 287, 16, S. 13279-13290.
- Lee, S. K., Harris, J. und Swanstrom, R. 2009.** *A strongly transdominant mutation in the human immunodeficiency virus type 1 gag gene defines an Achilles heel in the virus life cycle.* s.l. : J Virol, 2009. Bd. 83, 17, S. 8536-8543.
- Letcher, A. J., Schell, M. J. und Irvine, R. F. 2008.** *Do mammals make all their own inositol hexakisphosphate?* s.l. : Biochem J, 2008. Bd. 416, 2, S. 263-270.
- Lever, A., et al. 1989.** *Identification of a sequence required for efficient packaging of human immunodeficiency virus type 1 RNA into virions.* s.l. : J Virol, 1989. Bd. 63, 9, S. 4085-4087.
- Levin, J. G., et al. 2005.** *Nucleic acid chaperone activity of HIV-1 nucleocapsid protein: critical role in reverse transcription and molecular mechanism.* s.l. : Prog Nucleic Acid Res Mol Biol, 2005. Bd. 80, S. 217-286.
- Li, F., et al. 2003.** *PA-457: a potent HIV inhibitor that disrupts core condensation by targeting a late step in Gag processing.* s.l. : Proc Natl Acad Sci U S A, 2003. Bd. 100, 23, S. 13555-13560.
- Li, G., et al. 2013.** *Functional conservation of HIV-1 Gag: implications for rational drug design.* s.l. : Retrovirology, 2013. Bd. 10, S. 126.
- Li, M., et al. 2006.** *Retroviral DNA integration: reaction pathway and critical intermediates.* s.l. : EMBO J, 2006. Bd. 25, 6, S. 1295-1304.
- Li, S., et al. 2000.** *Image reconstructions of helical assemblies of the HIV-1 CA protein.* s.l. : Nature, 2000. Bd. 407, 6802, S. 409-413.
- Liu, J., et al. 2008.** *Molecular architecture of native HIV-1 gp120 trimers.* s.l. : Nature, 2008. Bd. 455, 7209.

- Liu, Y., et al. 2017.** *HIV-1 Sequence Necessary and Sufficient to Package Non-viral RNAs into HIV-1 Particles.* s.l. : J Mol Biol, 2017. Bd. 429, 16, S. 2542-2555.
- López, C. S., et al. 2013.** *Second site reversion of a mutation near the amino terminus of the HIV-1 capsid protein.* s.l. : Virology, 2013. Bd. 447, 1-2, S. 95-103.
- Lu, M. und Kim, P. S. 1997.** *A trimeric structural subdomain of the HIV-1 transmembrane glycoprotein.* s.l. : J Biomol Struct Dyn, 1997. Bd. 15, 3, S. 465-471.
- Lusic, M. und Siliciano, R. F. 2017.** *Nuclear landscape of HIV-1 infection and integration.* s.l. : Nat Rev Microbiol, 2017. Bd. 15, 2, S. 69-82.
- Lyonnais, S., et al. 2019.** *The HIV-1 ribonucleoprotein dynamically regulates its condensate behavior and drives acceleration of protease activity through membrane-less granular phase-separation.* s.l. : bioRxiv, 2019. S. 528638.
- Malet, I., et al. 2007.** *Association of Gag cleavage sites to protease mutations and to virological response in HIV-1 treated patients.* s.l. : J Infect, 2007. Bd. 54, 4, S. 367-374.
- Malim, M. H., et al. 1989.** *The HIV-1 rev trans-activator acts through a structured target sequence to activate nuclear export of unspliced viral mRNA.* s.l. : Nature, 1989. Bd. 338, 6212, S. 254-257.
- Mallery, D. L., et al. 2019.** *Cellular IP6 Levels Limit HIV Production while Viruses that Cannot Efficiently Package IP6 Are Attenuated for Infection and Replication.* s.l. : Cell Rep, 2019. Bd. 29, 12, S. 3983-3996.
- Mascher, a B., et al. 1996.** *Human immunodeficiency virus. Mutations in the viral protease that confer resistance to saquinavir increase the dissociation rate constant of the protease-saquinavir complex.* s.l. : J Biol Chem, 1996. Bd. 271, 52, S. 33231-33235.
- Mascola, J. R. und Montefiori, D. C. 2003.** *HIV-1: nature's master of disguise.* s.l. : Nat Med, 2003. Bd. 9, 4, S. 393-394.
- Matayoshi, E. D., et al. 1990.** *Novel fluorogenic substrates for assaying retroviral proteases by resonance energy transfer.* s.l. : Science, 1990. Bd. 247, 4945, S. 954-958.
- Mattei, S., et al. 2018.** *High-resolution structures of HIV-1 Gag cleavage mutants determine structural switch for virus maturation.* s.l. : Proc Natl Acad Sci U S A, 2018. Bd. 115, 40, S. E9401-E9410.
- Mattei, S., et al. 2014.** *Induced maturation of human immunodeficiency virus.* s.l. : J Virol, 2014. Bd. 88, 23, S. 13722-13731.
- Mattei, S., Schur, F. K. M. und Briggs, J. A. G. 2016.** *Retrovirus maturation — an extraordinary structural transformation.* s.l. : Current Opinion in Virology, 2016. Bd. 18, S. 27-35.
- McDonald, D., et al. 2002.** *Visualization of the intracellular behavior of HIV in living cells.* s.l. : J Cell Biol, 2002. Bd. 159, 3, S. 441-452.
- McDougal, J. S., et al. 1986.** *Binding of the human retrovirus HTLV-III/LAV/ARV/HIV to the CD4 (T4) molecule: conformation dependence, epitope mapping, antibody inhibition, and potential for idiotypic mimicry.* s.l. : J Immunol, 1986. Bd. 137, 9, S. 2937-2944.
- McKinstry, W. J., et al. 2014.** *Expression and purification of soluble recombinant full length HIV-1 Pr55(Gag) protein in Escherichia coli.* s.l. : Protein Expr Purif, 2014. Bd. 100, S. 10-18.
- Meng, B. und Lever, A. M. 2013.** *Wrapping up the bad news: HIV assembly and release.* s.l. : Retrovirology, 2013. Bd. 10:5.
- Meng, X., et al. 2012.** *Protease cleavage leads to formation of mature trimer interface in HIV-1 capsid.* s.l. : PLoS Pathog, 2012. Bd. 8, 8, S. e1002886.
- Mercredi, P. Y., et al. 2016.** *Structural and Molecular Determinants of Membrane Binding by the HIV-1 Matrix Protein.* s.l. : J Mol Biol, 2016. Bd. 428, 8, S. 1637-1655.

- Mervis, R. J., et al. 1988.** *The gag gene products of human immunodeficiency virus type 1: alignment within the gag open reading frame, identification of posttranslational modifications, and evidence for alternative gag precursors.* s.l. : Journal of Virology, 1988. Bd. 62, 11, S. 3993-4002.
- Mirambeau, G., et al. 2007.** *HIV-1 protease and reverse transcriptase control the architecture of their nucleocapsid partner.* s.l. : PLoS One, 2007. Bd. 2, 7, S. e669.
- Mirambeau, G., Lyonnais, S. und Gorelick, R. J. 2010.** *Features, processing states, and heterologous protein interactions in the modulation of the retroviral nucleocapsid protein function.* s.l. : RNA Biol, 2010. Bd. 7, 6, S. 724-734.
- Mücksch, F., et al. 2018.** *Synchronized HIV assembly by tunable PIP2 changes reveals PIP2 requirement for stable Gag anchoring.* s.l. : Elife, 2018. Bd. 6, S. e25287.
- Müller, B., et al. 2009.** *HIV-1 Gag processing intermediates trans-dominantly interfere with HIV-1 infectivity.* s.l. : J Biol Chem, 2009. Bd. 284, 43, S. 29692-29703.
- Munro, J. B., et al. 2014.** *A conformational transition observed in single HIV-1 Gag molecules during in vitro assembly of virus-like particles.* s.l. : J Virol, 2014. Bd. 88, 6, S. 3577-3585.
- Murray, P. S., et al. 2005.** *Retroviral matrix domains share electrostatic homology: models for membrane binding function throughout the viral life cycle.* s.l. : Structure, 2005. Bd. 13, 10, S. 1521-1531.
- Nakashima, H., et al. 1986.** *Inhibition of replication and cytopathic effect of human T cell lymphotropic virus type III/lymphadenopathy-associated virus by 3'-azido-3'-deoxythymidine in vitro.* s.l. : Antimicrobial agents and chemotherapy, 1986. Bd. 30, 6, S. 933-937.
- Nijhuis, M., et al. 2007.** *A novel substrate-based HIV-1 protease inhibitor drug resistance mechanism.* s.l. : PLoS Med, 2007. Bd. 4, 1, S. e36.
- Nijhuis, M., et al. 1999.** *Increased fitness of drug resistant HIV-1 protease as a result of acquisition of compensatory mutations during suboptimal therapy.* s.l. : AIDS, 1999. Bd. 13, 17, S. 2349-2359.
- Ning, J., et al. 2016.** *In vitro protease cleavage and computer simulations reveal the HIV-1 capsid maturation pathway.* s.l. : Nat Commun, 2016. S. 7:13689.
- Pak, A. J., et al. 2017.** *Immature HIV-1 lattice assembly dynamics are regulated by scaffolding from nucleic acid and the plasma membrane.* 2017.
- Partin, K., et al. 1991.** *Deletion of sequences upstream of the proteinase improves the proteolytic processing of human immunodeficiency virus type 1.* s.l. : Proc Natl Acad Sci U S A, 1991. Bd. 88, 11, S. 4776-4780.
- Partin, K., et al. 1990.** *Mutational analysis of a native substrate of the human immunodeficiency virus type 1 proteinase.* s.l. : J Virol, 1990. Bd. 64, 8, S. 3938-3947.
- Patarca, R. und Haseltine, W. A. 1985.** *A major retroviral core protein related to EPA and TIMP.* s.l. : Nature, 1985. Bd. 318, 6044, S. 390.
- Patick, A. K. und Potts, K. E. 1998.** *Protease inhibitors as antiviral agents.* s.l. : Clin Microbiol Rev, 1998. Bd. 11, 4, S. 614-627.
- Peters, R. W. und Ku, Y. 1988.** *The effect of tartrate, a weak complexing agent, on the removal of heavy metals by sulfide and hydroxide precipitation.* s.l. : Particulate science and technology, 1988. Bd. 6, 4, S. 421-439.
- Pettit, S. C., et al. 1994.** *The p2 domain of human immunodeficiency virus type 1 Gag regulates sequential proteolytic processing and is required to produce fully infectious virions.* s.l. : J Virol, 1994. Bd. 68, 12, S. 80-17-8027.

- Pettit, S. C., et al. 1991.** *Analysis of retroviral protease cleavage sites reveals two types of cleavage sites and the structural requirements of the P1 amino acid.* s.l. : J Biol Chem, 1991. Bd. 266, 22, S. 14539-14547.
- Pettit, S. C., et al. 2005.** *Ordered processing of the human immunodeficiency virus type 1 GagPol precursor is influenced by the context of the embedded viral protease.* s.l. : J Virol, 2005. Bd. 79, 16, S. 10601-10607.
- Pettit, S. C., et al. 2002.** *Replacement of the P1 amino acid of human immunodeficiency virus type 1 Gag processing sites can inhibit or enhance the rate of cleavage by the viral protease.* s.l. : J Virol, 2002. Bd. 76, 20, S. 10226-10233.
- Pettit, S. C., et al. 1998.** *The regulation of sequential processing of HIV-1 Gag by the viral protease.* s.l. : Adv Exp Med Biol, 1998. Bd. 436, S. 15-25.
- Pettit, S. C., et al. 2003.** *The dimer interfaces of protease and extra-protease domains influence the activation of protease and the specificity of GagPol cleavage.* s.l. : J Virol, 2003. Bd. 77, 1, S. 366-374.
- Pornillos, O. und Ganser-Pornillos, B. K. 2019.** *Maturation of retroviruses.* s.l. : Curr Opin Virol, 2019. Bd. 36, S. 47-55.
- Potempa, M., et al. 2015.** *A Direct Interaction with RNA Dramatically Enhances the Catalytic Activity of the HIV-1 Protease In Vitro.* s.l. : J Mol Biol, 2015. Bd. 427, 14, S. 2360-2378.
- Prabu-Jeyabalan, M., et al. 2004.** *Structural basis for coevolution of a human immunodeficiency virus type 1 nucleocapsid-p1 cleavage site with a V82A drug-resistant mutation in viral protease.* s.l. : J Virol, 2004. Bd. 78, 22, S. 12446-12454.
- ProteinCalculator v3.4. [Online] <http://protcalc.sourceforge.net/>.
- Purdy, M. D., et al. 2018.** *MicroED structures of HIV-1 Gag CTD-SP1 reveal binding interactions with the maturation inhibitor bevirimat.* s.l. : Proc Natl Acad Sci U S A, 2018. Bd. 115, 52, S. 13258-13263.
- Rambaut, A., et al. 2004.** *The causes and consequences of HIV evolution.* s.l. : Nat Rev Genet, 2004. Bd. 5, 1, S. 52-61.
- Ratner, L., et al. 1985.** *Complete nucleotide sequence of the AIDS virus, HTLV-III.* s.l. : Nature, 1985. Bd. 313, 6000, S. 277-284.
- Reeves, J. D. und Doms, R. W. 2002.** *Human immunodeficiency virus type 2.* s.l. : J Gen Virol., 2002. Bd. 83, 6, S. 1253-1265.
- Rein, A. 2010.** *Nucleic acid chaperone activity of retroviral Gag proteins.* s.l. : RNA Biology, 2010. Bd. 7, 6, S. 700-705.
- Rein, A., et al. 2011.** *Diverse interactions of retroviral Gag proteins with RNAs.* s.l. : Trends Biochem Sci, 2011. Bd. 36, 7, S. 373-380.
- Saad, J. S., et al. 2006.** *Structural basis for targeting HIV-1 Gag proteins to the plasma membrane for virus assembly.* s.l. : Proc Natl Acad Sci U S A, 2006. Bd. 103, 30, S. 11364-11369.
- Sadiq, S. K. 2016.** *Reaction-diffusion basis of retroviral infectivity.* s.l. : Philos Trans A Math Phys Eng Sci, 2016. Bd. 374, 2080.
- Sadiq, S. K., et al. 2011.** *Reaction kinetics of catalyzed competitive heteropolymer cleavage.* s.l. : J Phys Chem B, 2011. Bd. 115, 37, S. 11017-11027.
- Sadiq, S. K., Noé, F. und De Fabritiis, G. 2012.** *Kinetic characterization of the critical step in HIV-1 protease maturation.* s.l. : Proc Natl Acad Sci U S A, 2012. Bd. 109, 50, S. 20449-20454.
- Sattentau, Q. J. und Weiss, R. A. 1988.** *The CD4 antigen: physiological ligand and HIV receptor.* s.l. : Cell, 1988. Bd. 52, 5, S. 631-633.

- Sauter, D. und Kirchhoff, F. 2016.** *HIV replication: a game of hide and sense.* s.l. : Curr Opin HIV AIDS, 2016. Bd. 11, 2, S. 173-181.
- Schägger, H. 2006.** *Tricine-SDS-PAGE.* s.l. : Nat Protoc, 2006. Bd. 1, 1, S. 16-22.
- Schröder, A. R., et al. 2002.** *HIV-1 integration in the human genome favors active genes and local hotspots.* s.l. : Cell, 2002. Bd. 110, 4, S. 521-529.
- Schur, F. K., et al. 2016.** *An atomic model of HIV-1 capsid-SP1 reveals structures regulating assembly and maturation.* s.l. : Science, 2016. Bd. 353, 6298, S. 506-508.
- Schur, F. K., et al. 2015.** *Structure of the immature HIV-1 capsid in intact virus particles at 8.8 Å resolution.* s.l. : Nature, 2015. Bd. 517, 7535, S. 505-508.
- Shafer, R. W. und Schapiro, J. M. 2008.** *HIV-1 drug resistance mutations: an updated framework for the second decade of HAART.* s.l. : AIDS Rev, 2008. Bd. 10, 12, S. 67-84.
- Sheng, N., et al. 1997.** *Determinants of the human immunodeficiency virus type 1 p15NC-RNA interaction that affect enhanced cleavage by the viral protease.* s.l. : J Virol, 1997. Bd. 71, 8, S. 5723-5732.
- Skripkin, E., et al. 1994.** *Identification of the primary site of the human immunodeficiency virus type 1 RNA dimerization in vitro.* s.l. : Proc Natl Acad Sci U S A, 1994. Bd. 91, 11, S. 4945-4949.
- Sowd, G. A., et al. 2016.** *A critical role for alternative polyadenylation factor CPSF6 in targeting HIV-1 integration to transcriptionally active chromatin.* s.l. : Proc Natl Acad Sci U S A, 2016. Bd. 113, 8, S. 1054-1063.
- Spearman, P., et al. 1997.** *Membrane binding of human immunodeficiency virus type 1 matrix protein in vivo supports a conformational myristyl switch mechanism.* s.l. : J Virol, 1997. Bd. 71, 9, S. 6582-6592.
- Stephen, A. G., et al. 2007.** *Measuring the binding stoichiometry of HIV-1 Gag to very-low-density oligonucleotide surfaces using surface plasmon resonance spectroscopy.* s.l. : J Biomol Tech, 2007. Bd. 18, 4, S. 259-266.
- Stoye, J. P., et al. 2011.** *ICTV 9th Report.* s.l. : ICTV Reports, 2011.
- Studier, F. W. und Moffatt, B. A. 1986.** *Use of bacteriophage T7 RNA polymerase to direct selective high-level expression of cloned genes.* s.l. : J Mol Biol, 1986. Bd. 189, 1, S. 113-130.
- Sundquist, W. I. und Kräusslich, H. G. 2012.** *HIV-1 assembly, budding, and maturation.* s.l. : Cold Spring Harb Perspect Med, 2012. Bd. 2, 7.
- Swanstrom, R. und Coffin, J. 2012.** *HIV-1 pathogenesis: the virus.* s.l. : Cold Spring Harb Perspect Med, 2012. Bd. 2, 12.
- Swanstrom, R. und Wills, J. W. 1997.** *Synthesis, Assembly, and Processing of Viral Proteins.* s.l. : Cold Spring Harbor Laboratory Press, 1997.
- Szeltner, Z. und Polgár, L. 1996.** *Rate-determining steps in HIV-1 protease catalysis. The hydrolysis of the most specific substrate.* s.l. : J Biol Chem, 1996. Bd. 271, 50, S. 32180-32184.
- Tamburini, P. p., et al. 1990.** *A fluorometric assay for HIV-protease activity using high-performance liquid chromatography.* s.l. : Anal Biochem, 1990. Bd. 196, 2, S. 363-368.
- Tang, C., et al. 2004.** *Entropic switch regulates myristate exposure in the HIV-1 matrix protein.* s.l. : PNAS, 2004. Bd. 101, 2, S. 517-522.
- Tanwar, H. S., et al. 2017.** *The thermodynamics of Pr55Gag-RNA interaction regulate the assembly of HIV.* s.l. : PLoS Pathog, 2017. Bd. 13, 2, S. e1006221.
- Tessmer, U. und Kräusslich, H. G. 1998.** *Cleavage of human immunodeficiency virus type 1 proteinase from the N-terminally adjacent p6* protein is essential for efficient Gag polyprotein processing and viral infectivity.* s.l. : J Virol, 1998. Bd. 72, 4, S. 3459-3463.

- Todd, M. J., Semo, N. und Freire, E. 1998.** *The structural stability of the HIV-1 protease.* s.l. : J Mol Biol, 1998. Bd. 283, 2, S. 475-488.
- Tözsér, J., et al. 1991.** *Comparison of the HIV-1 and HIV-2 proteinases using oligopeptide substrates representing cleavage sites in Gag and Gag-Pol polyproteins.* s.l. : FEBS Lett, 1991. Bd. 281, 1-2, S. 77-80.
- Trinh, T., et al. 1994.** *STBL2: an Escherichia coli strain for the stable propagation of retroviral clones and direct repeat sequences.* s.l. : FOCUS, 1994. Bd. 16, S. 78-80.
- UNAIDS Press release. 2016.** *UNAIDS warns that after significant reductions, declines in new HIV infections among adults have stalled and are rising in some regions.* s.l. : UNAIDS, 2016.
- Van Lint, C. 1., Bouchat, S. und Marcello, A. 2013.** *HIV-1 transcription and latency: an update.* s.l. : Retrovirology, 2013. Bd. 10, 67.
- van Maarseveen, N. M., et al. 2007.** *Persistence of HIV-1 variants with multiple protease inhibitor (PI)-resistance mutations in the absence of PI therapy can be explained by compensatory fixation.* s.l. : J Infect Dis, 2007. Bd. 195, 3, S. 399-409.
- Veronese, F. D., et al. 1988.** *Biochemical and immunological analysis of human immunodeficiency virus gag gene products p17 and p24.* s.l. : J Virol, 1988. Bd. 62, 3, S. 795-801.
- Vogt, V. M. 1997.** *Retroviral Virions and Genomes.* s.l. : Cold Spring Harbor Laboratory Press, 1997.
- Voráčková, I., et al. 2011.** *Purification of proteins containing zinc finger domains using immobilized metal ion affinity chromatography.* s.l. : Protein Expr Purif, 2011. Bd. 79, 1, S. 88-95.
- Wagner, J. M., et al. 2016.** *Crystal structure of an HIV assembly and maturation switch.* s.l. : Elife, 2016. Bd. 5, S. e17063.
- Wain-Hobson, S., et al. 1985.** *Nucleotide sequence of the AIDS virus, LAV.* s.l. : Cell, 1985. Bd. 40, 1, S. 9-17.
- Wang, C. T. und Barklis, E. 1993.** *Assembly, processing, and infectivity of human immunodeficiency virus type 1 gag mutants.* s.l. : J Virol, 1993. Bd. 67, 7, S. 4264-4273.
- Watts, J. M., et al. 2009.** *Architecture and secondary structure of an entire HIV-1 RNA genome.* s.l. : Nature, 2009. Bd. 460, 7256, S. 711-716.
- Wensing, A. M., van Maarseveen, N. M. und Nijhuis, M. 2010.** *Fifteen years of HIV Protease Inhibitors: raising the barrier to resistance.* s.l. : Antiviral Res, 2010. Bd. 85, 1, S. 59-74.
- Wieggers, K., et al. 1998.** [Hrsg.] 2846-2854. *Sequential steps in human immunodeficiency virus particle maturation revealed by alterations of individual Gag polyprotein cleavage sites.* s.l. : J Virol, 1998. Bd. 72, 4.
- Wilén, C. B, Tilton, J. C. und Doms, R. W. 2012.** *Molecular Mechanisms of HIV Entry.* s.l. : Viral Molecular Machines, 2012. S. 223-242.
- Wills, J. W. und Craven, R. C. 1991.** *Form, function, and use of retroviral gag proteins.* s.l. : AIDS, 1991. Bd. 5, 6, S. 639-954.
- Woodward, C. L., Cheng, S. N. und Jensen, G. J. 2015.** *Electron cryotomography studies of maturing HIV-1 particles reveal the assembly pathway of the viral core.* s.l. : J Virol, 2015. Bd. 89, 2, S. 1267-1277.
- Wright, E. R., et al. 2007.** *Electron cryotomography of immature HIV-1 virions reveals the structure of the CA and SP1 Gag shells.* s.l. : EMBO J, 2007. Bd. 26, 8, S. 2218-2226.
- Wu, J. and Filutowicz, M. 1999.** *Hexahistidine (His6)-tag dependent protein dimerization: a cautionary tale.* s.l. : Acta Biochim Pol, 1999. Vol. 46, 3, pp. 591-599.
- Wu, L., et al. 1996.** *CD4-induced interaction of primary HIV-1 gp120 glycoproteins with the chemokine receptor CCR-5.* s.l. : Nature, 1996. Bd. 384, 6605, S. 179-183.

- Wyma, D. J., et al. 2004.** *Coupling of human immunodeficiency virus type 1 fusion to virion maturation: a novel role of the gp41 cytoplasmic tail.* s.l. : J Virol, 2004. Bd. 78, 7, S. 3429-3435.
- Yamashita, M: und Engelman, A. N. 2017.** *Capsid-Dependent Host Factors in HIV-1 Infection.* s.l. : Trends Microbiol, 2017. Bd. 25, 9, S. 741-755.
- Yang, F., et al. 2018.** *Prediction of the binding mode and resistance profile for a dual-target pyrrolyl dike to acid scaffold against HIV-1 integrase and reverse-transcriptase-associated ribonuclease H.* s.l. : Phys Chem Chem Phys, 2018. Bd. 20, 37, S. 23873-23884.
- Zhao, H., et al. 2019.** *Nucleic acid-induced dimerization of HIV-1 Gag protein.* s.l. : J Biol Chem, 2019. Bd. 294, 45, S. 16480-16493.
- Zhou, J., et al. 2004.** *Small-molecule inhibition of human immunodeficiency virus type 1 replication by specific targeting of the final step of virion maturation.* s.l. : J Virol, 2004. Bd. 78, 2, S. 922-929.
- Zhu, P., et al. 2003.** *Electron tomography analysis of envelope glycoprotein trimers on HIV and simian immunodeficiency virus virions.* s.l. : Proc Natl Acad Sci USA, 2003. Bd. 100, 26, S. 15812-15817.
- Zhu, T., et al. 1998.** *An African HIV-1 sequence from 1959 and implications for the origin of the epidemic.* s.l. : Nature, 1998. Bd. 391, 6667, S. 594-597.